CATALYSIS AND PHOTOCATALYSIS

BY PLATINIZED TITANIUM DIOXIDE

AND OTHER CATALYSTS

by

Keith Smallwood B.Sc.

Thesis submitted to the University of Nottingham

for the Degree of Doctor of Philosophy,

April, 1993.

To my late father,

who will always be

a source of inspiration for me.

ACKNOWLEDGEMENTS

The author wishes to express sincere gratitude to Dr. Rudham, under whose supervision and guidance this work was carried out. His advice, encouragement and patience have been much appreciated.

Thanks are due to members of the technical support staff at Nottingham University, whose expert assistance during the course of this project work was invaluable.

The author would also like to thank Mrs Sylvia Baguley (nee Smallwood) and Miss Debbie Towell in particular, but also his colleagues and friends at Nottingham and Unilever Research, Bedford, for their continued support and encouragement.

ABSTRACT

The work reported in this thesis was carried out between October 1986 and September 1989 at Nottingham University, under the supervision of Dr. R. Rudham. It is the original work of the author, except where indicated by reference to the open literature, and has not been submitted for any other degree.

The gas-phase, thermal hydrogenations of propene and cyclopropane over various titania-supported metal catalysts have been investigated. Catalysts were prepared either by a photodeposition or a thermal reduction method. Absolute initial hydrogenation rates were calculated from total gas pressure vs time measurements.

The activities of all catalysts were found to be very dependent upon catalyst state, as modified by reductive or oxidative pretreatments. These results are discussed in terms of reversible strong metal-support interactions, initiated via hydrogen spillover. For 0.5 %mass Pt on TiO_2, the order of reaction with respect to hydrocarbon was 0.5. An adsorption mechanism involving the alkylidene species is proposed as one possible explanation of this result. A negative order of reaction with respect to hydrogen was recorded. A Langmuir-Hinshelwood mechanism, involving competitive adsorption of hydrocarbon and hydrogen at supported metal sites, is proposed.

Differences in behaviour between catalysts prepared by photodeposition and the thermally-prepared catalyst were observed during the hydrogenation studies. These include different apparent activation

energies, maximum reaction rates at differing propene:hydrogen ratios and irreversible degradation of all photodeposited catalysts during cyclopropane hydrogenation. These differences are taken as being strongly indicative of differences in supported metal morphologies, arising as a consequence of the preparative routes employed. Temperature-programmed desorption and scanning electron microscopy studies were undertaken in an attempt to establish and characterise these potential morphological differences. Although the results of these studies were, at best, inconclusive, the possible nature of such supported metal morphological differences is discussed on the basis of available evidence generated within this and other, similar, studies.

The liquid-phase photocatalytic dehydrogenation of propan-2-ol, using the same catalysts, was also briefly investigated. Variations in measured activation energies suggest that photodeposited catalysts in the 'as prepared' state are contaminated with variable levels of impurity residues, particularly chloride ions.

TABLE OF CONTENTS

CHAPTER 1: INTRODUCTION

CHAPTER 2: EXPERIMENTAL

CHAPTER 3: RESULTS

CHAPTER 4: DISCUSSION

CHAPTER 1: INTRODUCTION

1.1 General Introduction

The word *catalysis* is used to describe the process in which one or more substances, known as catalysts, enhance the rate at which a chemical reaction occurs, without appearing in the overall stoichiometric equation. It is a purely kinetic phenomenon rather than a thermodynamic one, so that the position of chemical equilibrium remains unchanged. The function of a catalyst is essentially to provide a route towards equilibrium with a lower activation energy than that of the corresponding uncatalysed reaction.

Catalysis can be divided into two distinct categories:

1) *homogeneous* - in which no phase boundary exists between the catalyst and the reactant system, and

2) *heterogeneous* - in which a definite phase boundary exists between the catalyst and the reactant system.

The vast majority of heterogeneous catalysts are solid materials and the phase boundary between the catalyst and gas- or liquid-phase reactant-product system occurs at the surface of the catalyst particles. Surface phenomena have long been established as the origins of solid catalysis, and an outstanding feature of heterogeneous catalysts is the extent to which they can exert selective control during a reaction. In a catalytic reaction a number of products may be thermodynamically possible from the same reactants and the most dominant products will be those formed along the most energetically favourable pathway. The most favourable

route is determined by the nature of the catalyst used and in some cases the selectivity is so great that the catalyst is entirely specific for the reaction in question. A classical example of such extreme selectivity is the catalytic dehydration of formic acid, in which alumina gives CO and H_2O exclusively and zinc oxide gives CO_2 and H_2 exclusively.

The process of solid heterogeneous catalysis can be divided into five, fundamental consecutive steps:

1) transport of reactant(s) to the catalyst,

2) adsorption of reactant(s) onto the catalyst surface,

3) reaction of the adsorbed species to give product(s),

4) desorption of product(s) from the catalyst surface,

5) transport of product(s) away from the catalyst.

The rate at which a catalytic reaction proceeds will be determined by the slowest, or *rate-determining,* step in the above sequence. Steps (1) and (5) are transport phenomena and will only be rate-determining in cases where catalyst activity is extremely high and the catalytic reactor is of a poor design, or if the catalyst possesses small diameter pores, such as zeolites. Under these circumstances, the reaction is said to be *diffusion* or *mass-transport limited.* Steps (2) - (4) are concerned with chemical phenomena and step (3) is most frequently the rate-determining step, although some catalysts show activated adsorption or desorption kinetics, so that steps (2) or (4) become rate-determining.

The suitability of a substance as a catalyst for a particular type of reaction is determined by how it interacts with the reactant-product system, which in turn depends upon the general bulk properties of the

substance. This allows a general, somewhat superficial, classification of heterogeneous catalysts according to their primary catalytic functions, as shown in Table 1.1. Thus, metals tend to be very active in reactions involving hydrogen and hydrocarbons because of their ability to adsorb these compounds very strongly, but are not particularly efficient oxidation catalysts because many base metal are themselves oxidised under the reaction conditions frequently used.

Table 1.1 Broad Classification of Heterogeneous Catalysts According to Primary Catalytic Functions

Catalyst Class	Reactions	Examples
Metals	Hydrogenation	Ni, Pt, Pd, Fe
	Dehydrogenation	
	Hydrogenolysis	
Semiconducting Oxides/Sulphides	Oxidation	TiO_2, ZnO, MnO_2, WS_2
	Desulphurisation	
Insulating Oxides	Dehydration	Al_2O_3, SiO_2
Solid Acids	Cracking	Natural and Synthetic Zeolites
	Alkylation	
	Polymerisation	
	Skeletal Isomerisation	

It has long been recognised that adsorption processes are fundamental to heterogeneous catalysis and have consequently been studied in detail in this context. Two types of adsorption are known to occur on the surface of solids:

1) *Physical*, or *physisorption*, arises due to weak, short-range attractive molecular forces between the adsorbate and adsorbent. Physisorption can lead to the formation of more than one adsorbed layer and the process depends very little upon the chemical nature of the adsorbing solid.

2) *Chemical*, or *chemisorption*, involves the formation of either electrostatic or covalent bonds between the adsorbate and adsorbent and is consequently a much stronger interaction than physisorption. Chemisorption is restricted to a monolayer coverage of the surface and the process depends heavily upon the chemical nature of both the adsorbate and the adsorbent.

The thermodynamics of adsorption are represented by the equation:

$$\Delta G_{ads} = \Delta H_{ads} - T\Delta S_{ads} \qquad [1]$$

Since adsorption is a spontaneous process, the change in the Gibb's free energy of the system, ΔG_{ads}, will be negative and since there is a loss of at least one degree of freedom for the adsorbed species, the change in entropy, ΔS_{ads}, will also be negative. This implies that the enthalpy of adsorption, ΔH_{ads}, is also negative and therefore, adsorption is an exothermic process. In the case of physisorption, ΔH_{ads} is usually in the range 10 - 20kJ mol^{-1}, corresponding roughly to the heat of liquefaction of the adsorbed species. ΔH_{ads} for chemisorption is usually in the range 40 - 800kJ mol^{-1}, which is typical for chemical reactions.

The relationship between the amount of adsorbate on the surface of a solid and the gas pressure with which it is in dynamic equilibrium at constant temperature, is termed an *adsorption isotherm*. The most commonly used isotherm, derived by Langmuir, makes certain assumptions concerning the nature of the adsorbing surface and interactions occurring on the surface after adsorption. The most fundamental assumption is that the enthalpy of adsorption, ΔH_{ads}, is uniform for the whole surface and independent of the extent of surface coverage. However, the surface of a solid is not homogeneous and ΔH_{ads} is known to fall with increasing surface coverage. Consideration of surface heterogeneity has led to the development of the Freundlich and Tempkin isotherms, which assume an exponential and a linear fall in ΔH_{ads} with increasing surface coverage respectively. All three adsorption isotherms deal with monolayer adsorption; the Brunaeur, Emmett and Teller equation is an extension of the Langmuir equation applicable to multilayer adsorption processes.

Adsorption isotherms are extremely useful quantitative relationships that can describe the strength and extent of adsorption of molecules on the surface of solids. Furthermore, they can be used to estimate surface areas and, under appropriate conditions, the number of active sites on heterogeneous catalysts. Meaningful comparisons between catalysts with differing activities for a given reaction can be made on the basis of data obtained from adsorption studies.

The rate of a heterogeneous catalytic reaction can be described by the equation:

$$\text{Rate} = (1 / X).dn_i / dt \qquad [2]$$

- where X is some measure of the quantity of catalyst used and n_i is the number of moles of reactant consumed, or product formed, in time, t. X is often the volume of a large-scale reactor, giving a rate expressed in terms of mole m^{-3} s^{-1}. In catalysis research it is more appropriate if X is the mass, or even better, the surface area, of the catalyst sample, giving rates expressed in terms of moles kg^{-1} s^{-1} or moles m^{-2} s^{-1} respectively. In the most ideal situation, X represents the number of active sites per unit area of catalyst, in which case the rate can be expressed as:

$$\text{Rate} = (N_A / X.A).dn_i / dt \qquad [3]$$

- where A is the total surface area of the catalyst sample and N_A is the Avogadro number. This gives a rate expressed as the number of molecules reacting per active site per second, usually shortened to per second, and gives an excellent measure of the absolute activity of the catalyst. This quantity is known as the *turnover number* and is represented by the symbol, υ_t. A further quantity, known as the *total turnover number*, can be obtained if the number of active sites per unit area of catalyst is known. Total turnover number indicates the number of times a reaction occurs at each active site, assuming homogeneity of sites, for the duration of the overall catalytic reaction and its' value is a good guide as to whether or not a reaction is truly catalytic. Total turnover numbers close to unity suggest that a monolayer, surface-assisted reaction is occurring

rather than true catalysis, whereas total turnover numbers far in excess of unity are indicative of true catalysis. It is clear that in fundamental catalysis research, a knowledge of the total surface area and the number of active sites per unit area of the catalyst under study is of vital importance if meaningful comparisons between different catalysts are to be made.

Since a lowering of the activation energy is the fundamental principle behind catalysis, thermal activation is usually sufficient for a catalytic reaction to overcome the potential energy barrier between reactants and products. This is known as *thermal catalysis*. However, certain semiconducting oxides, because of their bulk electronic structure, possess the ability to absorb radiation of a specific wavelength with the concomitant production of excited electrons and positive holes, which can then migrate to the oxide surface and participate in catalytic redox reactions. This is known as *photocatalysis* and has been studied in detail since the early 1920's, when the photo-activity of semiconducting TiO_2 was first reported by Renz[1]. Recent years have seen the development and detailed investigation of metals supported on semiconductor oxides as efficient photocatalysts, with particular emphasis on their potential use in devices to convert solar energy to stored chemical energy, in the form of hydrogen via water photolysis and alcohol dehydrogenation. Supported metals are efficient photocatalysts because they combine the sorptive properties of the metal with the ability of the oxide support to utilise photon energy.

As in the case of photocatalysis, supported metal catalysts are also good thermal catalysts for reactions involving hydrogen and hydrocarbons because of the sorptive properties of the metal phase. The main advan-

tage of using a supported metal catalyst, rather than the free metal, is that the metal can be highly-dispersed on the support material, giving maximum surface area for a given mass of metal. In many early studies of these catalysts, it was often assumed that the support was just an inert carrier for the active metal phase and did not participate in the catalytic processes, or interact with the metal, in any way. However, over the last decade or so, it has been shown that this assumption does not hold and that both support and metal can interact with each other and consequently affect the reactant-product system. Such effects are collectively termed *metal-support interactions* and have been found to be particularly prominent in cases where the metal is supported on reducible transition metal oxides such as titanium dioxide.

The work reported in this thesis is concerned with the physical and catalytic properties of various metals, but in particular platinum, supported on TiO_2. Pt/TiO_2 catalysts have been prepared by two different methods and investigated as both photo- and thermal catalysts, with an emphasis on metal-support interactions. The rest of this introductory chapter reviews the physico-chemical properties of TiO_2 and $metal/TiO_2$ catalysts as reported in the literature to date.

1.2 Physical Properties of Titanium Dioxide

1.2.1 Crystal Structure

There are three morphological forms of titanium dioxide; rutile, anatase and the rare mineral form, brookite. To date, only rutile and anatase have been considered from the catalysis viewpoint. The crystal structures of both rutile and anatase were first investigated in 1916 by Vegard[2], who found that both forms have tetragonal unit cells exhibiting 6:3 coordination. Thus, each titanium cation is coordinated by six oxygen anions located at the corners of a slightly distorted octahedron and each oxygen anion is coordinated by three titanium cations lying in a plane at the corners of an approximately equilateral triangle. The difference between the two forms arises from the linkage of the titanium-oxygen octahedra[3]. In rutile, each octahedron shares two edges with other octahedra and each of the two remaining corners are shared with two other octahedra, whereas in anatase, four edges are shared with other octahedra. Furthermore, in anatase all Ti-O bond lengths are approximately equal, whereas in rutile the perpendicular Ti-O bonds are slightly longer (0.1988nm) compared to the planar Ti-O bonds (0.1944nm). Brookite has a more complicated crystal structure, in which the unit cell is orthorhombic[4].

Of the three morphological forms of TiO_2, rutile is the most thermodynamically stable and both anatase[5,6] and brookite[7] transform irreversibly to the rutile phase between 673 - 1373K. Generally, the temperature and rate at which the phase transition occurs depends markedly upon several factors, including the method of preparation, the amount of impurities

present and the surface area of the sample. It is thought that small particles, and consequently large surface areas, favour the transformation process, which is accelerated by the presence of oxygen vacancies but inhibited by interstitial cations. These variable factors account for the wide range of transition temperatures reported in the literature. High-pressure Raman spectroscopy has shown that rutile itself irreversibly transforms to a high-pressure phase, designated TiO_2-II, at about 26 kbar[8]. A further transition from TiO_2-II to TiO_2-III, at a pressure of 372 kbar has been reported by Mammone et al[9]. Bobyrenko et al[10] calculated the thermodynamics of the anatase to rutile phase transition from ultraviolet absorption spectra and concluded that the energy released during transition arises from a depression of the lower energy level of the valence electrons in rutile. This can be regarded as a strengthening of the chemical bonds, implying that rutile is more ionic in nature than anatase. However, on the basis of electronegativity parameters, Hannay and Smyth[11] and Boehm[12] calculated the theoretical percentage ionic characters for both rutile and anatase. The results of these calculations suggest that rutile has 43% ionic character compared to 63% ionic character for anatase.

1.2.2 Electronic Properties and Photoelectronic Processes

In terms of the band theory for electrical conductivity, pure stoichiometric TiO_2 is an insulating oxide with a full valence band and an empty conduction band. The energy difference between these two bands

is approximately 3eV, Fig. 1.1a. However, under normal conditions, TiO_2 possesses a certain degree of non-stoichiometry due to an oxygen deficiency, leading to the appearance of donor levels just below the bottom of the conduction band, Fig. 1.1b. Such defect donor levels can be ionised by thermal excitation of electrons into the conduction band. Earle[13] reported that the majority of charge carriers in non-stoichiometric TiO_2 are free electrons, so that it is an n-type extrinsic semiconductor.

TiO_2 absorbs strongly in the ultraviolet (UV) region of the electromagnetic spectrum; anatase at wavelengths < 400nm and rutile at wavelengths < 420nm. Companion and Wyatt[14] reported that absorption edges of 3.23eV and 3.0eV were observed in the reflectance spectra of TiO_2 samples. These values correspond to the band gap energies of anatase and rutile respectively, and represent the photo-induced promotion of electrons from the valence band to the conduction band. In many instances, the electron-hole pair generated by photon absorption does not dissociate immediately, but remains bound in a pre-ionisation state known as an *exciton*. Excitons can be readily produced by irradiation with light of wavelength close to the tail of the fundamental absorption band. Dissociation of excitons gives rise to mobile electrons and valence holes, which are independent of each other, as represented by the equation:

$$h\upsilon + TiO_2 \longrightarrow \underset{\text{exciton}}{(h^+\ e^-)^*} \longrightarrow VB_{h+} + CB_{e-} \qquad [4]$$

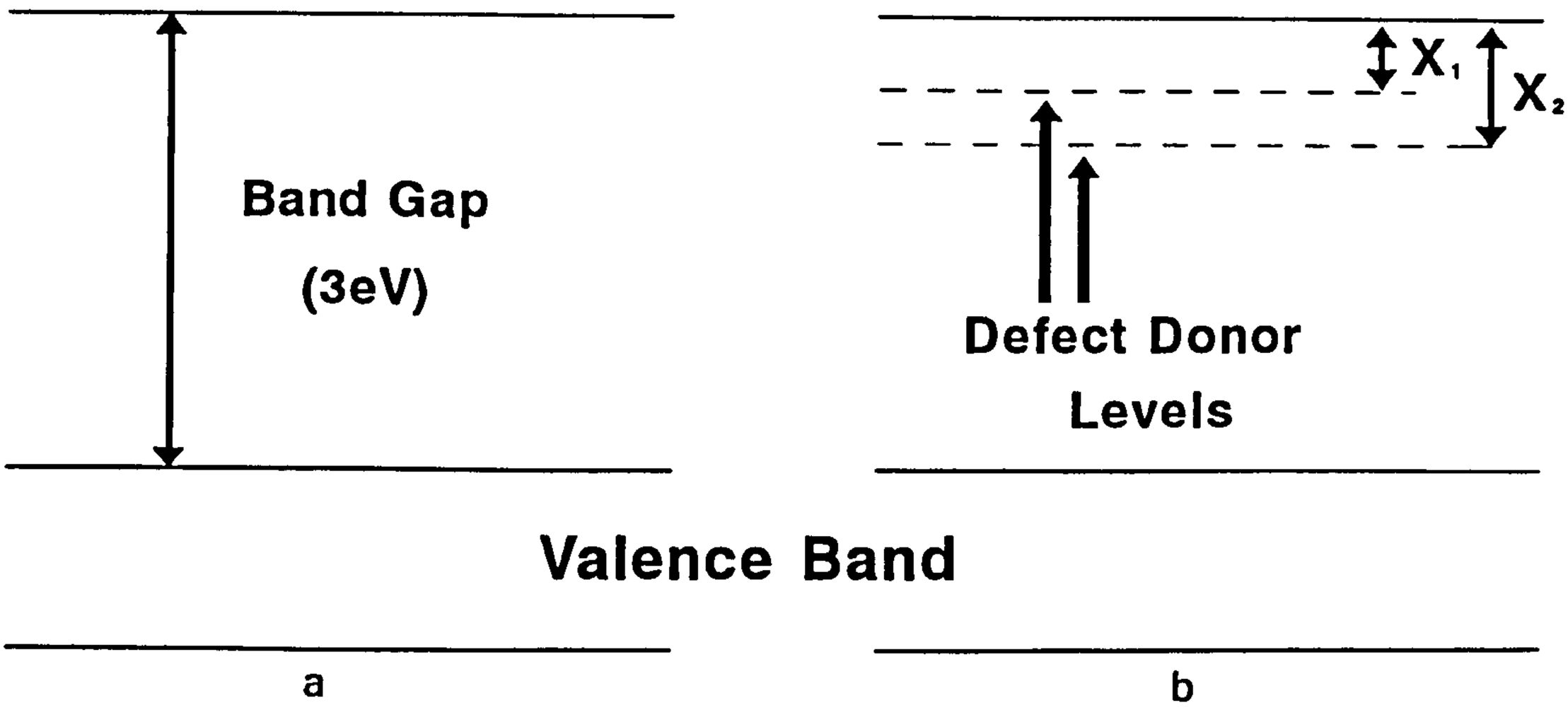

Fig. 1.1 Electronic Band Structure of TiO_2

a. Pure stoichiometric TiO_2

b. Non-stoichiometric TiO_2, showing the appearance of defect donor levels with ionisation energies X_1 and X_2 eV.

Thus, irradiation of TiO_2 with light of wavelength $< 400nm$, corresponding to an energy equal to, or greater than, the band gap energy, results in an increase in the electron population of the conduction band. Since photogenerated electrons and holes are mobile, an increase in the conductivity of TiO_2 is observed during UV irradiation, a process known as *photoconductivity*. Electron-hole pair generation is a non-equilibrium process which cannot occur indefinitely and a steady-state situation soon arises in which the rate of formation of electron-hole pairs equals the rate of their destruction by recombination and trapping processes. Wakim[15] studied the wavelength dependence of the time required for the photocurrent in TiO_2 to saturate and found that it increased with decreasing wavelength. It was proposed that when shorter wavelength light is used,

penetration of photons into the bulk lattice falls due to an increase in electron-hole recombination at the surface.

Recombination of electron-hole pairs can occur in three ways:

1) direct recombination, in which an excited electron in the conduction band falls directly to an unoccupied level within the valence band,

2) recombination at trap levels, which first capture an excited electron and then electrostatically attract a positive hole and,

3) surface recombination, in which the electrons and holes have migrated through the lattice to the surface where they recombine.

The energy generated by electron-hole recombination is dissipated either by photon and/or phonon emissions, or given to a third body in what is termed an *Auger recombination*[16]. Trap levels within titania, which correspond to defect sites having energies lying between the top of the valence band and the bottom of the conduction band, have been studied in detail by use of a wide variety of techniques. Ghosh et al[16] used a number of techniques to demonstrate the existence of at least eight shallow traps, having energies < 1eV, in non-stoichiometric rutile. One of these traps was assigned as probably being an oxygen vacancy in the lattice. Traps having optical ionisation energies in excess of 1.5eV, known as *deep traps*, were also reported, one of which was assigned as being interstitial Ti^{3+} cations possessing nearly octahedral coordination.

Marked changes in the electrical conductivity and optical properties of TiO_2 doped with impurity cations from other oxides have been observed by several workers[17-20]. Sullivan[19] reported that incorporation of cations having valency greater than four results in enhanced electrical

conductivity, whereas incorporation of cations having valency less than four results in a decrease in the electrical conductivity. From these results it was concluded that cations of valency > 4 act as donor impurities, whereas cations of valency < 4 act as acceptor impurities, thus modifying the concentration of free electrons in the TiO_2 conduction band.

Gerristen[21] studied the sites of incorporation of impurity cations in rutile single crystals via electron paramagnetic resonance (EPR) spectroscopy and concluded that most transition metal ions are substitutionally incorporated at Ti^{4+} sites, although Ni^{2+} ions were found to occupy interstitial sites. The results of EPR spectroscopic studies by Barry[22] have shown that impurity Cr^{3+} ions in anatase most probably occupy Ti^{4+} lattice sites. Gray and Lowery[23] used thermoluminescence (TL) and thermally-stimulated current (TSC) measurements to investigate shallow trap levels, with energies < 1eV, in both high purity and Nb-doped anatase. They found that some trap levels were common to both samples and some were restricted to the doped sample only. Six or more deeper lying traps were also noted, but were unsatisfactorily resolved or identified. Iida et al[24] suggested that impurity levels arising from the incorporation of Fe^{3+} into TiO_2, exist near to the top of the valence band and affect the photoconductivity response at the absorption edge of the doped sample.

The effect of surface-adsorbed species on photocurrent behaviour has also been studied in detail. Melnick[25] proposed a model to account for the photocurrent behaviour in ZnO, the essential feature of which is that there is a direct relationship between the photocurrent and the sorption of gases onto and from the surface of the sample. It was found that

chemisorption of gas produces a fall in the photocurrent due to surface trapping of excited electrons, whereas photodesorption of chemisorbed gas produces a rise in photoconduction due to the return of electrons to the conduction band. Addiss and Wakim[26] investigated the validity of this model for TiO_2 photocurrent behaviour and found that their observations agreed well with the results expected on the basis of the Melnick model.

1.2.3 Defect Structure of TiO_2

The defect structure of non-stoichiometric TiO_2 has been investigated by numerous workers, using a wide variety of techniques. Although it has been established that non-stoichiometry arises from an oxygen deficiency, the precise nature of the donor centres responsible for producing semiconductivity remains unclear. Oxygen deficiency in TiO_{2-x} can arise from two types of defect; namely macro and micro defects. Macro, or Wadsley, defects occur when complete planes of oxygen anions are absent in the crystal lattice, resulting in a shifting of the lattice planes either side of the fault so that ions of like charge are not adjacent to each other. This process is known as *crystallographic shear* and produces a whole family of higher titanium oxides conforming to the generic formula, Ti_nO_{2n-1}, where n is an integer. A detailed study of macro defects and the higher titanium oxides has been carried out by Bursill et al[27-29]. However, non-stoichiometry in TiO_2 can be mainly attributed to the presence of micro, or point, defects which occur randomly at single lattice sites. Although many investigations into the nature of such micro defects have

been conducted, it is still unclear as to whether they take the form of oxygen vacancies, interstitial titanium cations or a combination of both.

Cronemeyer and Gilleo[30] studied the optical absorption and photoconductivity of hydrogen-reduced rutile and concluded that the predominant point defect in non-stoichiometric TiO_2 is an oxygen vacancy associated with one or two trapped electrons. They also suggested the blue coloration of reduced rutile arises from the optical ionisation of these defect sites. Thermogravimetric analyses by Kofstad[31] and Førland[32] and detailed measurement of the absorption spectrum, over the range 430-720nm, by Coufova and Arend[33] for non-stoichiometric rutile provide further evidence to support this proposal. However, Hurlen[34], on the basis of data derived from lattice parameters, weight changes, electrical conductivity measurements and oxidation studies, proposed that interstitial titanium cations are the predominant point defect in non-stoichiometric TiO_2. EPR[35] and optical absorption studies[36] have also shown that the formation of Ti^{3+} interstitial cations is most likely to occur.

Watchman et al[37,38], on the basis of results obtained from internal friction measurements, concluded that the predominant point defect in vacuum-reduced rutile is neither a simple oxygen vacancy nor a simple interstitial titanium cation. They interpreted their results in terms of pairing of cation interstitials, within the temperature range of the experiments. The results of conductivity measurements on samples of TiO_2 reduced in CO - CO_2 mixtures, obtained by Kofstad[39] and Jakubowski[40], were interpreted in terms of a defect structure containing both oxygen vacancies and tri- and tetravalent interstitial titanium cations. More

specifically, Kofstad[39] proposed that low temperatures and high oxygen pressures favour the formation of oxygen vacancies, whereas interstitial titanium cations predominate under the reverse conditions. Barbenel' et al[41], from density change measurements on rutile, proposed that at temperatures below 873K, oxygen vacancies predominate since oxygen can readily diffuse along lattice channels to the surface of the sample. At temperatures above 873K, the presence of oxygen vacancies makes the transfer of lattice cations to interstitial sites easier, so that both types of point defect occur under these conditions. It was also suggested that the oxygen vacancies and the titanium interstitial cations are bound to each other.

In summary, it appears that the defect structure of TiO_2 is complicated, containing both oxygen vacancies and interstitial titanium cations. The extent to which each occurs, relative to the other, depends upon several factors, including the reduction process, the sample temperature and the ambient oxygen partial pressure.

1.3 Adsorption and Catalysis on TiO_2

1.3.1 Surface Structure

In investigations of the surface chemistry of TiO_2, it is generally accepted that small powder crystallites bear a strong resemblance to more massive crystals. Boehm[12,42], using chemical exchange techniques, and Yates[43], using infrared (IR) spectroscopy, demonstrated that the surface of rutile is extensively hydroxylated. Jones and Hockey[44], using IR

spectroscopy to study surface acidity via pyridine adsorption, concluded that there are two types of hydroxyl groups and adsorbed molecular water present on the surface of rutile. It was suggested that the undissociated water is held as a coordinating ligand at surface cationic sites. Further IR spectroscopic studies by the same workers[45,46] led to the proposal that the surface of rutile is composed mainly of three low index crystallographic planes; namely the {100}, {101} and {110} planes, occurring in the approximate ratio of 3:1:1 respectively. In the {100} and {101} planes, the Ti^{4+} cations have incomplete coordination; five lattice oxide anions leave a vacant ligand position which may coordinatively adsorb water. The {110} plane, which possesses equal quantities of four- and five-fold coordinated Ti^{4+} cations, may dissociatively adsorb water to give two types of hydroxyl groups. A theoretical value of 12.24 -OH groups nm^{-2} was calculated from this model of the rutile surface. From weight loss and tritium exchange studies, Yates et al[47] calculated a surface proton density of 12.5 nm^{-2}, in good agreement with the theoretical hydroxyl density calculated by Jones and Hockey. For anatase, the {001} plane has been assumed to be the most dominant surface plane[12,48] and a more recent study by Kozlowski et al[49], using extended X-ray absorption fine structure (EXAFS), provides evidence to support this assumption. Each Ti^{4+} cation in the {001} surface plane of anatase should be surrounded by five lattice oxide anions, leaving a vacant ligand position that can dissociatively adsorb water[12]. From D_2 exchange and reaction with acetylene and $SOCl_2$, Boehm and Herrmann[50] have estimated a surface density of 12 - 14 -OH groups nm^{-2} for fully hydroxylated anatase surfaces.

Primet et al[51], using IR spectroscopy to study the hydroxylated surfaces of both anatase and rutile, assigned bands observed at 3715 cm^{-1} (anatase) and 3685 cm^{-1} (rutile) to isolated terminal hydroxyl groups. Bands observed at 3665 cm^{-1} (anatase) and 3655 and 3410 cm^{-1} (rutile) were thought to arise from hydroxyl groups situated in adjacent unit cells that are hydrogen-bonded to each other. Exposure of the TiO_2 surface to D_2O and D_2 resulted in complete deuteration of all surface hydroxyl groups, although exchange with D_2 was observed to be an activated process that was only complete at ~470K. At temperatures above 523K, D_2 was observed to reduce TiO_2, as shown by the appearance of a signal due to surface Ti^{3+} cations in the EPR spectrum. The resulting D_2O was dissociatively re-adsorbed, giving rise to broad -OD bands in the 2500 - 2100 cm^{-1} region of the IR spectrum. The results of dehydroxylation-rehydroxylation studies suggested that dehydroxylation of the TiO_2 surface is only partially reversible. This observation cannot be entirely attributed to a loss of surface area and it was proposed that some sites capable of dissociatively adsorbing are eliminated during the dehydroxylation process. Below 623K, the lower wavenumber IR bands, corresponding to hydrogen-bonded hydroxyl groups, are preferentially removed by the following mechanism:

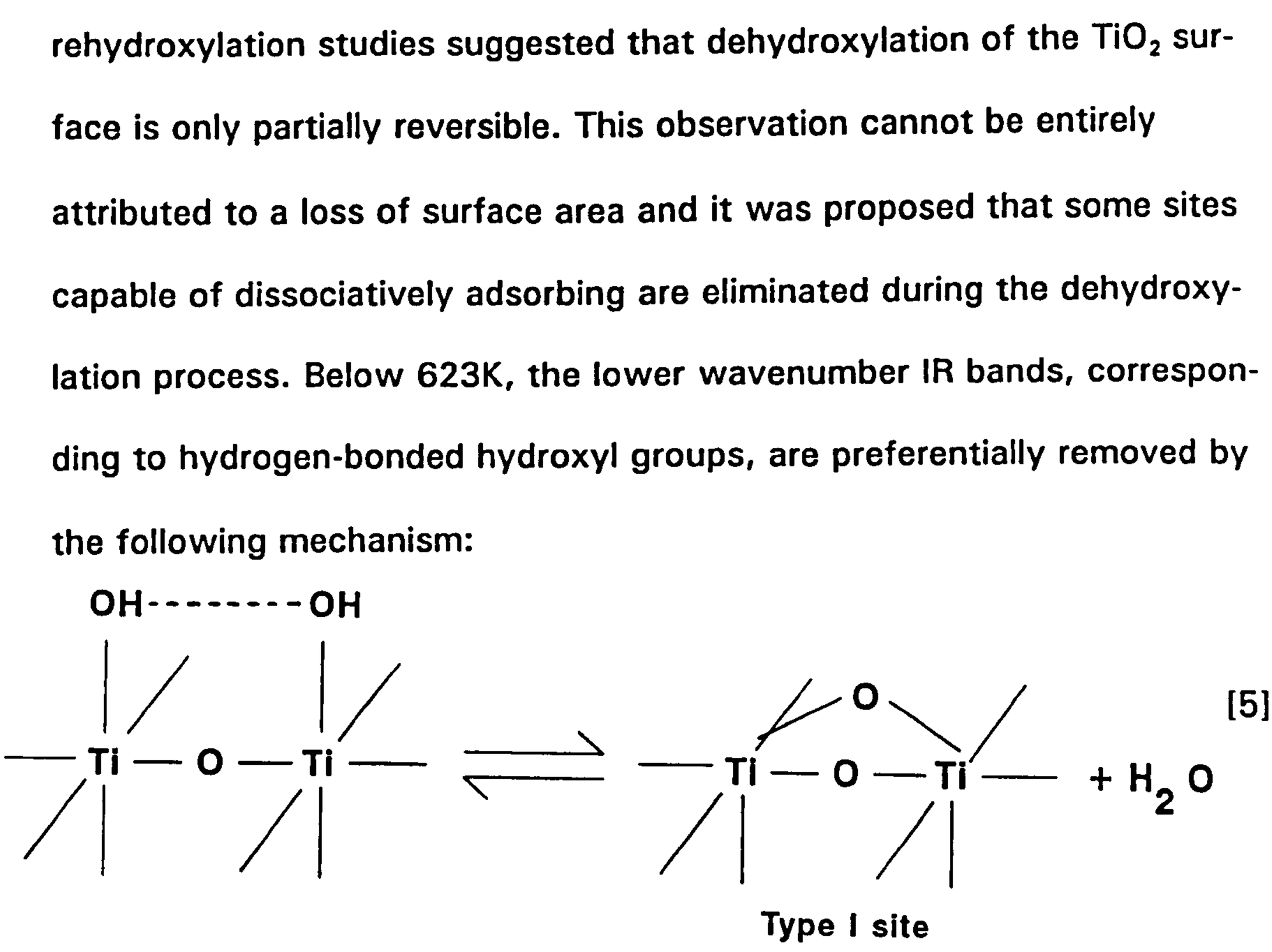

[5]

At temperatures above 673K, proton or hydroxyl group migration enables the removal of isolated -OH groups:

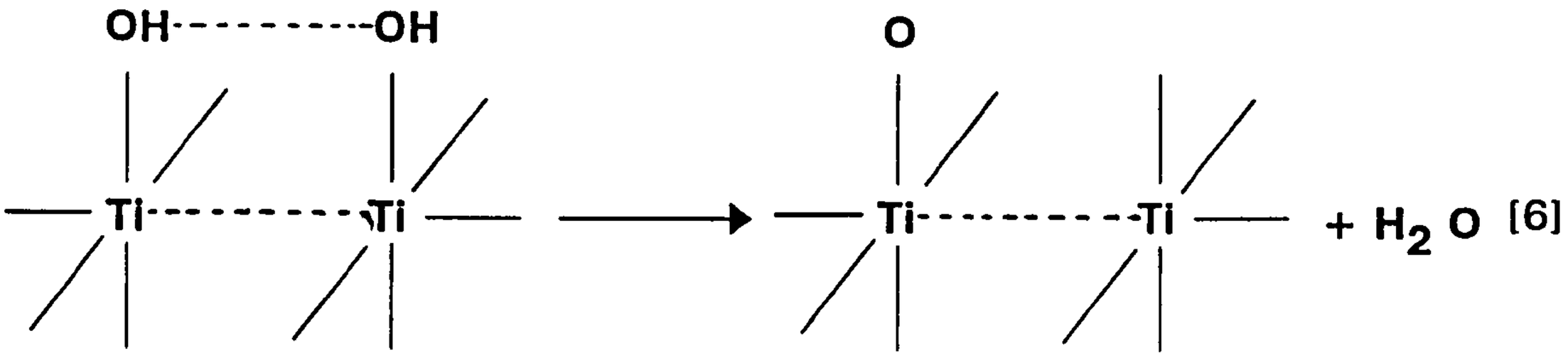

Type II site

Type I sites are capable of re-adsorbing water dissociatively, but Type II sites are incompletely coordinated surface cations which adsorb molecular water as a coordinating ligand. This produces a loss in the extent of rehydroxylation of the TiO_2 surface, although the extent of water uptake remains unchanged. Griffiths and Rochester[52] investigated the rehydroxylation of rutile calcined at 973K and observed enhanced chemisorption of H_2O on the {110} plane, but depleted adsorption on the {100} and {101} planes. This observation was explained in terms of the surface area of the {110} plane increasing at the expense of the other two planes.

Jackson and Parfitt[53] also studied the TiO_2 surface using IR spectroscopy and obtained similar results to Primet et al[51], assigning the observed IR bands to bridged, hydrogen-bonded and terminal hydroxyl groups. They also found that heat activation led to the removal of physisorbed water and -OH groups, with the hydrogen-bonded groups being the most thermally-labile. However, unlike Primet et al[51], it was found that exposure of dehydroxylated TiO_2 to water at room temperature, resulted in dissociative chemisorption to give a fully reversible surface. Munuera and Stone[54] studied the surface of TiO_2 using adsorption iso-

therm, temperature-programmed desorption (TPD) and IR spectroscopy techniques. They concluded that H_2O is adsorbed onto the surface in three forms by the following mechanism:

1) dissociative chemisorption at Ti-O pairs until approximately 50% of the surface is hydroxylated,

2) strong molecular adsorption at isolated surface Ti cations, and,

3) weak molecular adsorption at isolated surface O^{2-} anions.

This scheme is also supported by Jones and Hockey[39], although they reported physisorption of water at surface cation sites occurring before dissociative chemisorption was complete. From a combined secondary ion mass spectrometry (SIMS) - Auger electron spectroscopy (AES) study, De Pauw and Marlen[55] reported the presence of physisorbed water hydrogen-bonded to surface hydroxyl groups on the surface of anatase TiO_2. More recently, Morimoto and Iwaki[56,57] investigated the dielectric behaviour of water adsorbed on rutile and interpreted their results in terms of a previously proposed model[58] in which physisorbed water is hydrogen-bonded to surface hydroxyl groups.

Boehm[59], using chemical techniques, demonstrated the amphoteric nature of the hydroxylated surface of both anatase and rutile. It was concluded that approximately half the surface -OH groups are strongly acidic in nature, whilst the remainder are predominantly basic. Primet et al[60] studied the adsorption of ethanoic acid, phenol, CO_2, ammonia, pyridine and trimethylamine onto both rutile and anatase. Of the three acidic compounds, only CO_2 reacted with basic -OH groups, producing surface bicarbonate species. With anatase, some hydroxyl groups were

sufficiently acidic to protonate trimethylamine, but not ammonia or pyridine. No such acidic character towards any of the three basic compounds was found with rutile. Ammonia and pyridine adsorption gave evidence of two types of Lewis-acidic sites of differing strengths. It was proposed that these sites are incompletely coordinated Ti cations, the stronger ones formed by the removal of isolated -OH groups and the weaker sites by the removal of molecular water. However, Herrmann and Boehm[61] reported the presence of a band at 1400 cm^{-1}, characteristic of the ammonium ion, in the IR spectrum of ammonia adsorbed onto anatase, suggesting that some -OH groups on anatase are sufficiently acidic to protonate ammonia. Such variations in reactivity of the TiO_2 surface towards acids and bases are probably due to differing methods of preparation, with the subsequent incorporation of different impurities, rather than the result of some intrinsic property of the oxide. Evidence to support this proposal has been obtained by Parfitt et al[62], via IR spectroscopic studies of HCl adsorption onto the surface of rutile. It was observed that, following HCl adsorption, the $H_3O^+Cl^-$ species is formed, which acts as a Brønsted acid in the presence of ammonia or pyridine. Graham et al[63-65] carried out a series of IR spectroscopic studies of the adsorption of various hydrocarbon and carbonyl compounds onto the surface of rutile. In all experiments, they found that hydroxyl groups responsible for a maximum in the IR spectra at 3140 cm^{-1}, were unperturbed by the presence of the organic compound. It was proposed that these hydroxyl groups are located at sub-surface lattice sites where they are inaccessible to organic adsorbates. Morterra[66] recently studied the dehydration of the anatase

surface using IR spectroscopy and concluded that strong Lewis-acidic sites, capable of reversibly sorbing CO, can be generated by the vacuum removal of molecular water, which starts at low temperature and is complete at 470K. Removal of hydroxyl groups at temperatures above 450K was found to produce only a small number of additional Lewis-acidic sites strong enough to adsorb CO.

In summary, it is generally accepted that the rutile surface is composed mainly of the {100}, {101} and {110} planes in the ratio 3:1:1 respectively. For anatase, the {001} plane is generally thought to predominate at the surface. Water is dissociatively adsorbed on the {110} and {001} planes to produce two types of hydroxyl groups and is physisorbed as a coordinating ligand to surface cation sites on the other planes. The existence of molecular water hydrogen-bonded to surface hydroxyl groups has also been demonstrated. The surfaces of both anatase and rutile are amphoteric in nature, the former possessing stronger acidic sites. The structure of the TiO_2 surface and its' properties have been the subject of extensive reviews by Parfitt[67], Day[68] and Wiseman[69].

1.3.2 Adsorption and Thermal Decomposition of Alcohols

In view of the fact that titania is an active catalyst for alcohol dehydration and dehydrogenation, numerous investigations into the mechanism of alcohol adsorption onto TiO_2 have been undertaken. Although a variety of techniques have been employed, the exact nature of adsorbed

alcohol remains unclear and the literature contains much conflicting evidence. Shchekochikhin et al[70] and Jackson and Parfitt[71] interpreted IR spectra of various C_1 - C_8 aliphatic alcohols, adsorbed on rutile and anatase, in terms of dissociative chemisorption, giving alkoxide anions and surface -OH groups. The latter workers also reported that the extent of adsorption was independent of the degree of hydroxylation of the TiO_2 surface. A dual adsorption mechanism, involving classical esterification on fully hydroxylated surfaces and alkoxide anion formation on dehydroxylated surfaces, was proposed as an explanation of the results. However, Munuera and Carrizosa[72], on the basis of IR spectroscopic and adsorption isotherm data, concluded that C_1 - C_4 primary alcohols are adsorbed onto dehydroxylated anatase surfaces as coordinating ligands at Lewis-acidic and Lewis-basic surface sites. An 'irreversible adsorption' coverage of 2 molecules nm^{-2} was calculated from the results obtained. Rochester et al[73] investigated propan-2-ol adsorption on rutile using IR spectroscopy and concluded that both molecular alcohol, adsorbed at Lewis-acidic sites as a coordinating ligand, and alkoxide ions, formed at Ti^{4+} sites, were present on the oxide surface.

Thermal activation of alcohols adsorbed on titania produces alkenes, ethers and water from dehydration processes and aldehydes, ketones and CO from dehydrogenation processes. Much of the decomposition chemistry of alcohols adsorbed on TiO_2 has been ascribed to the formation, and subsequent reaction, of alkoxide species. However, other mechanisms involving molecularly-adsorbed alcohols[74,75], carbonium ions[76], Ti-alkyl[77], surface carboxylate[63] and surface carbonate[71] have also

been postulated. On the whole, alkene formation is thought to occur via proton abstraction from the β-methylene group of the adsorbed surface intermediate, with the concomitant formation of surface hydroxyl groups. Dehydrogenation processes are thought to depend upon surface hydroxyl groups and electron transfer steps, rather than the acid - base properties of the oxide surface[76]. In a more recent study, Kim et al[78] investigated the thermal decomposition of methanol, ethanol, propan-1-ol and propan-2-ol on anatase. They found that the temperature at which the maximum decomposition rate occurred decreased in the order, MeOH > EtOH > n-PrOH > i-PrOH. Furthermore, both uni- and bi-molecular decomposition products were observed for the primary alcohols, but only unimolecular products were found in the case of propan-2-ol. All alcohols were found to undergo dehydration and dehydrogenation processes, with the smaller alcohols favouring the latter decomposition route. A reaction mechanism based entirely on alkoxide intermediates was put forward to explain the above observations.

1.3.3 Adsorption of Oxygen

From an atomistic point of view, oxygen chemisorption on non-stoichiometric TiO_2 occurs at defect surface sites, which are most probably Ti^{3+} cations associated with oxygen vacancies[79]. On the basis of IR and EPR spectroscopic data[80,81], it has been suggested that oxygen is chemisorbed onto TiO_2 mainly as the O_2^- anion-radical. Furthermore, equilibrium oxygen coverages on the TiO_2 are low and never exceed 1% of a

monolayer[80]. These observations can be readily explained in terms of band theory, in which O_2 chemisorption occurs via thermal transfer of electrons from the conduction band of the oxide to oxygen. This is known as *depletive chemisorption* and is characterised by a decrease in the oxide conductivity, since the concentration of free electrons in the conduction band falls due to trapping by the adsorbed gas. Only low coverages of oxygen are observed because depletive chemisorption causes the valence and conduction bands of TiO_2 to bend upwards at the oxide surface, due to the formation of a space-charge in the TiO_2-O_2 boundary layer[82,83]. Upwards bending of the bands effectively presents a potential energy barrier which the conduction band electrons, in going from the oxide to the adsorbate, have to overcome. As oxygen adsorption continues, the height of this barrier increases and the Fermi level in the semiconductor is progressively depressed. Eventually, the potential energy of the electrons in the adsorbed oxygen equals that of the electrons in the oxide, after which no further net adsorption is possible. The O_2^- anion-radical is thought to be the predominant surface species formed during oxygen chemisorption on TiO_2. However, other species, including atomic oxygen[84], the O^- anion-radical[85,86] and the O_4^- anion-radical[87], have also been detected by IR and EPR spectroscopic techniques. Davydov et al[84] have investigated oxygen chemisorption on anatase with differing extents of non-stoichiometry. They reported that as the degree of reduction of anatase increases, the amount of $O^-_{2(ads)}$ also increases at the expense of $O_{2(ads)}$, such that on highly reduced TiO_2 the latter species was completely absent.

The low temperature homonuclear isotopic exchange of oxygen on reduced anatase has been investigated by Griva et al[86], using EPR spectroscopy. It was observed that exchange is accompanied by re-oxidation of the anatase and is catalysed by intermediate forms of oxygen, generated during the re-oxidation process. The $O^-_{2(ads)}$ anion-radical species was found not to be active in the exchange process and it was postulated that the $O^-_{(ads)}$ anion-radical is the active intermediate in this process, although the possibility of active non-paramagnetic oxygen intermediates was not precluded. Gundlach and Heusler[88,89] investigated oxygen chemisorption kinetics on non-stoichiometric TiO_2 films, by measuring changes in work function with time at different oxygen pressures, extents of non-stoichiometry and temperatures. The dependence of sorption and exchange rates and extent of equilibrium band bending on these factors were found to be in good agreement with theoretical expectations. After high temperature reduction, a second, fast process, possibly corresponding to a reaction between specific surface sites and oxygen and involving states in the valence band, were observed. From experimental evidence it was concluded that neutral oxygen atoms are transferred from the surface to the bulk of the oxide. A mechanism involving a rate-determining reaction between two adsorbed O^-_2 anion-radicals was proposed to account for the transfer process:

$$2\ O^-_{2(ads)} \longrightarrow O^-_{3(ads)} + O^-_{(ads)} \qquad [7]$$

$$O^-_{(ads)} + O_{2(ads)} \longrightarrow O^-_{3(ads)} \qquad [8]$$

$$2.\{\ O^-_{3(ads)} \longrightarrow O^-_{2(ads)} + O_{(ads)}\ \} \qquad [9]$$

$$O_{(ads)} + V_o \longrightarrow O_{(l)} \qquad [10]$$

- where V_o = oxygen vacancy and $O_{(l)}$ = lattice oxygen.

1.3.4 Adsorption of Hydrogen

Lo et al[90] studied the adsorption of hydrogen on model TiO_2 {100} surfaces, of variable stoichiometry, using ultraviolet photoemission spectroscopy (UPS). From spectral data and changes in the sign of the work function after adsorption, it was concluded that hydrogen is adsorbed as an electron donor on stoichiometric surfaces containing only Ti^{4+} cations, as shown in Eq. [11]. On non-stoichiometric surfaces, containing a large concentration of Ti^{3+} cations, hydrogen is adsorbed as an electron acceptor, as shown in Eq. [12].

$$\tfrac{1}{2}H_{2(g)} + \{ Ti^{4+} O^{2-} \}_{(s)} \longrightarrow \{ Ti^{3+} OH^{-} \}_{(s)} \qquad [11]$$

$$\tfrac{1}{2}H_{2(g)} + \{ Ti^{3+} OH^{-} \}_{(s)} \longrightarrow \{ Ti^{4+} \square^{2-} \}_{(s)} + H_2O \qquad [12]$$

- where $\square^{2-}$ = oxygen vacancy with two trapped electrons and $_{(s)}$ indicates surface species.

Serwicka et al[91] used EPR spectroscopy to study TiO_2 treated with atomic hydrogen at ambient temperatures. It was found that strong hydroxylation of the surface occurred, such that the concentration of Ti^{3+} cations generated during the process was comparable to that obtained by conventional reduction at high temperatures under vacuum or with molecular hydrogen. However, atomic hydrogen did not produce anionic vacancies,

as shown by the absence of the appropriate EPR signal and by the fact that O_2^- anion-radicals were not formed upon subsequent exposure to oxygen. The authors also reported that atomic hydrogen in contact with TiO_2 appeared to act as an electron donor and summarised the processes occurring during such treatment by the equation:

$$H_{(g)} + \{ Ti^{4+} O^{2-} \}_{(s)} \longrightarrow \{ Ti^{3+} OH^- \}_{(s)} \qquad [13]$$

Iwaki[92] studied hydrogen desorption from anatase and rutile over the temperature range 298 - 1078K, using TPD techniques. Chemisorption of hydrogen onto the TiO_2 surface was found to occur only at temperatures above 623K. Anatase produced two desorption peaks at 623 - 673K and 773 - 823K, whereas rutile only gave a single broad desorption peak at 923 - 973K. From these experimental observations, three mechanisms of hydrogen adsorption were postulated:

1) dissociative chemisorption to form surface hydroxyl groups, which subsequently condense to produce water and anionic oxygen vacancies,

2) dissociative chemisorption to form isolated surface hydroxyl groups, which are not removed from the surface, and

3) dissociative chemisorption followed by migration into the bulk lattice via oxygen channels to form sub-surface hydroxyl groups.

It was also suggested that anatase interacts more readily with hydrogen than rutile does, possibly due to differences in the ease of formation of surface hydroxyl groups. However, the TPD results obtained by Iwaki can be explained in terms of the formation of hydroxyl groups on the TiO_2

surface which are immobile in translation, but free in rotation. In this case, hydroxyl groups are formed as in mechanism (1) above, which are then randomly removed form the surface, which consequently gives rise to isolated hydroxyl groups as in (2). Sub-surface hydroxyl group formation, as in (3), can then be formed via proton transfer between freely rotating surface hydroxyl groups and sub-surface lattice oxygen anions. Iwaki et al[93] also investigated the H_2 - D_2 equilibration reaction, at temperatures above 473K, on anatase with differing extents of non-stoichiometry. On the basis of the results obtained, it was thought that the dissociation of hydrogen is not rate-determining in the reduction of TiO_2 by molecular hydrogen.

1.3.5 Adsorption of Hydrocarbons

From the literature it would appear that most studies of hydrocarbon adsorption onto titania have concentrated on alkenes, with reference to alcohol dehydration mechanisms. There is no evidence to suggest that alkenes are adsorbed via carbonium ion formation, presumably because neither the Lewis- nor the Brønsted-acidity of the TiO_2 surface is strong enough for this process to occur. However, weak physisorption of alkenes due to interaction between the hydrocarbon double bond and either surface hydroxyl groups or Ti^{4+} cations,depending upon the extent of surface hydroxylation, seems to occur to a certain degree. In the main, spectroscopic evidence strongly suggests that alkene adsorption onto the surface of titania occurs via the formation of alkoxide anions. Shchekochikhin et

al[70] have investigated ethylene adsorption on both pure and WO_3-doped anatase, in the temperature range 293 - 473K, using IR spectroscopy. The appearance of two intense bands in the 1150 - 1000 cm^{-1} region, absent in the IR spectrum of gaseous ethylene, were interpreted in terms of ethoxide anion formation during adsorption onto the oxide surface. No differences between the IR spectra of ethylene adsorbed on the pure and the doped anatase were observed, indicating that the presence of impurity cations had no effect on the adsorption process. Furthermore, it was found that ethylene adsorption onto anatase is temperature independent, since raising the adsorption temperature from 293K to 473K had no significant effect on the observed IR spectrum. Jackson and Parfitt[94], from IR spectroscopic data, concluded that but-1-ene interacts with the surface of hydroxylated rutile via hydrogen-bonding between the alkene double bond and surface -OH groups. Thermal activation at 423K resulted in the appearance of new bands at 2980, 2940 and 2890 cm^{-1}, which were attributed to the formation of surface butoxide anions. The presence of inaccessible, to the alkene, surface hydroxyl groups was also noted, although there was no evidence to suggest preferential reaction by one of the two types of surface hydroxyl groups. It seems likely that the inaccessible groups correspond to -OH groups at sub-surface lattice sites, as discussed earlier. The adsorption of propene onto TiO_2 has been investigated by Nakajima et al[95] and Graham et al[96], via IR spectroscopy. Both groups of workers concluded that, at ambient temperatures, propene is only weakly adsorbed onto the oxide surface via hydrogen-bonding interactions with surface hydroxyl groups. The latter workers also postulated

that weak π-complex formation with exposed Ti^{4+} cations in the {100} and {101} surface planes of rutile may also occur. Chemisorption, giving rise to adsorbed isopropoxide ions, was observed to occur at higher temperatures and preceded subsequent oxidation to surface carboxylate species, which was accompanied by a darkening of the white sample to a grey colour. Nakajima et al[95] attributed the appearance of an IR band at 1700 cm^{-1} to the formation of acetone, following propene chemisorption and subsequent heat treatment in oxygen. No further oxidation to carboxylate species was observed to occur under these conditions. Al-Mashta et al[97] studied the room temperature polymerisation of ethylene on the surface of anatase. This process was found to occur only on dehydroxylated surfaces, containing sulphate impurities. Evidence for the presence of an alkylidene - Ti^{4+} polymer end-group and for a 'hydrogen-bonding' - type interaction between CH bonds of the polymer chain and the oxide surface was obtained via IR spectroscopic studies. In a more recent study, Brookes et al[98] have investigated the isomerisation of cyclopropane, various methylcyclopropanes and C_6-alkenes on rutile catalysts. They proposed that isomerisation occurs via the formation of carbocationic intermediates σ-bonded to surface Lewis-acidic sites, followed by reactions involving 1,2- hydride and α-methyl shifts and hydrogen transfer processes, in which surface oxide anions may participate. The hydrogenation of various alkenes, H_2 - D_2 equilibration and the isomerisation of C_6-alkenes over anatase were also investigated. It appears that the catalytic properties of rutile and anatase are very similar with respect to these reactions and the relative rates of reaction over

both types of titania were found to be isomerisation > H_2 - D_2 equilibration > alkene hydrogenation. Self-poisoning, accompanied by a blackening of the catalyst, was observed to occur in a number of alkene hydrogenation reactions.

There is remarkably little, if any, work been reported in the literature concerning the adsorption of alkanes onto the surface of titania. This suggests that there is negligible interaction between the two and so alkane adsorption has not been worthwhile investigating. However, should alkane adsorption onto TiO_2 occur, the most likely mechanism would be one involving C-H bond cleavage, giving rise to Ti-alkyl complexes and surface hydroxyl groups, such as:

[14]

The formation of Ti-alkyl complexes has been proposed as an intermediate step in the thermal dehydration of alcohols adsorbed on titania[77]. However, there is no evidence for alkane formation during alcohol dehydration and so adsorption of alkanes onto the TiO_2 surface seems unlikely.

1.3.6 Adsorption of Carbon Monoxide and Carbon Dioxide

Adsorption of CO and CO_2 has frequently been used to investigate the surface properties of anatase and rutile[58,60,66] and has been briefly discussed in Section 1.3.1. Yates[43] studied the adsorption of CO and CO_2

onto various anatase and rutile surfaces, at ambient temperatures, using IR spectroscopy. He reported that CO is only weakly chemisorbed and could readily be removed by evacuation. No evidence for chemisorption at surface cationic sites was found and it was postulated that the adsorbed CO molecule is held by its' carbon atom at a surface oxygen site, in a linear configuration. CO_2 was found to be strongly chemisorbed on both anatase and rutile. The species on anatase was attributed to CO_2, whereas that on rutile was assigned as being a surface carbonate species. Jackson and Parfitt[94], using IR spectroscopy, identified a labile surface bicarbonate species, formed by the interaction of CO_2 with bridged hydroxyl groups, on the surface of rutile. IR data obtained by Primet et al[60] also suggested the formation of a bicarbonate species, following adsorption of CO_2 onto hydroxylated anatase and rutile surfaces. Using IR spectroscopic and gravimetric techniques, Primet et al[99,100] investigated the adsorption of CO onto TiO_2 at various temperatures. At ambient temperature, physisorption and reversible chemisorption at Ti^{4+} surface sites was considered to occur, in contradiction to Yates' findings[43]. Between 453K and 523K, surface carboxylate species were observed, formed by reversible CO adsorption at Ti^{4+} sites, followed by reaction with adjacent oxygen anions. At temperatures above 573K these species were destroyed, with the concomitant formation of CO_2. Tanaka and White[101] studied CO and CO_2 adsorption onto reduced and oxidised anatase, using IR spectroscopy. Two types of molecular CO were detected on oxidised anatase, both of which were removed during evacuation at ambient temperature. A limited amount of surface reduction, with the correspon-

ding formation of surface bicarbonate species, was also observed to occur. CO_2 adsorption onto oxidised anatase was found to occur readily at Ti^{4+} surface sites, with subsequent formation of bicarbonate species. Slow reaction between adjacent pairs of such bicarbonate species gave rise to adsorbed bidentate carbonate species and water. Subsequent room temperature evacuation resulted in the removal of both the carbonate and bicarbonate species and any residual CO_2, with rehydroxylation occurring to a limited extent, probably due to the dissociation of adsorbed water as the surface concentration of the other species fell. In a recent study of CO adsorption onto anatase, Bolis et al[102] identified two types of adsorbed CO, distinguished by different IR absorption frequencies, heats of adsorption and extents of surface coverage. No evidence for adsorption occurring at sites other than surface Ti^{4+} cations was found and it was postulated that the two types of adsorbed CO arise due to adsorption at Ti^{4+} surface sites capable of polarising the CO molecule to different extents.

1.3.7 Photosorption Processes on TiO_2

It has been well established, experimentally, that sorption kinetics and equilibria at semiconductor surfaces can be greatly influenced by illumination with radiation of the appropriate wavelength. This is known as *photosorption*, of which a detailed mathematical treatment has been conducted by Wolkenstein[103]. Many investigations into the photosorption behaviour of TiO_2 have been undertaken, mostly with respect to oxygen

sorption. EPR spectroscopic studies[80,104] have shown that the O_2^- anion-radical is the dominant species formed during oxygen photosorption onto TiO_2, although the formation of the O^- [105], the O_3^- and possibly the O_3^{3-} [106] anion-radicals have also been reported. Gravelle et al[80] found that the spectral dependence for O_2 photosorption onto titania shows a maximum at 390nm, with photosorption still detectable at 550nm, Since this latter wavelength is outside the absorption edge of TiO_2, it was presumed that photosorption at the higher wavelengths occurs via ionisation of defect donor levels situated in the TiO_2 band gap. Fukuzawa et al[107], using EPR spectroscopy, investigated the interaction of oxygen with illuminated anatase. Two paramagnetic species were detected, one of which was assigned to a solid state defect, most probably O_2^+, located in the TiO_2 band gap about 2.4eV below the bottom of the conduction band. The other species was thought to be the O_2^- anion-radical. It was also found that the photosorption behaviour of O_2 depends upon the ambient oxygen pressure, with high pressures favouring photo-adsorption and low pressures favouring photodesorption processes.

Bickley and Stone[108] reported that photo-adsorption of oxygen on illuminated rutile surfaces is enhanced by the presence of adsorbed water. Rutile subjected to prolonged outgassing at high temperatures, followed by re-oxidation in dry oxygen, was found to be inactive for oxygen photo-adsorption. The kinetics of oxygen photo-adsorption were observed to follow a parabolic rate law, suggesting a mechanism involving a surface-controlled diffusion step. It was postulated that surface hydroxyl groups act as photohole traps, thus allowing photo-electrons to participate in the

adsorption process to give O_2^- anion-radicals. No oxygen desorption was observed to occur upon termination of irradiation, indicating that the trapped photoholes are stable species. A prolonged period of darkness prior to secondary illumination was found to give enhanced oxygen photo-adsorption rates, indicating the existence of a more effective photohole trap than surface hydroxyl groups. This second photohole trap was thought to be the perhydroxyl anion, formed during the dark period via:

$$O^-_{2(ads)} + H\dot{O}_{(s)} \longrightarrow H\dot{O}_{2(s)} + O^-_{(ads)} \qquad [15]$$

$$H\dot{O}_{2(s)} + e^- \longrightarrow HO^-_{2(s)} \qquad [16]$$

A TPD study of oxygen photo-adsorption on reduced rutile, conducted by Bickley and Jayanty[109], revealed enhanced rates of photo-adsorption due to the presence of Ti^{3+} cations, which presumably also act as efficient photohole traps. Boonstra and Mutsaers[110] investigated oxygen photo-adsorption on both rutile and anatase, outgassed at differing temperatures. A direct linear relationship between the extent of oxygen uptake and the number of surface hydroxyl groups was discovered. This observation is supported by Oosawa and Grätzel[111], who found an inverse relationship between evolution rate and the number of surface hydroxyl groups during a study of photocatalytic oxygen evolution from aqueous TiO_2 suspensions. Munuera et al[112] studied oxygen photo-adsorption onto hydroxylated anatase surfaces and observed an initial fast uptake, followed by a prolonged period of slow oxygen photodesorption. Thermal dehydration of the surface resulted in reduced photo-adsorption, which

became a diffusion-controlled process. Re-hydration restored fast photo-adsorption, following first-order kinetics, accompanied by photodesorption of water. A mechanism involving the formation of OH radicals and their subsequent reaction to give hydrogen peroxide, which is then photo-decomposed to give oxygen, was proposed to account for these experi-mental observations. Further EPR spectroscopic investigations[113,114] revealed that the radical intermediates formed during oxygen photo-adsorption, depend upon the extent of surface hydroxylation. On the basis of these results, two different mechanisms for oxygen photo-adsorption onto hydroxylated and dehydroxylated TiO_2 surfaces were proposed, the former involving H_2O_2 formation.

Oxygen isotope exchange (OIE) reactions on illuminated TiO_2 sur-faces have been studied by several investigators attempting to elucidate the mechanisms of various photocatalytic oxidation reactions. Tanaka[115] investigated the gas-phase OIE reaction on illuminated rutile, using a combined mass spectrometry - thermal desorption technique. He con-cluded that the O_2^- anion-radical does not participate in the exchange process directly and proposed that the weakly-held O_3^- species, formed from adsorbed molecular oxygen and the O^- anion-radical, acts as the exchange intermediate. This proposal was supported by Courbon et al[116], who concluded the OIE process occurs via a single surface oxygen spe-cies, although the O^-, rather than the O_3^-, anion-radical was thought to be the exchange intermediate. Sato et al[117] investigated the room tempera-ture photo-induced exchange between $^{18}O_2$ and the lattice oxygen of TiO_2, prepared from titanium hydroxide calcined at various temperatures.

Little activity was observed for samples calcined below 473K, although increasing calcination temperature was observed to give increasing exchange activity, with a maximum in activity occurring at about 773K. Calcination at temperatures above 873K led to a sharp fall in exchange activity, such that calcination above 1023K rendered the titania samples virtually inactive for the exchange process. It was suggested that distortion of the TiO_2 lattice during initial calcination destabilises the lattice oxygen, leading to high exchange activity. High temperature calcination reduces the extent of lattice distortion, with the concomitant reduction in OIE activity. However, an alternative explanation for the experimental observations can be found by considering how calcination temperature influences the extent of surface hydroxylation and initiation of phase changes in TiO_2. Calcination of titanium hydroxide at temperatures below 473K probably results in the formation of hydrous titania, possessing little OIE activity. Increasing the calcination temperature above 473K leads to the formation of extensively hydroxylated anatase, which shows little OIE activity because the lattice oxygen is rendered inaccessible for the exchange process by the presence of surface hydroxyl groups. As the calcination temperature is further increased, the lattice oxygen become more accessible as the extent of dehydroxylation increases, such that a maximum in activity is observed at about 773K. Calcination above the temperature induces the anatase-to-rutile phase change, which leads to reduced OIE activity because rutile is the most stable polymorphic form of TiO_2. Calcination at 1023K leads to complete transition from anatase to rutile, so that little OIE activity is observed. More recently, Sato[118] has

studied the OIE reaction on illuminated TiO_2 samples with pretreated surfaces. From the experimental results obtained, it was concluded that surface hydroxyl groups also participate in the exchange process, most probably via interaction with surface oxygen species such as the O^- or O_3^- anion-radicals.

Although most studies of the photosorption behaviour of titania have concentrated on oxygen photo-adsorption and desorption, the photosorption of other species, such as NO[105], alkenes[119] and hydrogen and methane[120,] have also been investigated.

1.3.8 Photocatalysis on TiO_2

In general, photocatalysis on semiconductor surfaces utilises the redox capability arising from the photogeneration of electrons and positive holes. The first reported investigation into the photocatalytic activity of titania was undertaken by Renz[1], who was able to oxidise many organic molecules using TiO_2 irradiated with UV light. Since then, and particularly over the last two decades, the photocatalytic properties of TiO_2 have been studied in detail. This section briefly reviews some of the more frequently studied photocatalytic reactions on TiO_2 reported in the literature.

Both the gas-phase and liquid-phase partial oxidation of simple aliphatic alcohols to the corresponding carbonyl compounds, using UV-illuminated TiO_2, have been established as relatively efficient photocatalytic processes. It is generally accepted that UV radiation, of the

appropriate wavelength, and oxygen are required for sustained photocatalysis during these reactions. Although the role of water remains unclear, it is thought that the process is enhanced by the presence of surface hydroxyl groups[121]. However, the precise mechanism by which alcohol photo-oxidation over TiO_2 occurs remains unresolved and mechanisms involving O_2^-, formed via photo-electron trapping, and OH or O^- , formed via photohole trapping, have been proposed[109,121,122]. Bickley et al[121] have investigated the photocatalytic oxidation of propan-2-ol to propanone, using UV-illuminated rutile. They observed that when the amount of presorbed alcohol is increased, the rate of oxygen consumption increases to such an extent that oxygen photosorption follows a linear, rather than the usual parabolic, rate law. This was taken as an indication of very rapid oxygen consumption by the adsorbed alcohol, such that the surface diffusion step which normally controls oxygen uptake onto irradiated TiO_2 surfaces is eliminated. It was also concluded that surface hydroxyl groups participate in the photo-oxidative process, by acting as photohole traps. $O^-_{2(ads)}$ anion-radicals then react with adjacent adsorbed alcohol molecules, either by proton transfer Eq.[17] or by hydrogen atom transfer Eq.[18]:

$$O^-_{2(ads)} + Me_2CHOH_{(ads)} \longrightarrow HO_{2(ads)} + Me_2CHO^-_{(ads)} \qquad [17]$$

$$O^-_{2(ads)} + Me_2CHOH_{(ads)} \longrightarrow HO^-_{2(ads)} + Me_2C\dot{H}O_{(ads)} \qquad [18]$$

Propanone formation can then occur either by:

$$H\dot{O}_{2(ads)} + Me_2CHOH_{(ads)} \longrightarrow H_2O_{2(ads)} + Me_2C\dot{H}O_{(ads)} \quad [19]$$

$$H_2O_{2(ads)} + Me_2CHO^-_{(ads)} \longrightarrow Me_2CO_{(ads)} + H_2O_{(ads)}$$

$$+ OH_{(ads)} + e^-_{(to\ catalyst)} \quad [20]$$

$$\dot{O}H_{(ads)} + Me_2C\dot{H}O_{(ads)} \longrightarrow Me_2CO_{(ads)} + H_2O_{(ads)} \quad [21]$$

or by:

$$HO^-_{2(ads)} + Me_2CHOH_{(ads)} \longrightarrow H_2O_{2(ads)} + Me_2CHO^-_{(ads)} \quad [22]$$

$$H_2O_{2(ads)} + Me_2CHO_{(ads)} \longrightarrow Me_2CO_{(ads)} + H_2O_{(ads)}$$

$$+ \dot{O}H_{(ads)} \quad [23]$$

$$\dot{O}H_{(ads)} + Me_2CHO^-_{(ads)} \longrightarrow Me_2CO_{(ads)} + H_2O_{(ads)}$$

$$+ e^-_{(to\ catalyst)} \quad [24]$$

Cunningham et al[123] investigated the photo-oxidation of C_3 and C_4 alcohols, using $^{18}O_2$, over variously pretreated rutile surfaces. A mechanism involving photohole trapping at coordinatively unsaturated surface O^{2-} sites was proposed to account for the experimental results obtained. Harvey et al[124] investigated the photocatalytic oxidation of liquid propan-2-ol on TiO_2, irradiated with UV light of wavelength 366nm. The reaction was found to be dependent upon the square root of the incident light intensity which, taken together with observed low quantum yields, was thought to indicate the dominance of photo-electron and photohole recombination within the bulk of the catalyst. A further study of the photo-oxidation of liquid C_2 - C_4 aliphatic alcohols on UV-illuminated rutile was carried out by the same workers[125]. Within this study it was found that activities and activation energies for product formation were virtually identical for all the alcohols investigated. This single activation energy

value was considered to be the energy required to promote photogenerated electrons from traps into the conduction band of rutile. A radical mechanism similar to that proposed by Bickley et al[121] and Cundall et al[122] was postulated to account for these experimental results.

The photo-oxidation of hydrocarbons, including alkanes[126-128], alkenes[119,129] and aromatic molecules[130,131], on UV-irradiated TiO_2 has been studied extensively. Djeghri et al[126] investigated the interaction between oxygen and various C_1 - C_8 primary, secondary, tertiary and quaternary alkanes, on the surface of UV-illuminated anatase. The main reaction products observed were aldehydes and ketones, derived from partial oxidation processes, although CO_2 and H_2O from complete oxidation were also detected. A reactivity sequence, in decreasing order, of:

tertiary > quaternary > secondary > primary

was observed and the alkane carbon atom which is attacked is that which has the highest electron density, coupled with the least steric hinderance. A mechanism involving the formation of alcoholic intermediates, which are then oxidised to aldehydes and ketones, was proposed for 1°, 2° and 3° alkane photo-oxidation. Dehydration of 2° and 3° alcohol intermediates, to give alkenes which are then oxidised to aldehydes and/or ketones, was also considered to occur. Herrmann et al[127] simultaneously measured photoconductivity and the photocatalytic activity of TiO_2 during isobutane photo-oxidation at room temperature. It was found that the photoconductivity was inversely proportional to the partial oxygen pressure, which was attributed to the formation of the O_2^- anion-radical. However, the rate of propanone formation was found to be independent

of the oxygen partial pressure and it was postulated that the active oxygen intermediate for this process was the activated O^* species, formed via photohole trapping by the adsorbed O^- anion-radical. Childs and Ollis[132] considered that isobutane photo-oxidation on TiO_2 occurs by a two-step mechanism, involving a monatomic oxygen species which reacts with the adsorbed alkane to produce alcoholic intermediates. Two-site dehydration of the latter species, to give adsorbed alkene subsequently oxidised to propanone, was then thought to occur.

Numerous other photocatalytic reactions, using TiO_2 as the photocatalyst, have been reported in the literature. Some of the more significant reactions studied include the photohydrogenation of alkenes and alkynes using water[133-135], oxidation of various anions[136-138] and CO[139,140] and photo-Kolbe reactions[141-143]. However, an in-depth discussion of these reaction processes is not warranted in this thesis.

1.4 Preparation of Metallised TiO_2 Catalysts

The preparation of supported metal catalysts can be achieved in a variety of ways, including photodeposition[144-146], impregnation[147,148], ion-exchange[149,150], sol precipitation[151], co-precipitation[152] and metal vapour deposition[153]. In the majority of these techniques, the metal to be supported is initially in a high oxidation state, usually as an oxide or salt, and consequently a reduction step is required to produce the free metal on the support surface. Impregnation is the simplest and cheapest, and therefore the most commonly-used, method of preparing supported metal catalysts.

Photodeposition methods generally involve illumination, with band-gap radiation, of a semiconductor oxide suspended in a solution of the appropriate metal salt and a sacrificial electron donor, such as an alcohol or carboxylic acid. Production of small crystallites of the free metal on the oxide surface is achieved by reduction of the metal salt by photo-generated electrons. Photoholes are trapped at the surface by the sacrificial electron donor species, thereby reducing recombination processes and maximising the efficiency of the metal deposition process. Since photodeposition occurs under mild temperature conditions, surface diffusion of the deposited metal is minimised, giving rise to uniform, highly-dispersed, supported metal catalysts. This method was first proposed by Kraeutler and Bard[144], who used it to prepare Pt/TiO_2 catalysts from ethanoate-buffered hexachloroplatinic acid (H_2PtCl_6) solutions. Analysis of the dark deposits formed on the oxide during irradiation, by electron spectroscopy for chemical analysis (ESCA), showed that they were composed

of metallic platinum. Furthermore, scanning electron microscopy (SEM) failed to show the presence of any large Pt agglomerates on the surface of the oxide. Bickley[154] suggested that the efficiency of this procedure is due to the irreversible oxidation of ethanoate anions to CO_2, via trapping of photoholes. However, Koudelka et al[155], using X-ray photo-electron spectroscopy (XPS) and cyclic voltammetry techniques, investigated the platinisation of anatase films via H_2PtCl_6 / $CH_3CO_2^-$ and K_2PtCl_4 solutions. XPS showed that K_2PtCl_4 was readily reduced to metallic Pt during irradiation, whereas ethanoate-buffered H_2PtCl_6 gave rise to signals consistent with Pt^{II} and Pt^{IV} species. Although these species were not identified, XPS analysis for chlorine gave a surface Cl:Pt ratio < 1, indicating that partial or complete hydrolysis of $Pt[Cl_6]^{2-}$ had occurred. It was concluded that the first stage of platinum photodeposition from ethanoate-buffered H_2PtCl_6 solution involves strong, irreversible adsorption of Pt^{IV} species onto the oxide surface, followed by hydrolysis to give platinum oxychlorides and or platinum oxide. Cyclic voltammetry measurements revealed that Pt deposition from the ethanoate-buffered solution proceeds slower than from aqueous K_2PtCl_4 solution. It was proposed that a product or intermediate of the oxidative decarboxylation of the ethanoate anion, most probably CO_2, is adsorbed onto the TiO_2 surface, thereby blocking sites for Pt deposition. These results were confirmed by Sungbom et al[156], who used XPS to investigate how the oxidation state of Pt deposits on the surface of TiO_2 varied with increasing ethanoate concentration. It was found that the Pt^{II} and Pt^{IV} species dominated, even at low ethanoate concentrations.

Curran et al[157] investigated how the rate of Pt photodeposition onto TiO_2 varied when the reaction parameters were altered. It was found that low pH, low light intensity, high ionic strength and higher than ambient temperatures favoured the deposition process. The concentration of metal salt was found to have a secondary effect on the deposition rate, implying that deposition from dilute solutions is effective. Herrmann et al[158] investigated the rate of Pt photodeposition onto TiO_2 using various Pt complexes and found that the rate was identical for ionic complexes, but much slower for non-ionic complexes, supporting the results obtained by Curran and co-workers[157]. Furthermore, transmission electron microscopy (TEM) revealed that, for low metal loadings, Pt metal was uniformly distributed over the oxide surface in the form of small crystallites of diameter approximately 1nm. Higher metal loadings and longer irradiation times tended to produce larger agglomerates of Pt metal. It was also shown that other metals, such as Pd, Ag, Rh, Au and Ir, could be photodeposited onto semiconductor oxide supports, such as TiO_2, ZnO, Nb_2O_5 and ThO_2.

The exact mechanism by which photodeposition occurs is still not fully understood. Yoneyama et al[159] studied the process of metal deposition onto TiO_2 single crystals, illuminated on one side only. They observed that the metal was preferentially deposited on the dark side of the crystal, which was taken as a strong indication that photodeposition proceeds via an electrochemical mechanism. This mechanism envisages that photogenerated electrons and holes move in opposite directions within the oxide, due to strong internal electric fields. It was proposed that the electrons move into the bulk of the crystal, whilst holes migrate to the

illuminated surface where they are trapped. The accumulation of electrons in the oxide conduction band causes the band to bend upwards to such an extent that the excess electrons escape from the dark side of the crystal to the metal cations. In the photodeposition of metals onto oxide powders, the entire surface of the individual particles is never illuminated simultaneously, so the electrochemical mechanism is applicable to powder samples as well as single crystal models. Nakamatsu et al[160] found that the shape and dispersion of Pt photodeposited onto TiO_2 was governed by the choice of sacrificial electron donor. The average nearest neighbour distance of the Pt particles, as determined by TEM, was taken as an indication of the degree of dispersion. This decreased in the sequence: ethanoic acid ~ 2-methylpropan-2-ol (100nm) > methanol ~ propan-2-ol (30nm) > ethanol (5nm). Thus, the use of ethanol as the sacrificial electron donor produced the greatest degree of Pt dispersion, with particle diameters in the range 1-4nm. Methanol produced particles with diameters in the range of a few to >10nm, with diffraction studies indicating that the larger particles were single crystals. Use of ethanoic acid as the sacrificial electron donor resulted in the formation of polycrystalline Pt deposits. The conventional model of photodeposition assumes that only electrons excited to the conduction band of the oxide are available to reduce the metal ions, so that the choice of sacrificial hole scavenger should not affect the degree of metal dispersion achieved. Nakamatsu and co-workers[160] proposed that the sacrificial reagent is adsorbed onto the oxide surface, where it is converted to a radical species via photohole trapping. The radical then furnishes an electron to the metal salt co-

adsorbed on the oxide surface. Since, in the case of methanol and ethanol at least, the reducing power of the corresponding radical is greater than that of the excited electrons present in the TiO_2 conduction band, the degree of metal dispersion may be governed by the choice of sacrificial photohole scavenger.

Preparation of supported metal catalysts via the impregnation/ reduction method generally involves slurrying the support material in an aqueous solution of the desired metal salt, at the appropriate concentration. The resulting impregnated support is then usually calcined in air at 373 - 393K, followed by reduction in a flowing hydrogen atmosphere and then cooling to ambient temperature under a flow of either H_2 or an inert gas[161,162]. The average metal particle size produced during the reductive stage tends to depend upon the initial concentration of the metal salt solution, with higher metal loadings resulting in larger metal particles. Furthermore, slow evaporation of the solvent favours migration of the metal salt to the external surface of the support particle, whereas rapid drying tends to produce a more uniform distribution of metal throughout the support material[162]. Frequently, a concentration of metal salt is used such that the volume of aqueous solvent required to give the desired loading of metal is approximately the same as the pore volume of the support material, giving rise to a paste rather than a slurry. This is known as *impregnation to incipient wetness* and often gives a more uniform distribution of metal on the support because nucleation and growth of the metal crystallites is limited by the amount of metal salt solution contained within each pore.

In cases where the support material is not readily reduced, such as SiO_2 or Al_2O_3, the temperature at which reduction in H_2 is carried out is not critical in terms of the properties of the resultant catalyst, provided that the metal is fully reduced. However, in systems where the support is either reducible or has strong tendencies toward non-stoichiometry, such as TiO_2 or Nb_2O_5, the temperature at which the reductive step is carried out can markedly affect both the chemisorptive and catalytic properties of the resulting catalyst. Tauster et al[147] prepared a series of TiO_2-supported noble metal catalysts, with a metal loading of 2 mass%, via impregnation/reduction. Reduction at 473K was found to produce well-dispersed metal catalysts exhibiting normal chemisorptive properties, whereas reduction at 773K resulted in severe depression of the chemisorptive, and hence catalytic, properties of all catalysts. Subsequent analysis of the high temperature reduced metal/TiO_2 catalysts by X-ray diffraction and electron microscopy failed to reveal the presence of any large agglomerates of metal on the oxide surface, a result which ruled out loss of metal surface area due to sintering effects. It was proposed that the loss of chemisorption and catalytic activity was due to bonding between the deposited metal and either titanium cations or titanium atoms, the latter involving the formation of intermetallic compounds. This effect was termed *strong metal-support interaction (SMSI)* and has been the subject of detailed investigation over the last decade. A review of the literature concerning the physical characteristics of metal/TiO_2 catalysts in the SMSI state and possible causes of this effect is given in the next section.

1.5 Metal - Support Effects in Metallised TiO_2 Catalysts

1.5.1 Hydrogen Spillover

Generally, the process of hydrogen spillover in catalytic systems is one in which molecular hydrogen is dissociatively adsorbed at metal sites, followed by H atom migration to an adjacent substance not normally capable of the direct chemisorption of H_2. The first convincing evidence for hydrogen spillover was obtained by Khoobiar[163], who found that the formation of hydrogen tungsten bronzes, H_xWO_3, from WO_3 and H_2 is catalysed by the presence of Pt/Al_2O_3. This observation was explained in terms of dissociative hydrogen chemisorption at Pt sites, followed by the migration of H atoms onto the alumina support and subsequent transfer to WO_3. Benson et al[164], using Pt/Al_2O_3-WO_3, demonstrated that the presence of water on the catalyst surface is essential for hydrogen spillover to occur. Spillover hydrogen is not thought to be particularly reactive[165] and reverse migration of such hydrogen from the support to the metal sites is the normal mechanism for reactions between spillover hydrogen and hydrogen acceptor molecules[166].

Using ^1H nuclear magnetic resonance (NMR) spectroscopy, Gajardo et al[167] investigated the surface adsorption states of hydrogen on Rh/TiO_2 catalyst. They observed two distinct forms of adsorbed hydrogen on the catalyst surface; a weakly-bound, mobile species, which was removed on outgassing at ambient temperature, and a more strongly-bound species. These observations were interpreted in terms of a mobile hydrogenic species formed on the support TiO_2 via a spillover mechanism and more strongly-bound H atoms associated with the Rh metal sites. Conesa and

Soria[168] studied the reversible formation of Ti^{3+} cations during hydrogen adsorption onto metal/TiO_2 catalysts, using EPR spectroscopy. Strong EPR signals corresponding to Ti^{3+} cations were observed following contact with H_2 at room temperature. Outgassing of the samples at room temperature for a short time resulted in the disappearance of the EPR signals and it was found that this process could be repeated many times in a cyclic manner. Dehydroxylation or reduction in H_2 at temperatures above 473K resulted in a marked decrease in the effect. These observations were interpreted in terms of a hydrogen spillover mechanism as outlined below:

$$H_{2(g)} + Pt_{(s)} \longrightarrow Pt{-}H_{(ads)} \qquad [25]$$

H atom migration to the support then occurs by either:

$$Pt{-}H_{(ads)} + \{ Ti^{4+}\ O^{2-} \} \longrightarrow Pt_{(s)} + \{ Ti^{3+}\ OH^{-} \} \qquad [26]$$

or by:

$$Pt{-}H_{(ads)} \longrightarrow \{ H^{+} + e^{-} \}_{(s)} \qquad [27]$$

$$e^{-} + Ti^{4+} \longrightarrow Ti^{3+} \qquad [28]$$

Huizinga and Prins[169], using EPR spectroscopy, have also investigated the behaviour of Ti^{3+} cations during the low- and high-temperature reduction of Pt/TiO_2 catalysts. They found that exposure to hydrogen at 573K leads to the formation of a Ti^{3+} signal in the EPR spectrum, which can be removed by subsequent outgassing at 573K. The signal can then be regenerated by treatment in hydrogen at ambient temperature. These observations support the hydrogen spillover mechanism, and the reverse pro-

cess, as postulated by Conesa and Soria[168]. However, hydrogen spillover on high-temperature reduced catalysts was found to irreversible, which was attributed to dehydration of the reduced TiO_2 support around the metal deposits. This is discussed in more detail later, in Section 1.5.2.

Herrmann and Pichat[170] have investigated hydrogen spillover on Pt/TiO_2, Rh/TiO_2 and Ni/TiO_2 catalysts by means of electrical conductivity measurements. They concluded that hydrogen spillover occurs via dissociative adsorption at metal sites, followed by the migration of atomic hydrogen onto the oxide support with subsequent protonation of surface O^{2-} anions, as evidenced by an increase in the electrical conductivity of the sample, arising from an increase in the concentration of defect Ti^{3+} sites. The influence of the extent of surface hydroxylation and the presence of molecular water upon the hydrogen spillover process was also investigated. The presence of both these species on the TiO_2 surface was found to favour spillover by the provision of proton switch routes that facilitate the migration of atomic hydrogen away from the metal sites:

$$H_{(s)} + H_2O_{(ads)} \longrightarrow \{ H_3O^+ \}_{(ads)} \quad [29]$$

$$\{ H_3O^+ \}_{(ads)} + H_2O_{(ads)} \longrightarrow H_2O_{(ads)} + \{ H_3O^+ \}_{(ads)} \quad [30]$$

and:

$$Ti^{3+}(OH)_{(s)} + H_{(s)} \longrightarrow \{ Ti^{4+}(OH_2) \}_{(s)} \quad [31]$$

$$\{ Ti^{4+}(OH_2) \}_{(s)} + Ti^{3+}(OH)_{(s)} \longrightarrow Ti^{3+}(OH)_{(s)} + \{ Ti^{4+}(OH_2) \}_{(s)} \quad [32]$$

Evacuation of samples previously exposed to hydrogen resulted in a fall in the electrical conductivity, indicating that spillover is, at least partially, reversible. The presence of an "electron pumping effect" was also proposed, whereby the presence of the metal on the TiO_2 surface reduces the free electron concentration in the support, according to the equation:

$$e^- + M_{(s)} \longrightarrow \{ M_{(s)} \}^- \qquad [33]$$

- where $\{ M_{(s)} \}^-$ represents excess electron density trapped at surface metal sites. This effect was evidenced by the lower conductivities of the metallised catalysts, relative to pure TiO_2 samples that been subjected to similar pretreatments.

Beck and White[171], using TPD techniques, have studied hydrogen isotope scrambling during spillover processes on Pt/TiO_2 catalysts. Sequential dosing of H_2 and D_2 onto the catalyst, followed by thermal desorption into vacuum, showed incomplete isotope mixing. This was interpreted in terms of a spillover mechanism in which the hydrogen isotope is dissociatively adsorbed at Pt sites and then slowly diffuses away from these sites onto the surrounding oxide in a radial manner. The mean diffusion length was found to increase non-linearly with both temperature and exposure time and for H_2 and D_2 sequentially dosed at different temperatures this has the effect of preserving the spatial separation of the two isotopes on the oxide surface. Hence, only a small quantity of HD, formed via isotope scrambling, was observed. In further TPD studies by White and co-workers[172,173], the spillover of deuterium on Pt/TiO_2 was investigated. In addition to chemisorption at Pt sites, two thermally-acti-

vated states, attributed to spillover species, were observed. One of these states was thought to arise from spillover to a special oxide site,possibly TiO_x particles associated with the Pt metal. The extent of D_2 spillover, as with H_2 spillover, was found to be dependent upon a variety of factors, including the degree of reduction and hydroxylation of the catalyst surface. Oxygen titration experiments[172] revealed that the desorption of spillover deuterium occurs via migration back to Pt sites, rather than by direct recombination and subsequent desorption from the oxide surface. Detailed reviews of hydrogen spillover in general have been published by Bond and Sermon[174,175].

1.5.2 Strong Metal - Support Interactions (SMSI)

Following the paper by Tauster et al[147], in which the discovery of the SMSI effect was reported, many investigations, using a wide variety of techniques, have been carried out in attempts to elucidate the exact origin and nature of this phenomenon. Although the literature contains a great deal of conflicting evidence, it shows that hydrogen spillover, and subsequent reduction of the TiO_2 support, plays an important role in the generation of SMSI. The catalytic reduction of TiO_2 to suboxide Ti_4O_7 by deposits of Pt metal on the oxide surface has been proposed by Baker et al[153,176]. These workers investigated the morphological behaviour of Pt deposited on various supports, including TiO_2, when treated in hydrogen in the temperature range 473 - 1075K. Analysis of these materials by TEM revealed that metal dispersion was more stable on TiO_2 in compari-

son to other support materials and examination of Pt/TiO_2 at high resolution (HRTEM) showed the metal particles to be predominantly hexagonal, very thin and of uniform thickness. This was termed *pill-box morphology*. The unique behaviour of Pt deposited on TiO_2 was thought to arise from a strong metal - support interaction of unknown origin. In a further HRTEM study, Baker et al[177] investigated the role of the supported metal in SMSI using Ag/TiO_2 and $PtAg/TiO_2$ catalysts. Examination of the Ag/TiO_2 catalysts after treatment in hydrogen at 823K showed the metal particles to be fairly large, dense and globular in outline. Also, electron diffraction measurements revealed that the TiO_2 support remained in the rutile phase, consistent with the catalyst being in a normal state. However, in the presence of Pt metal, reduction at 823K resulted in massive morphological changes in the Ag deposits, which were subsequently observed to be predominantly thin pill-box structures virtually indistinguishable from the Pt deposits. The support was also found to have been reduced from rutile to the Ti_4O_7 suboxide. On the basis of these results it was proposed that, with Pt present, Ag exhibits characteristic SMSI behaviour and that the function of the Pt metal is to dissociatively adsorb H_2, which Ag is incapable of, thereby providing a H atom source which initiates SMSI via spillover. Huizinga and Prins[169] found that hydrogen spillover was reversible on Pt/TiO_2 catalysts reduced in H_2 at 573K, but irreversible on samples similarly reduced at 773K. The authors supported the idea that during high temperature reduction, the oxide surface around the metal particles is first reduced and then dehydrated to form a Ti_4O_7 suboxide layer, which inhibits the reverse process of spillover. It was suggested

that SMSI might arise as a consequence of the formation of this suboxide layer via a special interaction, of unknown origin, between the metal and the reduced oxide. Morphological changes in the Pt crystallites, observed as a spreading of the metal over the Ti_4O_7 layer, occurred during the high temperature reduction stage. In a further study by the same workers[178], EPR spectroscopy was used to investigate changes in the oxidation state of the Pt metal during both oxidation and reduction of the catalyst. Two sets of EPR signals, assigned to Pt^+ and Pt^{3+}, were observed in these experiments. The Pt^+ cation, formed during reduction, was thought to be situated at the metal - support interface, in contact with the Pt particle. The Pt^{3+} cation was formed either by direct oxidation or by re-oxidation of reduced Pt/TiO_2. However, the shape and intensity of the Pt^{3+} EPR signal was found to be different after re-oxidation, compared with that observed after direct oxidation of the catalyst. This was taken as evidence that the metal oxide crystallites were more agglomerated following re-oxidation of reduced Pt/TiO_2, relative to those formed during direct oxidation.

Reduction of the TiO_2 support by hydrogen at high temperatures, giving rise to mobile suboxide species, nominally TiO_x, which then migrate and encapsulate the metal crystallites has also been proposed as the cause of SMSI in TiO_2-supported metal catalysts[179-182]. Jiang et al[179] observed slow hydrogen uptake by Ni/TiO_2, $NiFe/TiO_2$ Pt/TiO_2 catalysts, previously reduced in H_2 at 770K. It was postulated that partial blocking of the metal surface by an electronegative titanium species, possibly TiO_x ($1 < x < 2$), was the cause of the characteristic SMSI behaviour. Fur-

thermore, it was also suggested that such species may decrease the rate and strength of hydrogen adsorption onto the remaining accessible metal sites. The idea of encapsulation of metal sites by titanium-oxygen species has been supported by Simeons et al[180], who used a number of analytical techniques to investigate the SMSI effect in high temperature reduced Ni/TiO_2 catalysts. Brumberger et al[183] used small-angle X-ray diffraction methods to investigate Pt/TiO_2 catalysts reduced in hydrogen at both low and high temperatures. It was found that the free metal surface area decreased by approximately 25% in going from the normal to the SMSI condition, which was in good agreement with electron microscopic measurements. The results of temperature-programmed reduction (TPR) experiments provided some evidence to suggest that Pt oxides were present in both normal and SMSI catalysts. However, the discrepancy between metal surface areas calculated from X-ray scattering and from electron microscopy was large, particularly for the SMSI catalyst, when platinum oxides were taken into consideration. From these results, the authors concluded that the majority of metal deposits, in both types of catalyst, consist of metallic Pt, rather than platinum oxides. Sun et al[184], using XPS, investigated thin film models of Pt supported on both oxidised and reduced TiO_2. On fully oxidised titania, annealing at high temperature was observed to cause the migration and coalescence of small metal particles, to give larger, isolated regions of Pt on the oxide surface, a process termed *"islanding"*. There was no evidence for encapsulation of the Pt metal during this treatment of the model catalyst. However, on reduced titania, annealing above 673K resulted in support migration and

subsequent encapsulation of the Pt deposits. XPS characterisation of the encapsulating species indicated the presence of Ti^{2+} cations. In a recent HRTEM study of Rh/TiO_2 SMSI catalysts, Logan and co-workers[185] reported the direct observation of amorphous surface layers surrounding small Rh crystallites. These layers were still evident after re-oxidation of the SMSI catalyst at 473K, which partially restored the chemisorption capacity of the catalyst.

In the paper reporting the discovery of the SMSI effect, Tauster et al[147] postulated that electron transfer from Ti^{3+} cations to the supported metal may be responsible for the observed depression in chemisorptive capacity of the metal for electron-donating adsorbents, such as H_2 and CO. Soon afterwards, Horsley[186] carried out a theoretical molecular orbital study of Pt/TiO_2 SMSI catalysts, using two different cluster models. The calculations suggested that the most favourable model of SMSI is one in which the Pt atoms reside in surface oxygen vacancies, generated during high temperature reduction of the catalyst. The presence of significant metal-metal bonding between Pt atoms and Ti^{3+} cations was also indicated within the calculations, arising from electron transfer from Ti^{3+} to Pt. Electrical conductivity measurements of low and high temperature reduced Pt/TiO_2 catalysts have been carried out by Herrmann and Pichat[161,187]. In the SMSI state, the Pt metal was found to be markedly enriched in electrons, which was interpreted in terms of filling of the metal d-orbitals, such that they approached the d^{10} configuration, thereby reducing the chemisorptive capacity of the metal. Fung[188] and Sexton et al[189] used XPS to measure the core level electron binding energies of

titania-supported metal catalysts in the SMSI state. In both studies, the XPS spectra indicated that at least some electron transfer from Ti^{3+} to the metal had occurred. However, Meriaueau et al[190] pointed out that reduction of Pt/TiO_2 catalysts at both 473K and 773K resulted in the formation of Ti^{3+} cations, but that the SMSI effect only manifests itself after high temperature reduction. Furthermore, EPR spectroscopy of Ti^{3+} and Rh^0 species located in the supercages of Y zeolite showed that the close proximity of the two species did not result in electron transfer from Ti^{3+} to the metal. The authors[190] proposed that SMSI arises from the bulk electronic properties of highly-reduced TiO_2, rather than from direct Ti^{3+}-metal electron transfer processes. High temperature reduction of TiO_2 produces a large concentration of surface defects, which raises the Fermi level of the reduced oxide above that of the metal. When the metal particles are in contact with reduced TiO_2, the Fermi levels of the two balance out via electron density accumulating at the metal sites, thus producing the SMSI effect. Chen and White[191], using bulk electrical conductivity and XPS data, demonstrated that the presence of surface Ti^{3+} cations is not necessary for the generation of SMSI in TiO_2-supported Pt catalysts. Pt supported on reduced TiO_2, TiO and Ti_2O_3, in which the surface region had been fully oxidised to TiO_2, was found to be very active for the H_2-D_2 equilibration reaction, although only very limited H_2 uptake was observed. It was suggested that electrons from the reduced bulk oxide tunnel through the thin TiO_2 surface layer and become trapped at Pt sites. The negatively-charged Pt crystallites can readily dissociate dihydrogen, but only have weak binding for the resulting hydrogen atoms.

Further work by the same authors[192] revealed that H_2 chemisorption by Pt/TiO_2 catalysts can be suppressed by the addition of small amounts of potassium to the catalyst. This was attributed to the transfer of electrons from K to Pt, rendering the sample in a state analogous to that found in SMSI catalysts. EPR spectroscopy of Pt/TiO_2, with and without added K, showed that the concentration of surface Ti^{3+} cations remained essentially unchanged, suggesting that the presence of this species was not necessary for the generation of the SMSI effect. However, Spencer[193], on the basis of theoretical calculations, concluded that re-arrangement of the TiO_2 support, promoted by the formation of K_2TiO_3 and resulting in the encapsulation of the Pt deposits by TiO_x species, was the most likely cause of the observed SMSI effect in $Pt/TiO_2/K$ catalysts.

Thin films of Pt deposited on oxidised Ti foil, to give $Ti/TiO_2/Pt$ wafer models of high surface area Pt/TiO_2 catalysts exhibiting SMSI, have been investigated by Belton et al[194] using XPS and AES. Suppression of CO and H_2 chemisorption on reduced, as compared to fully oxidised, titania films with Pt overlayers was interpreted in terms of two factors:

a) flatter Pt particles, dominated by {110} terraces, and

b) enhanced electronic interaction between the Pt metal and the reduced TiO_2 substrate. More recently, Martens et al[195] have investigated the SMSI effect in Rh/TiO_2 catalysts, using EXAFS and HRTEM techniques. In the SMSI state, no evidence was found for coverage of the metal by suboxide species, although it was concluded that the support surrounding the metal deposits had been reduced to a TiO_x species. The possibility of a loosely-bound TiO_x suboxide layer covering the metal surface was not

precluded, but it was thought that an electronic perturbation of the metal is the most likely cause of SMSI in highly-dispersed Rh/TiO_2 catalysts. In a series of studies, in which a wide variety of techniques were employed, Belton et al[196-198] have investigated the origins of SMSI in Rh/TiO_2 and Pt/TiO_2 thin film model catalysts. On the basis of the results obtained in these experiments, it was concluded that high temperature reduction of such catalysts produces a mobile suboxide species, TiO_x, which segregates to the surface from the bulk oxide, where it encapsulates the metal particles. However, the authors considered that the effects of encapsulation alone are insufficient to account for the entire SMSI effect observed; they suggested that enhanced electronic interaction between the metal and the suboxide, relative to fully oxidised TiO_2, also contributes to the SMSI effect. The idea that SMSI might arise from a combination of both encapsulation and electronic interactions between the metal and TiO_x suboxides has also been supported by Takatani and Chung[199]. These workers used Auger and vibrational spectroscopic techniques to investigate CO adsorption on high temperature reduced Ni/TiO_2 catalysts.

Tauster et al[147], in their original paper, also suggested that SMSI in titania-supported metal catalysts may result from the formation of intermetallic compounds, between the supported metal and the reduced oxide support. Sheng et al[200] have used a wide variety of analytical techniques to investigate high temperature reduced Pt/TiO_2, TiO_2/Pt and co-sputtered $Pt\text{-}TiO_2$ model catalysts. From the observations that the surfaces of these materials were enriched with, rather than depleted of, Pt and that TiO_x species ($x \sim 1$) diffused into Pt, it was postulated that SMSI

in Pt/TiO_2 catalysts arises from the formation of intermediate surface compounds of the type Pt_nTiO_x ($n > 1$, $x \sim 1$). The presence of hydrogen was thought to greatly facilitate the formation of such surface compounds. A similar conclusion has been reached by zur Loye and Stacy[201], who proposed that SMSI in high temperature reduced Ni/TiO_2 catalysts arises from the formation of a reduced ternary oxide of the type, Ni_yTiO_x.

The recovery of H_2 and CO chemisorptive capacity in $metal/TiO_2$ SMSI catalysts, by treatment in oxygen at high temperatures and followed by mild reduction in hydrogen at 400 - 500K, has been demonstrated by Tauster et al[147,202] and confirmed by many other workers. Obviously, the process by which SMSI is destroyed the oxidation/reduction procedure depends upon the mechanism by which the SMSI effect is initially generated. Thus, workers favouring the encapsulation model or formation of intermetallic surface compounds have proposed that SMSI is destroyed by re-oxidation of TiO_x suboxide to TiO_2, with the concomitant liberation of the supported metal. On the other hand, workers favouring the electron charge transfer model of SMSI postulate that electron density is transferred from the metal back to the support during re-oxidation.

In summary, high temperature reduction of $metal/TiO_2$ catalysts results in a strong metal - support interaction, characterised by a severe depression in the H_2 and CO chemisorptive capacity of these catalysts. SMSI appears to be a complex phenomenon, the exact origin of which remains unclear. Although the literature contains much conflicting evidence, it seems likely that a variety of factors, including metal morphology, electronic perturbations and suboxide encapsulation of the metal,

play a role in the generation of SMSI. The situation is further complicated by the fact that the dominant cause of SMSI would seem to vary according to the metal/TiO_2 catalyst, the method of preparation and the analytical techniques used to investigate the SMSI effect.

Apart from suppressing H_2 and CO chemisorption, SMSI has a marked effect on the catalytic properties of TiO_2-supported metal catalysts, particularly with respect to structure-sensitive reactions such as alkane hydrogenolysis[203-205] and CO hydrogenation[206-208]. A review of the literature, up to mid-1982, concerning the nature, possible origins and influence on catalytic properties of metal/TiO_2 catalysts, of SMSI has been conducted by Bond and Burch[209]. However, the effect of SMSI on the catalytic properties of TiO_2-supported metal catalysts will be discussed in more detail, in relation to the results obtained during the course of this research project, at a later stage.

1.6 Photocatalysis on Metallised TiO_2

This section briefly reviews photocatalysis by supported metals, with particular emphasis on Pt/TiO_2 catalysts. In addition to metal - support interaction studies, a large proportion of the work on metal/TiO_2 catalysts has been carried out in the context of photon-to-chemical energy conversion, with respect to potential solar energy devices. Focus has centred on hydrogen production via various photo-assisted reactions,

including gas-phase[210,211] and liquid-phase[212,213] alcohol dehydrogenation, hydrazine dehydrogenation[214,215] photo-electrochemical water cleavage[216-218] and CO oxidation by water[219,220].

The photo-electrochemical (PEC) cleavage of water using pure and metallised semiconductor oxides, particularly TiO_2, in the context of alternative energy sources, has received considerable attention in recent years. Fujishima and Honda[216] reported the photodecomposition of water using a PEC cell incorporating a TiO_2 photo-anode and a Pt black cathode. The following mechanism involving photohole trapping by water molecules at the titania electrode to form molecular oxygen and protons was proposed:

$$TiO_2 + h\upsilon \longrightarrow h^+ + e^- \quad [34]$$

$$4h^+ + 2H_2O \longrightarrow O_{2(g)} + 4H^+ \quad [35]$$

Protons then migrate to the Pt electrode where they combine with electrons to form molecular hydrogen:

$$2e^- + 2H^+ \longrightarrow H_{2(g)} \quad [36]$$

Overall, the reaction is:

$$H_2O + 4h\upsilon \longrightarrow O_{2(g)} + 2H_{2(g)} \quad [37]$$

However, metallised semiconductor oxide photocatalysts have several advantages over PEC cells, not least that they are cheaper to construct and can be made with large surface areas. Bard[221] considered that a particle of platinised TiO_2 is analogous to a short-circuited PEC cell, where reactions occur by photogenerated electrons and holes at two different sites on the particle surface. Sato and White[222] reported that the photo-

decomposition of water could be achieved at 298K, by use of UV-illuminated Pt/TiO_2 catalysts. They found that a steady-state condition was rapidly reached, in which the rate of catalytic recombination of O_2 and H_2 at the metal sites equalled the rate of water photodecomposition. In a further study by the same workers[223], it was revealed that catalytic water reformation on Pt metal could be significantly reduced by coating the catalyst with NaOH.

Grätzel and co-workers[217,224,225] developed a bi-functional redox catalyst consisting of ultrafine deposits of Pt and RuO_2 supported on colloidal TiO_2. Band-gap irradiation of this catalyst resulted in efficient photodecomposition of water. It was proposed that water decomposition at the Pt deposits occurs via photo-electron trapping, whilst the RuO_2 deposits facilitate photohole transfer from the semiconductor valence band to species in solution. Sensitisation of the $Pt/RuO_2/TiO_2$ catalyst using the tris-chelate ruthenium complex, $[Ru(bpy)_3]^{2+}$ - where (bpy) represents the 2,2'-bipyridyl group - enables water photodecomposition to be achieved using visible, rather than UV, light. Furthermore, the addition of an electron relay, namely methyl viologen, significantly increased the hydrogen yield. Laser photolysis and conductance experiments[226,227] revealed that positive hole transfer from $[Ru(bpy)_3]^{2+}$ ions to the catalyst particle is accompanied by proton release from water molecules. Furthermore, it was found that only surface-adsorbed species could act as electron and hole scavengers. A number of reviews describing the UV and visible light-induced cleavage of water and photo-electrochemical aspects of solar energy conversion have been published[154,228-232].

The yield of hydrogen from the photodecomposition of water, using metallised titania catalysts, can be improved by the removal of monatomic oxygen generated during the reaction. This can be achieved by the addition of CO, which is subsequently oxidised to CO_2 according to the equation:

$$H_2O_{(g)} + CO_{(g)} + h\upsilon \longrightarrow CO_{2(g)} + H_{2(g)} \qquad [38]$$

The above reaction is known as the *water-gas shift (WGS) reaction*. Fang et al[233] investigated how catalyst preparation and reaction parameters influence the rate of the WGS reaction. They found that the rate of reaction does not depend upon either the method of Pt deposition or the Pt loading, above 2 mass%, and that the rate is first-order with respect to light intensity. The extent of reduction and the surface concentration of NaOH was found to affect the reaction rate considerably. It was concluded that when NaOH is present on the catalyst surface, the overall reaction rate is determined by the rate of photohole trapping by surface hydroxyl anions. Sato and White[219] proposed a mechanism for the WGS reaction involving photohole trapping by surface water molecules and hydroxyl groups:

$$h^+ + H_2O_{(s)} \longrightarrow OH_{(ads)} + H^+ \qquad [39]$$

$$h^+ + OH_{(ads)} \longrightarrow O_{(ads)} + H^+ \qquad [40]$$

$$CO_{(ads)} + OH_{(ads)} \longrightarrow CO_{2(g)} + H_{(ads)} \qquad [41]$$

$$CO_{(ads)} + O_{(ads)} \longrightarrow CO_{2(g)} \qquad [42]$$

$$2H^+ + 2e^- \longrightarrow 2H_{(ads)} \longrightarrow H_{2(g)} \qquad [43]$$

Tsai et al[220] have studied the WGS reaction over UV-illuminated Pt/TiO_2 model catalysts, prepared by deposition of the metal onto a sliced TiO_2 single crystal exhibiting {100} orientation. They concluded that photo-reduction of the support at Pt/TiO_2 peripheral sites is the rate-determining step, according to the mechanism:

$$\{Pt\ Ti^{4+}\ O^{2-}\} + 2h^+ + CO_{(ads)} \longrightarrow \{Pt\ Ti^{4+}\ \square_s\} + CO_{2(g)} \qquad [44]$$

$$\{Pt\ Ti^{4+}\ \square_s\} + H_2O_{(ads)} + 2e^- \longrightarrow \{Pt\ Ti^{4+}\ O^{2-}\} + H_{2(g)} \qquad [45]$$

- where $\{Pt\ Ti^{4+}\ O^{2-}\}$ represents a Pt/TiO_2 peripheral site and $\square_s$ represents a surface oxygen vacancy.

Sato and White[234,235] have also investigated the photocatalytic reaction of gas-phase water with active carbon and ethylene over platinised TiO_2. With active carbon, CO_2 and H_2, and a small quantity of O_2, are evolved, although it was found that the reaction rate declines with time. This was thought to be due to hydrogen accumulation and the loss of good contact between the catalyst and the carbon reactant. In the presence of liquid-phase water, the oxidation of carbon is inhibited and O_2 and H_2 are evolved. The reaction between gas-phase water and ethylene was observed to produce ethane, CO_2 and H_2 as the main reaction products, although a small amount of methane was also detected. A reaction mechanism involving the formation of OH radicals, via photohole trapping

by water molecules, was proposed to account for these experimental results.

Photocatalytic dehydrogenation of aliphatic alcohols over Pt/TiO_2 catalysts appears to occur in a similar manner to alcohol dehydration on pure TiO_2, in that alkoxide intermediates are presumed to be formed upon adsorption of the alcohol. Carbonyl product formation is then thought to occur via a radical mechanism, initiated by photohole trapping at negatively-charged surface species. It is generally agreed that this process is enhanced by photo-electron capture at surface Pt deposits, represented as $(Pt_s)^-$, which consequently reduces the extent of photohole and photo-electron loss by non-radiative recombination processes. However, the nature of the photohole trapping surface species, and hence the complete reaction mechanism, remains unclear. Pichat et al[148] proposed a mechanism for propan-2-ol dehydrogenation over UV-illuminated Pt/TiO_2, in which the adsorbed isopropoxide anion acts as the photohole trap:

$$TiO_2 + h\upsilon \longrightarrow h^+ + e^- \qquad [46]$$

$$Me_2CHO^-_{(ads)} + h^+ \longrightarrow Me_2C\dot{H}O_{(ads)} \qquad [47]$$

Propanone formation then occurs by unimolecular hydrogen atom loss:

$$Me_2C\dot{H}O_{(ads)} \longrightarrow Me_2CO_{(ads)} + H_{(ads)} \qquad [48]$$

Further dissociative chemisorption of propan-2-ol regenerates isopropoxide, with the concomitant release of protons:

$$Me_2CHOH \longrightarrow Me_2CHO^-_{(ads)} + H^+_{(ads)} \qquad [49]$$

The role of $(Pt_s)^-$ is thought to be in converting protons to H atoms, which then combine to evolve H_2 in a process which is essentially the reverse of hydrogen spillover:

$$(Pt_s)^- + H^+_{(ads)} + H_{(ads)} \longrightarrow (Pt_s)\begin{matrix}H\\|\\H\end{matrix} \longrightarrow (Pt_s) + H_{2(g)} \qquad [50]$$

Although given for propan-2-ol dehydrogenation, the above reaction mechanism is equally applicable to the photocatalytic dehydrogenation of other aliphatic alcohols. On the basis of the mechanism, a limiting quantum yield of unity would be expected since absorption of one photon results in the formation of one carbonyl molecule. However, Hussein and Rudham[213] found a limiting quantum yield of only 0.5 for the photocatalytic dehydrogenation of various aliphatic alcohols over UV-illuminated Pt/TiO_2. The authors considered that there is no direct evidence for photohole trapping by surface-adsorbed alkoxide anions and, therefore, postulated a mechanism in which surface hydroxyl anions act as photohole traps:

$$OH^-_{(s)} + h^+ \longrightarrow \dot{O}H_{(s)} \qquad [51]$$

Following interaction of the hydroxy radical with propan-2-ol:

$$Me_2CHOH + \dot{O}H_{(s)} \longrightarrow Me_2C\dot{H}O_{(ads)} + H_2O_{(ads)} \qquad [52]$$

propanone formation, with a limiting quantum yield of 0.5, could occur either by:

$$2Me_2CH\dot{O}_{(ads)} \longrightarrow Me_2CO + Me_2CHOH \qquad [53]$$

or by:

$$Me_2CH\dot{O}_{(ads)} + \dot{O}H_{(s)} \longrightarrow Me_2CO + H_2O \qquad [54]$$

Surface hydroxyl ions are then regenerated by interaction of water with $(Pt_s)^-$:

$$(Pt_s)^- + H_2O \longrightarrow (Pt_s)\ H + OH^-_{(s)} \qquad [55]$$

$$2(Pt_s)\text{—}H \longrightarrow (Pt_s) + H_{2(g)} \qquad [56]$$

Thus, there are two possible mechanisms for the photocatalytic dehydrogenation of simple aliphatic alcohols over Pt/TiO_2 catalysts, each determined by the manner in which photoholes are trapped. However, it appears to be difficult to decide which mechanism actually occur because the rate-determining step is normally that of photo-electron transport from the bulk to the surface of the oxide support.

1.7 The Present Work

This thesis reports an investigation into the performance of various TiO_2-supported metal catalysts, prepared by photodeposition. A platinised TiO_2 catalyst, prepared by impregnation/reduction, was used as a comparative reference to aid assessment of the behaviour of the photo-deposited materials. The bulk of the work has concentrated on the thermal hydrogenation of propene and cyclopropane in the gas-phase, although the liquid-phase dehydrogenation of propan-2-ol has also been briefly investigated for all catalysts. The project work has been directed towards answering the following questions:

1. Does the method of preparation of TiO_2-supported metal catalysts effect their subsequent performance, and if so, why?
2. Does the nature of the supported metal, and the extent of loading, have any affect on catalyst activity and stability?
3. What effects arise by changing the crystalline habit of the TiO_2 support?
4. What are the mechanisms of the gas-phase hydrogenation of propene and cyclopropane over metal/TiO_2 catalysts?

An ultra-high vacuum system was used for the hydrogenation studies, with analysis of reactant-product mixtures being achieved by means of mass spectrometry. A microcomputer system, the development of which is reported in this thesis, was employed to determine hydrogenation reaction rates via pressure measurements.

CHAPTER 2 - EXPERIMENTAL

2.1 Gas-Phase Experimental Apparatus

The experimental vacuum system used to study gas-phase thermal catalytic reactions was divided into two distinct parts. The first part comprised a high vacuum gas purification, storage and dosing system, whilst the second part comprised an ultra-high vacuum (UHV) system, containing the catalytic reactor and associated data collection instruments. More detailed descriptions of each part of the vacuum system, including their operation, are given below.

2.1.1 The High Vacuum System

A detailed schematic representation of this system, constructed from hard Pyrex glass, is shown in Fig. 2.1. The vacuum was achieved using Jencons electric type 1 two-stage mercury diffusion pumps, backed by Speedivac 2S2 OB rotary oil pumps. Liquid nitrogen cold traps were used to prevent contamination of the system by backstreaming of either oil or mercury vapour. Edwards IG5G ion gauges were used to measure base vacua, which were typically 5 - 8 x 10^{-7} kPa. Ground glass taps, lubricated with Apiezon 'N' grease, were used throughout the system.

As shown in Fig. 2.1, the top line comprised 3dm^3 storage bulbs for the reactant gases, all of which, apart from hydrogen, were purified prior to storage via a "freeze-pump-thaw" method. In this procedure, the gas to be purified was condensed to the solid phase by cooling to liquid

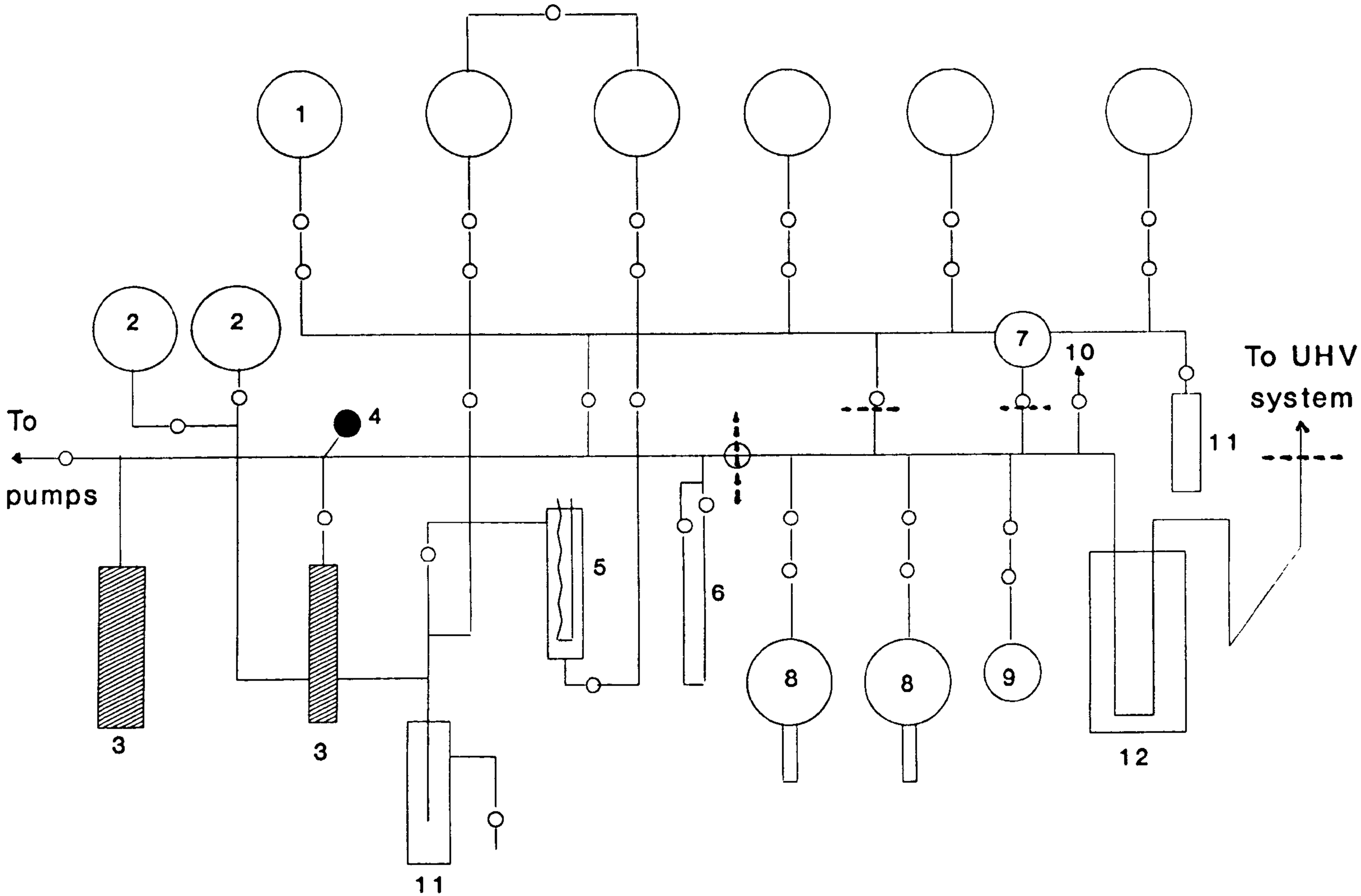

1 - 31 storage bulbs
2 - 3l ballsat bulbs
3 - liquid nitrogen trap
4 - Edwards IG5G ion gauge
5 - palladium thimble
6 - Hg manometer
7 - known volume bulb (1058.8)
8 - 3l reaction gas bulbs
9 - 1l He bulb
10 - pressure transducer
11 - cold finger
12 - dry ice / acetone slush bath

○ - Apiezon 'N' greased glass taps

••••• - volume of gas dosing line (= 0.480l)

Fig. 2.1: Schematic Representation of the High Vacuum Gas Storage and Dosing System

nitrogen temperature (77K), enabling the more volatile contaminants to be pumped away, and then allowed to evaporate again. This cycle was repeated at least three times. Hydrogen gas was purified by allowing it to diffuse slowly through an electrically-heated palladium thimble. Since a high positive pressure of gas was required to maintain the diffusion process, the impure hydrogen was stored prior to purification in two $3dm^3$ ballast bulbs at pressures slightly above atmospheric pressure. Research grade helium and CO were supplied in $1dm^3$ bulbs, fitted with glass breaker seals, which were glassblown directly onto the vacuum system. Hydrocarbon/H_2 mixtures for reaction purposes were prepared and stored in two $3dm^3$ bulbs on the lower line, by condensing a known pressure of hydrocarbon gas in the finger of the bulb at 77K and then placing a known pressure of H_2 above the solid gas. By using this procedure, the hydrocarbon/H_2 ratio could be varied as desired. Known pressures of the mixed gases were placed in the gas dosing line, which were then allowed to expand into the UHV system where the catalyst sample was situated. For the high vacuum system, all pressure measurements were obtained by use of pressure transducers, previously calibrated against mercury manometers.

2.1.2 The Ultra-High Vacuum System

Detailed schematic representations of this system and the catalytic reactor are shown in Figs. 2.2 and 2.3, respectively. For gas-phase hydrogenation studies, all glassware was constructed from wide-bore

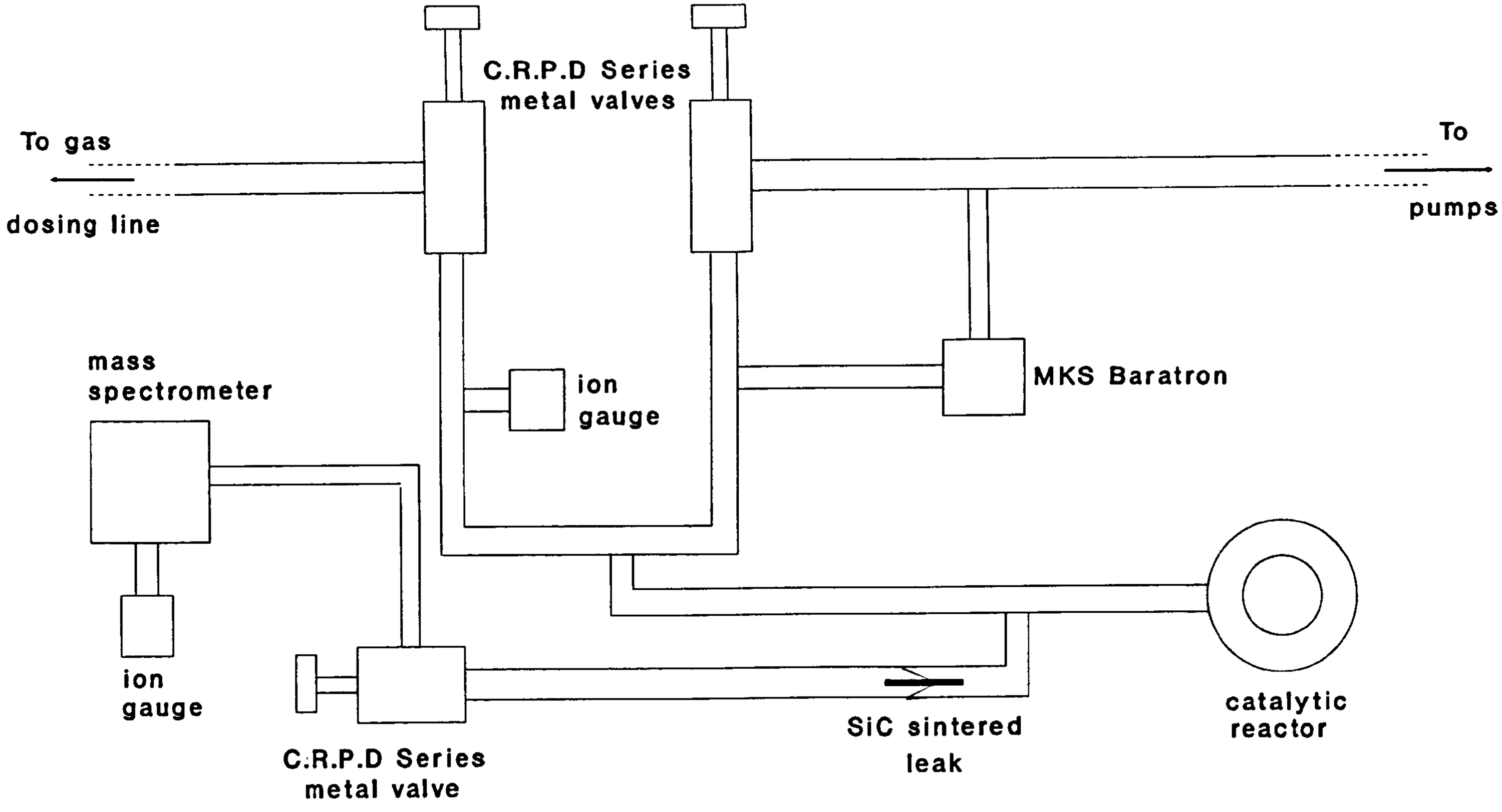

Fig. 2.2: Schematic Representation of the Ultra-High Vacuum System (Plan View)

hard Pyrex in order to facilitate efficient pumping of the system. Vacua were achieved by means of two Jencons electric type 1 two-stage mercury diffusion pumps in series, backed by a Speedivac 2S2 OB rotary oil pump. Contamination of the system was prevented by use of two liquid nitrogen cold traps. The whole system was mounted on a heat-resistant asbestos cement table, along the edges of which were mounted four 1kW heating elements. An insulated oven, suspended above the system by a counterweighted chain, could be lowered onto the table to facilitate baking of the system. Following a full 'bake-out' (~600K, 18hrs) using this set-up, typical base vacua of 4 - 6 x 10^{-8} kPa were obtained, as measured using a Mullard IOG22 ion gauge. As shown in Fig. 2.2, the UHV system could be isolated from both the high vacuum dosing line and the pump system by means of two Vacuum Generators C.R.P.D Series metal valves with glass tubulations.

Fig. 2.3 shows a schematic representation of the catalytic reactor, which comprised two parts; an outer Pyrex glass sleeve and a hollow Pyrex glass inner tube, terminating in a small cradle in which the catalyst sample was held. The two parts were coupled together by means of two Vacuum Generators metal-to-glass tubulation flanges, fitted with an internal copper gasket to ensure an effective seal. This arrangement allowed a chromel-alumel thermocouple to be in contact with the catalyst cradle, thereby enabling accurate measurements of the catalyst temperature. The flange connection part of the reactor was supported on a small metal plate, with the remainder, including the catalyst cradle, projecting below the asbestos cement table. This configuration enabled the catalyst sample

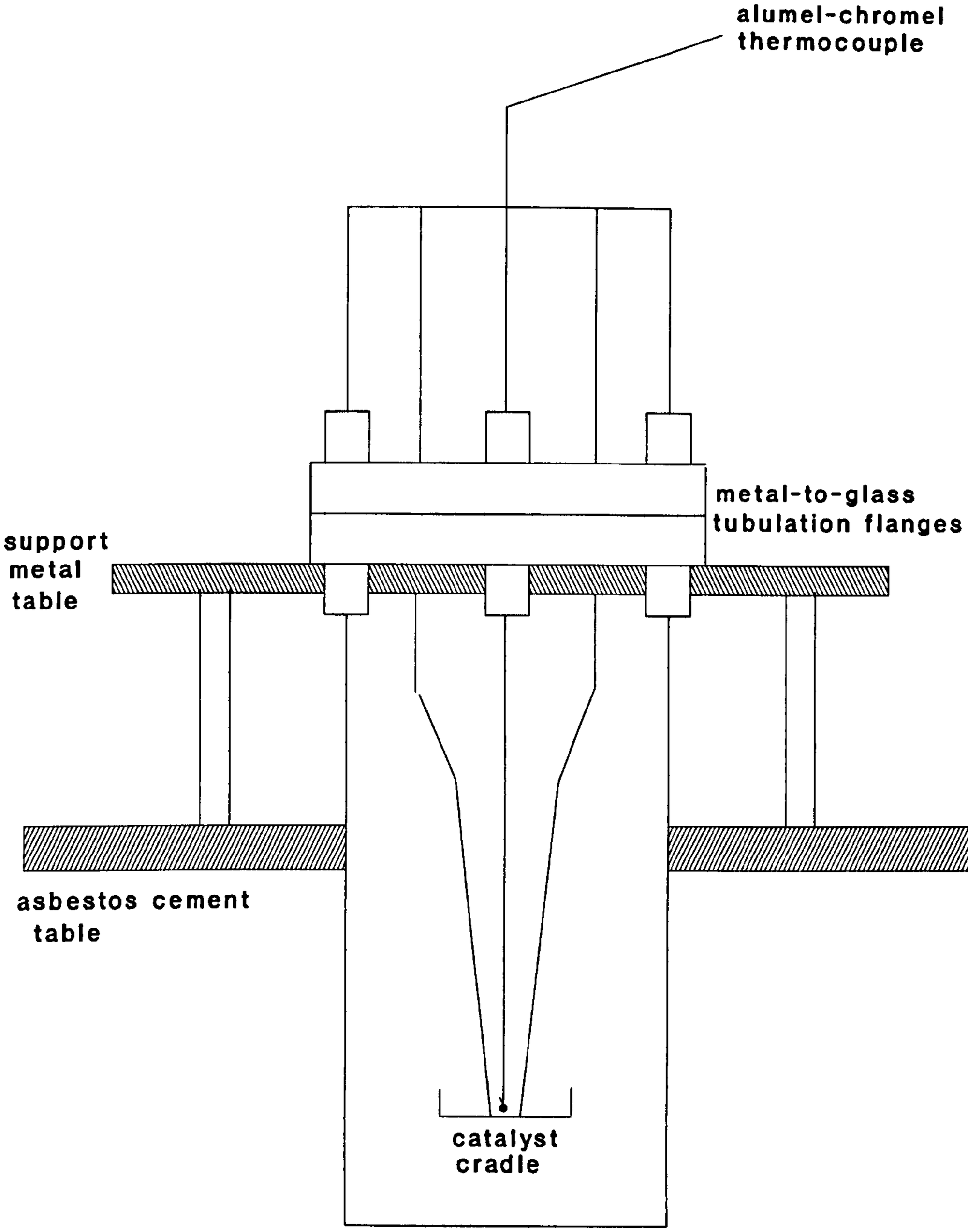

Fig. 2.3: Schematic Representation of the Catalytic Reactor (Side View)

to be heated independently by means of either a water-jacket or an electric furnace.

2.1.3 Pressure Measurements and Product Analysis

Measurement of gas pressures within the UHV system were made using an MKS Instruments Baratron, (Type 170M-6C Electronic Control Unit; Type 170M-27D Digital Readout Unit), fitted with a differential STD-315 bakeable head. Throughout this project, pressure readings from the Baratron were automatically recorded at set time intervals using a microcomputer system. Initially, the analogue output of the Baratron was measured by use of a calibrated Keithley Instruments 177 Microvolt DMM digital voltmeter, interfaced by means of an IEEE 488 board to a Commodore 4302 PET microcomputer, with associated Commodore 4023 dot matrix printer and 4040 dual floppy diskette drive. However, it was found that a computer system of greater speed and sensitivity was necessary to record and process the Baratron output signal in a satisfactory manner. The preferred system comprised a Control Universal Cuban-12A analogue-to-digital integrating board, operating in Real Time BASIC, interfaced to a BBC Master Series microcomputer via a Beebex i/o board, along the 1MHz bus. The Baratron analogue output signal was attenuated from 10V to 4V maximum, the limit of the Cuban-12A board, via a voltage divider. A UFD 80/40 track dual floppy diskette drive unit and an Epson LX-800 dot matrix printer were the associated peripheral devices. The software driver

for the Cuban-12A, a mixture of Real Time Basic and 6507 assembly language, is given in Appendix 1.

Analysis of reactant and product gases during catalytic experiments was achieved by use of an Associated Electronic Instruments MS10 mass spectrometer, connected to the UHV system via a Metrosil fine sintered SiC leak. A Vacuum Generators C.R.P.D Series metal valve, with glass tubulations, was used to isolate the mass spectrometer from the vacuum system. The mass spectrometer vacuum was maintained by an integral Apiezon B.S. oil diffusion pump, backed by a Speedivac 2S2 OB rotary oil pump. Vacua, as measured by an Edwards IG5G ion gauge, were approximately 1 x 10^{-8} kPa, following a full 'bake-out' of the system. Analysis of gas-phase species by the instrument was achieved by varying the accelerating voltage and positive ions in the mass/charge (m/e) range of 2 - 100 could be detected. Gas molecules were ionised by a 7.65eV electron beam, generated by a hot rhenium filament, and then trapped by a 10μA ion trap current. Mass spectrographs were recorded by feeding the analogue output signal of the mass spectrometer to a Tekman TE200 Series single pen chart recorder.

2.1.4 Measurement of the Volume of the UHV System

The above measurement was carried out using the following procedure. A known pressure, P_1, of pure helium was placed in the gas dosing line, between the points marked in Fig. 2.1, corresponding to an unknown volume, V_1. The gas was then expanded into a bulb of known

volume (1.059dm^3), giving a new pressure, P_2, in volume, V_2. Volume V_2 was then calculated using Boyle's Law:

$$P_1V_1 = P_2V_2 \quad [57]$$

where:

$$V_1 = V_2 - 1.059 \quad [58]$$

giving:

$$P_1(V_2 - 1.059) = P_2V_2 \quad [59]$$

enabling volume V_1 to be found. The gas was then expanded into the UHV system, giving a new pressure, P_3 and the volume of the UHV system, V_3 calculated from the equation:

$$P_2V_2 = P_3V_3 \quad [60]$$

The values of V_1 and V_3 were then re-calculated by reversing the measurement process and expanding helium, at a known pressure, from the UHV system into the gas dosing line. The calculated average volumes of the gas dosing line, between the points marked in Fig. 2.1, and the UHV system were 0.480 ± 0.002 dm^3 and 0.670 ± 0.003 dm^3, respectively.

2.1.5 Temperature Programmed Desorption Apparatus

The UHV system, as represented in Fig. 2.2, served as the apparatus for temperature programmed desorption (TPD) experiments, although two modifications were made to the system prior to conducting these studies. Firstly, the lower part of the catalytic reactor was changed from

hard Pyrex glass to silica glass, enabling temperatures above 800K to be attained. Secondly, the SiC leak connecting the UHV system to the mass spectrometer was removed, enabling gas desorbed from the catalyst sample to be pumped directly through the spectrometer. A Eurotherm Type 812 programmable temperature controller was used to heat the catalyst sample at a controlled rate (K min^{-1}). The actual temperature of the catalyst was measured using a chromel-alumel thermocouple and monitored by the BBC Master Series microcomputer, via the Cuban-12A integrating card. The thermocouple signal was calibrated to either 5mV K^{-1} or 10mV K^{-1} by means of a voltage amplification circuit. The analogue output signal of the mass spectrometer, tuned to monitor the appropriate m/e signal, was also recorded by the microcomputer system, via the Cuban-12A integrating card, giving TPD profiles in terms of temperature (K) versus mass spectrometer signal (arbitrary units).

2.2 Liquid-Phase Experimental Apparatus

2.2.1 Photocatalytic Reactor Unit

The apparatus used for both the preparation of TiO_2-supported metal catalysts via photodeposition and for photocatalytic alcohol dehydrogenation studies is shown in Fig. 2.4. A Pyrex glass cylinder (25mm diameter, 80mm length), with a small side-arm (10mm diameter) fitted with a rubber septum cap to allow access to the reaction solution, served as the reactor vessel. A small glass paddle, driven by a Crouzet

82-330 synchronous motor operating at 600rpm, was used to maintain the solid material in suspension. An inert atmosphere of N_2 was maintained within the vessel by passing a slow flow of the gas through two small glass side-arms, situated at the top of the reactor. The lower half of the reactor vessel was held in a close-fitting, aluminium block, insulated with polystyrene. The temperature of this block, as measured by a chromel-alumel thermocouple, was controlled accurately by means of a frigister and associated electronic control unit. A slow flow of water through a jacket in contact with the frigister served as a heat sink. Previous measurements[124,125] have shown that a constant temperature, to ± 0.02K in the range 273 - 313K, could be achieved using this apparatus.

The ultraviolet (UV) radiation source was initially a Thorn ME/D 250W medium pressure mercury lamp, although a Woton Ultramed® 400W metal halide lamp was employed at a later stage. The spectral characteristics of both lamps are given in Fig. 2.5. The UV lamp was housed in a tall metal chimney, fitted with a Pyrex window, to help convect away heat generated by the lamp. With the 400W lamp, a small fan circulating air was utilised, to keep it within the specified operating temperature range. Two silica glass lenses, of focal length 50mm, were used to concentrate and focus the radiation into the centre of the reactor vessel. A heat filter, in the form of a Pyrex glass cylinder (50mm diameter, 100mm length) containing 2M ethanoic acid, was used to remove IR radiation from the incident light. For the photocatalytic alcohol dehydrogenation studies, UV light of wavelength > 316nm and < 400nm was isolated by use of a combination of soda glass and Chance OX1 filters.

The whole apparatus, except the associated electronic control units, was housed in a matt black wooden box, in order to minimise the effects of external air currents and radiation.

Reaction mixture analysis during photocatalytic alcohol dehydrogenation studies was conducted by use of a Pye Series 104 single flame ionisation detector gas-liquid chromatogram, (GLC). Separation of the reaction components was achieved using a 3.2m column of 10% polyethylene glycol 400 supported on Chromosorb W, maintained at 353K, with nitrogen, at a flow-rate of $1cm^3\ s^{-1}$, acting as the carrier gas. The ionisation flame was maintained by a flow of air, at a rate of $6.5cm^3\ s^{-1}$, and hydrogen, at a rate of $0.8cm^3\ s^{-1}$. The injection port and detector were kept at a constant temperature of 398K. Chromatograms were recorded by feeding the analogue output of the detector to a Tekman TE200 Series chart recorder.

2.2.2 Measurement of UV Lamp Intensity

The intensity of light from each UV lamp was measured using the standard technique of uranyl ethandioate actinometry[236-238], in which the photodecomposition of $H_2C_2O_4$ is sensitised by the presence of UO_2^{2+} ions. The actinometer solution consisted of uranyl sulphate hydrate, $UO_2.SO_4.3½H_2O$ (0.432g, 0.001M), and ethandioic acid dihydrate, $H_2C_2O_4.2H_2O$ (0.630g, 0.005M), dissolved in triply distilled water ($100cm^3$). Stirred portions of this solution ($25cm^3$) were irradiated with optically unfiltered light from the UV lamp at 298K, for 100 minutes,

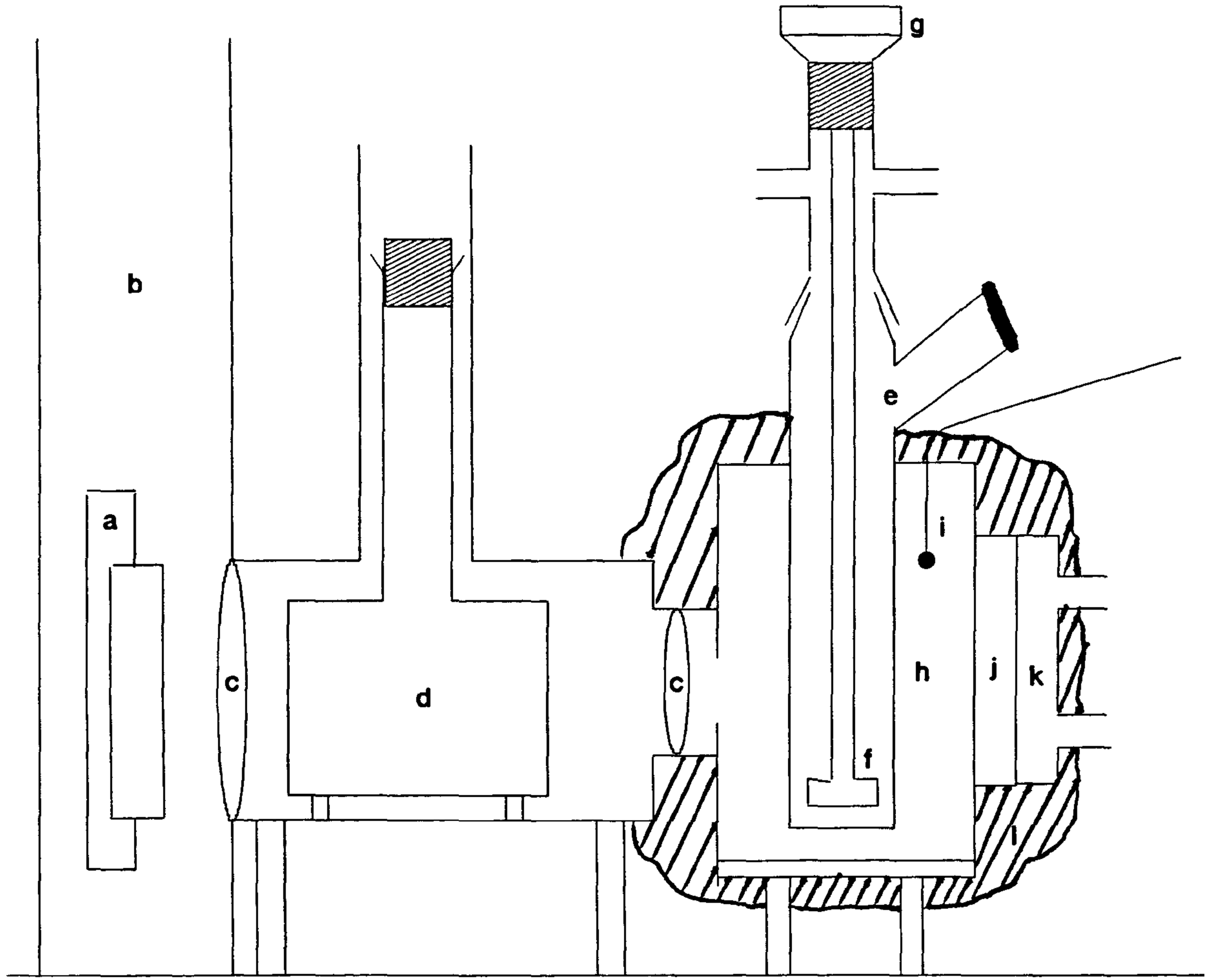

KEY

a - U.V. lamp

b - chimney

c - silica lens

d - heat filter

e - reaction vessel

f - stirrer

g - synchronous motor

h - aliminium block

i - thermocouple

j - frigister

k - water jacket

l- foam lagging

Figure 2.4: Photocatalytic Reactor Unit (Side View)

under a flowing O_2 atmosphere. Samples of the irradiated solution ($10cm^3$) were acidified with concentrated sulphuric acid ($3cm^3$) and then titrated, at 323 - 333K, with potassium permanganate solution, previously standardised by titration with a solution of ferrous ammonium sulphate hexahydrate, $FeSO_4.(NH_4)_2SO_4.6H_2O$, dissolved in 1% v/v concentrated sulphuric acid in triply distilled water. The net reaction is:

$$2MnO_4 + 5C_2O_4^{2-} + 8H^+ \longrightarrow 2Mn^{2+} + 4H_2O + 10CO_2 \qquad [61]$$

A similar titration procedure was repeated for non-irradiated samples of the actinometer solution and the difference in titres between the two solutions was used to calculate the amount of ethandioate consumed during irradiation, A, according to the equation:

$$A = V_1/1000 \times M \times 5/2 \times V_2/V_3 \qquad [62]$$

- where M = molarity of standardised $KMnO_4$ solution,

V_1 = difference between titres for irradiated and non-irradiated actinometer solutions (cm^3),

V_2 = volume of actinometer solution irradiated (cm^3),

V_3 = volume of actinometer solution titrated (cm^3).

The average intensity of radiation over the spectral range of the UV lamp, I_a, was then calculated using the equation:

$$I_a = A/\phi_o^a \times t \times (1-10^{-O.D.}) \qquad [63]$$

- where ϕ_o^a = average quantum yield for ethandioate loss over the spectral range of the lamp at 298K,

t = time of irradiation,

O.D. = average optical density of the actinometer solution over the spectral range of the lamp.

An average value of the quantum yield, ϕ_o^a, for ethandioate loss over the spectral range 255 - 435nm, at 298K, was calculated according to the equation:

$$\phi_o^a = (\Sigma\phi_o\lambda) / (\Sigma\lambda) \qquad [64]$$

$$= 0.563$$

as calculated using data from Ref. 236.

The average optical density of the uranyl ethandioate solution was measured using a Perkin-Elmer 522 UV-Vis spectrophotometer, in standard 10mm silica glass cells. This value was then corrected, in accordance with the Beer-Lambert law, for the internal path length of the reactor vessel, estimated to be 22mm.

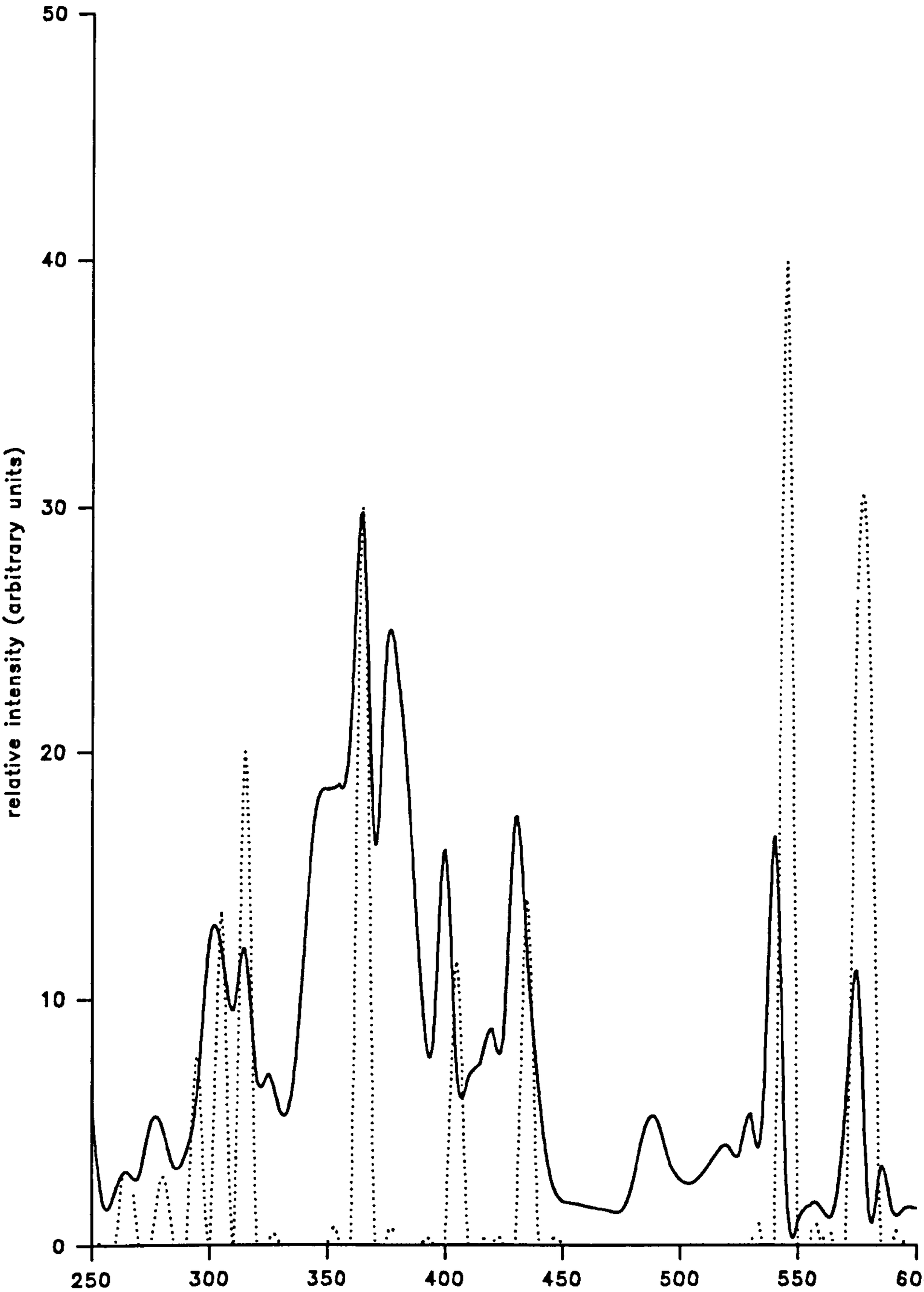

Figure 2.5: Spectral Characteristics of the Ultraviolet Lamps

2.3 Chemicals

Pure anatase TiO_2 (CLDD2078/1) Pure rutile TiO_2 (CLDD2078/2)	Tioxide UK Ltd.
P25 TiO_2	Degussa AG.
$KMnO_2$ (ARG) $FeSO_4.(NH_4)_2SO_4.6H_2O$ (ARG) $UO_2SO_4.3½H_2O$ (LRG)	BDH Ltd.
Ethandioic acid (LRG) 40% aqueous methanal solution (LRG)	East Anglia Chemicals.
Methanol (LRG) Propan-2-ol (ARG) Propanone (ARG) Diethylether (ARG)	May & Baker Ltd.
H_2PtCl_6 $Rh[(NH_3)_5Cl]Cl_2$ $IrCl_3.nH_2O$ (assay 49.77% Ir) H_2IrCl_6 (assay 44.50% Ir)	Johnson Matthey Ltd.
$PdCl_2$	Engelhard Ltd.
Oxygen (RG) Propene (RG)	Messer Grieshiem GmBH.
Carbon monoxide (RG) Helium (RG)	BOC Gases Ltd.
Propane (RG)	BDH Ltd.
Cyclopropane (RG)	Air Products Ltd.

H_2, N_2, O_2 and air supplied in cylinders by Air Products Ltd.

LRG = Laboratory Grade Reagent
ARG = Analytical Grade Reagent
RG = Research Grade

2.4 Catalyst Preparation

2.4.1 Origin of TiO_2 Supports

Three samples of TiO_2 were employed as supports for various metals. Pure anatase and pure rutile, with quoted surface areas of 63m^2 g^{-1} and 15m^2 g^{-1} respectively, were kindly supplied by Tioxide UK Ltd. The other sample, known as P25 TiO_2, was obtained from Degussa AG, with a quoted surface area of 50 ± 15m^2 g^{-1}. This material was mainly the anatase form of titania, but also contained a small percentage of the rutile phase. The physical and chemical characteristics of all three TiO_2 samples are given in Appendix 2.

2.4.2 Preparation of Metallised TiO_2 Catalysts by Photodeposition

Titania-supported metal catalysts were prepared using the photo-reactor described in Section 2.2.1, following a similar method to that described by Grätzel et al[224,225]. The soda glass and Chance OX1 filters were removed during the preparation procedure to allow the maximum intensity of radiation into the reaction vessel. Such catalysts were given the general designation of M(x)/S(P) - where M = Pt, Pd, Rh or Ir, x = %mass of supported metal, S = P25 TiO_2, anatase or rutile and (P) denotes preparation via photodeposition.

A known mass, approximately 2g, of TiO_2 was suspended, with continual stirring, in a solution comprising 40% aqueous methanal solution (20cm^3), methanol (5cm^3) and the appropriate volume of metal salt solution. The metal salt solutions and the conditions used for the prep-

aration of titania-supported metal catalysts via photodeposition are summarised in Table 2.1. The reaction slurry was maintained at 318K, under a flowing nitrogen atmosphere (0.5cm^3 s^{-1}), and irradiated with optically unfiltered UV light for 4 - 8 hours, until complete deposition of the metal, as determined by UV-visible spectrophotometry, had been achieved. Catalysts were then repeatedly washed with triply distilled water and centrifuged until all chloride ions had been removed, as indicated by a negative silver nitrate test. Drying at 383K for 24 hours yielded catalysts as light-to-dark grey powders, which were stored in Pyrex glass sample vials, under ambient atmosphere, for future use.

2.4.3 Preparation of Pt/TiO_2 by Impregnation/Reduction

0.5 %mass Pt supported on P25 TiO_2 - designated Pt(0.5)/P25(T) - was prepared by a method similar to that described by Pichat et al[148]. A known mass, approximately 2g, of P25 TiO_2 was suspended in triply distilled water (100cm^3) and the appropriate volume of 1%(w/v) H_2PtCl_6 in 0.1M HCl was added. The aqueous solvent was evaporated to dryness at 303K and the resulting impregnated solid dried at 393K for 2 hours. After transferring to the Pyrex glass vessel shown in Fig. 2.6, the solid was heated to 573K under a flowing N_2 atmosphere (0.5cm^3 s^{-1}) and then reduced in flowing H_2 (0.5cm^3 s^{-1}) at 753K for 16 hours. The resulting dark grey catalyst was allowed to cool to room temperature under flowing N_2 (0.5cm^3 s^{-1}) and then stored in a Pyrex glass sample vial, under ambient atmosphere, for future use.

Table 2.1 Photodeposition Conditions for Preparation of Titania-Supported Metal Catalysts

Metal (%mass)	Support	Precursor Metal Salt[a]	10^{-7}Intensity (moles s^{-1})	Irradiation Time (hrs)
Pt(0.25)	P25	H_2PtCl_6	2.62[c]	4
Pt(0.5)	P25	H_2PtCl_6	2.62	4
Pt(1.0)	P25	H_2PtCl_6	2.62	4
Pt(2.0)	P25	H_2PtCl_6	2.62	4
Pt(0.5)	anatase	H_2PtCl_6	2.62	5
Pt(0.5)	rutile	H_2PtCl_6	2.62	5
Pd(0.5)	P25	$PdCl_2$	2.62	4
Rh(0.5)	P25	$Rh[(NH_3)_5Cl]Cl_2$	2.62	8
Ir(0.5)[b]	P25	$IrCl_3$	2.62	12
Ir(0.5)	P25	H_2IrCl_6	4.31[d]	6

a) All metal salts were dissolved in 0.1M HCl, except the Rh salt which was dissolved in triply distilled water.

b) Although the photodeposition solution changed from pale yellow to colourless, during UV irradiation, UV-visible spectrophotometry suggested that much of the Ir species (peak = 195nm) remained in solution, even after a 12 hour irradiation period. Consequently, this material was not used for catalytic studies.

c) Thorn ME/D 250W medium pressure Hg lamp.

d) Woton Ultramed™ 400W metal halide lamp.

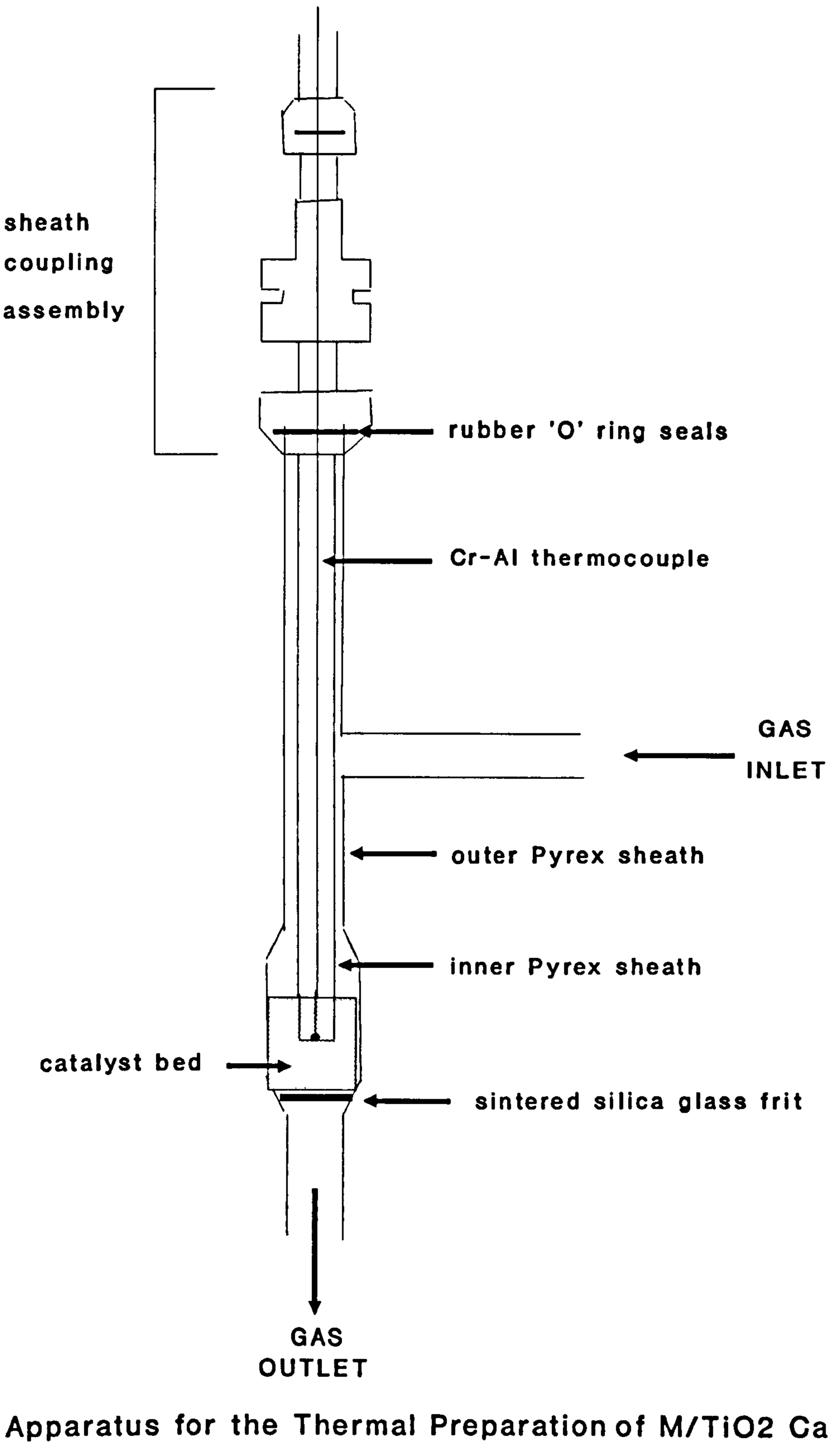

Figure 2.6: Apparatus for the Thermal Preparation of M/TiO2 Catalysts

2.5 Experimental Procedures

2.5.1 Gas-Phase Hydrogenation Reactions

Two gas-phase thermally catalysed reactions, propene and cyclopropane hydrogenation, were chosen in order to investigate the relative properties of metallised TiO_2 catalysts, prepared by photodeposition and impregnation/reduction. Propene hydrogenation was found to occur readily at room temperature, but cyclopropane hydrogenation required a higher reaction temperature to proceed at a comparable rate. Under the experimental conditions used, hydrogenation of both propene and cyclopropane over M/TiO_2 catalysts gave rise to propane as the sole reaction product. Repeated analysis of reaction mixtures using mass spectrometry, m/e range 2 - 60, failed to show any signs of side reactions occurring and it was assumed that in both reactions hydrogen consumption was due solely to addition of hydrogen to the reactant hydrocarbon gas. Initially pressure fall due to hydrogen consumption was monitored indirectly via the mass spectrometer, the data being interpreted in terms of first- and second-order reaction kinetics. However, this method proved unsatisfactory and a microcomputer-based system for monitoring the rate of hydrogen consumption was developed. Details of both procedures for following catalytic hydrogenation reactions are given below.

2.5.2 Analysis using the Mass Spectrometer

a) Calibration

Since both propene and cyclopropane hydrogenation, under the reaction conditions employed, gave rise to propane alone, it was more expedient to follow reactions in terms of product formation rather than reactant consumption. The mass spectral cracking patterns for propene, propane and cyclopropane are given in Table 2.2. The m/e 29 peak, present only in the mass spectrum of propane and being the most intense peak, was selected in order to follow rates of hydrogenation. Calibration of the mass spectrometer for propane, on x25, x100 and x250 attenuation ranges, was achieved by varying the propane pressure in the UHV system, with no catalyst present, and measuring the corresponding height of the m/e 29 peak. A good linear correlation between propane pressure (kPa) and m/e 29 peak height (mm), for all three attenuation ranges, was found, as shown in Fig. 2.7, allowing direct conversion of peak height to pressure.

b) Mathematical Treatment of Mass Spectral Data

Data obtained from the mass spectrometer were used to assess the order of reaction for propene and cyclopropane hydrogenations in the following manner:

$$P_{t(propane)} = \text{(m/e peak height)} \times \text{(calibration factor)} \quad [65]$$

$$P_{i(total)} = P_{i(hc)} + P_{i(h)} = \text{initial total pressure} \quad [66]$$

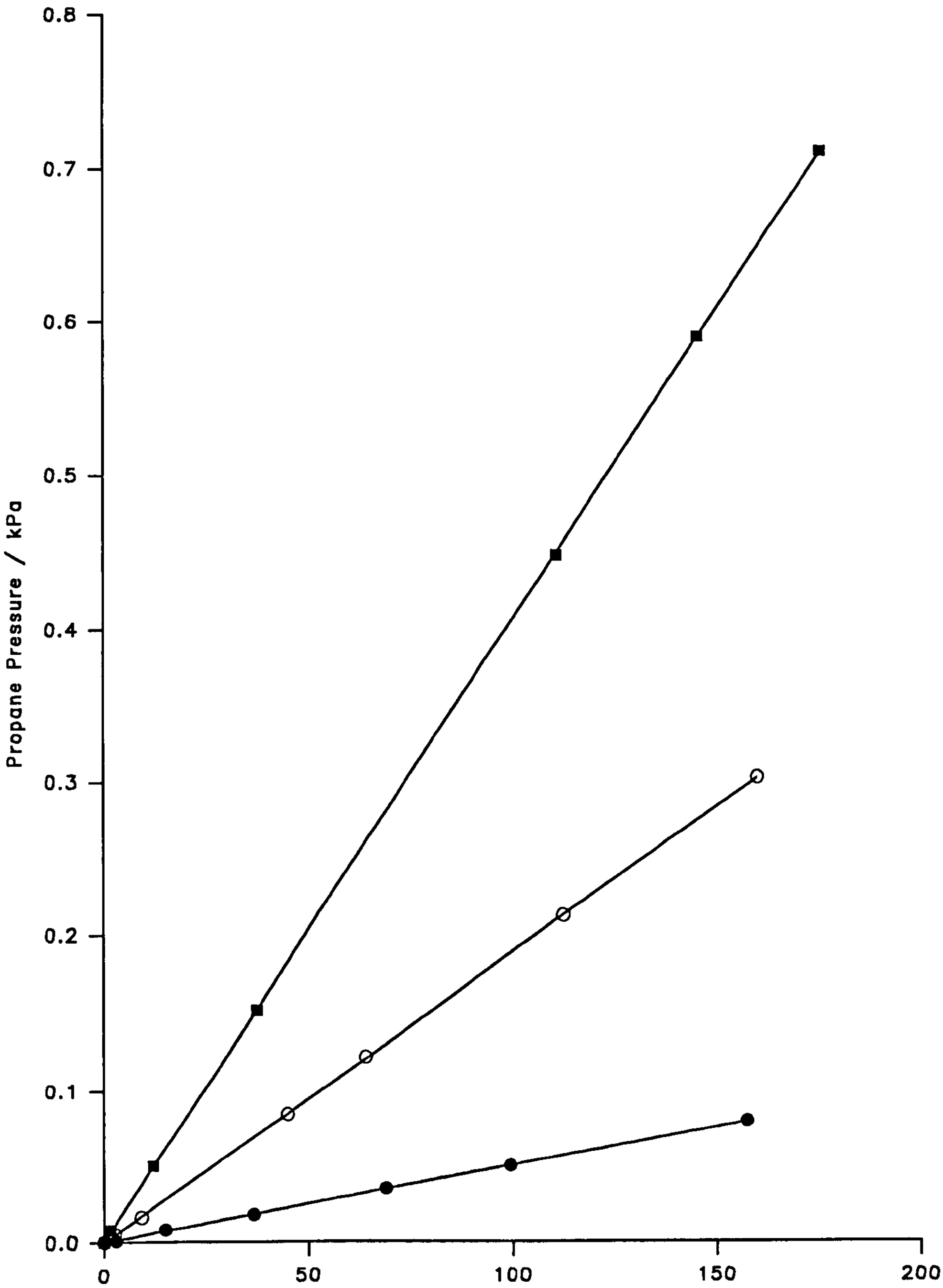

Figure 2.7: Calibration Plots for the Determination of Propane Pressures in the Ultra–High Vacuum System via Mass Spectrometer Response (m/e = 29)

- where $P_{t(propane)}$ = propane partial pressure at time,t (kPa),

$P_{i(hc)}$ = initial hydrocarbon partial pressure (kPa),

$P_{i(h)}$ = initial hydrogen partial pressure (kPa).

If $P_{i(total)}$ is known, then:

$$P_{i(hc)} = [X/(X+Y)]P_{i(total)} \quad [67]$$

$$P_{i(h)} = [Y/(X+Y)]P_{i(total)} \quad [68]$$

- where X and Y are the respective partial pressures (kPa) of hydrocarbon and hydrogen in the stored gas mixture.

The rate of formation of propane was then converted to the rate of consumption of hydrocarbon via:

$$P_{t(hc)} = P_{i(hc)} - P_{t(propane)} \quad [69]$$

This data was then used to calculate the order of reaction with respect to propene and cyclopropane for the catalytic hydrogenation reactions.

2.5.3 Analysis by Direct Pressure Measurement

In this method of analysis, pressure changes due to hydrogen consumption were monitored by feeding the output signal of the Baratron directly to a microcomputer system, as described in Section 2.3.1.

a) Calibration

The Keithley 177 digital voltmeter and the Cuban-12A analogue-to-digital board were calibrated against the Baratron by varying the pressure of hydrogen gas in the UHV system, with no catalyst present, and recording the corresponding output voltage. In the case of the Cuban-12A

Table 2.2 Major Mass Spectral Cracking Patterns for Propene, Propane and Cyclopropane
(Source: American Petroleum Research Institute Project 44)

m/e ratio	Relative Intensity (*for ionisation voltage of 50V*)		
	Propene	Cyclopropane	Propane
1	3.21	3.02	1.41
12	0.88	1.02	-
13	1.43	1.91	-
14	3.44	5.99	1.78
15	5.52	5.40	5.90
19	2.18	2.33	-
20	1.84	1.88	-
25	1.77	1.77	-
26	10.5	12.7	8.22
27	38.7	35.0	40.3
28	1.42	2.45	59.5
29	-	-	100.
30	-	-	2.19
36	1.83	1.46	-
37	12.7	9.92	2.63
38	19.4	14.4	4.66
39	72.5	67.2	17.5
40	29.1	31.4	2.63
41	100.	88.7	12.9
42	70.3	100.	5.86
43	2.30	3.33	23.1
44	-	-	29.2

board, it was necessary to attenuate the output of the Baratron from 10V to 4V maximum by means of an appropriate voltage divider. A good linear correlation between pressure and measured voltage was found for both the Keithley 177 voltmeter and the Cuban-12A board, as shown in Fig. 2.8.

b) Mathematical Treatment of Baratron Data

For both the Commodore PET and the BBC Master Series micro-computer systems, BASIC programs were written in which the overall experiment time and the sampling interval could be varied as desired. The data collected was then fitted to a polynomial of general formula:

$$P_t = a_1 + a_2t + a_3t^2 + a_4t^3 \text{ ---------- } + a_it^{i-1} \qquad [70]$$

- where P_t = total pressure at time,t and a_1, a_2 .... a_i are constants. Any order of polynomial, within the confines of computer capacity, could be calculated and a comparison between calculated and experimentally measured pressures was used to help assess the best-fit polynomial. From co-efficient a_1, corresponding to the total initial pressure, the initial pressures of hydrocarbon and hydrogen could be calculated accurately. Differentiation of the polynomial, with respect to time, allowed co-efficient a_2, corresponding to the initial rate of reaction at time zero (kPa s^{-1}), to be found. This value was then used to calculate absolute initial rates of reaction, expressed in molecules s^{-1} g^{-1} catalyst, according to Eq.[73].

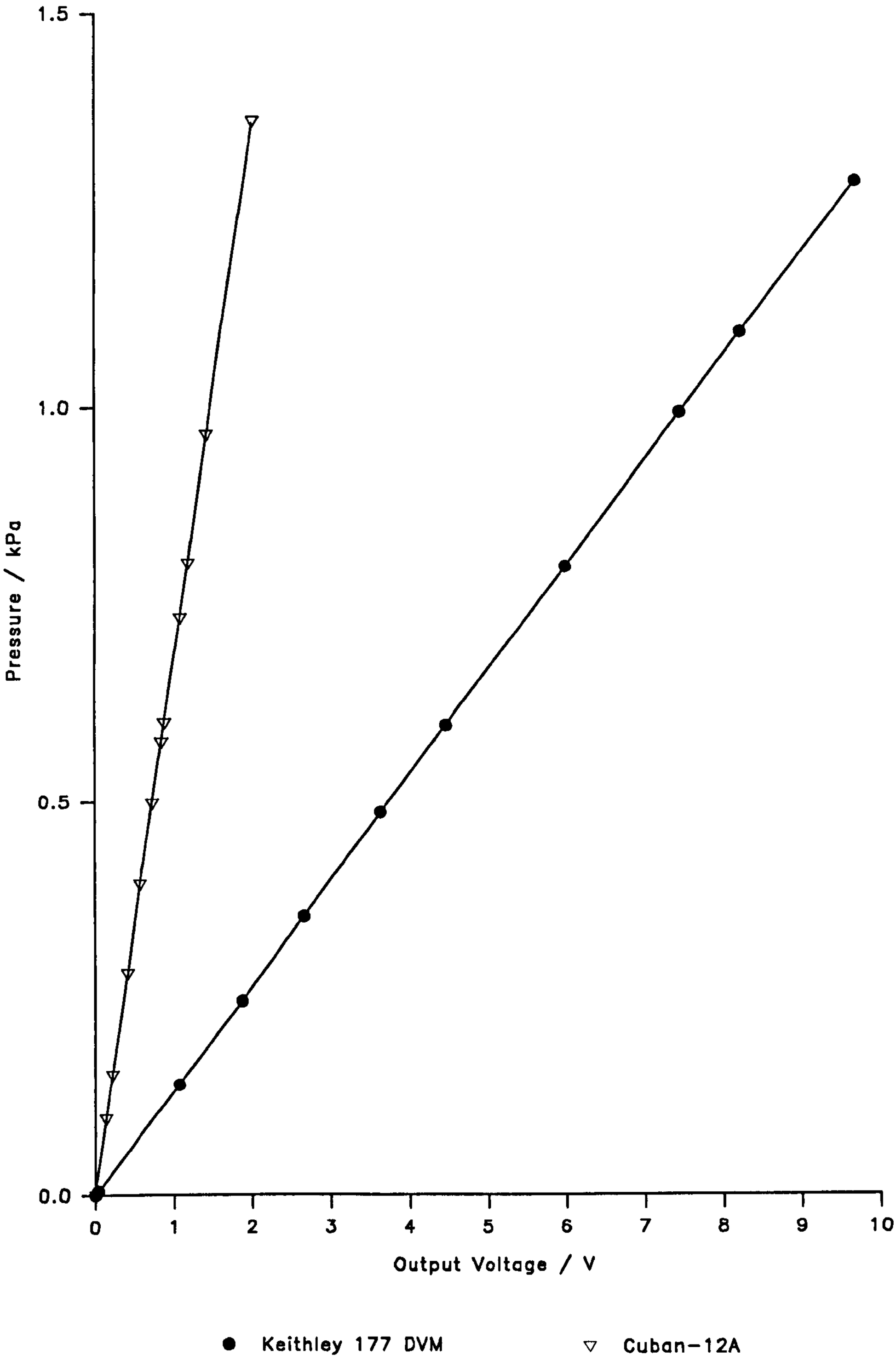

Figure 2.8: Calibration Plots for the Determination of Gas Pressure within the Ultra-High Vacuum System via a Keithley 177 DVM Voltmeter and a Cuban-12A Analogue-to-Digital Integrating Card

2.5.4 Reaction Procedures

The same general reaction procedure was used for all gas-phase catalytic hydrogenation studies. A known mass of catalyst was placed in the cradle of the reactor and the UHV system was then baked overnight to obtain a good vacuum, which was checked by pressure measurements and by recording a background mass spectrum. The catalyst was then raised to the required reaction temperature and allowed to equilibrate for at least 30 minutes. Where no further surface pretreatment was given, presorbed gases were removed from the catalyst surface by dosing the system with the hydrocarbon/H_2 mixture being used, to a pressure of about 1kPa, for 10 minutes. The system was then pumped down again for 30 minutes, prior to commencing the experiment. A known pressure of the hydrocarbon/H_2 mixture, as measured by the calibrated pressure transducer, was placed in the high vacuum dosing line, between the points marked in Fig. 2.1, and then expanded into the UHV system. Reaction progress was monitored using the mass spectrometer, repeatedly scanning the m/e 25 - 30 range and, when used, by the microcomputer system. When pressure data was obtained by mass spectrometry alone, the reaction was allowed to proceed until no further hydrogenation could be detected, as shown by a constant m/e 29 peak height. In the case of data collection via the microcomputer system, the overall run time and sampling interval, often found by trial and error, were defined in the BASIC program prior to commencement of reaction. In most experiments, rapid sampling of the Baratron output voltage during the first 1 or 2 minutes of reaction was carried out, followed by a longer sampling interval

until the reaction was at least 80% complete. In all cases, the UHV system was evacuated for at least 15 minutes prior to commencing the next experiment on the same catalyst sample.

If required, the above procedure was repeated for catalyst samples subjected to high temperature reduction in H_2 or reduction, followed by high temperature re-oxidation in O_2. Such pretreatment of catalyst samples was achieved by heating the catalyst to the appropriate temperature and then dosing the UHV system with either H_2 or O_2, to a pressure of approximately 1kPa. The catalyst was then held at the set temperature for a known length of time, usually 3 hours, and then allowed to cool to ambient temperature before the system was evacuated for at least 1 hour before commencement of the experiment.

2.5.5 Temperature Programmed Desorption Procedure

The surfaces of Pt(0.5)/P25(P) and Pt(0.5)/P25(T) were investigated by the technique of linear temperature programmed desorption, using the UHV system as described in Section 2.1.5. Carbon monoxide, propene and propene/H_2 were used as adsorbates for untreated, reduced and reduced/oxidised catalyst samples. TPD spectra were also recorded for each adsorbate gas in the presence of untreated, reduced and oxidised P25 TiO_2 and with no adsorbent present in the UHV system. Pretreatment of the adsorbents in either hydrogen or oxygen at high temperatures was achieved using the method described in Section 2.5.4 above. The mass spectrometer, set on x250 attenuation, was used to follow desorption of

the adsorbed species as a function of increasing temperature. For propene and propene/H_2, the m/e 29 peak was monitored, but since CO_2 was also desorbed following CO adsorption, both the m/e 28 and the m/e 44 peaks were monitored in separate experiments. A linear temperature rise of 5K min^{-1}, maintained by the Eurotherm temperature controller, between the limits of 300 - 900K , was used in all TPD runs. A 50mg sample of the catalyst was placed in the reactor cradle and the UHV system evacuated overnight at ambient temperature. The adsorbate gas was then allowed to expand into the UHV system, until a pressure of 1.0 - 1.1kPa was reached, and then pumped away after 5 minutes. After a further 5 minutes, the temperature programme was commenced and the system isolated from the vacuum pumps. The valve between the vacuum system and the mass spectrometer was then quickly opened to allow unrestricted flow of the desorbing gas through to the instrument. The temperature of the catalyst, measured by a chromel-alumel thermocouple, and the mass spectrometer signal were sampled by the Cuban-12A board and recorded by the microcomputer system every 15 seconds, until the maximum temperature had been attained.

2.5.6 Liquid-Phase Photocatalytic Dehydrogenation of Propan-2-ol

a) Calibration of the Gas-Liquid Chromatogram

The concentration of propanone formed during the photocatalytic dehydrogenation of propan-2-ol was measured indirectly by gas-liquid chromatography, following a procedure, described below, first devised by

Cundall et al[122]. 100μl aliquots of a standard diethylether solution (20μl in 20cm^3 propan-2-ol) were mixed with 100μl aliquots of a series of standard propanone solutions (20 - 80μl in 20cm^3 propan-2-ol), at 273K. 0.3μl samples of each of these mixtures were then injected onto the GLC and the heights of the propanone peak (H_p) and the ether peak (H_e) were measured. A good linear correlation between the ratio of the two peak heights (H_p/H_e) and original propanone concentration was found and typical calibration values are given in Table 2.3 and plotted in Fig. 2.9.

Table 2.3 Typical Calibration Values for GLC Determination of Propanone Concentrations

10^2 [propanone] / moles dm^{-3}	H_p/H_e
0.00	0.00
1.36	0.48
2.72	1.01
4.08	1.42
5.44	1.93

b) Reaction Procedure

A common experimental procedure was used for all photocatalytic experiments,. Before any experiment was initiated, the UV lamp was allowed to warm up for about 2 hours so that maximum light intensity was always achieved. The wavelength region of 316 - 400nm was isolated from the lamp spectrum by a combination of soda glass and Chance OX1 filters. The intensity of radiation over this spectral range, for each

lamp, was measured via uranyl ethandioate actinometry, as described in Section 2.2.2.

150mg of catalyst were suspended in propan-2-ol, with continual stirring, and the reaction vessel purged with a flow of nitrogen (0.6cm^3 s^{-1}), which was maintained throughout the course of the experiment. The required reaction temperature was set via the frigister control unit, allowing at least 30 minutes for the apparatus and reaction solution to equilibrate prior to commencing the experiment. Reaction was initiated by raising a brass shutter, located between the UV lamp and the reaction vessel, to a pre-set mark, which ensured that the same amount of UV radiation entered the reaction vessel in all experiments. A 0.3cm^3 sample of the reaction solution was obtained just prior to raising the brass shutter and at regular intervals of 20 minutes, for 100 minutes, thereafter. The reaction solution samples were then centrifuged in a MSE Micro Centaur centrifuge for 4 minutes and then cooled to 273K. 100μl aliquots of the supernatant liquid and standard diethylether solution were thoroughly mixed at 273K and 0.3μl of the resulting solution injected onto the GLC. Propanone concentrations at time,t were found via the equation:

$$[\text{propanone}]_t = K(H_p/H_e)_t \qquad [71]$$

- where K = calibration factor (dm^3 mol^{-1})

A typical value of K, calculated from the calibration data given in Table 2.3, was 35.5 dm^3 mol^{-1}.

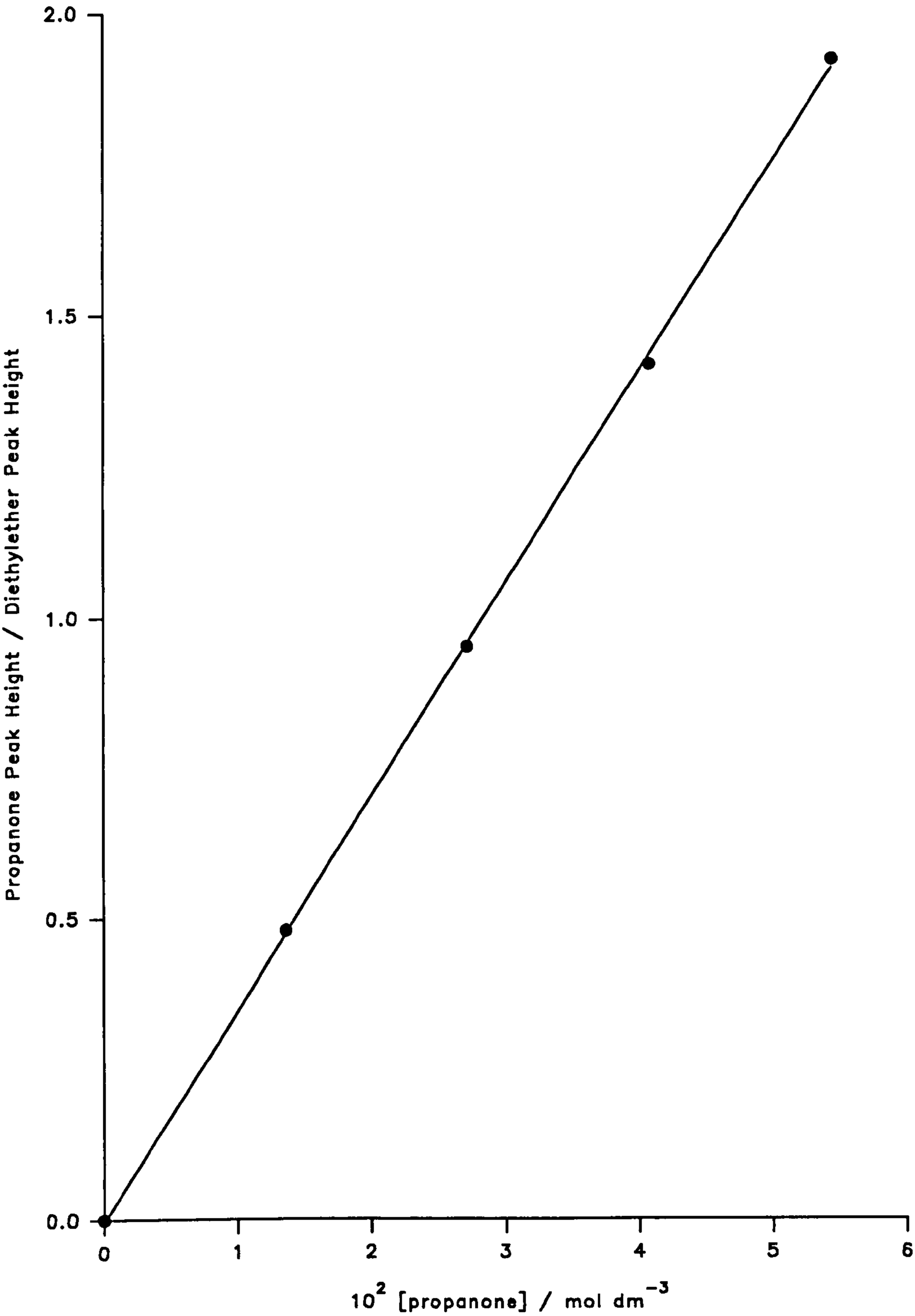

Figure 2.9: Calibration Plot for the Determination of Propanone Concentration via Gas–Liquid Chromatograhpy
(x1000 attenuation; 0.5μl injection)

CHAPTER 3: RESULTS

3.1 Gas Phase Hydrogenation Studies

3.1.1 Preliminary Investigations using Mass Spectrometry

At the beginning of this project, propene hydrogenation over Pt(0.5)/TiO_2(P) catalyst was investigated under a variety of reaction conditions, including temperature, pressure and initial state of catalyst. The primary objective of these initial studies was to assess the behaviour of platinised titania catalysts when functioning as thermal hydrogenation catalysts. Although only a first approximation, it was expected that these results would give a good indication of the sensitivity of the hydrogenation reactions to variations in reaction conditions. On the basis of these data, further detailed investigations, with well-defined reaction parameters, could then be planned. Two reasons can be given to justify the choice of reaction and catalyst used in these preliminary experiments. Firstly, the hydrogenation of propene is a facile reaction at room temperature in the presence of platinum metal and was, therefore, suitable for initial exploratory experiments. Secondly, previous studies have shown that photodeposition of Pt metal onto the surface of TiO_2 produces catalysts which are active for the photocatalytic dehydrogenation of alcohols[250,251]. During these preliminary studies, reaction progress was monitored by following the growth of the propane m/e 29 peak as a function of time, using the MS10 mass spectrometer. Raw data obtained

using this method were analyzed in terms of first-order reaction kinetics, from which initial absolute reaction rates, with respect to propene, were calculated, according to the equation:

$$k_a = (k_1 P_i C)/m \qquad [72]$$

where: k_a = initial absolute reaction rate (molecules s^{-1} g^{-1})

k_1 = experimental first-order rate constant (s^{-1})

P_i = initial propene partial pressure (kPa)

C = no. of molecules in reaction volume per unit pressure at 295K (molecules kPa^{-1})

m = mass of catalyst (g)

The value of C was obtained from the reaction volume measurements described in Section 2.1.4.

i) Propene Hydrogenation over Pt(0.5)/P25(P):

Temperature Dependency

A series of propene hydrogenation experiments was carried out in the temperature range 300-600K, using a Pt(0.5)/P25(P) catalyst. The results are summarised in Table 3.1, with first-order plots shown in Fig. 3.1. The dependence of the absolute initial reaction rate, calculated using Eq.[72], upon temperature is shown in Fig. 3.2. It can be seen that the absolute rate falls only slightly with increasing temperature over the range 300-500K; above this temperature a dramatic decrease in absolute rate is

observed, such that at 600K the rate was found to be an order of magnitude less that measured at 300K. Catalyst activity was not recovered when the reaction temperature was reduced to 300K after such high temperatures had been reached, indicating that the loss in catalyst activity was not reversible.

Table 3.1

Temperature/K	$10^3 k_1/s^{-1}$	10^{-18}Initial Absolute Rate/ molecules s^{-1} g^{-1}
300	5.95	5.00
350	4.85	4.06
400	5.00	4.19
500	4.90	4.11
600	0.50	0.42

Reaction parameters:

Catalyst mass = 32mg

Propene:H_2 = 1:3.2

$P_{i(propene)}$ = 0.163 ± 0.012kPa

ii) Propene Hydrogenation over Pt(0.5)/P25(P):

Pressure Dependency

A series of propene hydrogenation experiments was carried out at 273K, using a Pt(0.5)/P25(P) catalyst. In these experiments the effect of varying the initial propene partial pressure, keeping the propene:H_2 ratio constant, upon the initial absolute reaction rate was investigated. The results are summarised in Table 3.2, with the corresponding first-order

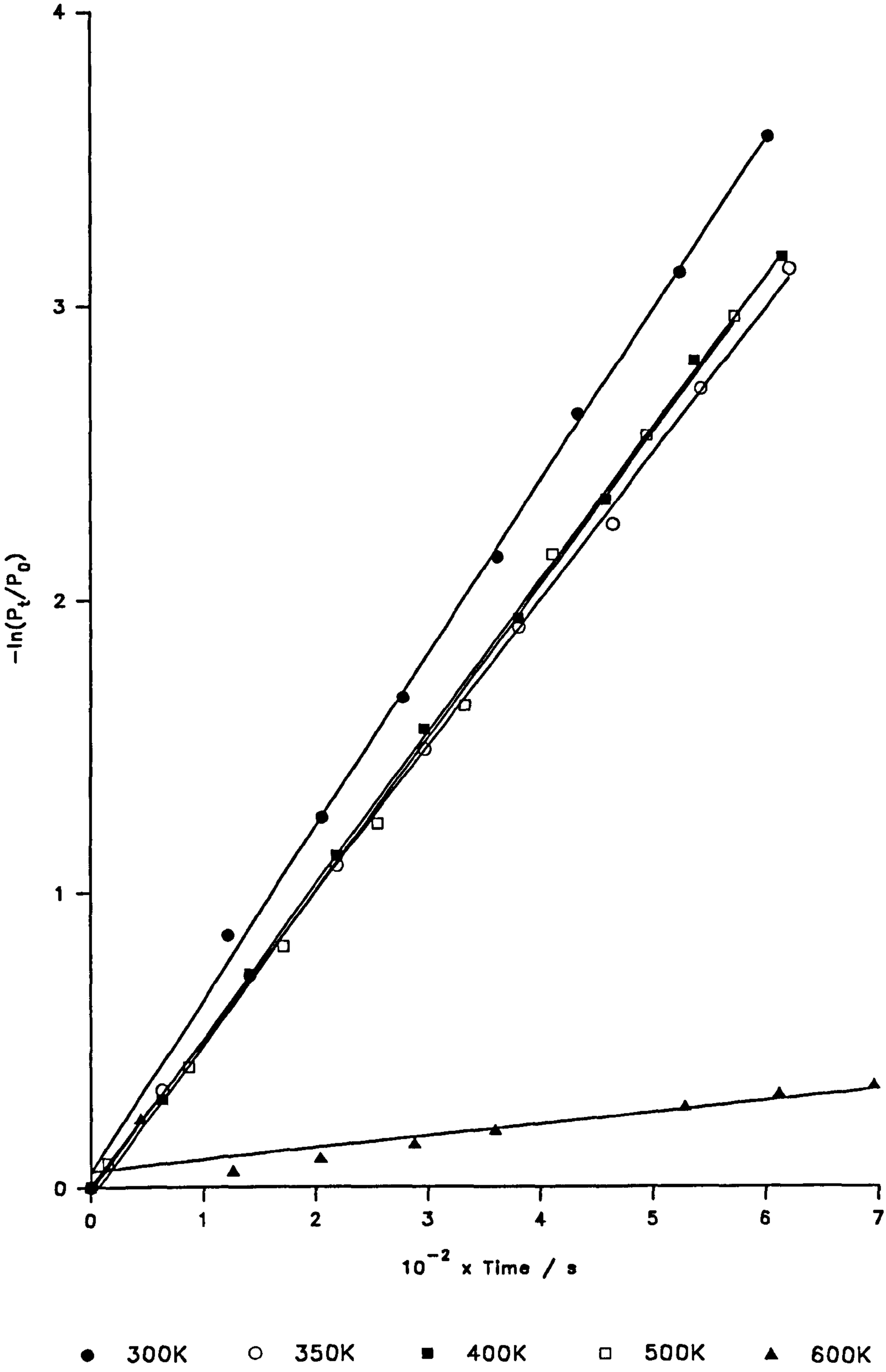

Figure 3.1: First–Order Plots for Propene Hydrogenation over Untreated Pt(0.5)/P25(P) at Various Temperatures

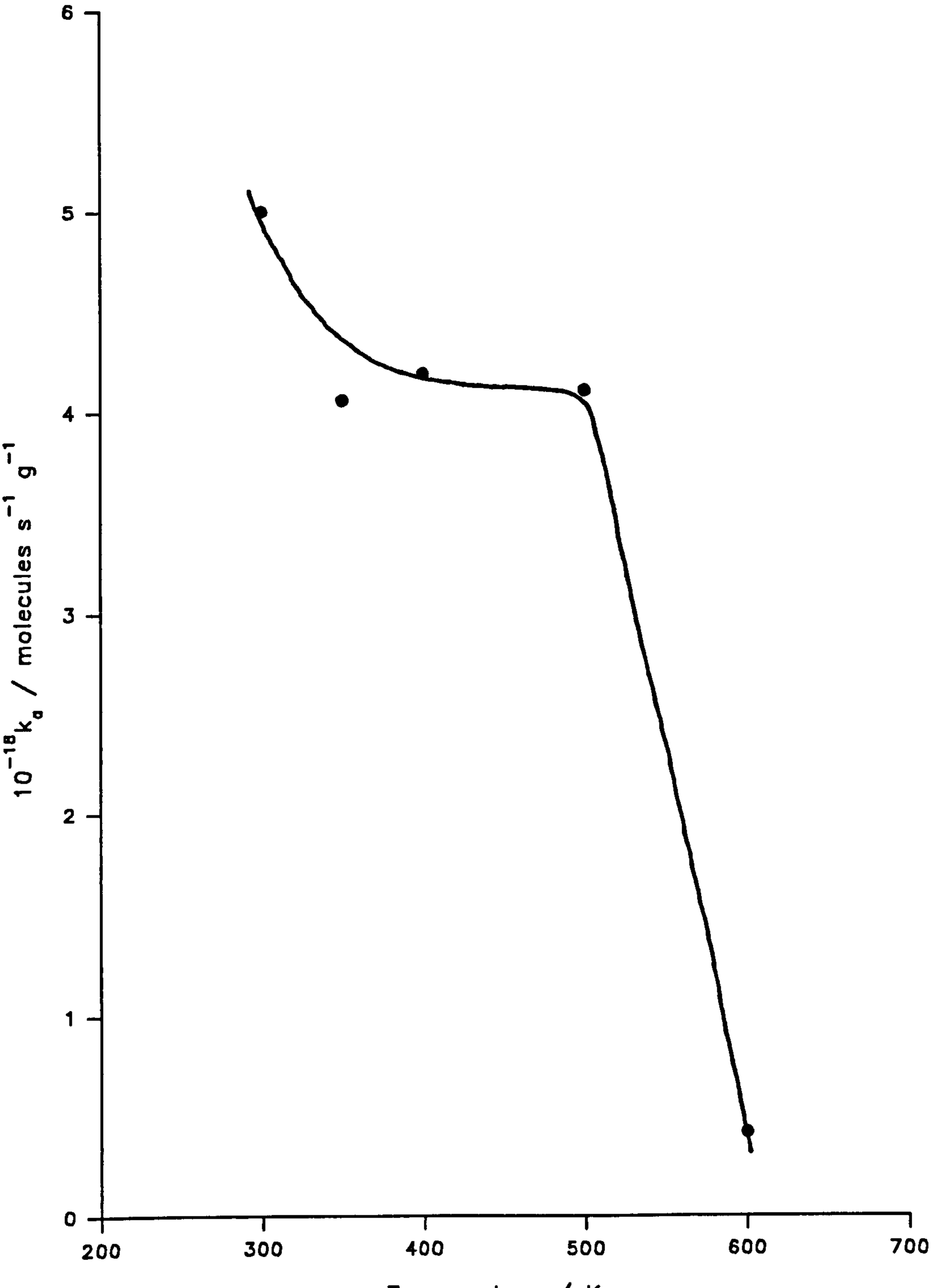

Figure 3.2: Absolute Initial Reaction Rate as a Function of Temperature for Propene Hydrogenation over Untreated Pt(0.5)/P25(P)

plots shown in Fig. 3.3, and the variation in absolute initial rate with increasing propene pressure is shown in Fig. 3.4. The results show that overall the hydrogenation reaction is less than 1st order with respect to propene, although individual runs obey 1st order with respect to departure from equilibrium.

Table 3.2

$P_{i(propene)}$/kPa	$10^3 k_1/s^{-1}$	10^{-18}Initial Absolute Rate/ molecules s^{-1} g^{-1}
0.081	4.13	1.08
0.148	2.13	1.02
0.177	1.96	1.12
0.266	1.46	1.35
0.422	1.18	1.61

Reaction parameters: Reaction temperature = 273K

Catalyst mass = 51mg

Propene:H_2 = 1:3.2

iii) Propene Hydrogenation over Pt(0.5)/P25(P):

Effect of Catalyst Pretreatment

A series of propene hydrogenation experiments was carried out at 300K, using a Pt(0.5)/P25(P) catalyst. Prior to reaction, the same catalyst sample was subjected to either reduction in hydrogen or oxidation in oxygen at an elevated temperature for a known period of time. The

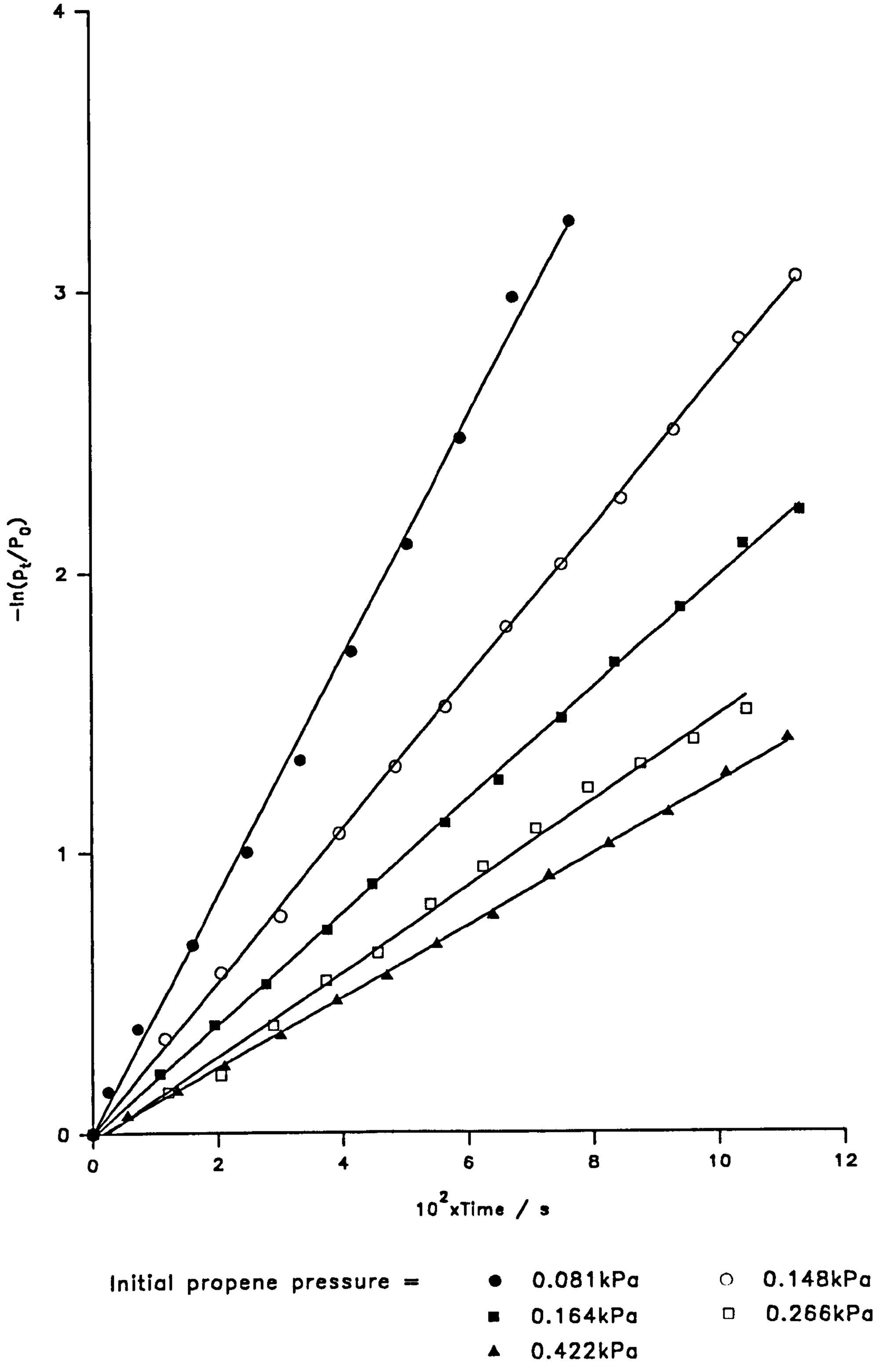

Figure 3.3: First-Order Plots for Propene Hydrogenation over Untreated Pt(0.5)/P25(P) at Various Initial Propene Partial Pressures

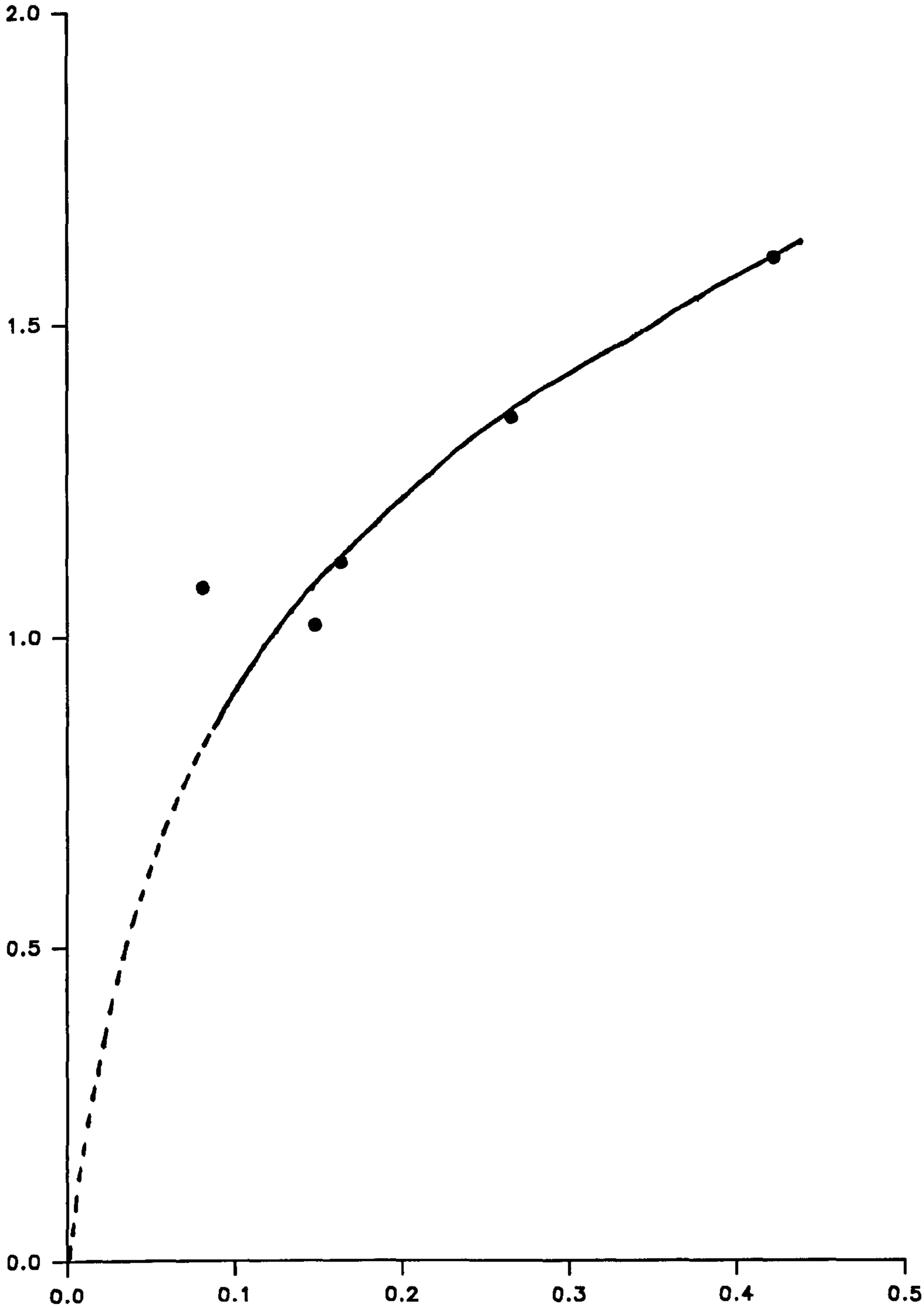

Figure 3.4: Absolute Initial Reaction Rate as a Function of Initial Propene Partial Pressure for Propene Hydrogenation over Untreated Pt(0.5)/P25(P)

results of these experiments are summarised in Table 3.3, with the corresponding first-order plots shown in Fig. 3.5. The results show that high-temperature reduction in H_2 renders the catalyst virtually inactive for the hydrogenation reaction. The effect is reversible by treating the prereduced catalyst in O_2, although the recovered activity is dependent upon the oxidation temperature. Thus, at a fairly low oxidation temperature the recovered activity is much less than that exhibited by the original untreated catalyst, whereas a much higher oxidation temperature gives a significantly increased activity compared with the untreated catalyst. These experiments show, therefore, that the measured absolute initial rate of reaction is highly dependent upon the initial state of the catalyst.

Table 3.3

Catalyst Pretreatment	$10^3 k_1/s^{-1}$	10^{-18}Initial Absolute Rate/ molecules s^{-1} g^{-1}
None	1.16	0.72
H_2;18hrs;671K	*	*
O_2;18hrs;430K	0.29	0.12
O_2;23hrs;673K	4.52	1.29
H_2;3hrs;673K	*	*

* Activity of catalyst too low to measure accurately

Reaction parameters:

Reaction temperature = 300K

Catalyst mass = 50mg

Propene:H_2 = 1:3.2

$P_{i(propene)}$ = 0.136 ± 0.043kPa

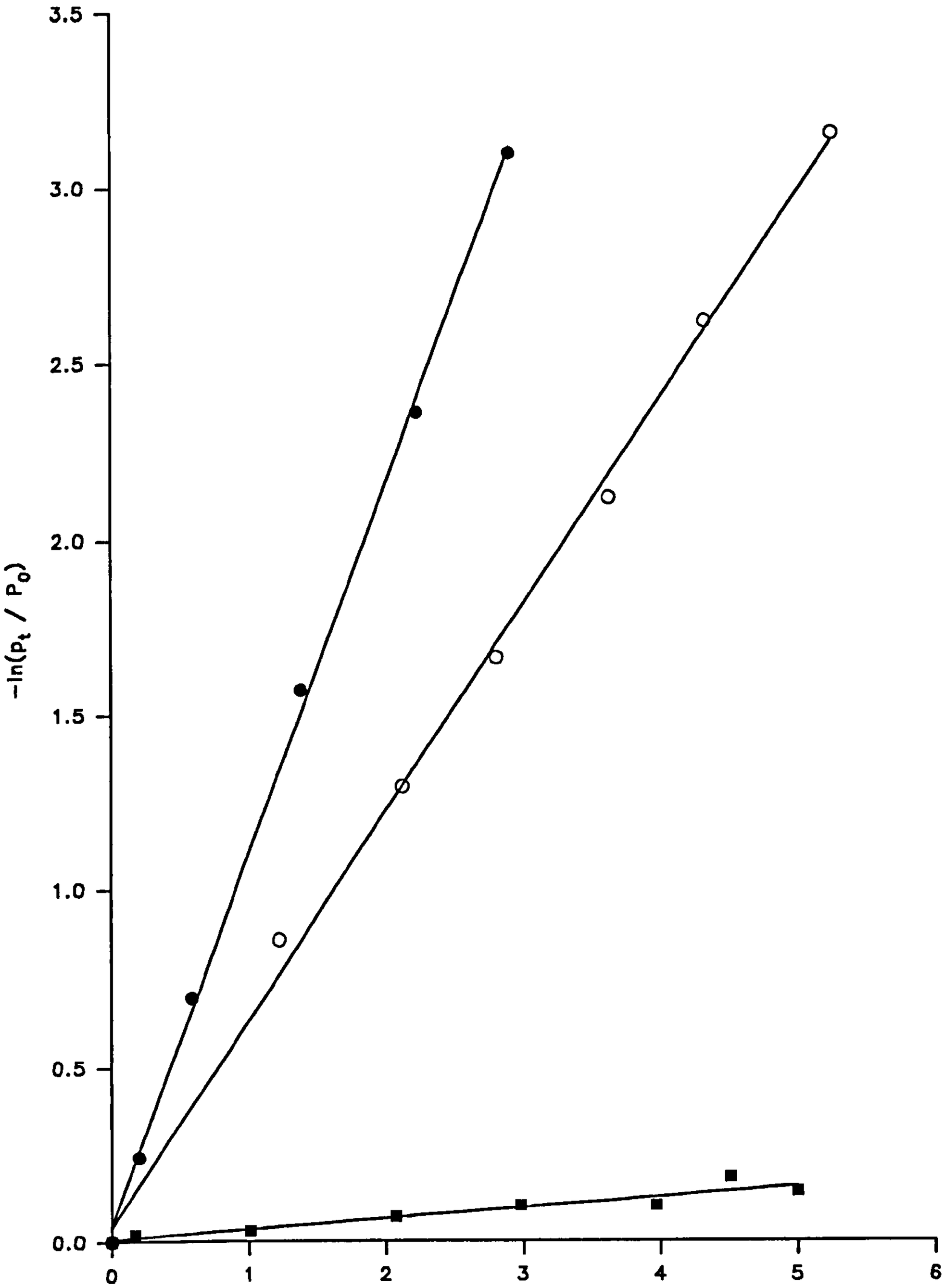

Figure 3.5: First-Order Plots for Propene Hydrogenation over Various Pretreated Pt(0.5)/P25(P) Catalysts

iv) Disadvantages of the Technique

Although the technique of following the rate of hydrogenation via mass spectrometry yielded useful preliminary results, it was found that the data obtained were not always reliable. A serious disadvantage of using mass spectrometry to obtain kinetic data from product formation is that the reaction must be allowed to proceed for as long as possible, in order that an accurate "infinity" reading may be taken. In this case, the "infinity" reading gave the maximum pressure of propane formed, which was assumed to equal the initial propene pressure. The necessity of having to allow the reaction to proceed for as long as possible can affect the quality of data obtained in several ways. Firstly, any error in finding and/or measuring the "infinity" will consistently reappear in later calculations. Such errors are more likely to occur in protracted runs, where the catalyst activity is low, due to the pumping of gas through the mass spectrometer leak, giving a lower than actual "infinity" value. Also, chart recorders have a finite time of indication, which means that the true maximum of each m/e peak, as measured by the mass spectrometer, may not always be recorded, especially when short cycling times are employed. Another important point is that as the reaction proceeds to virtual completion, it becomes diffusion-controlled, giving rise to misleading data.

With these problems in mind, it was decided that use of the mass spectrometer, as an analytical tool for obtaining kinetic data, was unsatisfactory. A new method of data acquisition and analysis, based on a microcomputer system, was devised and implemented, as previously described. However, by use of mass spectrometry in the initial stages of

this project it was shown that the hydrogenation of both propene and cyclopropane proceeded cleanly over all the catalysts used, giving propane as the sole reaction product. This is an extremely important result since all kinetic data reported hereafter are assumed to relate solely to the process of hydrogenation, with no contribution from other side-reactions, such as hydrogenolysis to methane and ethane. It is accepted that this is only a close approximation since some hydrogen will be consumed through the processes of spillover onto the titania support and of activated adsorption. Furthermore, mass spectrometry was also used to show that TiO_2 alone was inactive, at the same reaction temperatures, for the hydrogenation reactions studied.

3.1.2 Preliminary Investigations: Commodore Microcomputer System

In view of the problems associated with using mass spectrometry as a means of obtaining kinetic data, an automated system, comprising a Commodore 4302 PET microcomputer interfaced to the Baratron via a Keithley 177 DVM voltmeter, was implemented. This recorded data in terms of changing pressure in the reaction vessel as a function of time, which was then described by a best-fit polynomial as outlined in Section 2.5.3(b). Determination of co-efficient a_2, via differentiation of the polynomial with respect to time, enabled initial absolute rates of reaction to be determined according to the equation:

$$k_a = bc/m \qquad [73]$$

where: k_a = initial absolute reaction rate (molecules s^{-1} g^{-1})

b = initial reaction rate (kPa s^{-1})

c = no. of molecules in reaction volume per unit pressure at 295K

m = mass of catalyst (g)

Using this system, a series of preliminary experiments, in which the activities of pretreated Pt(0.5)/P25(P) catalysts were measured as a function of the total amount of propene hydrogenated, was undertaken. The results of these experiments, calculated using Eq.[73], are summarised in Tables 3.4 - 3.6 and shown in Fig. 3.6.

Notes:

1. In some experiments the initial state of the catalyst(s) was not known and consequently the first point(s) are omitted from the line plots, (see, for example, Fig. 3.7).

2. Where shown, error bars were calculated on the basis of at least three repeat experiments and the plot points represent mean value ± S.D.

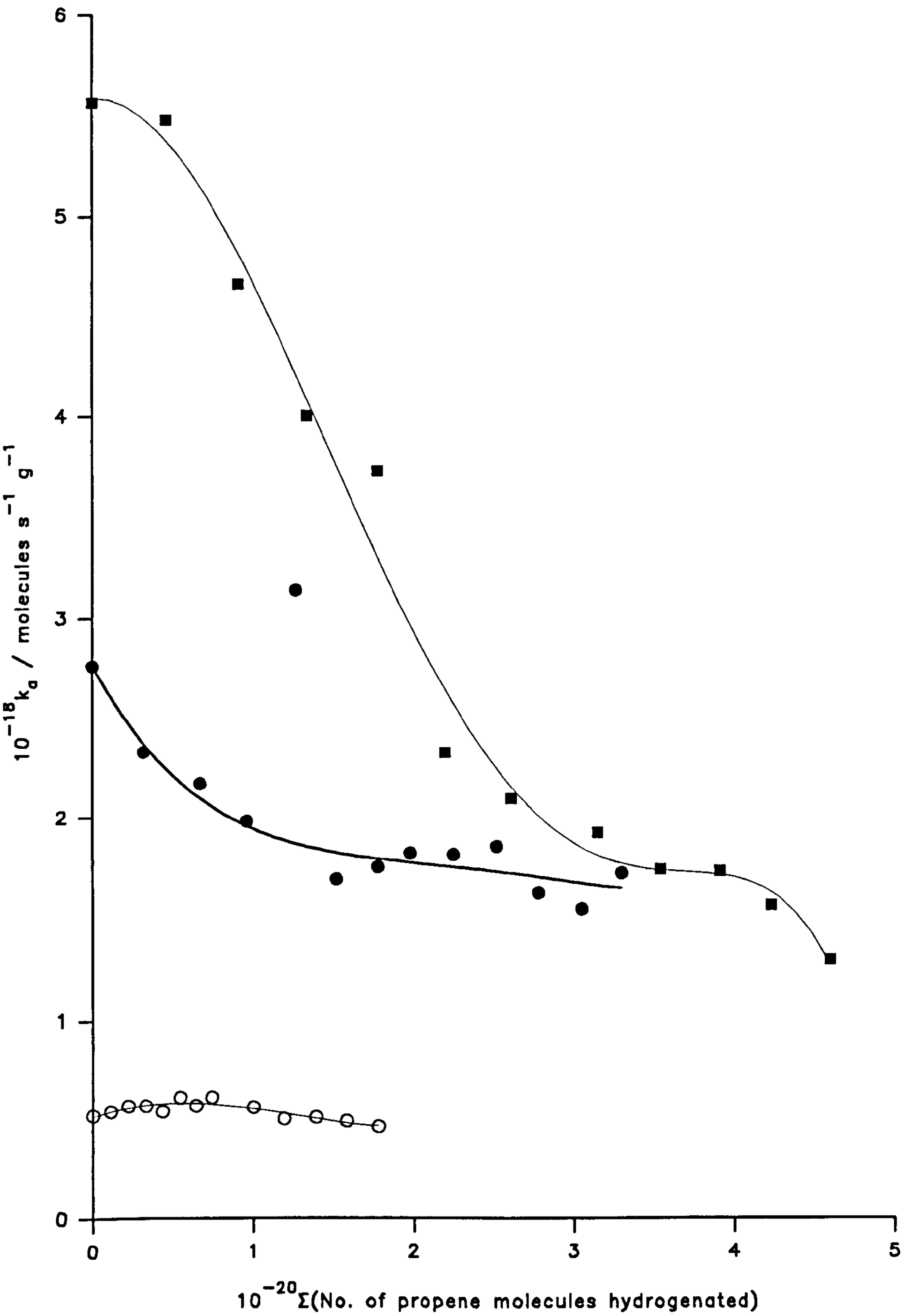

Figure 3.6: Prolonged Propene Hydrogenation Activites for Various Pretreated Pt(0.5)/P25(P) Catalysts

Table 3.4

i	$10^{-20}\sum_i$(No. of propene molecules hydrogenated)	10^4b/ kPa s^{-1}	$10^{-18}k_a$/molecules s^{-1} g^{-1}
1	0.00	4.18	2.76
2	0.32	3.53	2.33
3	0.67	3.29	2.17
4	0.96	3.00	1.98
5	1.27	4.75	3.14
6	1.52	2.56	1.69
7	1.78	2.65	1.75
8	1.98	2.75	1.82
9	2.25	2.74	1.81
10	2.52	2.80	1.85
11	2.78	2.45	1.62
12	3.05	2.33	1.54
13	3.30	2.60	1.72

Reaction parameters:

Catalyst pretreatment = Evac.18hrs

Reaction temperature = 300K

Catalyst mass = 25mg

$P_{i(propene)}$ = 0.278 ± 0.004kPa

Propene:H_2 = 1:3.2

Table 3.5

i	$10^{-20}\sum_i$(No. of propene molecules hydrogenated)	10^4b/ kPa s^{-1}	$10^{-18}k_a$/molecules s^{-1} g^{-1}
1	0.00	0.79	0.52
2	0.11	0.81	0.54
3	0.22	0.87	0.57
4	0.33	0.86	0.57
5	0.43	0.82	0.54
6	0.54	0.92	0.61
7	0.64	0.86	0.57
8	0.74	0.93	0.61
9	1.00	0.85	0.56
10	1.19	0.76	0.50
11	1.39	0.77	0.51
12	1.58	0.74	0.49
13	1.78	0.70	0.46

Reaction parameters:

Catalyst pretreatment = H_2;3hrs;405K

Reaction temperature = 300K

Catalyst mass = 25mg

$P_{i(propene)}$ = 0.277 ± 0.002kPa

Propene:H_2 = 1:3.2

Table 3.6

i	$10^{-20}\sum_i$(No. of propene molecules hydrogenated)	10^4b/ kPa s^{-1}	$10^{-18}k_a$/molecules s^{-1} g^{-1}
1	0.00	8.44	5.57
2	0.46	8.30	5.48
3	0.91	7.06	4.66
4	1.34	6.06	4.00
5	1.78	5.65	3.73
Catalyst evacuated for 16hrs at ambient temperature			
6	2.20	3.52	2.32
7	2.61	3.17	2.09
8	3.15	2.91	1.92
9	3.54	2.63	1.74
10	3.91	2.62	1.73
11	4.23	2.37	1.56
12	4.60	1.96	1.29

Reaction parameters:

Catalyst pretreatment = O_2;4hrs;402K

Reaction temperature = 300K

Catalyst mass = 25mg

$P_{i(propene)}$ = 0.279 ± 0.002kPa

Propene:H_2 = 1:3.2

3.1.3 Experimental Investigations: BBC Microcomputer System

Following critical assessment of the performance of the Commodore microcomputer system, a decision was made to upgrade the data acquisition and processing technique by employing a faster and more sensitive microcomputer. As described in Section 2.1.3, the chosen system comprised a BBC Master Series microcomputer, interfaced to the Baratron via a Cuban-12A analogue-to-digital converter. The system operated in real time, using Real Time BASIC language, and the software program written for the data acquisition and analysis is listed in Appendix 1.

3.1.4 Propene Hydrogenation over Reduced and Reduced/Oxidised Pt(0.5)/P25(P): Prolonged Catalyst Activity

A systematic series of experiments was undertaken to assess the variation in activity for Pt(0.5)/P25(P) catalysts, subjected to reduction in H_2 and also reduction in H_2 followed by oxidation in O_2 at various temperatures between 300 - 700K. Each catalyst sample was repeatedly exposed to fixed doses of propene/H_2 mixture at 300K and the initial absolute rate of hydrogenation was then calculated at time zero, following each dosing. In this manner, the prolonged activity of the catalyst sample could be determined as a function of the cumulative amount of propene hydrogenated. The results of these experiments, calculated using Eq.[73], are given in Tables 3.7 - 3.14 and plotted in terms of initial absolute reaction rate vs total amount of propene hydrogenated in Fig. 3.7. The

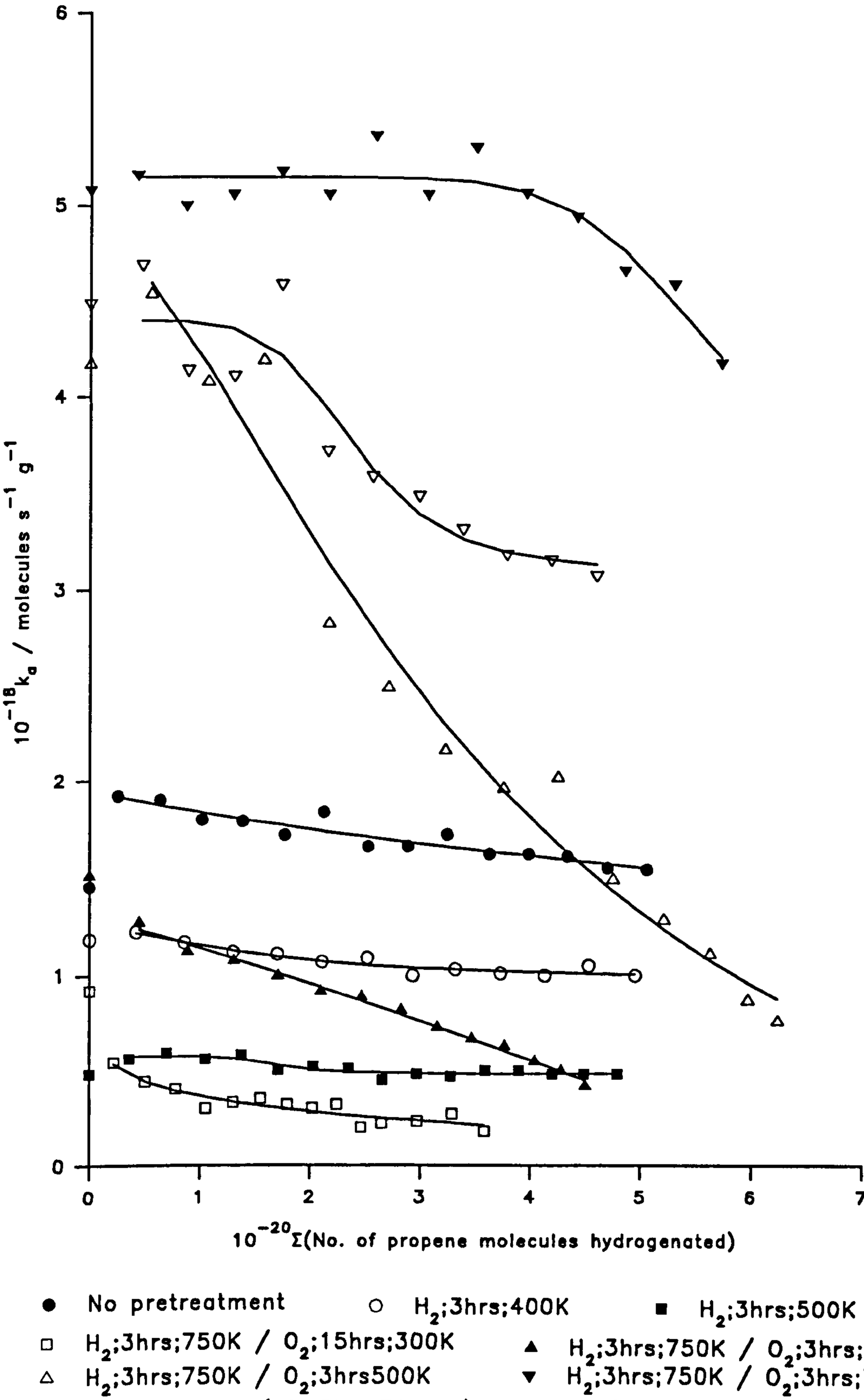

● No pretreatment ○ H_2;3hrs;400K ■ H_2;3hrs;500K

□ H_2;3hrs;750K / O_2;15hrs;300K ▲ H_2;3hrs;750K / O_2;3hrs;400K

△ H_2;3hrs;750K / O_2;3hrs500K ▼ H_2;3hrs;750K / O_2;3hrs;700K

▽ H_2;3hrs;750K / O_2;3hrs;700K / H_2;3hrs;445K

Figure 3.7: Prolonged Propene Hydrogenation Activities for Various Reduced and Reduced/Oxidised Pt(0.5)/P25(P) Catalysts

overall effect of increasing the reduction and the re-oxidation temperatures on catalyst activity immediately following such pretreatments, relative to the untreated catalyst, is shown in Fig. 3.8. The vertical bars at each point represent the difference between the initial and final activities of that particular catalyst sample, following prolonged propene hydrogenation.

A number of significant results, relative to untreated Pt(0.5)/P25(P), were found during these experiments:

i) Increasing the temperature at which the catalyst was reduced in H_2 produced a correspondingly greater fall in the initial rate of hydrogenation, such that reduction above 600K rendered the catalyst inactive.

ii) Reduction in H_2 at 750K, followed by re-oxidation in O_2 at increasingly higher temperatures, gradually restored catalyst activity, such that re-oxidation above 500K produced activities greater than that observed for the untreated catalyst.

iii) Reduction at 750K, re-oxidation at 700K, followed by a further mild reduction at 445K, produced a similar catalyst activity to that observed following just reduction/re-oxidation.

iv) Increasing the reduction temperature conferred greater stability on the catalyst, with respect to activity, although overall the activity was lower.

v) In order to obtain good catalyst stability, as well as enhanced activity, it was necessary to re-oxidise catalyst samples at temperatures well above 500K, following previous reduction at 750K.

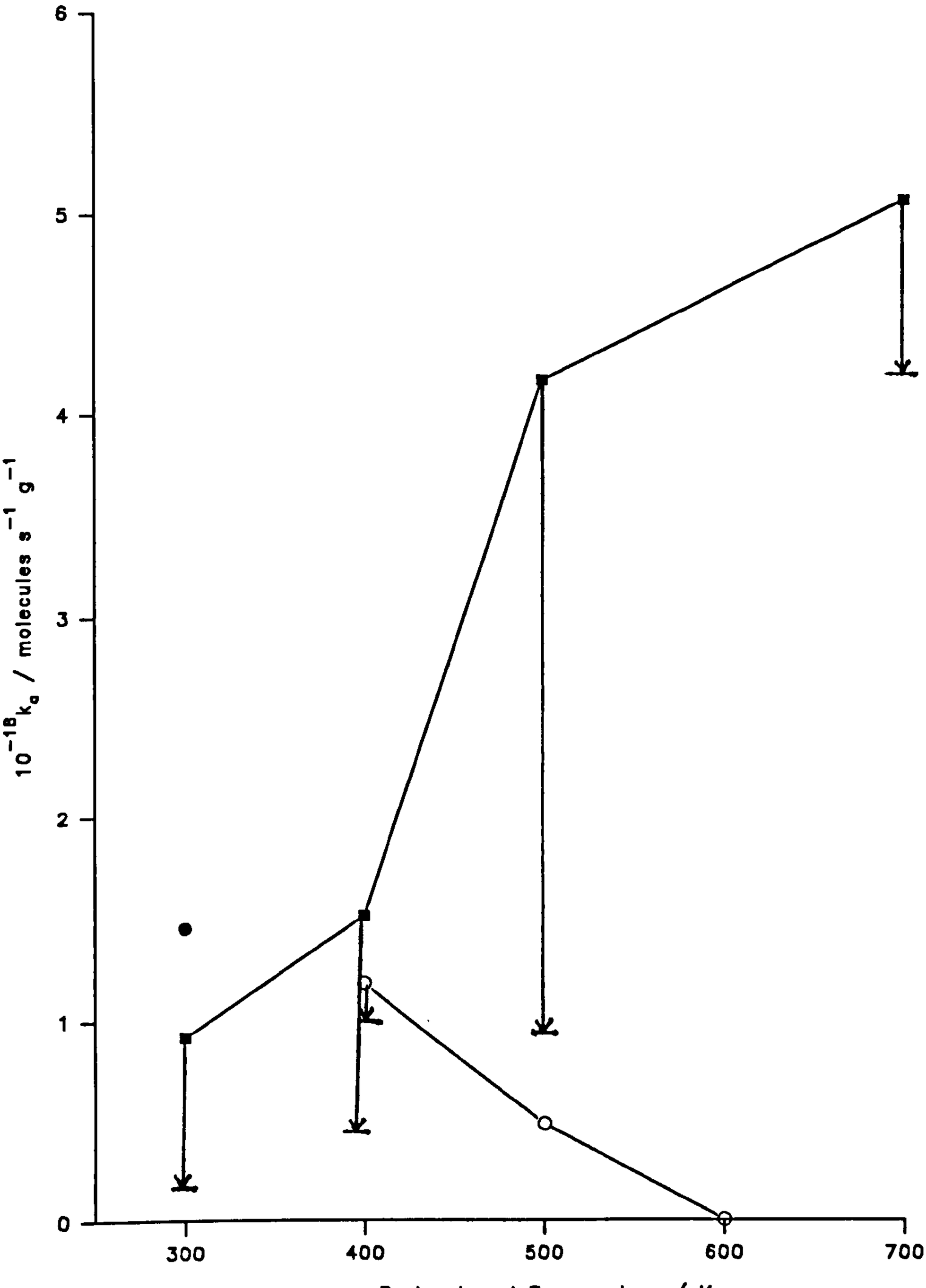

- ● No pretreatment
- ○ Reduction in H_2 for 3hrs
- ■ Reduction in H_2 for 3hrs, then oxidation in O_2 for 3hrs

Figure 3.8: Summary of the Effect of Reduction and Reduction/ Oxidation on the Absolute Initial Propene Hydrogenation Rate over Pt(0.5)/P25(P) Catalyst

Table 3.7

i	$10^{-20}\Sigma_i$(No. of propene molecules hydrogenated)	10^4b/ kPa s^{-1}	$10^{-18}k_a$/ molecules s^{-1} g^{-1}
1	0.00	4.44	1.45
2	0.26	5.93	1.92
3	0.64	5.86	1.90
4	1.02	5.56	1.80
5	1.39	5.53	1.79
6	1.77	5.33	1.72
7	2.13	5.70	1.84
8	2.53	5.13	1.66
9	2.89	5.12	1.66
10	3.25	5.31	1.72
11	3.63	5.01	1.62
12	3.99	5.01	1.62
13	4.34	4.96	1.61
14	4.70	4.80	1.55
15	5.06	4.77	1.54

Reaction parameters:

Catalyst pretreatment = None

Reaction temperature = 300K

Catalyst mass = 51mg

$P_{i(propene)}$ = 0.277 ± 0.004kPa

Propene:H_2 = 1:3.1

Table 3.8

i	$10^{-20}\sum_i$(No. of propene molecules hydrogenated)	10^4b/ kPa s^{-1}	$10^{-18}k_a$/ molecules s^{-1} g^{-1}
1	0.00	3.64	1.18
2	0.42	3.78	1.22
3	0.86	3.62	1.17
4	1.30	3.47	1.12
5	1.70	3.42	1.11
6	2.11	3.30	1.07
7	2.52	3.36	1.09
8	2.93	3.09	1.00
9	3.32	3.17	1.03
10	3.73	3.12	1.01
11	4.13	3.10	1.00
12	4.53	3.25	1.05
13	4.95	3.08	1.00

Reaction parameters:

Catalyst pretreatment = H_2;3hrs;400K

Reaction temperature = 300K

Catalyst mass = 51mg

$P_{i(propene)}$ = 0.279 ± 0.002kPa

Propene:H_2 = 1:3.1

Table 3.9

i	$10^{-20}\sum_i$(No. of propene molecules hydrogenated)	10^4b/ kPa s^{-1}	$10^{-18}k_a$/ molecules s^{-1} g^{-1}
1	0.00	1.49	0.48
2	0.36	1.73	0.56
3	0.70	1.81	0.59
4	1.05	1.74	0.56
5	1.38	1.79	0.58
6	1.71	1.55	0.50
7	2.03	1.60	0.52
8	2.35	1.58	0.51
9	2.66	1.39	0.45
10	2.97	1.49	0.48
11	3.28	1.44	0.47
12	3.59	1.53	0.50
13	3.90	1.55	0.50
14	4.20	1.49	0.48
15	4.49	1.49	0.48
16	4.79	1.47	0.48

Reaction parameters:

Catalyst pretreatment = H_2;3hrs;500K

Reaction temperature = 300K

Catalyst mass = 51mg

$P_{i(propene)}$ = 0.280 ± 0.001kPa

Propene:H_2 = 1:3.0

Table 3.10

i	$10^{-20}\Sigma_i$(No. of propene molecules hydrogenated)	10^4b/ kPa s^{-1}	$10^{-18}k_a$/ molecules s^{-1} g^{-1}
1	0.00	2.84	0.92
2	0.22	1.68	0.54
3	0.50	1.37	0.44
4	0.78	1.24	0.40
5	1.05	0.93	0.30
6	1.30	1.03	0.33
7	1.55	1.07	0.35
8	1.79	0.99	0.32
9	2.02	0.94	0.30
10	2.24	0.98	0.32
11	2.46	0.61	0.20
12	2.65	0.68	0.22
13	2.97	0.72	0.23
14	3.29	0.84	0.27
15	3.58	0.56	0.18

Reaction parameters:

Catalyst pretreatment = H_2;3hrs;750K

O_2;15hrs;300K

Reaction temperature = 300K

Catalyst mass = 51mg

$P_{i(propene)}$ = 0.335 ± 0.003kPa

Propene:H_2 = 1:2.4

Table 3.11

i	$10^{-20}\sum_i$(No. of propene molecules hydrogenated)	10^4b/ kPa s^{-1}	$10^{-18}k_a$/ molecules s^{-1} g^{-1}
1	0.00	4.39	1.51
2	0.45	3.70	1.27
3	0.89	3.30	1.13
4	1.31	3.13	1.08
5	1.71	2.92	1.00
6	2.10	2.67	0.92
7	2.47	2.58	0.89
8	2.83	2.37	0.82
9	3.16	2.12	0.73
10	3.47	1.94	0.67
11	3.77	1.83	0.63
12	4.04	1.61	0.55
13	4.28	1.45	0.50
14	4.50	1.21	0.42

Reaction parameters:

Catalyst pretreatment = H_2;3hrs;750K
O_2;3hrs;400K

Reaction temperature = 300K

Catalyst mass = 48mg

$P_{i(propene)}$ = 0.334 ± 0.001kPa

Propene:H_2 = 1:2.4

Table 3.12

i	$10^{-20}\sum_i$(No. of propene molecules hydrogenated)	10^4b/ kPa s^{-1}	$10^{-18}k_a$/ molecules s^{-1} g^{-1}
1	0.00	12.12	4.17
2	0.55	13.19	4.54
3	1.07	11.86	4.08
4	1.58	12.18	4.19
5	2.17	8.20	2.82
6	2.71	7.25	2.49
7	3.23	6.28	2.16
8	3.76	5.70	1.96
9	4.25	5.87	2.02
10	4.75	4.33	1.49
11	5.21	3.71	1.28
12	5.63	3.24	1.11
13	5.97	2.52	0.87
14	6.24	2.22	0.76

Reaction parameters:

Catalyst pretreatment = H_2;3hrs;750K

O_2;3hrs;500K

Reaction temperature = 300K

Catalyst mass = 48mg

$P_{i(propene)} = 0.343 \pm 0.002$kPa

Propene:H_2 = 1:2.4

Table 3.13

i	$10^{-20}\sum_i$(No. of propene molecules hydrogenated)	10^4b/ kPa s^{-1}	$10^{-18}k_a$/ molecules s^{-1} g^{-1}
1	0.00	14.77	5.08
2	0.43	15.01	5.16
3	0.87	14.53	5.00
4	1.30	14.71	5.06
5	1.74	15.06	5.18
6	2.17	14.72	5.06
7	2.60	15.62	5.37
8	3.07	14.73	5.06
9	3.51	15.46	5.31
10	3.96	14.76	5.07
11	4.42	14.39	4.95
12	4.85	13.58	4.67
13	5.30	13.37	4.60
14	5.73	12.15	4.18

Reaction parameters:

Catalyst pretreatment = H_2;3hrs;750K

O_2;3hrs;700K

Reaction temperature = 300K

Catalyst mass = 48mg

$P_{i(propene)}$ = 0.279 ± 0.001kPa

Propene:H_2 = 1:3.0

Table 3.14

i	$10^{-20}\sum_i$(No. of propene molecules hydrogenated)	10^4b/ kPa s^{-1}	$10^{-18}k_a$/ molecules s^{-1} g^{-1}
1	0.00	13.06	4.49
2	0.47	13.64	4.69
3	0.89	12.04	4.14
4	1.31	11.95	4.11
5	1.74	13.36	4.59
6	2.16	10.81	3.72
7	2.57	10.43	3.59
8	2.99	10.15	3.49
9	3.39	9.65	3.32
10	3.79	9.29	3.19
11	4.19	9.20	3.16
12	4.60	8.96	3.08

Reaction parameters:

Catalyst pretreatment = H_2;3hrs;750K

O_2;3hrs;700K

H_2;3hrs;445K

Reaction temperature = 300K

Catalyst mass = 48mg

$P_{i(propene)}$ = 0.282 ± 0.001kPa

Propene:H_2 = 1:3.0

3.1.5 Propene Hydrogenation over Pt(x)/P25(P) and Pt(0.5)/P25(T): Prolonged Catalyst Activity

a) Untreated Catalysts

In this series of experiments, catalyst activity and behaviour during prolonged propene hydrogenation, as a function of Pt metal content, was investigated. Four catalysts prepared by photodeposition having Pt contents in the range 0.25 - 2.0 mass% and, for comparative purposes, a sample of Pt(0.5)/P25(T) catalyst were included in the study. Each untreated catalyst was repeatedly exposed to doses of propene/H_2 mix at 300K and the initial absolute rate of hydrogenation was calculated for time zero, following each dosing. The results of this study are summarised in Tables 3.15 - 3.19 and plotted in terms of initial absolute reaction rate vs total amount of propene hydrogenated in Fig. 3.9.

From the plots shown in Fig. 3.9 it can be seen that, generally speaking, as the metal content of the catalyst increases, so does its activity. There is, however, no direct relation between activity and metal content. Compared with the other catalysts, both Pt(0.5)/P25(P) and Pt(0.5)/P25(T) exhibited greater than expected activity,in view of their metal content. This is particularly true for Pt(0.5)/P25(P) which was found to be almost as active as Pt(2.0)/P25(P), with a metal content some four times greater. All catalysts were found to be reasonably stable with respect to prolonged propene hydrogenation, with activities tending to fall to a constant level during the course of the experiment.

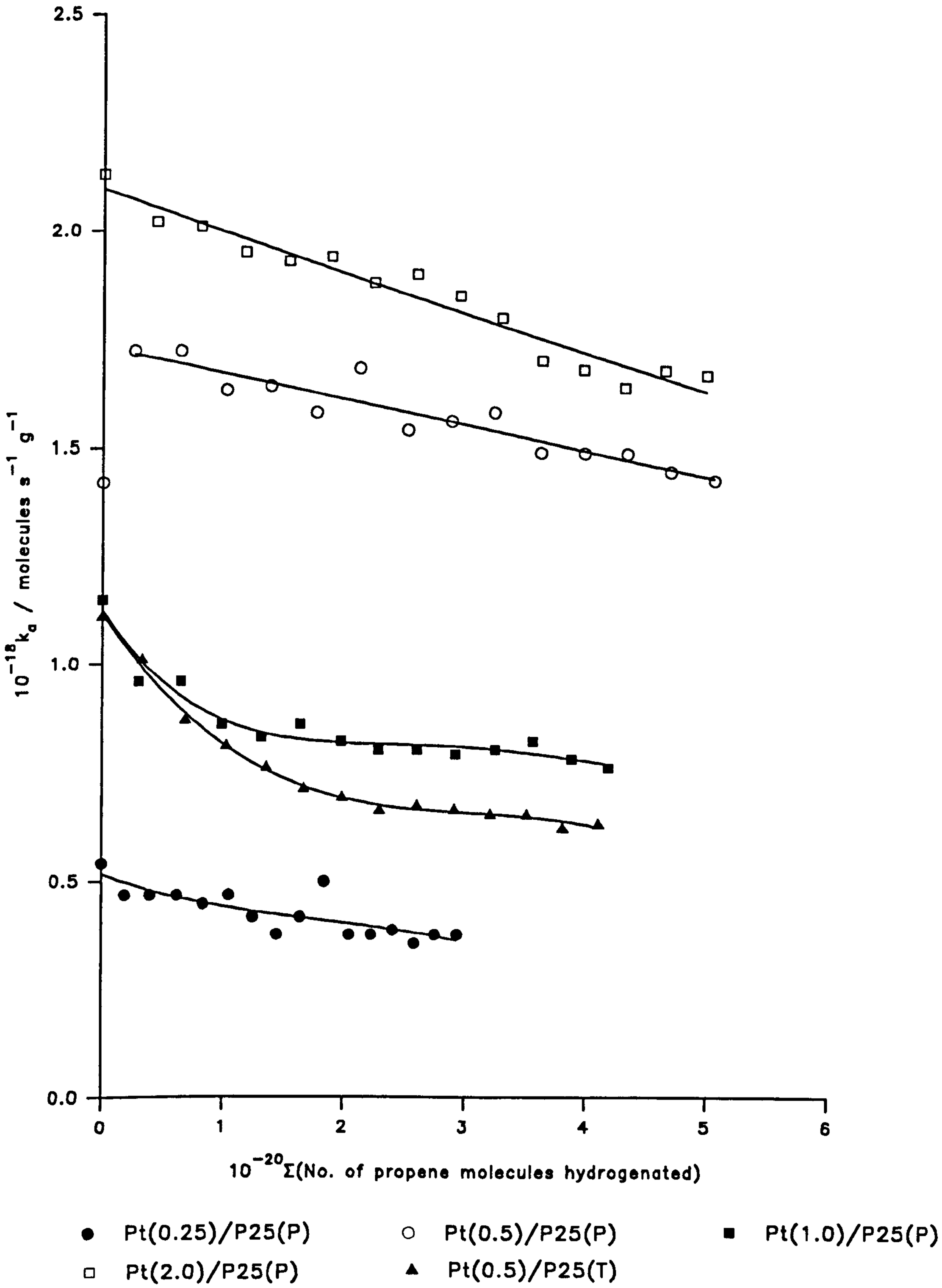

Figure 3.9: Prolonged Propene Hydrogenation Activity as a Function of Metal Content for Untreated Pt/P25 Catalysts

b) Reduced/Oxidised Catalysts

A similar series of experiments to that described in (a) above was carried out using the same five catalysts. However, in this series the catalyst samples were first reduced in H_2 at 750K and then subsequently re-oxidised in O_2 at 700K, prior to reaction. The results of these experiments are summarised in Tables 3.20 - 3.24 inclusive and plotted in terms of initial absolute reaction rate vs total amount of propene hydrogenated in Fig. 3.10.

From these experiments, it was observed that all the catalysts studied exhibited very similar activities for propene hydrogenation immediately after the reduction/ oxidation pretreatment. The exception to this was Pt(0.25)/P25(P), which was found to be nearly 50% less active than the other catalysts during the initial stages of propene hydrogenation. Furthermore, both Pt(0.25) and Pt(0.5)/P25(P) were found to be very unstable during prolonged propene hydrogenation, their activities falling significantly as the total amount of propene hydrogenated increased. The other two catalysts prepared by photodeposition, having higher Pt contents, were found to much more stable, with their activities only just beginning to fall towards the end of the experiment. Pt(0.5)/P25(T), prepared by impregnation/reduction, exhibited the greatest stability during prolonged propene hydrogenation, showing no appreciable fall in activity during the entire experiment.

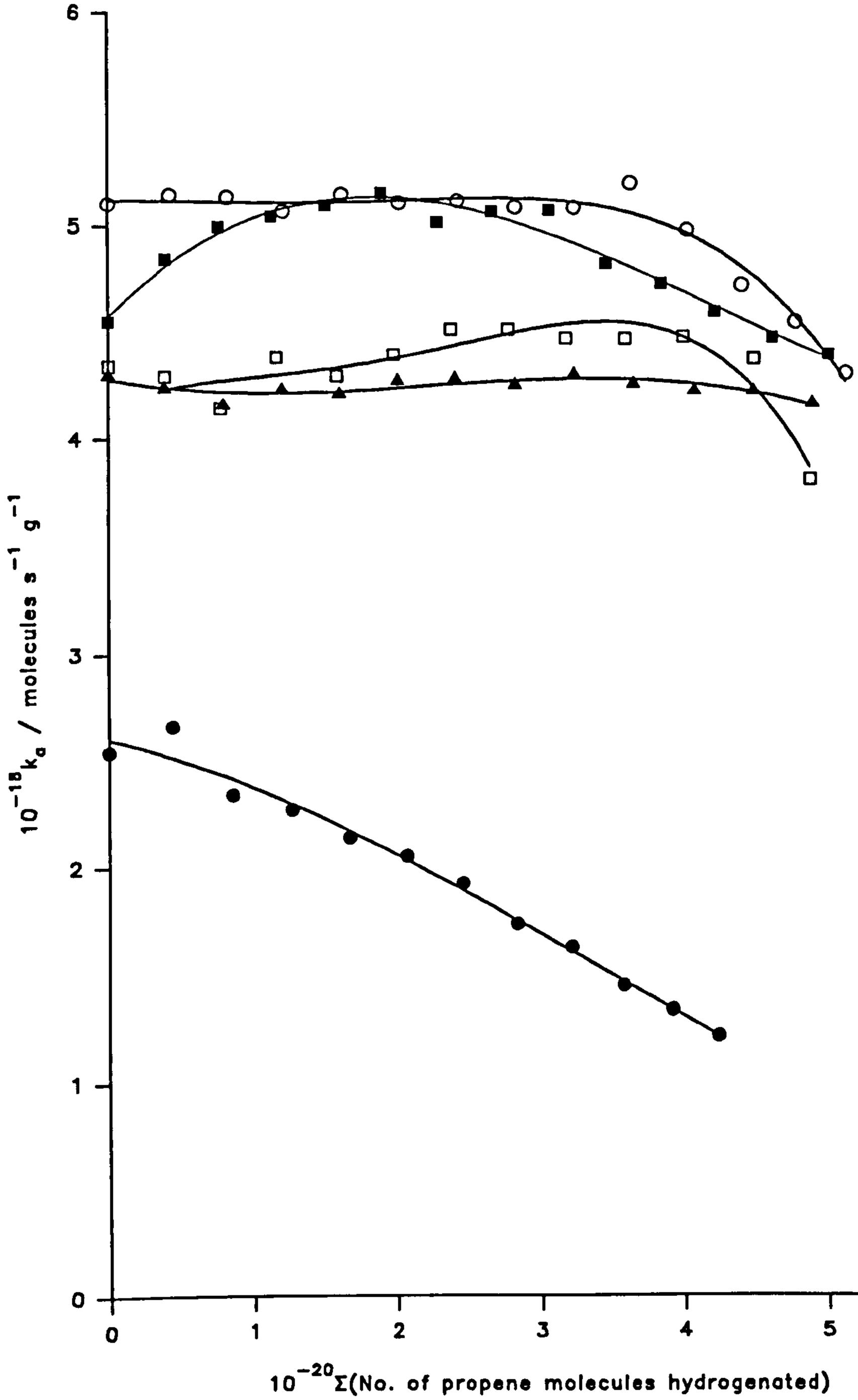

Figure 3.10: Propene Hydrogenation Activities as a Function of Metal Content for Reduced/Oxidised Pt/P25 Catalysts

Table 3.15

i	$10^{-20}\sum_i$(No. of propene molecules hydrogenated)	10^4b/ kPa s^{-1}	$10^{-18}k_a$/ molecules s^{-1} g^{-1}
1	0.00	1.57	0.54
2	0.19	1.36	0.47
3	0.40	1.38	0.47
4	0.62	1.38	0.47
5	0.84	1.30	0.45
6	1.05	1.37	0.47
7	1.25	1.21	0.42
8	1.45	1.10	0.38
9	1.64	1.21	0.42
10	1.84	1.45	0.50
11	2.05	1.09	0.38
12	2.23	1.09	0.38
13	2.41	1.12	0.39
14	2.59	1.04	0.36
15	2.76	1.11	0.38
16	2.94	1.10	0.38

Reaction parameters:

Catalyst = Pt(0.25)/P25(P)

Catalyst pretreatment = None

Catalyst mass = 48mg

Reaction temperature = 300K

$P_{i(propene)}$ = 0.285 ± 0.001kPa

Propene:H_2 = 1:3.0

Table 3.16

i	$10^{-20}\Sigma_i$(No. of propene molecules hydrogenated)	10^4b/ kPa s^{-1}	$10^{-18}k_a$/ molecules s^{-1} g^{-1}
1	0.00	4.39	1.42
2	0.26	5.32	1.72
3	0.64	5.32	1.72
4	1.02	5.04	1.63
5	1.39	5.07	1.64
6	1.77	4.88	1.58
7	2.13	5.19	1.68
8	2.53	4.76	1.54
9	2.89	4.82	1.56
10	3.25	4.88	1.58
11	3.63	4.61	1.49
12	3.99	4.61	1.49
13	4.34	4.61	1.49
14	4.70	4.48	1.45
15	5.06	4.42	1.43

Reaction parameters:

Catalyst = Pt(0.5)/P25(P)

Catalyst pretreatment = None

Catalyst mass = 51mg

Reaction temperature = 300K

$P_{i(propene)}$ = 0.277 ± 0.004kPa

Propene:H_2 = 1:3.1

Table 3.17

i	$10^{-20}\sum_i$(No. of propene molecules hydrogenated)	10^4b/ kPa s^{-1}	$10^{-18}k_a$/ molecules s^{-1} g^{-1}
1	0.00	3.33	1.15
2	0.30	2.79	0.96
3	0.65	2.78	0.96
4	0.99	2.50	0.86
5	1.32	2.42	0.83
6	1.64	2.49	0.86
7	1.98	2.37	0.82
8	2.29	2.34	0.80
9	2.61	2.32	0.80
10	2.93	2.29	0.79
11	3.26	2.32	0.80
12	3.57	2.39	0.82
13	3.89	2.26	0.78
14	4.19	2.21	0.76

Reaction parameters:

Catalyst = Pt(1.0)/P25(P)

Catalyst pretreatment = None

Catalyst mass = 48mg

Reaction temperature = 300K

$P_{i(propene)}$ = 0.284 ± 0.002kPa

Propene:H_2 = 1:3.0

Table 3.18

i	$10^{-20}\sum_i$(No. of propene molecules hydrogenated)	10^4b/ kPa s^{-1}	$10^{-18}k_a$/ molecules s^{-1} g^{-1}
1	0.00	6.33	2.13
2	0.44	6.01	2.02
3	0.81	5.98	2.01
4	1.18	5.78	1.95
5	1.54	5.73	1.93
6	1.89	5.75	1.94
7	2.25	5.58	1.88
8	2.60	5.63	1.90
9	2.96	5.49	1.85
10	3.31	5.33	1.80
11	3.64	5.06	1.70
12	3.98	4.98	1.68
13	4.32	4.86	1.64
14	4.65	4.98	1.68
15	4.99	4.97	1.67

Reaction parameters:

Catalyst = Pt(2.0)/P25(P)

Catalyst pretreatment = None

Catalyst mass = 49mg

Reaction temperature = 300K

$P_{i(propene)}$ = 0.279 ± 0.001kPa

Propene:H_2 = 1:3.0

Table 3.19

i	$10^{-20}\sum_i$(No. of propene molecules hydrogenated)	10^4b/ kPa s^{-1}	$10^{-18}k_a$/ molecules s^{-1} g^{-1}
1	0.00	3.37	1.11
2	0.33	3.06	1.01
3	0.69	2.63	0.87
4	1.03	2.45	0.81
5	1.36	2.29	0.76
6	1.67	2.14	0.71
7	1.99	2.08	0.69
8	2.30	2.00	0.66
9	2.61	2.03	0.67
10	2.92	2.00	0.66
11	3.22	1.97	0.65
12	3.52	1.98	0.65
13	3.82	1.89	0.62
14	4.11	1.90	0.63

Reaction parameters:

Catalyst = Pt(0.5)/P25(T)

Catalyst pretreatment = None

Catalyst mass = 50mg

Reaction temperature = 300K

$P_{i(propene)}$ = 0.276 ± 0.001kPa

Propene:H_2 = 1:3.0

Table 3.20

i	$10^{-20}\sum_i$(No. of propene molecules hydrogenated)	10^4b/ kPa s^{-1}	$10^{-18}k_e$/ molecules s^{-1} g^{-1}
1	0.00	7.38	2.54
2	0.44	7.75	2.66
3	0.86	6.80	2.34
4	1.27	6.60	2.27
5	1.67	6.23	2.14
6	2.07	5.97	2.05
7	2.46	5.58	1.92
8	2.84	5.02	1.73
9	3.22	4.71	1.62
10	3.58	4.19	1.44
11	3.92	3.86	1.33
12	4.24	3.51	1.21

Reaction parameters:

Catalyst = Pt(0.25)/P25(P)

Catalyst pretreatment = H_2;3hrs;750K

O_2;3hrs;700K

Catalyst mass = 48g

Reaction temperature = 300K

$P_{i(propene)}$ = 0.278 ± 0.001kPa

Propene:H_2 = 1:3.0

Table 3.21

i	$10^{-20}\sum_i$(No. of propene molecules hydrogenated)	10^4b/ kPa s^{-1}	$10^{-18}k_a$/ molecules s^{-1} g^{-1}
1	0.00	15.76	5.10
2	0.43	15.88	5.14
3	0.83	15.87	5.13
4	1.22	15.64	5.06
5	1.63	15.88	5.14
6	2.03	15.76	5.10
7	2.44	15.79	5.11
8	2.84	15.70	5.08
9	3.25	15.70	5.08
10	3.64	16.07	5.20
11	4.03	15.39	4.98
12	4.41	14.59	4.72
13	4.78	14.06	4.55
14	5.13	13.32	4.31

Reaction parameters:

Catalyst = Pt(0.5)/P25(P)

Catalyst pretreatment = H_2;3hrs;750K

O_2;3hrs;700K

Catalyst mass = 51mg

Reaction temperature = 300K

$P_{i(propene)}$ = 0.279 ± 0.001kPa

Propene:H_2 = 1:3.0

Table 3.22

i	$10^{-20}\Sigma_i$(No. of propene molecules hydrogenated)	10^4b/ kPa s^{-1}	$10^{-18}k_a$/ molecules s^{-1} g^{-1}
1	0.00	13.24	4.55
2	0.40	14.09	4.84
3	0.77	14.51	4.99
4	1.14	14.66	5.04
5	1.52	14.80	5.09
6	1.91	14.97	5.15
7	2.30	14.56	5.01
8	2.68	14.71	5.06
9	3.08	14.74	5.07
10	3.47	14.03	4.82
11	3.85	13.76	4.73
12	4.22	13.39	4.60
13	4.62	13.04	4.48
14	5.01	12.80	4.40

Reaction parameters:

Catalyst = Pt(1.0)/P25(P)

Catalyst pretreatment = H_2;3hrs;750K

O_2;3hrs;700K

Catalyst mass = 48mg

Reaction temperature = 300K

$P_{i(propene)}$ = 0.280 ± 0.001kPa

Propene:H_2 = 1:3.0

Table 3.23

i	$10^{-20}\sum_i$(No. of propene molecules hydrogenated)	10^4b/ kPa s^{-1}	$10^{-18}k_a$/ molecules s^{-1} g^{-1}
1	0.00	12.92	4.34
2	0.39	12.74	4.29
3	0.78	12.30	4.14
4	1.17	13.01	4.38
5	1.59	12.74	4.29
6	1.99	13.05	4.39
7	2.39	13.40	4.51
8	2.79	13.39	4.51
9	3.19	13.26	4.47
10	3.60	13.27	4.47
11	4.00	13.29	4.48
12	4.49	13.00	4.38
13	4.88	11.31	3.81

Reaction parameters:

Catalyst = Pt(2.0)/P25(P)

Catalyst pretreatment = H_2;3hrs;750K

O_2;3hrs;700K

Catalyst mass = 49mg

Reaction temperature = 300K

$P_{i(propene)}$ = 0.282 ± 0.001kPa

Propene:H_2 = 1:3.0

Table 3.24

i	$10^{-20}\sum_i$(No. of propene molecules hydrogenated)	10^4b/ kPa s^{-1}	$10^{-18}k_a$/ molecules s^{-1} g^{-1}
1	0.00	13.03	4.30
2	0.39	12.84	4.24
3	0.80	12.60	4.16
4	1.21	12.81	4.23
5	1.61	12.76	4.21
6	2.02	12.95	4.27
7	2.42	12.96	4.28
8	2.84	12.87	4.25
9	3.25	13.04	4.30
10	3.66	12.91	4.26
11	4.08	12.81	4.23
12	4.49	12.81	4.23
13	4.90	12.63	4.17

Reaction parameters:

Catalyst = Pt(0.5)/P25(T)

Catalyst pretreatment = H_2;3hrs;750K

O_2;3hrs;700K

Catalyst mass = 50mg

Reaction temperature = 300K

$P_{i(propene)}$ = 0.274 ± 0.001kPa

Propene:H_2 = 1:3.0

3.1.6 Propene Hydrogenation over Reduced/Oxidised Pt(0.5)/P25 Catalysts: Temperature Dependence

a) Pt(0.5)/P25 Prepared by Photodeposition

The temperature dependence for the catalytic hydrogenation of propene over Pt(0.5)/P25(P), previously reduced in H_2 at 750K, then oxidised in O_2 at 700K prior to reaction, was measured over the range 273 - 345K. Throughout the course of the experiment, the propene:H_2 ratio and the total initial gas pressure in the reaction vessel was kept constant. The results are summarised in Table 3.25 and plotted in terms of absolute initial reaction rate vs temperature in Fig. 3.11. Measurement of the absolute reaction rates at the various selected reaction temperatures was carried out in a random manner, shown by the appropriate run number in Table 3.25. By using this procedure, any effect on the measured reaction rate due to catalyst deterioration would be immediately apparent. The results obtained suggest that no significant deterioration of the catalyst occurred during the course of the experiment, although reproducibility is rather poor. Fig. 3.12 gives the corresponding Arrhenius plot, constructed using this data.

From Fig. 3.11 it can be seen that the reaction rate increased with increasing temperature over the approximate range, 273 - 298K. Although the data is not particularly consistent at the lower end of this range, an activation energy of ~ +55kJ mol^{-1} was estimated for the hydrogenation reaction. Between 298 - 345K, the reaction rate was observed to fall non-linearly with increasing temperature.

b) Pt(0.5)/P25 Prepared by Impregnation/Reduction

The temperature dependence for the catalytic hydrogenation of propene over Pt(0.5)/P25(T), previously reduced in H_2 at 750K, then oxidised in O_2 at 700K prior to reaction, was measured over the range 260 - 343K. As in the previous experiment, absolute initial reaction rates were measured at selected temperatures in the order shown, so that any effects arising from catalyst deterioration would be immediately apparent. The results of this experiment are summarised in Table 3.26 and plotted in terms of absolute initial reaction rate vs temperature in Fig. 3.11. The corresponding Arrhenius plot, constructed from the results obtained in this experiment, is shown in Fig. 3.12.

As can be seen from Fig. 3.11, the measured reaction rate was found to fall very slightly, in a linear manner, over the range 273 - 343K. An activation energy of effectively zero was estimated for the hydrogenation reaction, over this temperature range. Below 273K, the rate of hydrogenation was observed to fall dramatically and activation energy of $\sim +45 kJ\ mol^{-1}$ was estimated for the reaction between 263 - 273K.

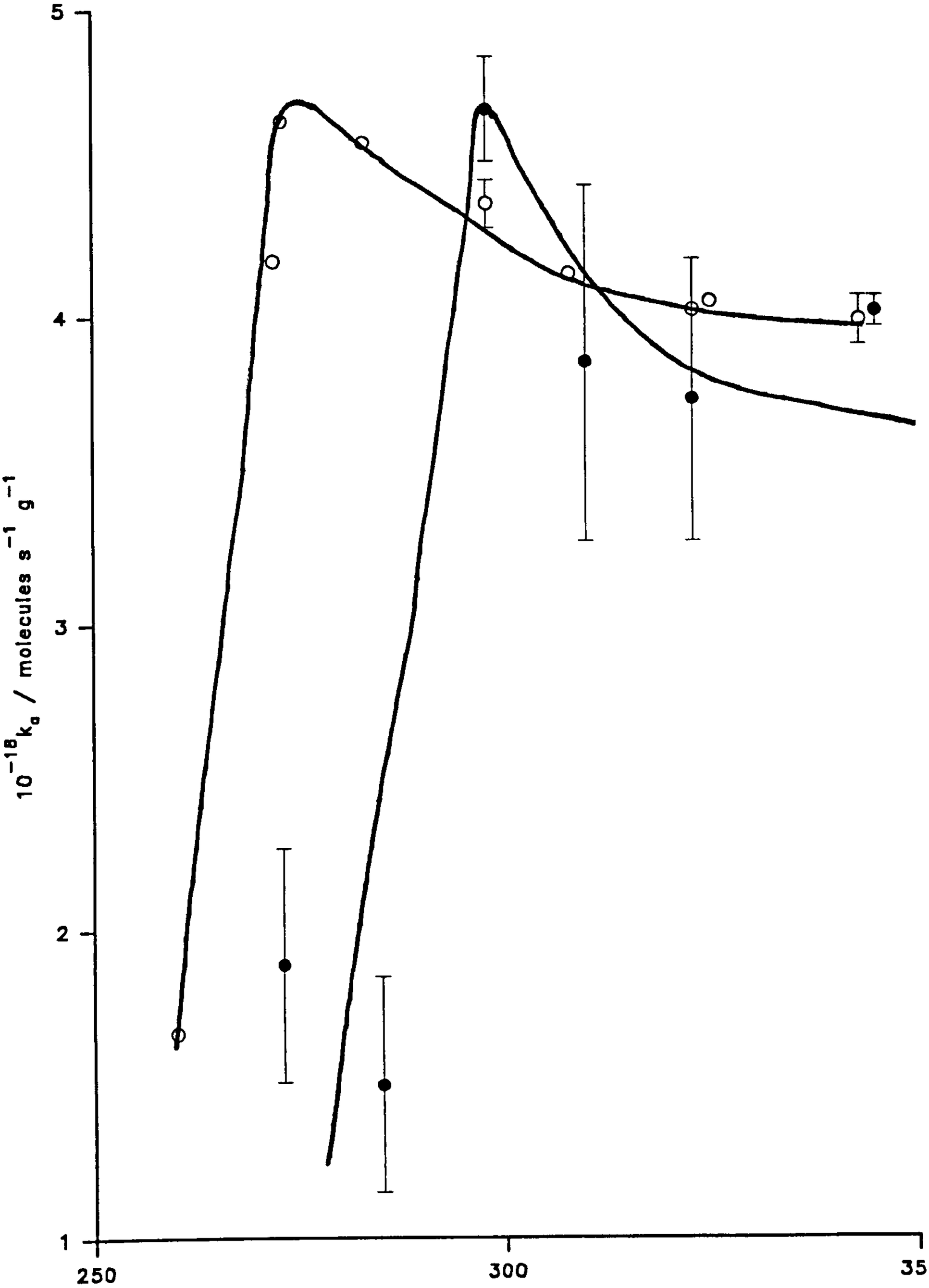

Figure 3.11: Effect of Temperature on Absolute Initial Propene Hydrogenation Rate over Reduced/Oxidised Pt(0.5)/P25(P) and Pt(0.5)/P25(T) Catalysts

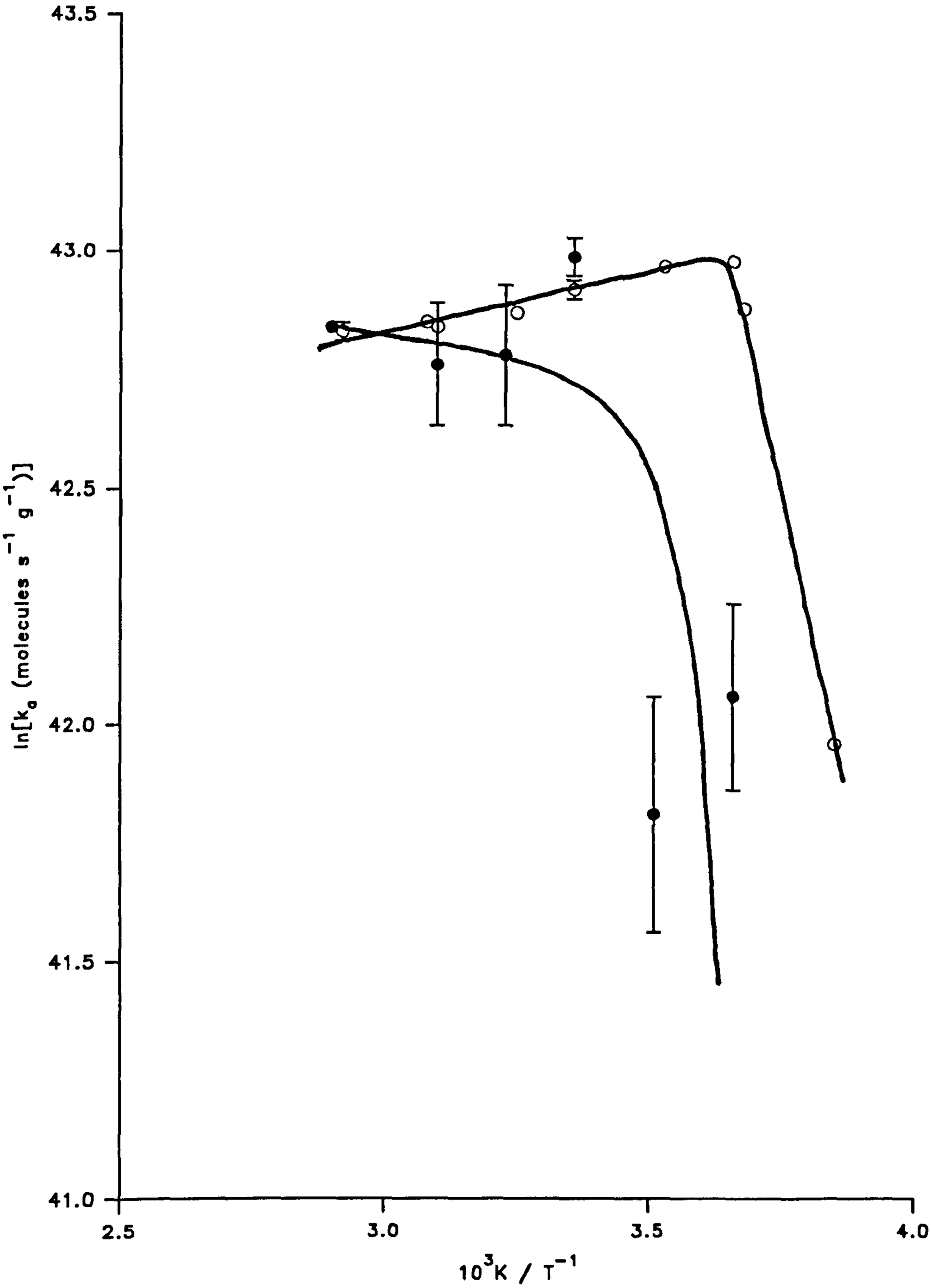

Figure 3.12: Arrhenius Plots for Propene Hydrogenation over Reduced/Oxidised Pt(0.5)/P25(P) and Pt(0.5)/P25(T) Catalysts

Table 3.25

Temp./ K	10^3K / T	10^4b/ kPa s^{-1}	$10^{-18}k_a$/ molecules s^{-1} g^{-1}	ln(k_a)	Run No.
273	3.66	6.58	2.26	42.26	2
		4.39	1.51	41.86	5
285	3.51	5.38	1.85	42.06	7
		3.35	1.15	41.56	12
298	3.36	14.08	4.84	43.02	1
		13.12	4.51	42.95	4
310	3.23	12.86	4.42	42.93	8
		9.51	3.27	42.63	11
323	3.10	12.19	4.19	42.88	3
		9.51	3.27	42.63	6
345	2.90	11.55	3.97	42.83	9
		11.81	4.06	42.85	10

Reaction Parameters:

Catalyst = Pt(0.5)/P25(P)

Catalyst pretreatment = H_2;3hrs;750K

O_2;3hrs;700K

Catalyst mass = 48mg

$P_{i(propene)}$ = 0.273 ± 0.001kPa

Propene:H_2 = 1:3.0

Table 3.26

Temp./ K	10^3K / T	10^4b/ kPa s^{-1}	$10^{-18}k_a$/ molecules s^{-1} g^{-1}	ln(k_a)	Run No.
260	3.85	4.96	1.67	41.96	12
272	3.68	12.41	4.18	42.88	11
273	3.66	13.78	4.64	42.98	10
283	3.53	13.57	4.57	42.97	9
298	3.36	13.19	4.44	42.94	1
		12.74	4.29	42.90	8
308	3.25	12.30	4.14	42.87	2
		12.30	4.14	42.87	7
323	3.10	11.94	4.02	42.84	3
325	3.08	12.03	4.05	42.85	6
343	2.92	11.61	3.91	42.81	4
		12.09	4.07	42.85	5

Reaction Parameters:

Catalyst = Pt(0.5)/P25(T)

Catalyst pretreatment = H_2;3hrs;750K

O_2;3hrs;700K

Catalyst mass = 49mg

$P_{i(propene)}$ = 0.269 ± 0.002kPa

Propene:H_2 = 1:3.0

3.1.7 Propene Hydrogenation over Reduced/Oxidised Pt(0.5)/P25: Effect of Variation in Initial Propene Partial Pressure

The dependence of the absolute initial reaction rate upon initial propene partial pressure was investigated for propene hydrogenation over Pt(0.5)/P25(P) and Pt(0.5)/P25(T) catalysts, at 300K. Both catalyst samples were reduced in H_2 at 750K, then re-oxidised in O_2 at 700K, prior to commencement of the experiment. In both experiments, the initial ratio of propene:H_2 in the reaction mixture was varied over the approximate range 0.1 - 0.5, with the initial H_2 partial pressure kept constant throughout.

The order of reaction with respect to propene can be calculated according via:

$$k_a = k P_h^m P_c^n \qquad [74]$$

where: k_a = absolute initial reaction rate (molecules s^{-1} g^{-1})

k = rate constant

P_h = initial hydrogen partial pressure (kPa)

P_c = initial propene partial pressure (kPa)

m,n = order of reaction with respect to hydrogen and propene respectively.

In this experiment, the initial partial hydrogen partial pressure was kept constant, giving:

$$k_a = K' P_c^n \qquad [75]$$

where: $K' = kP_h^m$ = constant

and taking logs gives:

$$\log(k_a) = \log(K') + n\log(P_c) \qquad [76]$$

Thus, plots of $\log(k_a)$ vs $\log(P_c)$ will have gradients equal to n, the order of reaction with respect to initial propene partial pressure.

a) Pt(0.5)/P25(P)

The dependency of the absolute initial reaction rate upon initial propene partial pressure for propene hydrogenation over Pt(0.5)/P25(P), at 300K, was investigated as outlined above. The results are summarised in Table 3.27 and plotted in terms of absolute initial reaction rate vs initial propene partial pressure in Fig. 3.13. As can be seen, the reaction rate was observed to increase linearly with increasing propene pressure, over the approximate range 0.05 - 0.20kPa. Above this pressure, the rate plateaued out and then began to fall as the propene pressure was further increased to ~ 0.40kPa. Fig. 3.14 shows the appropriate $\log(k_a)$ vs $\log(P_c)$ plot, derived from Eq.[76] using the results obtained in this experiment. From the linear part of the plot, corresponding to initial propene partial pressures in the approximate range 0.05 - 0.30kPa, the order of reaction, with respect to propene, was calculated to be +0.56. Above 0.30kPa, the plot becomes distinctly curved, indicating a change in reaction order as the initial propene partial pressure is further increased.

b) Pt(0.5)/P25(T)

The dependency of the absolute initial reaction rate upon initial propene partial pressure for propene hydrogenation over Pt(0.5)/P25(T), at 300K, was investigated as outlined above. The results are summarised in Table 3.28 and plotted in terms of absolute initial reaction rate vs initial propene partial pressure in Fig. 3.13. As can be seen, the reaction rate was found to increase in a non-linear manner over the whole partial pressure range investigated. The corresponding $\log(k_a)$ vs $\log(P_c)$ plot, derived using Eq.[76], is shown in Fig. 3.14 and can be seen to have good linearity. From this plot, the order of reaction, with respect to propene, was calculated to be +0.46.

3.1.8 Propene Hydrogenation over Reduced/Oxidised Pt(0.5)/P25: Effect of Variation in Initial Hydrogen Partial Pressure

The dependence of the absolute initial reaction rate upon initial hydrogen partial pressure was investigated for propene hydrogenation over Pt(0.5)/P25(P) and Pt(0.5)/P25(T) catalysts, at 300K. Both catalyst samples were reduced in H_2 at 750K, then re-oxidised in O_2 at 700K, prior to commencement of the experiment. In both experiments, the initial ratio of propene:H_2 in the reaction mixture was varied over the approximate range 0.1 - 1, with the initial propene partial pressure kept constant throughout.

Using Eq.[74], the order of reaction with respect to hydrogen, m, can be calculated for the hydrogenation reaction. Thus:

$$\log(k_a) = \log(K'') + m\log(P_h) \quad [77]$$

where - $K'' = kP_c^n$ = constant

Thus, plots of $\log(k_a)$ vs $\log(P_h)$ will have gradients equal to m, the order of reaction with respect to initial hydrogen partial pressure.

a) Pt(0.5)/P25(P)

The dependency of the absolute initial reaction rate upon initial hydrogen partial pressure for propene hydrogenation over Pt(0.5)/P25(P), at 300K, was investigated as outlined above. The results are summarised in Table 3.29 and plotted in terms of absolute initial reaction rate vs initial propene partial pressure in Fig. 3.15. As can be seen, the reaction rate was at first observed to increase sharply with increasing hydrogen partial pressure, over the range 0.2 - 0.4kPa, before reaching a plateau value. Above ~ 0.6kPa, the reaction rate decreased linearly, as the hydrogen partial pressure was further increased.

The appropriate $\log(k_a)$ vs $\log(P_h)$ plot, derived from the results obtained in this experiment using Eq.[77], is shown in Fig. 3.16. From the linear part of this plot, corresponding to initial hydrogen partial pressures in the approximate range 0.2 - 0.4kPa, the order of reaction with respect to hydrogen is calculated to be +0.60. Within the approximate range 0.4 - 0.6kPa, the plot is observed to curve significantly, indicating a changing reaction order, Above ~ 0.60kPa, the plot becomes linear once again and the reaction order with respect to hydrogen is calculated to be -0.55.

b) Pt(0.5)/P25(T)

The dependency of the absolute initial reaction rate upon initial hydrogen partial pressure for propene hydrogenation over Pt(0.5)/P25(T), at 300K, was investigated as outlined above. The results are summarised in Table 3.30 and plotted in terms of absolute initial reaction rate vs initial propene partial pressure in Fig. 3.15. As can be seen from this plot, the reaction rate was observed to increase sharply as the propene:H_2 ratio was reduced from 1:1, peaking at a ratio of 0.5:1 and then fall non-linearly as the ratio was further reduced to a limit of 0.1:1.

The appropriate $\log(k_a)$ vs $\log(P_h)$ plot, derived from the results obtained in this experiment using Eq.[77], is shown in Fig. 3.16. The plot is seen to be linear over the approximate range corresponding to initial hydrogen partial pressures of 0.25 - 0.65kPa, and the order of reaction, with respect to hydrogen, is calculated to be -0.30. Outside this stated range, on either side, the log-log plot is non-linear, indicating a variable reaction order.

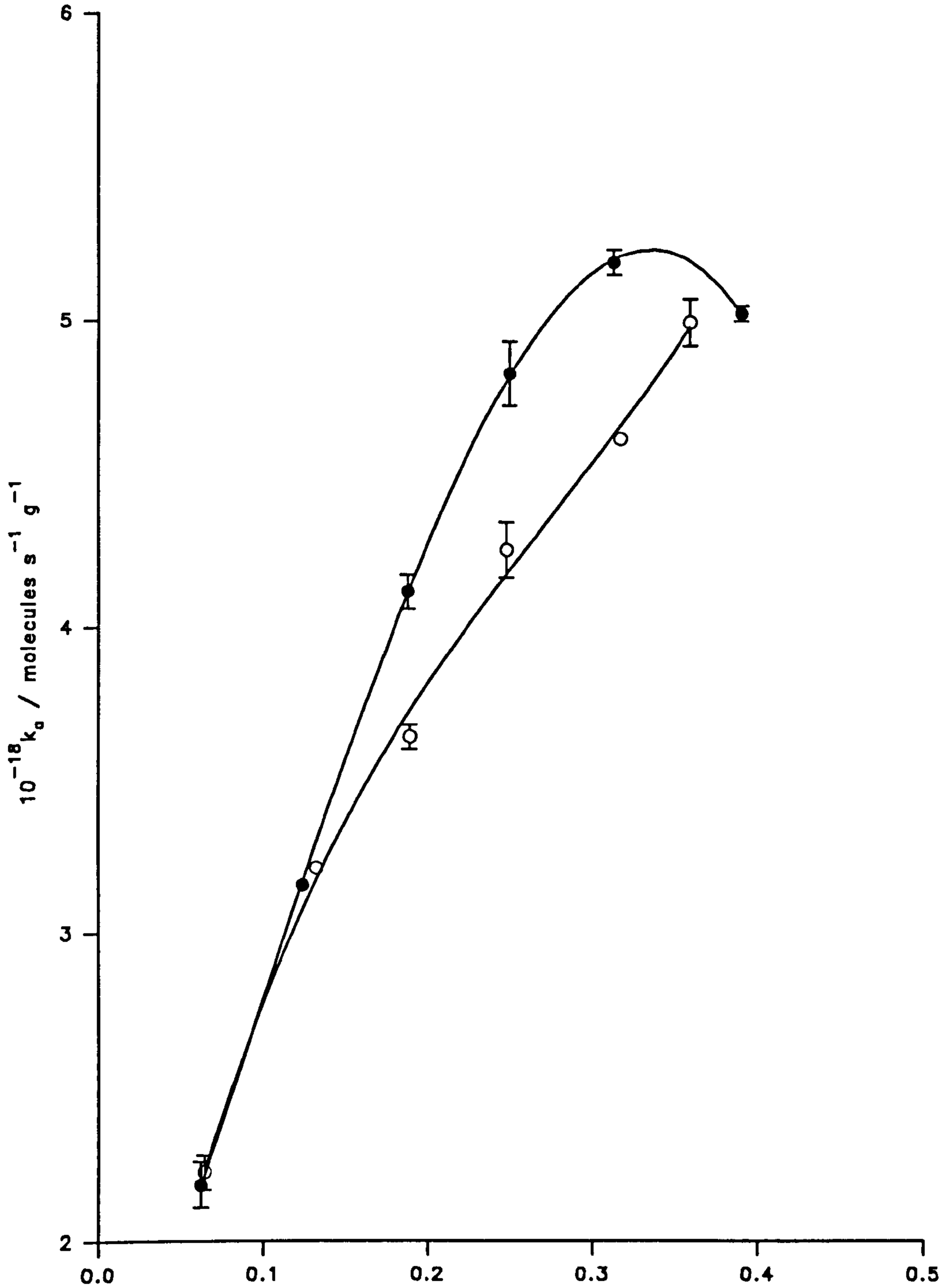

Figure 3.13: Absolute Initial Propene Hydrogenation Rate as a Function of Initial Propene Partial Pressure over Reduced/Oxidised Pt(0.5)/P25(P) and Pt(0.5)/P25(T)

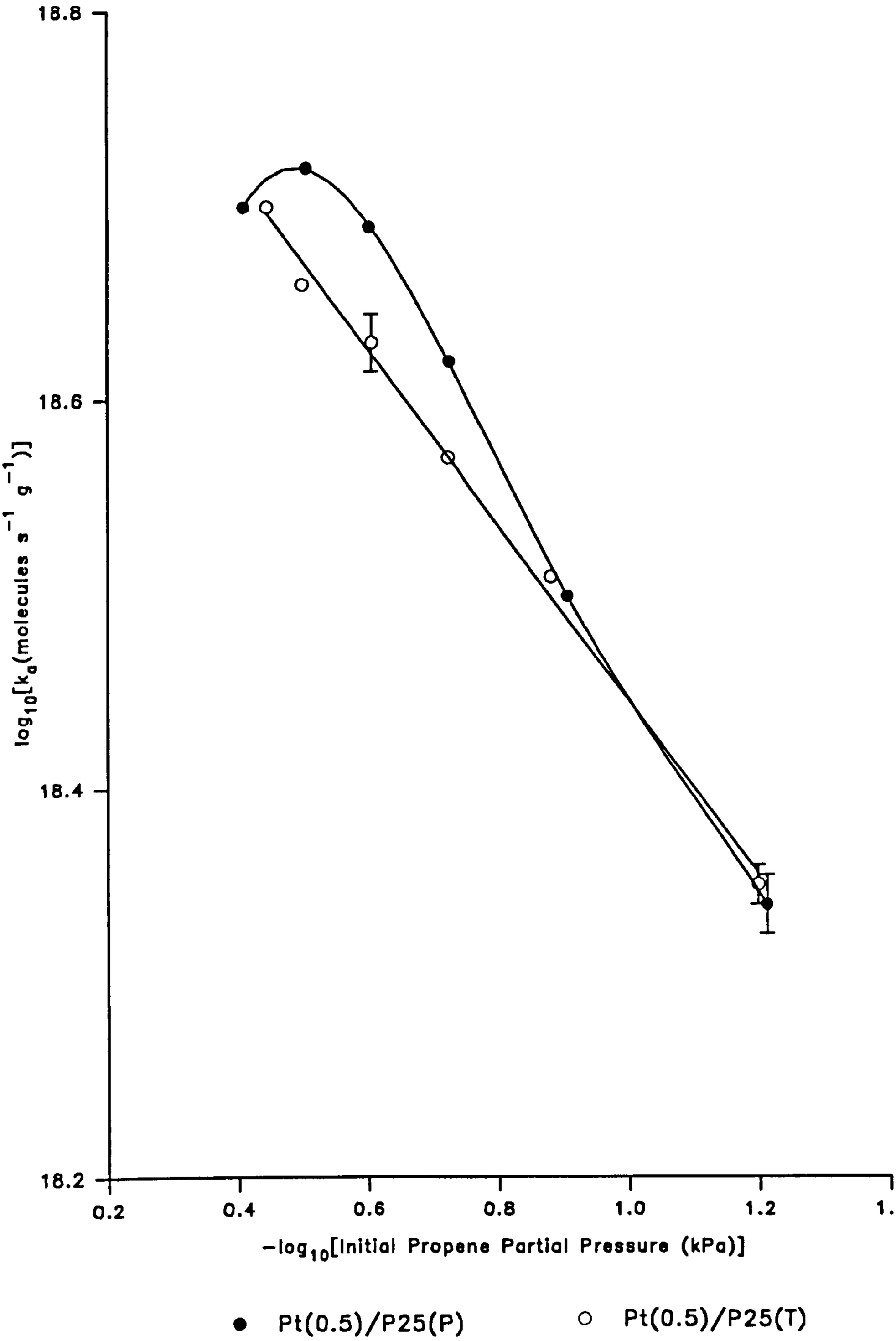

Figure 3.14: Plots of $\log_{10}$(Absolute Initial Propene Hydrogenation Rates) vs $\log_{10}$(Initial Propene Partial Pressure) for Reduced/Oxidised Pt(0.5)/P25(P) and Pt(0.5)/P25(T)

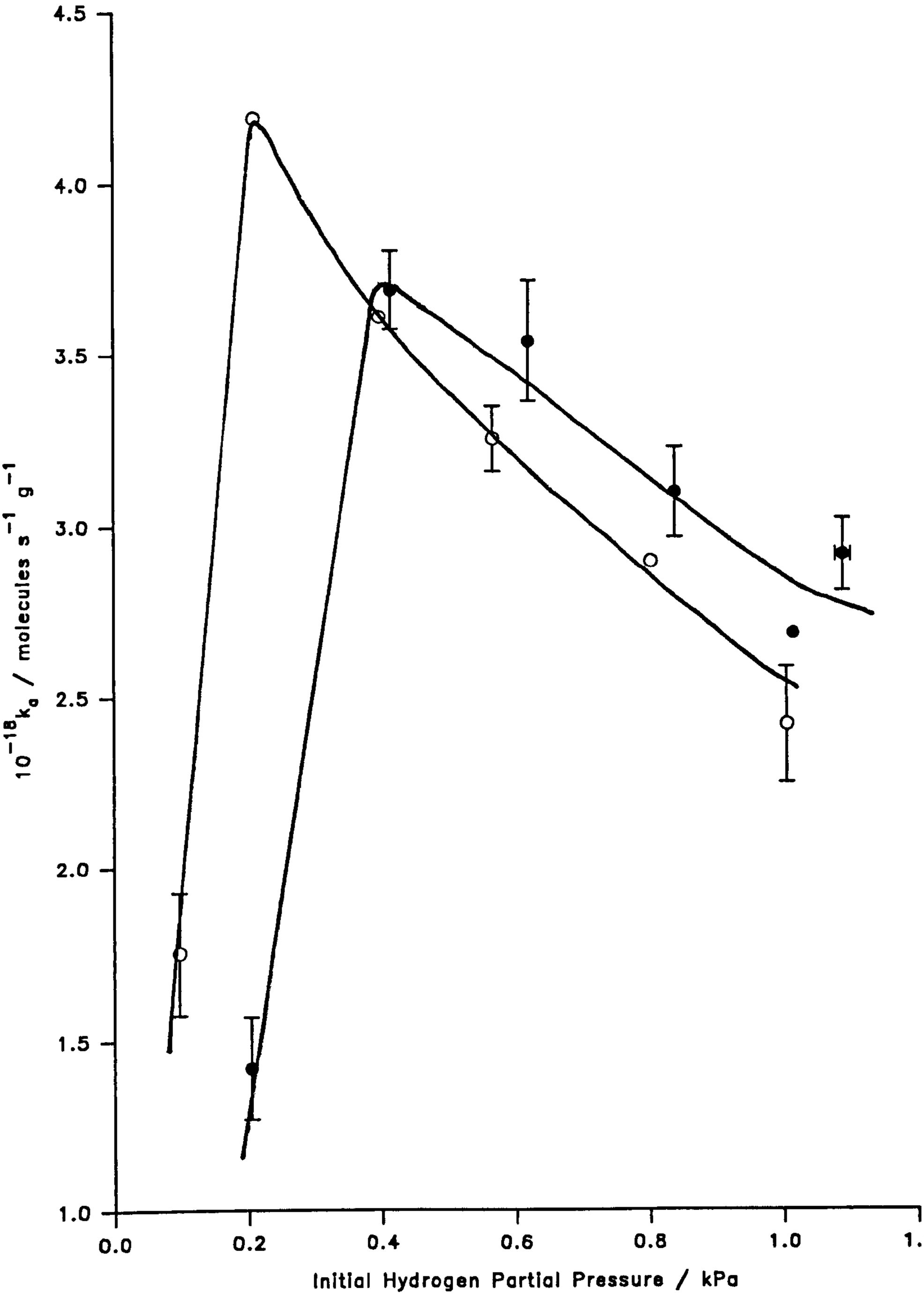

Figure 3.15: Absolute Initial Propene Hydrogenation Rates as a Function of Initial Hydrogen Partial Pressure for Reduced/Oxidised Pt(0.5)/P25(P) and Pt(0.5)/P25(T)

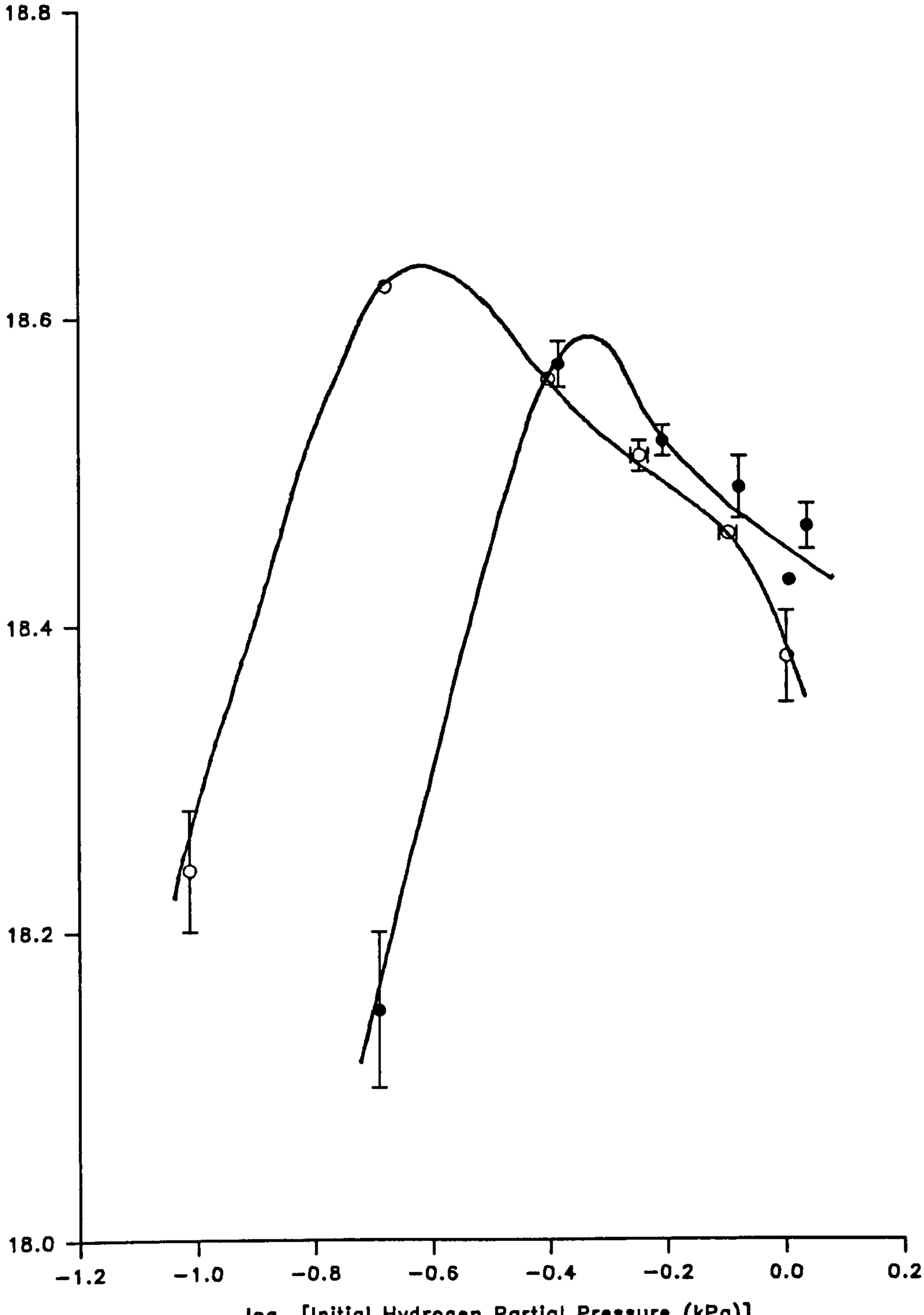

Figure 3.16: Plots of $\log_{10}$(Absolute Initial Propene Hydrogenation Rate) vs $\log_{10}$(Initial Hydrogen Partial Pressure) for Reduced/Oxidised Pt(0.5)/P25(P) and Pt(0.5)/P25(T)

Table 3.27

Initial C_3H_6:H_2	$P_{i(propene)}$/ kPa	10^4b/ kPa s^{-1}	$10^{-18}k_a$ / molecules s^{-1} g^{-1}	log $[P_{i(propene)}]$	log $[k_a]$
0.512	0.388	16.83	5.05	0.411	18.70
	0.392	16.66	5.00	0.407	18.70
0.415	0.312	17.17	5.15	0.506	18.71
	0.313	17.42	5.23	0.505	18.72
0.330	0.248	15.84	4.75	0.606	18.68
	0.251	16.33	4.90	0.600	18.69
0.249	0.188	13.91	4.17	0.726	18.62
	0.188	13.54	4.06	0.726	18.61
0.166	0.124	10.56	3.17	0.907	18.50
	0.124	10.46	3.14	0.907	18.50
0.083	0.061	7.02	2.11	1.215	18.32
	0.062	7.54	2.26	1.208	18.35

Reaction parameters:

Catalyst = Pt(0.5)/P25(P)

Catalyst pretreatment = H_2;3hrs;750K

O_2;3hrs;700K

Catalyst mass = 55mg

Reaction temperature = 300K

$P_{i(hydrogen)}$ = 0.752 ± 0.008kPa

Propene:H_2 = variable

Table 3.28

Initial $C_3H_6:H_2$	$P_{i(propene)}$/ kPa	10^4b/ kPa s^{-1}	$10^{-18}k_a$/ molecules s^{-1} g^{-1}	-log $[P_{i(propene)}]$	log $[k_a]$
0.466	0.360	16.27	5.07	0.444	18.71
	0.358	15.79	4.92	0.446	18.69
0.412	0.320	14.82	4.61	0.495	18.66
	0.314	14.81	4.61	0.503	18.66
0.324	0.248	13.95	4.34	0.606	18.64
	0.248	13.37	4.16	0.606	18.61
0.247	0.188	11.57	3.60	0.726	18.56
	0.190	11.82	3.68	0.721	18.57
0.173	0.131	10.26	3.19	0.883	18.50
	0.132	10.38	3.23	0.879	18.51
0.084	0.063	7.33	2.28	1.201	18.36
	0.064	6.98	2.17	1.194	18.34

Reaction parameters:

Catalyst = Pt(0.5)/P25(T)

Catalyst pretreatment = H_2;3hrs;750K

O_2;3hrs;700K

Catalyst mass = 53mg

Reaction temperature = 300K

$P_{i(hydrogen)}$ = 0.763 ± 0.005kPa

Propene:H_2 = variable

Table 3.29

Initial $C_3H_6:H_2$	$P_{i(hydrogen)}$/ kPa	10^4b/ kPa s^{-1}	$10^{-18}k_a$/ molecules s^{-1} g^{-1}	log $[P_{i(hydrogen)}]$	log $[k_a]$
0.500	0.205	4.23	1.27	-0.688	18.10
	0.203	5.23	1.57	-0.693	18.20
0.249	0.420	11.89	3.57	-0.377	18.55
	0.409	12.67	3.80	-0.388	18.58
0.166	0.626	12.40	3.72	-0.203	18.57
	0.618	11.19	3.36	-0.209	18.53
0.122	0.842	10.76	3.23	-0.075	18.51
	0.835	9.89	2.97	-0.078	18.47
0.103	1.013	8.94	2.68	0.006	18.43
	1.016	8.96	2.69	0.007	18.43
0.095	1.099	10.07	3.02	0.041	18.48
	1.078	9.38	2.81	0.033	18.45

Reaction parameters:

Catalyst = Pt(0.5)/P25(P)

Catalyst pretreatment = H_2;3hrs;750K

O_2;3hrs;700K

Catalyst mass = 54mg

Reaction temperature = 300K

$P_{i(propene)}$ = 0.103 ± 0.001kPa

Propene:H_2 = variable

Table 3.30

Initial $C_3H_6:H_2$	$P_{i(hydrogen)}$/ kPa	10^4b/ kPa s^{-1}	$10^{-18}k_a$/ molecules s^{-1} g^{-1}	log $[P_{i(hydrogen)}]$	log $[k_a]$
1.000	0.097	5.05	1.57	-1.013	18.20
	0.097	6.15	1.92	-1.013	18.28
0.474	0.212	13.47	4.19	-0.674	18.62
	0.208	13.46	4.19	-0.682	18.62
0.250	0.401	11.53	3.59	-0.397	18.56
	0.395	11.65	3.63	-0.403	18.56
0.174	0.570	10.13	3.15	-0.244	18.50
	0.566	10.72	3.34	-0.247	18.52
0.125	0.806	9.33	2.91	-0.094	18.46
	0.800	9.24	2.88	-0.097	18.46
0.100	1.003	7.21	2.25	0.001	18.35
	1.007	8.33	2.59	0.003	18.41

Reaction parameters:

Catalyst = Pt(0.5)/P25(T)

Catalyst pretreatment = H_2;3hrs;750K

O_2;3hrs;700K

Catalyst mass = 55mg

Reaction temperature = 300K

$P_{i(propene)}$ = 0.099 ± 0.001kPa

Propene:H_2 = variable

3.1.9 Cyclopropane Hydrogenation over Metallised TiO_2 Catalysts

Up to now, all the experiments described have been associated with the thermal hydrogenation of propene in the presence of platinised TiO_2 catalysts. As stated previously, this reaction was chosen for the initial experiments because it occurs readily at room temperature in the presence of Pt/TiO_2 and therefore, presented few experimental difficulties. The results of these initial experiments highlight some interesting aspects of platinised TiO_2, when used as a thermal hydrogenation catalyst. Not least are the obvious differences in behaviour observed between Pt/TiO_2 catalysts prepared by photodeposition and that prepared by impregnation/ reduction. At this stage it was decided that further information concerning the behaviour of metallised TiO_2 substrates, acting as thermal hydrogenation catalysts, could be obtained by extending this study. In particular, it was thought that the catalysts prepared by photodeposition and that prepared by impregnation/reduction might show more pronounced differences if a more demanding reaction, compared with propene hydrogenation, was investigated. For this reason, the hydrogenation of cyclopropane to propane, via C - C σ-bond hydrogenolysis, was chosen as the next reaction to study. Furthermore, the range of catalysts used in this particular study was extended to include the metals Pd, Rh and Ir, supported on P25 titania at a level of 0.5 mass%. These new catalysts were prepared using the same photodeposition technique as that used to prepare Pt/P25 catalysts. The role of the titania support in determining catalyst activity and stability was also briefly investigated by use of catalysts comprised of 0.5 mass% Pt deposited on pure anatase and on pure rutile.

These latter two catalysts were also prepared using the photodeposition method.

In preliminary experiments, designed to optimise the reaction conditions for cyclopropane hydrogenation, it was noticed that an increase in reaction temperature was often accompanied by a fall in catalyst activity. It was thought that this effect would arise if either the reaction was associated with an apparently negative activation energy or irreversible deterioration of the catalyst active sites occurred during the hydrogenation process. Differentiating between these two possible causes was achieved by measuring the activity of a catalyst as a function of increasing reaction temperature, within certain limits, and then again at the initial starting temperature. If the effect was due entirely to an apparently negative activation energy, then the two activity values measured at the lower reaction temperature limit would be roughly the same. However, if catalyst deterioration was occurring during hydrogenation, then the second value for the catalyst activity measured at the lower reaction temperature limit would be less than all previous values measured within the chosen temperature range. It is worth reiterating at this point that, by use of mass spectrometry, it was found that the hydrogenation of cyclopropane under the chosen reaction conditions gave propane as the sole reaction product.

Due consideration of these preliminary findings led to a common experimental procedure being adopted for all cyclopropane hydrogenation studies. Each investigation was repeated twice; the first time using catalyst samples which had been pre-reduced in H_2 at 750K and the second

time using catalyst samples which had been pre-reduced in H_2 at 750K, then re-oxidised in O_2 at 700K, prior to reaction. Catalyst activity was assessed by repeatedly dosing with a fixed composition c-C_3H_6/H_2 mixture and measuring the absolute initial reaction rate observed at each dosing. The reaction temperature was increased by approximately 10K, between the limits 370 - 420K, before each subsequent dosing. If the increase in reaction temperature was accompanied by a fall in catalyst activity, then a second measurement of catalyst activity was made at ~370K in order to determine the cause of this effect. The catalyst variables investigated using this experimental procedure, and the results obtained, are detailed below. It should be noted that the rate of reaction over the reduced photodeposited catalysts was below that detectable using the experimental set-up described. This led to quantisation of the data in the range 0.0 - 7.0 x 10^{-16} molecules s^{-1} g^{-1} and consequently only the points are depicted in the relevant plots, (e.g. Fig. 3.17).

3.1.10 Cyclopropane Hydrogenation over M(0.5)/P25 Catalysts: Effect of Supported Metal Type

In this series of experiments, catalyst activity for cyclopropane hydrogenation was investigated using various metals supported on P25 TiO_2, at a level of 0.5 mass%. Four catalysts, namely Pt(0.5), Pd(0.5), Rh(0.5) and Ir(0.5)/P25, were prepared via the photodeposition technique described earlier. A fifth catalyst, Pt(0.5)/P25(T), was also included in this study for comparative purposes.

a) Reduced Catalysts

The results obtained for this series of pretreated catalysts are summarised in Tables 3.31 - 3.35, and plotted in terms of absolute initial reaction rate vs temperature in Fig. 3.17. For all catalysts prepared by photodeposition, it is immediately obvious that high temperature reduction in H_2 rendered them virtually inactive for cyclopropane hydrogenation, within the temperature range investigated. In contrast, Pt(0.5)/P25(T) catalyst, pretreated in the same manner, was found to exhibit significantly higher activity under the same reaction conditions. Furthermore, it can be seen that the catalyst activity increased with increasing reaction temperature, which is the opposite trend to that observed in many preliminary experiments. A second measurement of activity at the lower temperature limit gave a value which was significantly higher than that initially recorded at this temperature.

b) Reduced/Oxidised Catalysts

The results obtained for this series of pretreated catalysts are summarised in Tables 3.36 - 3.39, and plotted in terms of absolute initial reaction rate vs temperature in Fig. 3.18. These results show that, immediately following pretreatment, catalyst activity for cyclopropane hydrogenation at 370K, in order of decreasing activity, was:

$$Pt(0.5)(T) \sim Pt(0.5)(P) \sim Pd(0.5)(P) > Rh(0.5)(P) >> Ir(0.5)(P) \sim 0.$$

Except for Ir(0.5)/P25(P), all the initial activities were far greater than those measured for the corresponding reduced catalysts. In the case of the iridium catalyst, reduction in H_2 at 750K, followed by re-oxidation in

O_2 at 700K failed to produce any significant activity for the reaction, within the temperature range investigated. For each of the remaining three active catalysts prepared by photodeposition it was observed that as the reaction temperature increased, catalyst activity decreased. Re-measurement of absolute initial reaction rates at 370K for a second time gave values which were much lower than all previously calculated rates, indicating irreversible deterioration in catalyst activity. In contrast, for Pt(0.5)/P25(T), increasing the reaction temperature from 370K to 420K had the effect of very slightly increasing the activity of the catalyst. Lowering the temperature from 420K to 370K returned the catalyst to its original activity, indicating that no deterioration of the catalyst had occurred during the hydrogenation reaction. The difference between the first and second measurements of absolute initial reaction rate at ~370K, for each of the active catalysts, was taken as a good indication of catalyst stability during cyclopropane hydrogenation and gave, in terms of decreasing stability, the order:

$$Pt(0.5)(T) > Pd(0.5)(P) >> Rh(0.5)(P) > Pt(0.5)(P).$$

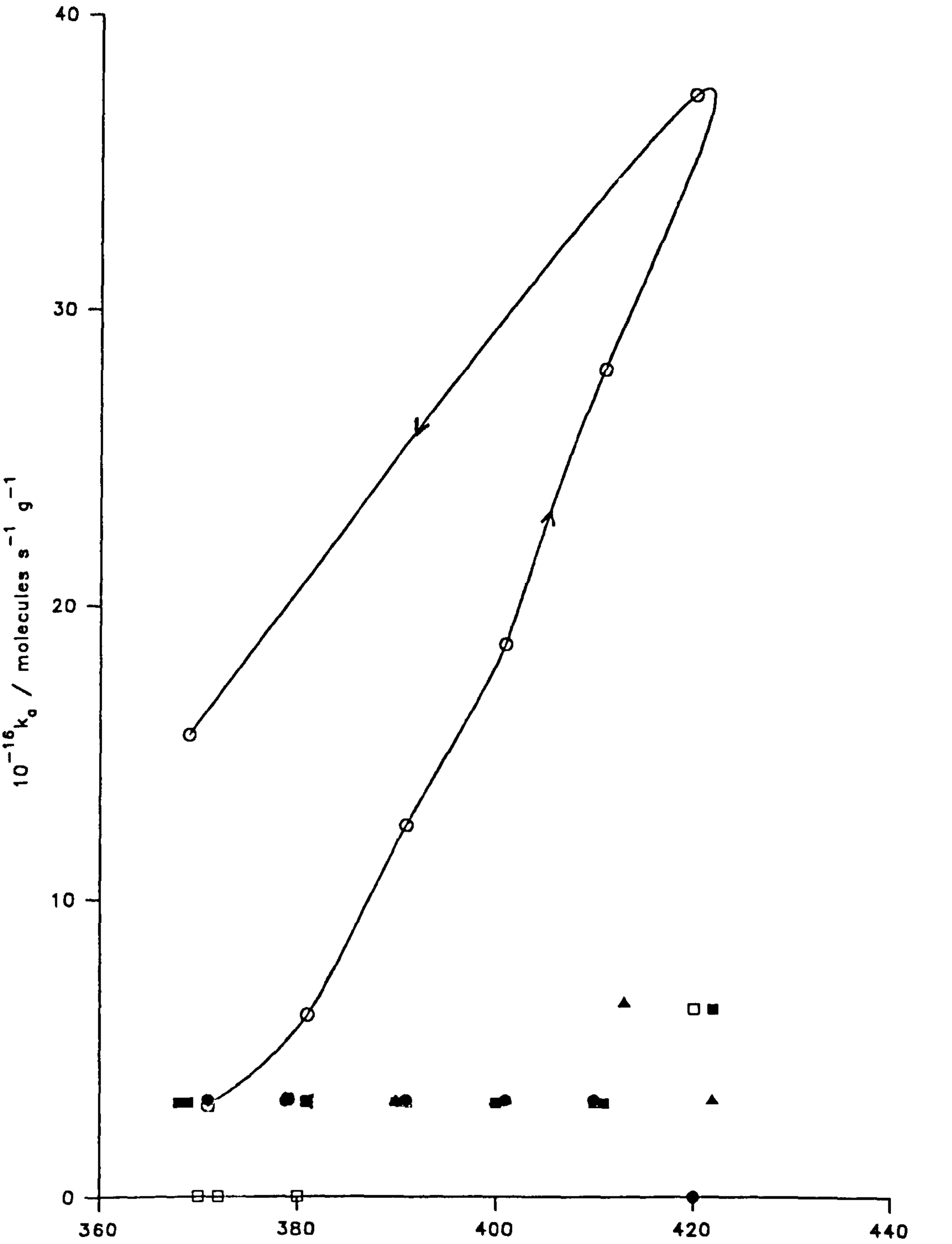

Figure 3.17: Effect of Temperature on Absolute Initial Cyclopropane Hydrogenation Rate for Various Reduced M(0.5)/P25 Catalysts

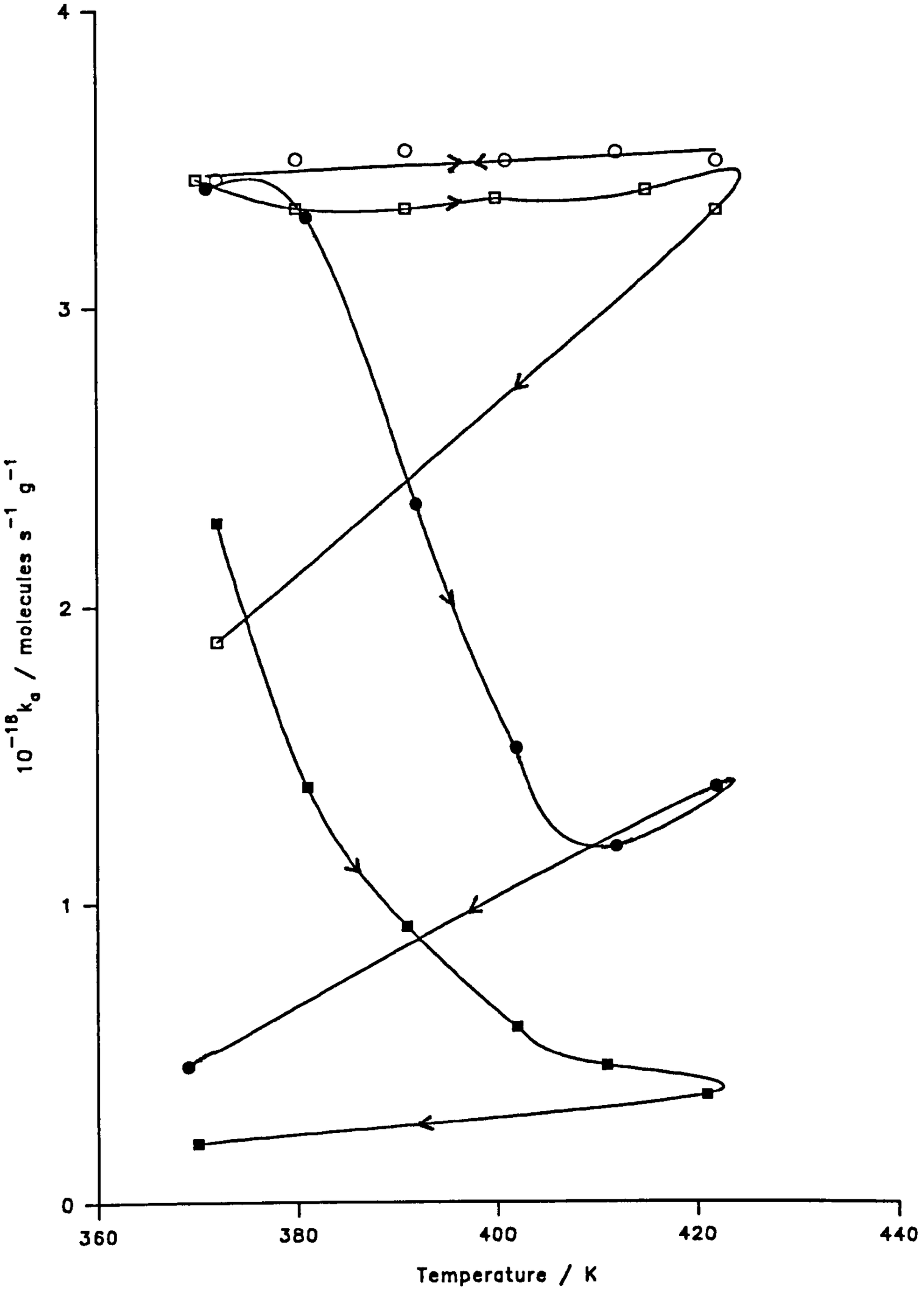

Figure 3.18: Effect of Temperature on Absolute Initial Cyclopropane Hydrogenation Rate for Various Reduced/Oxidised M(0.5)/P25 Catalysts

Table 3.31

i	Temp. /K	$10^{-18}\Sigma_i$(No. of c-C_3H_6 molecules hydrogenated)	-10^4b/ kPa s^{-1}	$10^{-16}k_a$/ molecules s^{-1} g^{-1}
1	371	0.00	0.0	3.3
2	379	0.28	0.1	3.3
3	391	0.79	0.1	3.3
4	401	1.33	0.1	3.3
5	410	2.14	0.1	3.3
6	420	2.92	0.0	0.0

Reaction parameters:

Catalyst = Pt(0.5)/P25(P)

Catalyst pretreatment = H_2;3hrs;750K

Catalyst mass = 50.0mg

$P_{i(cyclopropane)}$ = 0.290 ± 0.003kPa

Cyclopropane:H_2 = 1:2.913

Table 3.32

i	Temp. /K	$10^{-18}\Sigma_i$(No. of c-C_3H_6 molecules hydrogenated)	-10^4b/ kPa s^{-1}	$10^{-16}k_a$/ molecules s^{-1} g^{-1}
1	371	0.00	0.1	3.1
2	381	1.21	0.2	6.2
3	391	3.01	0.4	12.5
4	401	6.02	0.6	18.7
5	411	10.24	0.9	28.0
6	420	16.86	1.2	37.4
7	369	25.30	0.5	15.6

Reaction parameters:

Catalyst = Pt(0.5)/P25(T)

Catalyst pretreatment = H_2;3hrs;750K

Catalyst mass = 50.3mg

$P_{i(cyclopropane)}$ = 0.289 ± 0.002kPa

Cyclopropane:H_2 = 1:2.913

Table 3.33

i	Temp. /K	$10^{-18}\sum_i$(No. of c-C_3H_6 molecules hydrogenated)	-10^4b/ kPa s^{-1}	$10^{-16}k_a$/ molecules s^{-1} g^{-1}
1	368	0.00	0.1	3.2
2	381	0.60	0.1	3.2
3	390	1.21	0.1	3.2
4	400	2.41	0.1	3.2
5	411	3.01	0.1	3.2
6	422	4.22	0.2	6.4
7	369	5.42	0.1	3.2

Reaction parameters:

Catalyst = Rh(0.5)/P25(P)

Catalyst pretreatment = H_2;3hrs;750K

Catalyst mass = 51.7mg

$P_{i(cyclopropane)}$ = 0.291 ± 0.001kPa

Cyclopropane:H_2 = 1:2.913

Table 3.34

i	Temp. /K	$10^{-18}\sum_i$(No. of c-C_3H_6 molecules hydrogenated)	-10^4b/ kPa s^{-1}	$10^{-16}k_a$/ molecules s^{-1} g^{-1}
1	370	0.00	0.0	0.0
2	380	0.60	0.0	0.0
3	391	1.21	0.1	3.2
4	400	1.81	0.1	3.2
5	410	2.41	0.1	3.2
6	420	3.01	0.2	6.4
7	372	4.22	0.0	0.0

Reaction parameters:

Catalyst = Pd(0.5)/P25(P)

Catalyst pretreatment = H_2;3hrs;750K

Catalyst mass = 51.8mg

$P_{i(cyclopropane)}$ = 0.289 ± 0.004kPa

Cyclopropane:H_2 = 1:2.913

Table 3.35

i	Temp. /K	$10^{-18}\sum_i$(No. of c-C_3H_6 molecules hydrogenated)	-10^4b/ kPa s^{-1}	$10^{-16}k_a$/ molecules s^{-1} g^{-1}
1	371	0.00	0.1	3.3
2	381	0.63	0.1	3.3
3	390	1.22	0.1	3.3
4	401	1.82	0.1	3.3
5	413	2.41	0.2	6.6
6	422	3.03	0.1	3.3
7	371	4.20	0.1	3.3

Reaction parameters:

Catalyst = Ir(0.5)/P25(P)

Catalyst pretreatment = H_2;3hrs;750K

Catalyst mass = 49.8mg

$P_{i(cyclopropane)}$ = 0.285 ± 0.001kPa

Cyclopropane:H_2 = 1:3.0

Table 3.36

i	Temp. /K	$10^{-20}\sum_i$(No. of c-C_3H_6 molecules hydrogenated)	-10^4b/ kPa s^{-1}	$10^{-18}k_a$/ molecules s^{-1} g^{-1}
1	371	0.00	10.3	3.40
2	381	0.34	10.0	3.30
3	392	0.68	7.1	2.34
4	402	0.98	4.6	1.52
5	412	1.21	3.6	1.19
6	422	1.41	4.2	1.39
7	369	1.62	1.4	0.46

Reaction parameters:

Catalyst = Pt(0.5)/P25(P)

Catalyst pretreatment = H_2;3hrs;750K

O_2;3hrs;700K

Catalyst mass = 50.0mg

$P_{i(cyclopropane)}$ = 0.290 ± 0.002kPa

Cyclopropane:H_2 = 1:2.913

Table 3.37

i	Temp. /K	$10^{-20}\sum_i$(No. of c-C_3H_6 molecules hydrogenated)	-10^4b/ kPa s^{-1}	$10^{-18}k_a$/ molecules s^{-1} g^{-1}
1	371	0.00	10.3	3.40
2	380	0.33	10.6	3.50
3	391	0.66	10.7	3.53
4	401	0.99	10.6	3.50
5	412	1.30	10.7	3.53
6	422	1.60	10.6	3.50
7	372	1.90	10.4	3.43

Reaction parameters:

Catalyst = Pt(0.5)/P25(T)
Catalyst pretreatment = H_2;3hrs;750K
O_2;3hrs;700K
Catalyst mass = 50.3mg
$P_{i(cyclopropane)}$ = 0.285 ± 0.001kPa
Cyclopropane:H_2 = 1:2.913

Table 3.38

i	Temp. /K	$10^{-20}\sum_i$(No. of c-C_3H_6 molecules hydrogenated)	-10^4b/ kPa s^{-1}	$10^{-18}k_a$/ molecules s^{-1} g^{-1}
1	372	0.00	6.9	2.28
2	381	0.34	4.2	1.39
3	391	0.63	2.8	0.92
4	402	0.86	1.8	0.59
5	411	1.05	1.4	0.46
6	421	1.19	1.1	0.36
7	370	1.30	0.6	0.20

Reaction parameters:

Catalyst = Rh(0.5)/P25(P)
Catalyst pretreatment = H_2;3hrs;750K
O_2;3hrs;700K
Catalyst mass = 48.4mg
$P_{i(cyclopropane)}$ = 0.287 ± 0.001kPa
Cyclopropane:H_2 = 1:2.913

Table 3.39

i	Temp. /K	$10^{-20}\sum_i$(No. of c-C_3H_6 molecules hydrogenated)	-10^4b/ kPa s^{-1}	$10^{-18}k_a$/ molecules s^{-1} g^{-1}
1	370	0.00	10.4	3.43
2	380	0.34	10.1	3.33
3	391	0.67	10.1	3.33
4	400	0.99	10.2	3.37
5	415	1.31	10.3	3.40
6	422	1.62	10.1	3.33
7	372	1.92	5.7	1.88

Reaction parameters:

Catalyst = Pd(0.5)/P25(P)

Catalyst pretreatment = H_2;3hrs;750K

O_2;3hrs;700K

Catalyst mass = 51.8mg

$P_{i(cyclopropane)}$ = 0.282 ± 0.002kPa

Cyclopropane:H_2 = 1:3.0

3.1.11 Cyclopropane Hydrogenation over Pt(x)/P25(P):

Effect of Pt Content

In this group of experiments, activity for cyclopropane hydrogenation as a function of metal content was investigated for a series of platinised P25 titania catalysts. The activities of reduced and reduced/oxidised samples of three catalysts, prepared by photodeposition and having Pt contents of 0.25, 1.0 and 2.0 mass%, were measured. The results obtained in these experiments were compared alongside those

obtained for Pt(0.5)/P25(P) and Pt(0.5)/P25(T) catalysts, given in Section 3.1.10 above.

a) Reduced Catalysts

The results for this series of catalyst samples are summarised in Tables 3.40 - 3.42, and plotted in terms of absolute initial reaction rate vs temperature in Fig. 3.19. As would be expected in view of the pretreatment, these catalyst samples also exhibited very low activities for cyclopropane hydrogenation, in the temperature range investigated. Only Pt(2.0)/P25(P) showed any significant activity, which, despite a much higher metal content, was comparable with that observed for Pt(0.5)/P25(T), under similar conditions.

b) Reduced/Oxidised Catalysts

The results for this series of catalyst samples are summarised in Tables 3.43 - 3.45, and plotted in terms of absolute initial reaction rate vs temperature in Fig. 3.20. The results show that immediately after pretreatment, all catalysts exhibited roughly similar activities for cyclopropane hydrogenation at 370K. Increasing the reaction temperature within the range 370 - 420K was invariably accompanied by a corresponding fall in catalyst activity for all samples, with the photodeposited catalysts showing the greatest decrease overall. Re-measuring the activities of the catalysts for a second time, at 370K, revealed that irreversible deterioration had occurred for all photodeposited catalysts, but not for Pt(0.5)/P25(T), as noted in Section 3.1.10b above.

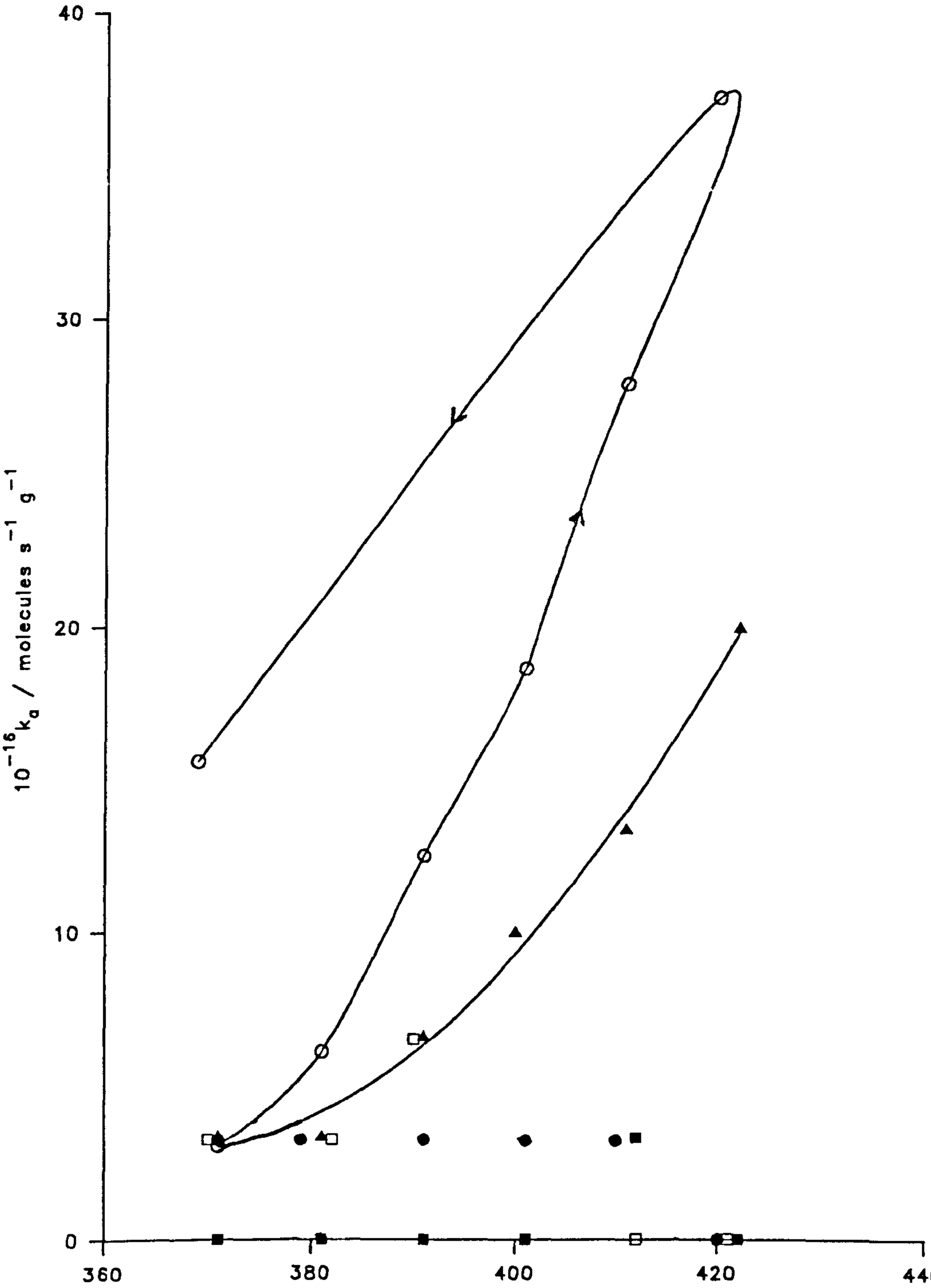

Figure 3.19: Effect of Temperature on Absolute Initial Cyclopropane Hydrogenation Rate for Various Reduced Pt(x)/P25(P) and Pt(0.5)/P25(T) Catalysts

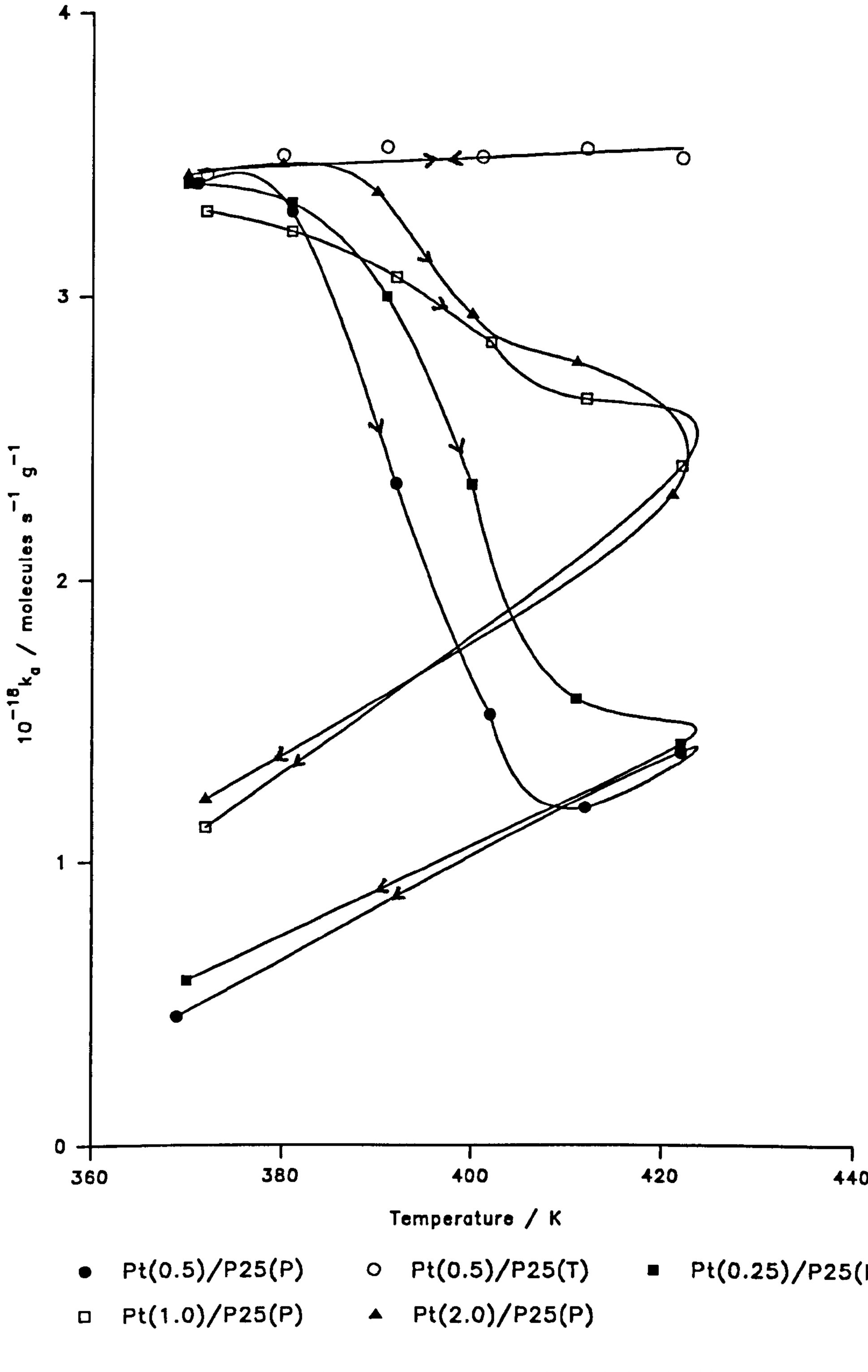

Figure 3.20: Effect of Temperature on Absolute Initial Cyclopropane Hydrogenation Rate for Various Reduced/Oxidised Pt(x)/P25(P) and Pt(0.5)/P25(T) Catalysts

Table 3.40

i	Temp. /K	$10^{-18}\Sigma_i$(No. of c-C_3H_6 molecules hydrogenated)	-10^4b/ kPa s^{-1}	$10^{-16}k_a$/ molecules s^{-1} g^{-1}
1	371	0.00	0.0	0.0
2	381	0.00	0.0	0.0
3	391	0.00	0.0	0.0
4	401	0.00	0.0	0.0
5	412	0.00	0.1	3.4
6	422	0.00	0.0	0.0

Reaction parameters:

Catalyst = Pt(0.25)/P25(P)

Catalyst pretreatment = H_2;3hrs;750K

Catalyst mass = 48.8mg

$P_{i(cyclopropane)}$ = 0.285 ± 0.001kPa

Cyclopropane:H_2 = 1:3.0

Table 3.41

i	Temp. /K	$10^{-18}\Sigma_i$(No. of c-C_3H_6 molecules hydrogenated)	-10^4b/ kPa s^{-1}	$10^{-16}k_a$/ molecules s^{-1} g^{-1}
1	370	0.00	0.1	3.3
2	382	0.00	0.1	3.3
3	390	0.60	0.2	6.6
4	401	1.21	0.0	0.0
5	412	1.81	0.0	0.0
6	421	2.41	0.0	0.0

Reaction parameters:

Catalyst = Pt(1.0)/P25(P)

Catalyst pretreatment = H_2;3hrs;750K

Catalyst mass = 50.1mg

$P_{i(cyclopropane)}$ = 0.286 ± 0.003kPa

Cyclopropane:H_2 = 1:2.997

Table 3.42

i	Temp. /K	$10^{-18}\Sigma_i$(No. of c-C_3H_6 molecules hydrogenated)	-10^4b/ kPa s^{-1}	$10^{-16}k_a$/ molecules s^{-1} g^{-1}
1	371	0.00	0.1	3.4
2	381	1.21	0.1	3.4
3	391	3.01	0.2	6.7
4	400	5.42	0.3	10.0
5	411	8.43	0.4	13.4
6	422	12.64	0.6	20.1

Reaction parameters:

Catalyst = Pt(2.0)/P25(P)

Catalyst pretreatment = H_2;3hrs;750K

Catalyst mass = 49.3mg

$P_{i(cyclopropane)}$ = 0.284 ± 0.001kPa

Cyclopropane:H_2 = 1:2.997

Table 3.43

i	Temp. /K	$10^{-20}\Sigma_i$(No. of c-C_3H_6 molecules hydrogenated)	-10^4b/ kPa s^{-1}	$10^{-18}k_a$/ molecules s^{-1} g^{-1}
1	370	0.00	10.3	3.40
2	381	0.34	10.1	3.33
3	391	0.67	9.1	3.00
4	400	0.99	7.1	2.34
5	411	1.30	4.8	1.58
6	422	1.54	4.3	1.42
7	370	1.78	1.8	0.59

Reaction parameters:

Catalyst = Pt(0.25)/P25(P)

Catalyst pretreatment = H_2;3hrs;750K

O_2;3hrs;700K

Catalyst mass = 48.8mg

$P_{i(cyclopropane)}$ = 0.284 ± 0.002kPa

Cyclopropane:H_2 = 1:3.0

Table 3.44

i	Temp. /K	$10^{-20}\sum_i$(No. of c-C_3H_6 molecules hydrogenated)	-10^4b/ kPa s^{-1}	$10^{-18}k_a$/ molecules s^{-1} g^{-1}
1	372	0.00	10.0	3.30
2	381	0.34	9.8	3.23
3	392	0.67	9.3	3.07
4	402	0.98	8.6	2.84
5	412	1.29	8.0	2.64
6	422	1.59	7.3	2.41
7	372	1.89	3.4	1.12

Reaction parameters:

Catalyst = Pt(1.0)/P25(P)
Catalyst pretreatment = H_2;3hrs;750K
O_2;3hrs;700K
Catalyst mass = 51.0mg
$P_{i(cyclopropane)}$ = 0.282 ± 0.002kPa
Cyclopropane:H_2 = 1:2.997

Table 3.45

i	Temp. /K	$10^{-20}\sum_i$(No. of c-C_3H_6 molecules hydrogenated)	-10^4b/ kPa s^{-1}	$10^{-18}k_a$/ molecules s^{-1} g^{-1}
1	370	0.00	10.4	3.43
2	380	0.33	10.5	3.47
3	390	0.66	10.2	3.37
4	400	0.99	8.9	2.94
5	411	1.31	8.4	2.77
6	421	1.62	7.0	2.31
7	372	1.90	3.7	1.22

Reaction parameters:

Catalyst = Pt(2.0)/P25(P)
Catalyst pretreatment = H_2;3hrs;750K
O_2;3hrs;700K
Catalyst mass = 49.3mg
$P_{i(cyclopropane)}$ = 0.283 ± 0.002kPa
Cyclopropane:H_2 = 1:2.997

3.1.12 Cyclopropane Hydrogenation over Pt(0.5)/TiO_2(P):

Effect of Titania Morphology

In this series of experiments, the effect of changing the morphology of the titania support material on catalyst activity for cyclopropane hydrogenation was investigated. Pure rutile, surface area 15.4 m^2g^{-1}, and pure anatase, surface area 63 m^2g^{-1}, were used as supports for 0.5 mass% Pt catalysts, prepared by photodeposition. The results of the experiments, detailed below, were compared with those obtained for Pt(0.5)/P25(P) and Pt(0.5)/P25(T) catalysts, determined under similar conditions.

a) Reduced Catalysts

The results obtained for this series of pretreated catalyst samples are summarised in Tables 3.46 - 3.47, and plotted in terms of absolute initial reaction rate vs temperature in Fig. 3.21. As can be seen from the results, high temperature reduction in H_2 rendered both catalysts virtually inactive for cyclopropane hydrogenation over the temperature range 370 - 420K. This behaviour is the same as that observed for Pt(0.5)/P25(P), which was also found to be inactive for the reaction following similar pretreatment, but in contrast to that of Pt(0.5)/P25(T), which exhibited a slight recovery in activity during cyclopropane hydrogenation under similar conditions.

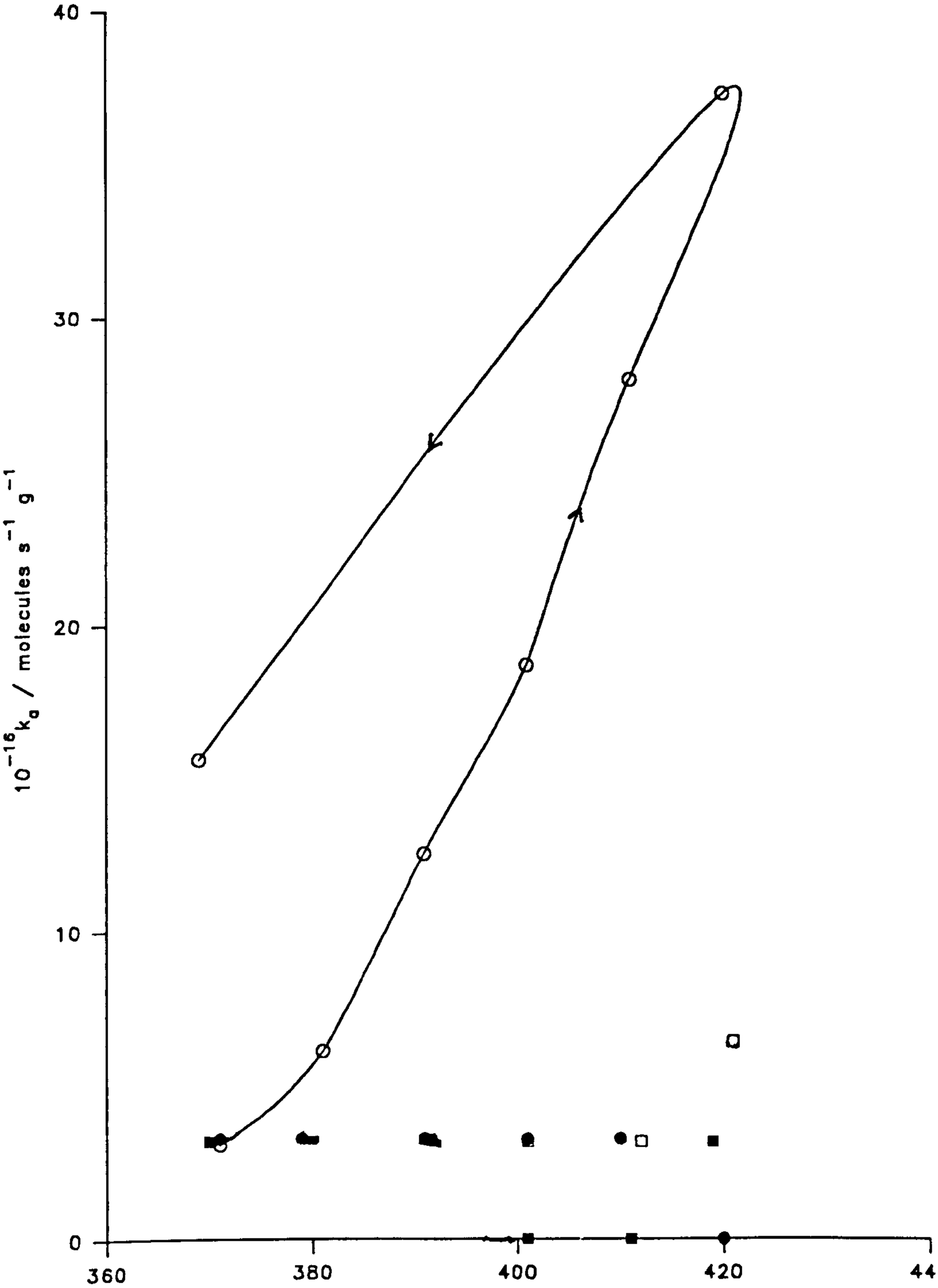

Figure 3.21 Effect of Temperature on Absolute Initial Cyclopropane Hydrogenation Rate for Reduced 0.5 mass% Pt on Various TiO_2 Supports

Table 3.46

i	Temp. /K	$10^{-18}\sum_i$(No. of c-C_3H_6 molecules hydrogenated)	-10^4b/ kPa s^{-1}	$10^{-16}k_a$/ molecules s^{-1} g^{-1}
1	370	0.00	0.1	3.2
2	380	0.00	0.1	3.2
3	392	0.60	0.1	3.2
4	401	1.22	0.0	0.0
5	411	1.81	0.0	0.0
6	419	2.41	0.1	3.2

Reaction parameters:

Catalyst = Pt(0.5)/anatase(P)

Catalyst pretreatment = H_2;3hrs;750K

Catalyst mass = 51.6mg

$P_{i(cyclopropane)}$ = 0.282 ± 0.002kPa

Cyclopropane:H_2 = 1:3.0

Table 3.47

i	Temp. /K	$10^{-18}\sum_i$(No. of c-C_3H_6 molecules hydrogenated)	-10^4b/ kPa s^{-1}	$10^{-16}k_a$/ molecules s^{-1} g^{-1}
1	370	0.00	0.1	3.2
2	380	0.00	0.1	3.2
3	392	0.00	0.1	3.2
4	401	0.00	0.1	3.2
5	412	0.60	0.1	3.2
6	421	1.21	0.2	6.5

Reaction parameters:

Catalyst = Pt(0.5)/rutile(P)

Catalyst pretreatment = H_2;3hrs;750K

Catalyst mass = 51.0mg

$P_{i(cyclopropane)}$ = 0.284 ± 0.002kPa

Cyclopropane:H_2 = 1:3.0

b) Reduced/Oxidised Catalysts

The results for this series of pretreated catalyst samples are summarised in Tables 3.48 - 3.49, and plotted in terms of absolute initial reaction rate vs temperature in Fig. 3.22. It can be seen that immediately following pretreatment, the activities of these two catalysts, for cyclo-propane hydrogenation at 370K, were virtually identical, and very similar to those observed for Pt(0.5)/P25(P) and Pt(0.5)/P25(T) catalysts under the same conditions. Again, the activities of both catalysts were observed to fall as the reaction temperature was increased gradually to ~ 420K. As with reduced/ oxidised Pt(0.5)/P25(P), the decline in the activities of these two catalysts was irreversible, since re-measurement of absolute initial reaction rates at 370K, for a second time, yielded values much lower than all preceding values for the rates of hydrogenation. The overall fall in the activity was considerable and approximately equal for both catalysts. This behaviour is in contrast to that observed for reduced/ oxidised Pt(0.5)/P25(T), in which case increasing the reaction temperature in the range 370 - 420K had very little effect on catalyst activity or stability.

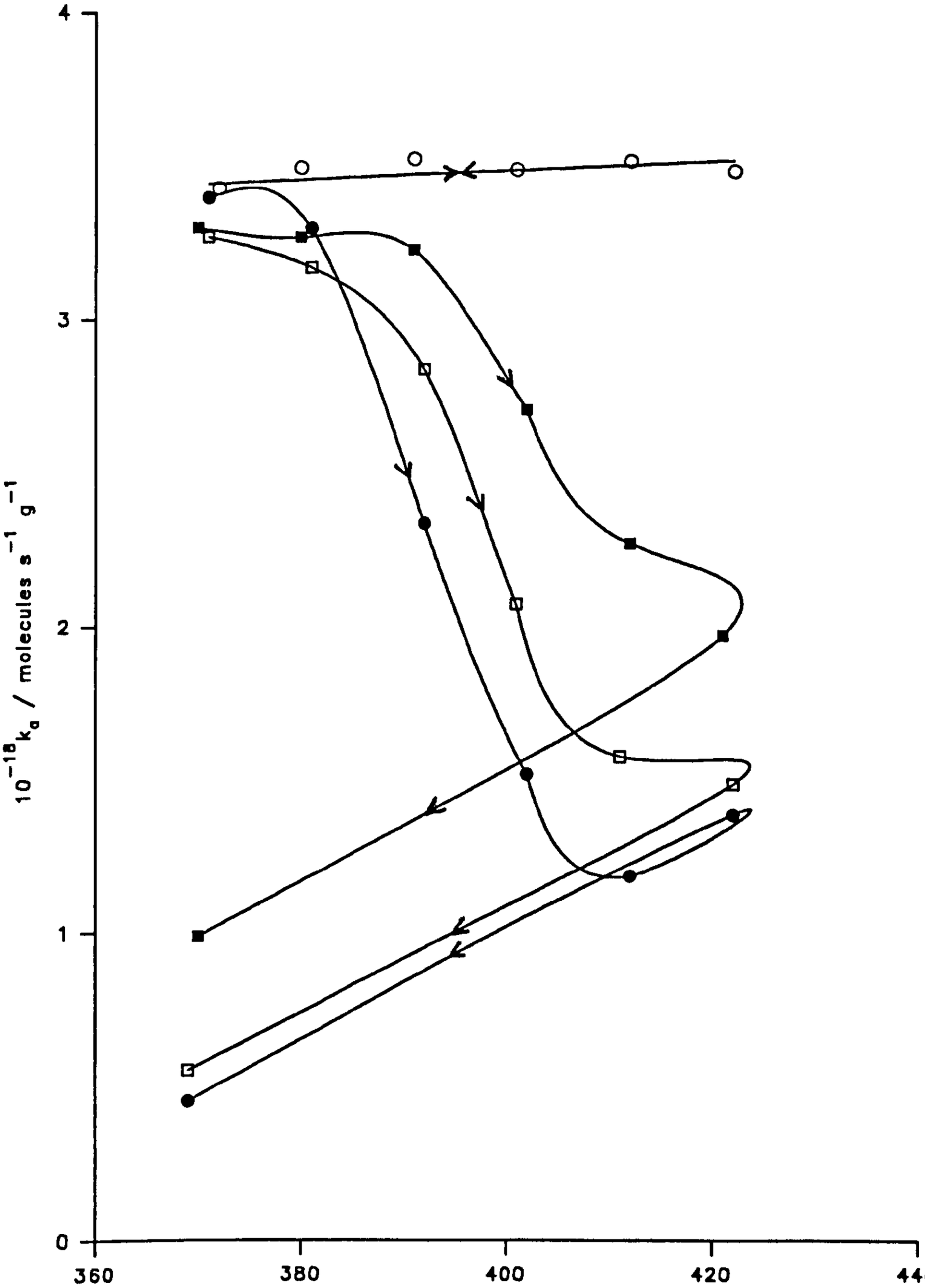

Figure 3.22: Effect of Temperature on Absolute Initial Cyclopropane Hydrogenation Rate for Reduced/Oxidised 0.5 mass% Pt on Various TiO_2 Supports

Table 3.48

i	Temp. /K	$10^{-20}\sum_i$(No. of c-C_3H_6 molecules hydrogenated)	-10^4b/ kPa s^{-1}	$10^{-18}k_a$/ molecules s^{-1} g^{-1}
1	370	0.00	10.1	3.30
2	380	0.34	9.9	3.27
3	391	0.67	9.8	3.23
4	402	1.01	8.2	2.71
5	412	1.31	6.9	2.28
6	421	1.60	6.0	1.98
7	370	1.87	3.0	0.99

Reaction parameters:

Catalyst = Pt(0.5)/anatase(P)
Catalyst pretreatment = H_2;3hrs;750K
O_2;3hrs;700K
Catalyst mass = 51.6mg
$P_{i(cyclopropane)}$ = 0.284 ± 0.002kPa
Cyclopropane:H_2 = 1:3.0

Table 3.49

i	Temp. /K	$10^{-20}\sum_i$(No. of c-C_3H_6 molecules hydrogenated)	-10^4b/ kPa s^{-1}	$10^{-18}k_a$/ molecules s^{-1} g^{-1}
1	371	0.00	9.9	3.27
2	381	0.34	9.6	3.17
3	392	0.68	8.6	2.84
4	401	1.00	6.3	2.08
5	411	1.29	4.8	1.58
6	422	1.55	4.5	1.49
7	369	1.80	1.7	0.56

Reaction parameters:

Catalyst = Pt(0.5)/rutile(P)
Catalyst pretreatment = H_2;3hrs;750K
O_2;3hrs;700K
Catalyst mass = 51.0mg
$P_{i(cyclopropane)}$ = 0.282 ± 0.002kPa
Cyclopropane:H_2 = 1:3.0

3.1.13 Cyclopropane Hydrogenation over Pt(0.5)/P25(T): Effect of Reactant Partial Pressures

a) Cyclopropane

The dependence of the absolute initial reaction rate upon initial cyclopropane partial pressure was investigated for cyclopropane hydrogenation over Pt(0.5)/P25(T) catalyst, at 300K. Prior to commencing the experiment, the catalyst sample was reduced in H_2 at 750K, then re-oxidised in O_2 at 700K. The initial cyclopropane:H_2 ratio was varied over the approximate range 0.09 - 0.54, whilst the initial hydrogen partial pressure was kept constant at 0.723 ± 0.006 kPa throughout the experiment. The results are summarised in Table 3.50 and plotted in terms of absolute initial reaction rate vs initial cyclopropane pressure in Fig. 3.23. As can be seen from these results, the reaction rate was observed to increase non-linearly as the initial cyclopropane partial pressure was gradually increased over the range investigated. The corresponding plot of $\log(k_a)$ vs $\log(P_c)$, derived by using Eqs.[74 - 76] given in Section 3.1.7, is shown in Fig. 3.24 and can be seen to exhibit good linearity. From this plot, the order of reaction, with respect to cyclopropane, for the hydrogenation of cyclopropane over reduced/oxidised Pt(0.5)/P25(T) catalyst, at 300K, was calculated to be +0.50.

b) Hydrogen

In a similar experiment to that described in part (a) above, the effect of varying the initial hydrogen partial pressure upon absolute initial

reaction rate was investigated for cyclopropane hydrogenation over Pt(0.5)/P25(T) catalyst, at 300K. As before, the catalyst sample was reduced in H_2 at 750K, then re-oxidised in O_2 at 700K, prior to commencing the experiment. The initial cyclopropane:H_2 ratio was varied over the approximate range 0.09 - 0.66, whilst the initial cyclopropane partial pressure was kept constant at 0.101 ± 0.002 kPa throughout the experiment. The results are summarised in Table 3.51 and plotted in terms of absolute initial reaction rate vs initial hydrogen partial pressure in Fig. 3.25. The results show that as the initial hydrogen partial pressure was gradually increased over the range investigated, the reaction rate gradually fell in a non-linear manner. The corresponding $\log(k_a)$ vs $\log(P_h)$, derived using Eqs. [74] and [77], is shown in Fig. 3.26 and can be seen to exhibit reasonably good linearity. The order of reaction, with respect to hydrogen, for the hydrogenation of cyclopropane over reduced/oxidised Pt(0.5)/P25(T) catalyst, at 300K, was calculated to be -0.31.

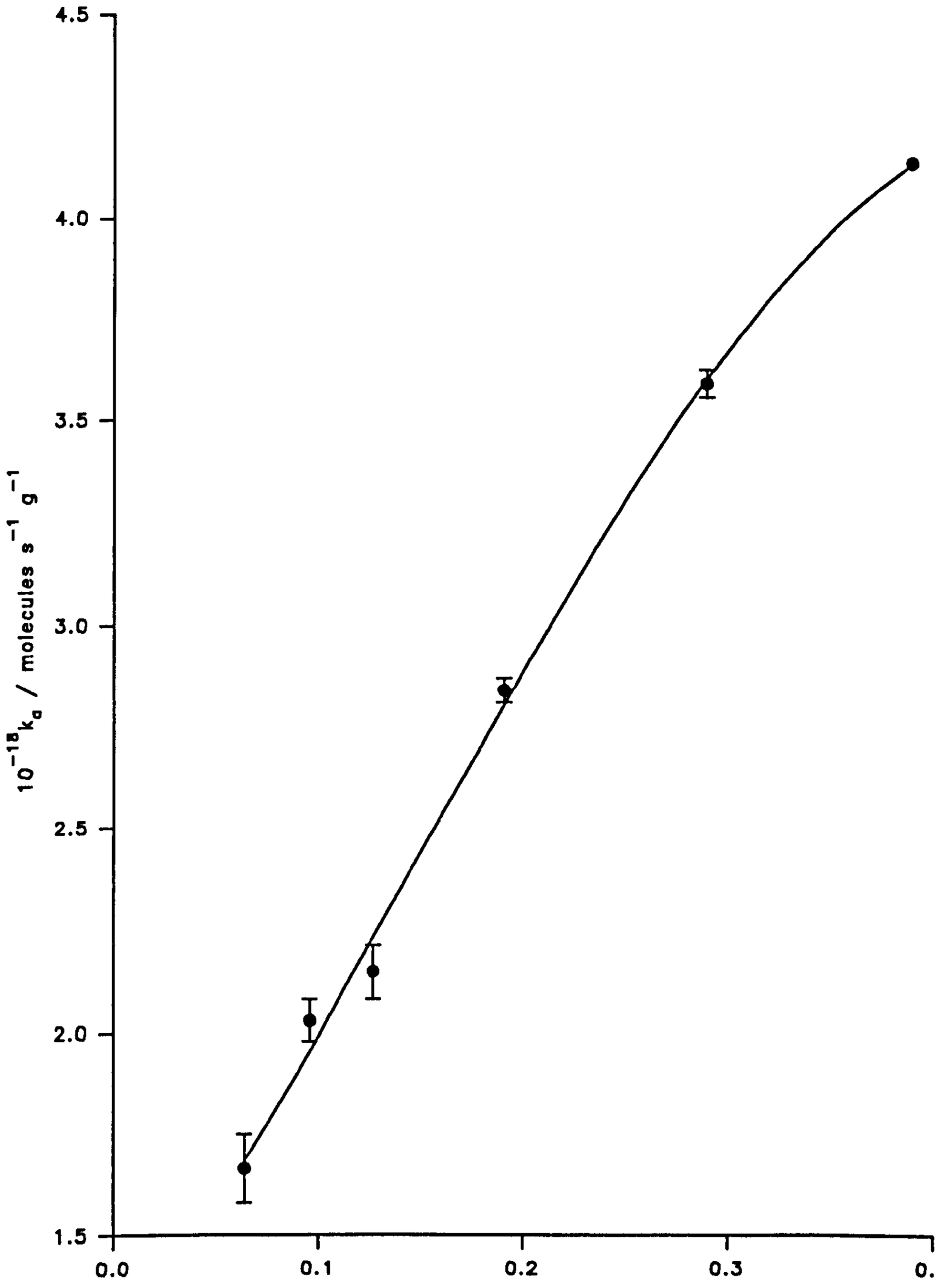

Figure 3.23: Absolute Initial Cyclopropane Hydrogenation Rate as a Function of Initial Cyclopropane Partial Pressure for Reduced/Oxidised Pt(0.5)/P25(T)

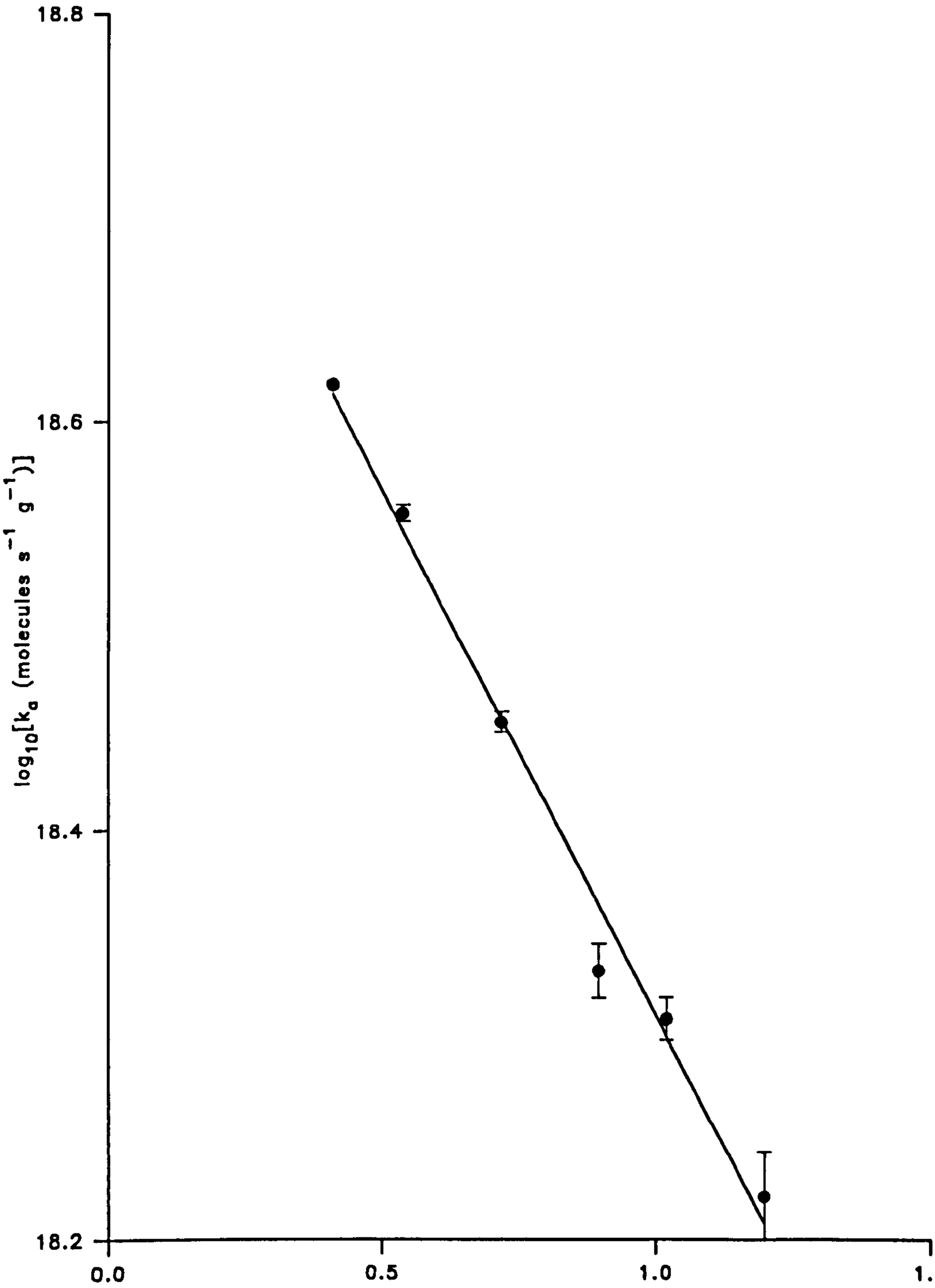

Figure 3.24: Plot of $\log_{10}$(Absolute Initial Cycloprpane Hydrogenation Rate) vs $\log_{10}$(Initial Cyclopropane Partial Pressure for Reduced/Oxidised Pt(0.5)/P25(T)

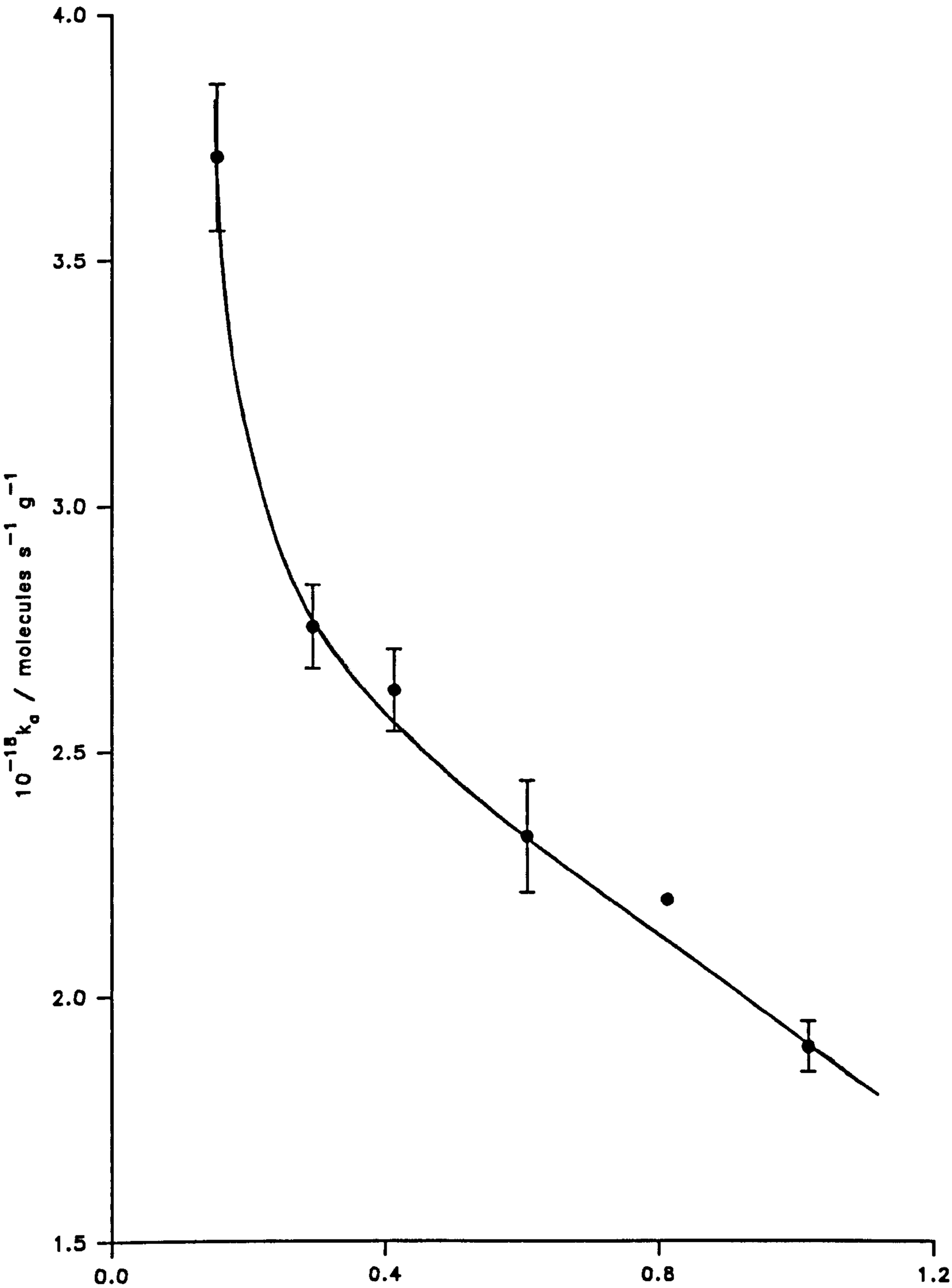

Figure 3.25: Absolute Initial Cycloropane Hydrogenation Rate as a Function of Initial Hydrogen Partial Pressure for Reduced/Oxidised Pt(0.5)/P25(T)

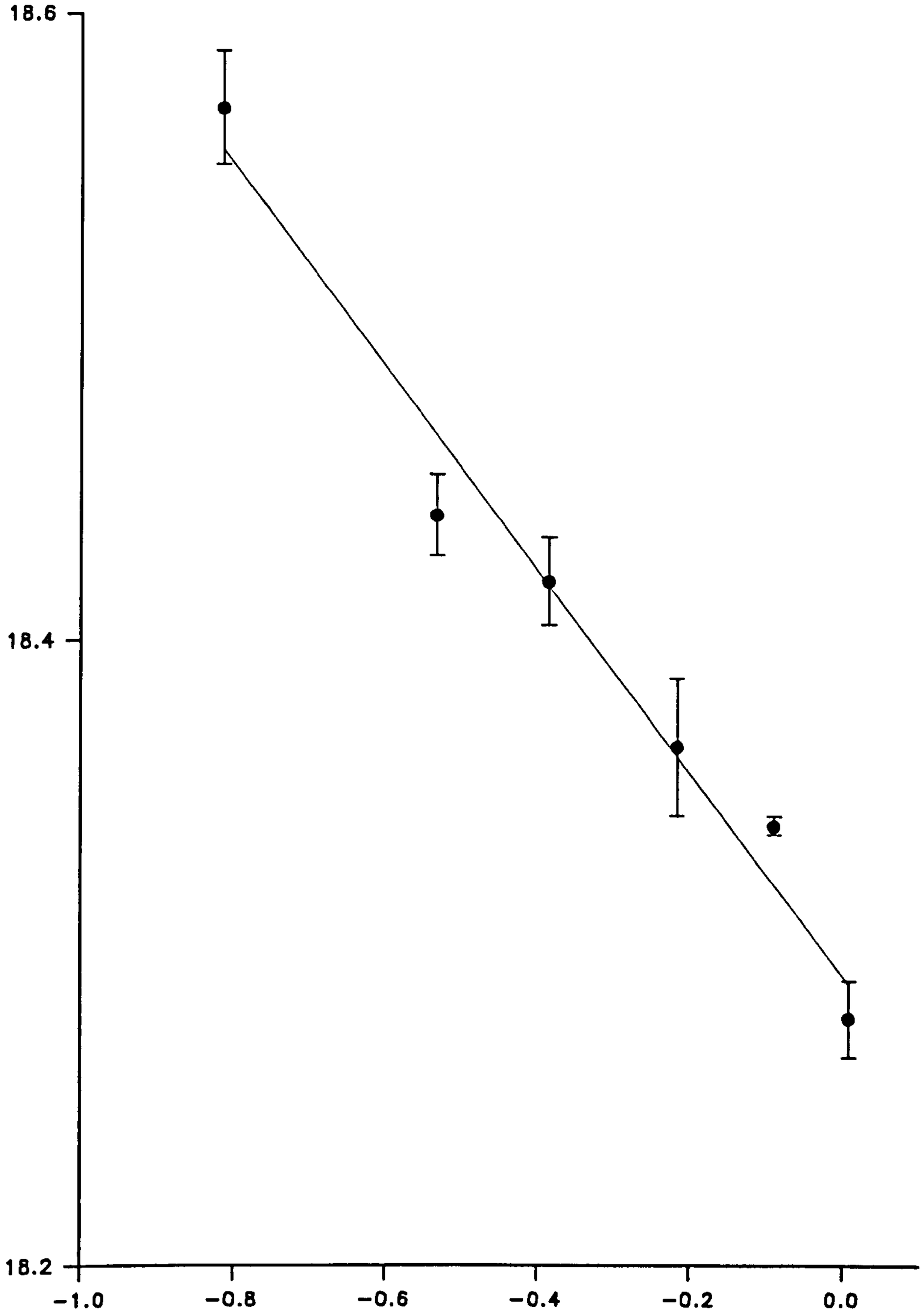

Figure 3.26: Plot of $\log_{10}$(Absolute Initial Cyclopropane Hydrogenation Rate) vs $\log_{10}$(Initial Hydrogen Partial Pressure) for Reduced/Oxidised Pt(0.5)/P25(T)

Table 3.50

Initial $c\text{-}C_3H_6:H_2$	$P_i(c\text{-}C_3H_6)$ / kPa	$-10^4 b$ / kPa s^{-1}	$10^{-18}k_a$ / molecules s^{-1} g^{-1}	$-\log_{10}[P_{i(c\text{-}C3H6)}]$	$\log_{10}[k_a]$
0.538	0.389	12.6	4.16	0.410	18.619
	0.388	12.5	4.13	0.411	18.616
0.401	0.289	10.8	3.56	0.539	18.552
	0.291	11.0	3.63	0.536	18.560
0.264	0.191	8.7	2.87	0.719	18.458
	0.191	8.5	2.81	0.719	18.449
0.176	0.127	6.3	2.08	0.896	18.318
	0.127	6.7	2.21	0.896	18.344
0.133	0.095	6.0	1.98	1.022	18.297
	0.096	6.3	2.08	1.018	18.318
0.089	0.063	5.3	1.75	1.201	18.243
	0.064	4.8	1.58	1.194	18.199

Reaction parameters:

Catalyst = Pt(0.5)/P25(T)
Catalyst pretreatment = H_2;3hrs;750K
O_2;3hrs;700K
Catalyst mass = 50.2mg
$P_{i(hydrogen)}$ = 0.723 ± 0.006 kPa
Cyclopropane:H_2 = variable

Table 3.51

Initial c-C_3H_6:H_2	$P_i(H_2)$ / kPa	$-10^4 b$ / kPa s^{-1}	$10^{-18} k_a$ / molecules s^{-1} g^{-1}	$\log_{10}[P_{i(hydrogen)}]$	$\log_{10}[k_a]$
0.660	0.153	10.8	3.56	-0.815	18.552
	0.154	11.7	3.86	-0.813	18.587
0.344	0.296	8.1	2.67	-0.529	18.427
	0.291	8.6	2.84	-0.536	18.453
0.245	0.410	8.2	2.71	-0.387	18.433
	0.415	7.7	2.54	-0.382	18.405
0.166	0.603	6.7	2.21	-0.220	18.344
	0.612	7.4	2.44	-0.213	18.387
0.124	0.807	6.7	2.21	-0.093	18.344
	0.818	6.6	2.18	-0.087	18.339
0.099	1.018	5.9	1.95	0.008	18.290
	1.017	5.6	1.85	0.007	18.267

Reaction parameters:

Catalyst = Pt(0.5)/P25(T)
Catalyst pretreatment = H_2;3hrs;750K
O_2;3hrs;700K
Catalyst mass = 50.2mg
$P_{i(cyclopropane)}$ = 0.101 ± 0.002 kPa
Cyclopropane:H_2 = variable

3.2 Temperature Programmed Desorption Experiments

The results obtained during the investigations into the behaviour of metallised TiO_2 substrates, acting as thermal hydrogenation catalysts, clearly show that significant differences exist between those catalysts prepared by photodeposition and that prepared by impregnation/reduction. This is particularly true for catalyst stability, since Pt(0.5)/P25(T) was invariably found to be much more stable, although usually no more active, than all photodeposited catalysts during the hydrogenation studies. At this point, it was decided to attempt to probe the surfaces of the two types of catalysts by undertaking a series of linear temperature-programmed desorption (TPD) experiments, using several different gaseous adsorbates. A standard experimental procedure, described in detail in Section 2.5.5, was used for all TPD investigations, the results of which are given below. To briefly recapitulate, the substrates investigated were untreated, reduced and reduced/oxidised P25 titania, Pt(0.5)/P25(P) and Pt(0.5)/P25(T), using propene, propene/H_2 and CO as adsorbate gases. Background desorption profiles of these adsorbates from the ultra-high vacuum system were also recorded, with no adsorbent present.

Desorption profiles of propene, CO and CO_2 were obtained via mass spectrometry, by continuously monitoring the m/e 41, m/e 28 and m/e 44 peaks respectively.

3.2.1 Propene Desorption Experiments

a) Untreated Catalysts

The results of these experiments are plotted in terms of mass spectrometer detector response (arbitrary units) vs temperature (K) in Fig. 3.27. It can be seen that the TPD profiles obtained when no adsorbent was present and for Pt(0.5)/P25(P) are very similar, indicating little or no propene desorption from the catalyst in the temperature range investigated. The profile obtained for Pt(0.5)/P25(T) shows a fairly small, sharp desorption peak between 300 - 350K, with the maximum occurring at ~325K, with no further significant desorption occurring beyond 350K. This suggests the presence of a single adsorption site for propene on the untreated surface of Pt(0.5)/P25(T) catalyst. Compared with the metallised adsorbents, the TPD profile for pure P25 titania is significantly different, showing a very broad propene desorption region over the approximate temperature range 450 - 800K. Within this region, two distinct peaks, having maxima at ~540K and at ~650K, can be distinguished, indicating either two different modes of desorption or the presence of two different adsorption sites on the surface of untreated P25 titania.

b) Reduced Catalysts

The results obtained from this series of experiments are plotted in terms of mass spectrometer detector response (arbitrary units) vs temperature (K) in Fig. 3.28. From these results, it can be seen that the propene desorption profiles of both platinised catalysts are very similar,

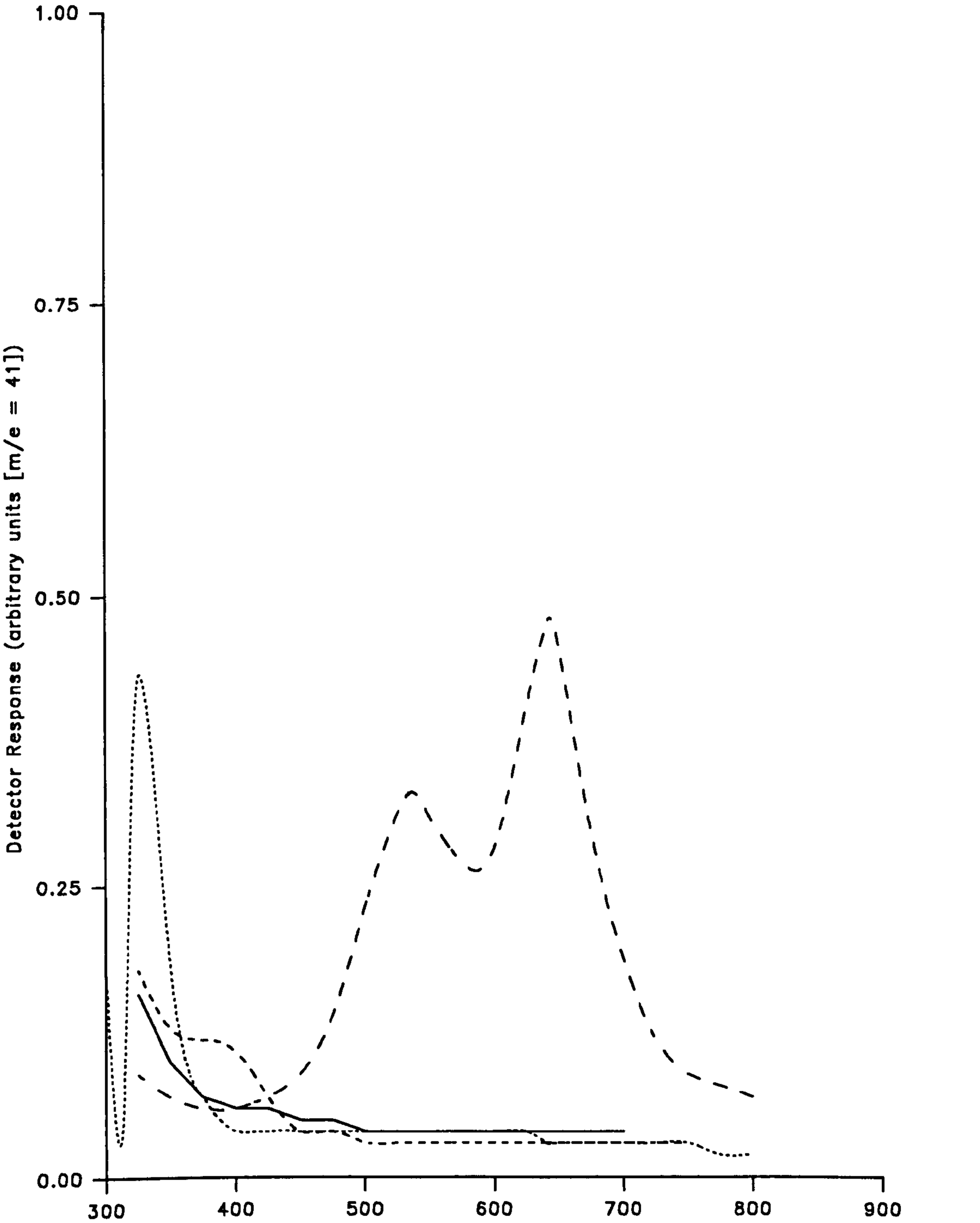

Figure 3.27: T.P.D. Spectra of Propene Desorption from Pure and Metallised Titanium Dioxide (Untreated Samples)

each showing a single low temperature desorption peak, with a maximum at ~350K, although the peak for Pt(0.5)/P25(P) appears to have a very long tail. The quantity of desorbed propene from reduced Pt(0.5)/P25(T) is significantly greater than the quantity desorbed from reduced Pt(0.5)/ P25(P). These observations suggest that for both reduced platinised catalysts, a single propene adsorption site exists on the surfaces, although the adsorption strength for propene may be different for the two types of catalyst. Reduced P25 titania shows very little propene desorption over the temperature range investigated, since the TPD profile obtained for this adsorbent is virtually identical to that obtained with no adsorbent present in the vacuum system.

c) Reduced/Oxidised Catalysts

The results from this series of experiments are plotted in terms of mass spectrometer detector response (arbitrary units) vs temperature (K) in Fig. 3.29. For both reduced/oxidised Pt(0.5)/P25(P) and Pt(0.5)/P25(T) catalysts, a single sharp propene desorption peak, having a maximum at ~325K, is observed. The TPD profiles are very similar to those observed for the two catalysts following high temperature reduction, although the propene desorption peak for Pt(0.5)/P25(P) does not have the long tail observed for the reduced catalyst. Again, the quantity of propene desorbed from the thermally-produced catalyst is much greater than that desorbed from the photodeposited catalyst, which in both cases is similar to that desorbed from the corresponding reduced samples. The TPD profile for reduced/oxidised P25 titania shows that propene desorption

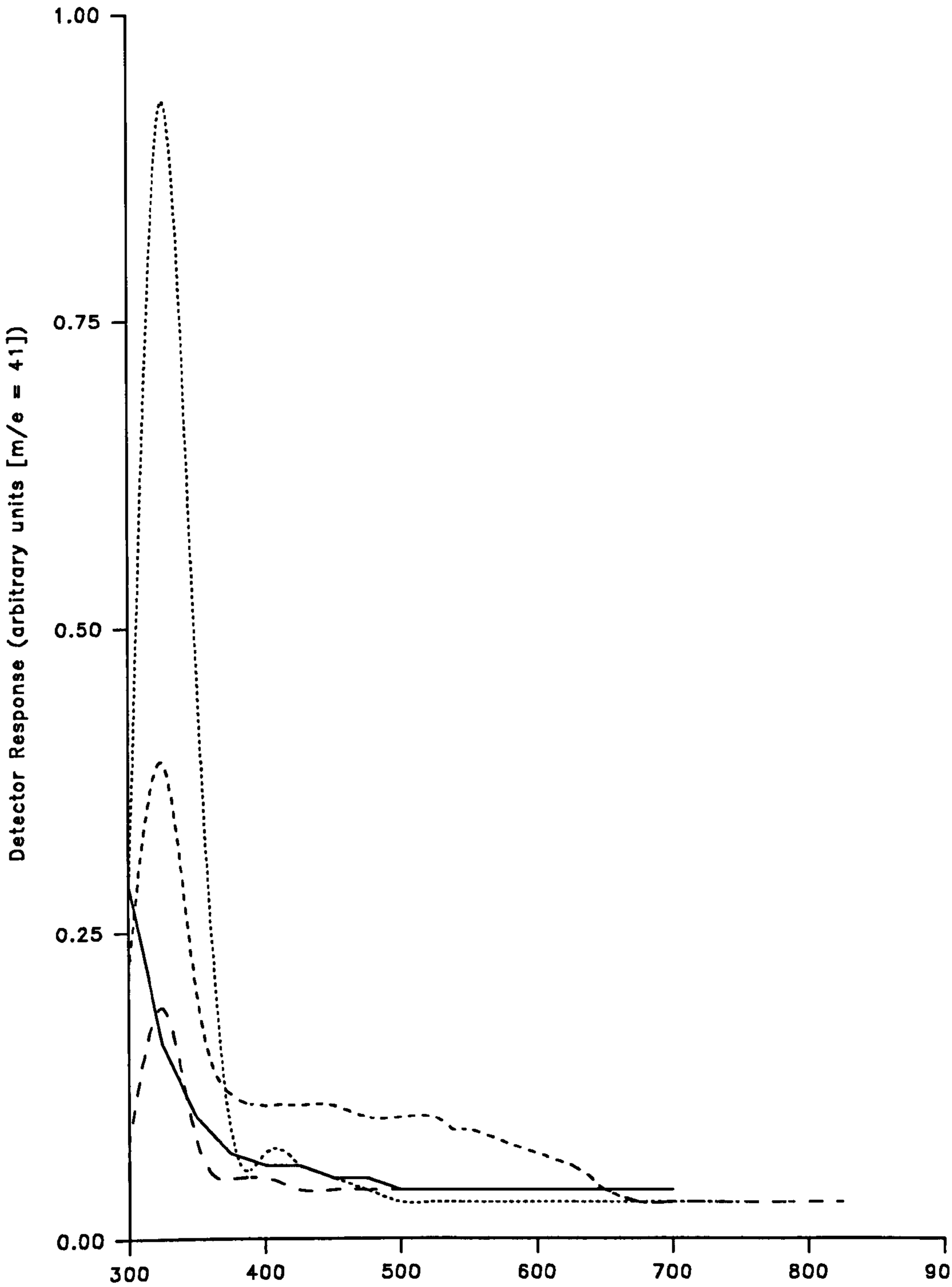

Figure 3.28: T.P.D. Spectra of Propene Desorption from Pure and Metallised Titanium Dioxide (Reduced Samples)

occurs over the fairly broad temperature range 300 - 500K, although two distinct peaks, having maxima at 325K and 400K can be distinguished. This indicates that, as with untreated P25 titania, propene desorbs from two different sites on the surface of the reduced/oxidised material. However, the temperatures at which the peak maxima occur and the quantities of propene desorbed are significantly different for the two samples, suggesting that the changes occurring on the surface of titania during high temperature reduction, are not readily reversed by high temperature re-oxidation in oxygen.

3.2.2 Propene/H_2 Desorption Experiments

a) Untreated Catalysts

The results obtained from this series of experiments are plotted in terms of mass spectrometer detector response (arbitrary units) vs temperature (K) in Fig. 3.30. From the TPD profile obtained with no adsorbent present shows that very little propene is desorbed from the vacuum system, as observed in the case of pure propene. For untreated P25 titania, the profile shows propene desorption occurring over the entire temperature range investigated. It can be seen that there is no distinct structure to the TPD profile, although a maximum at ~650K is observed. Similarly for Pt(0.5)/P25(P), propene is found to desorb over the broad temperature range 300 - 750K. However, in this case the profile shows two distinct desorption peaks, having maxima at ~315K and 635K, indicating the presence of two different adsorption sites on the surface of the

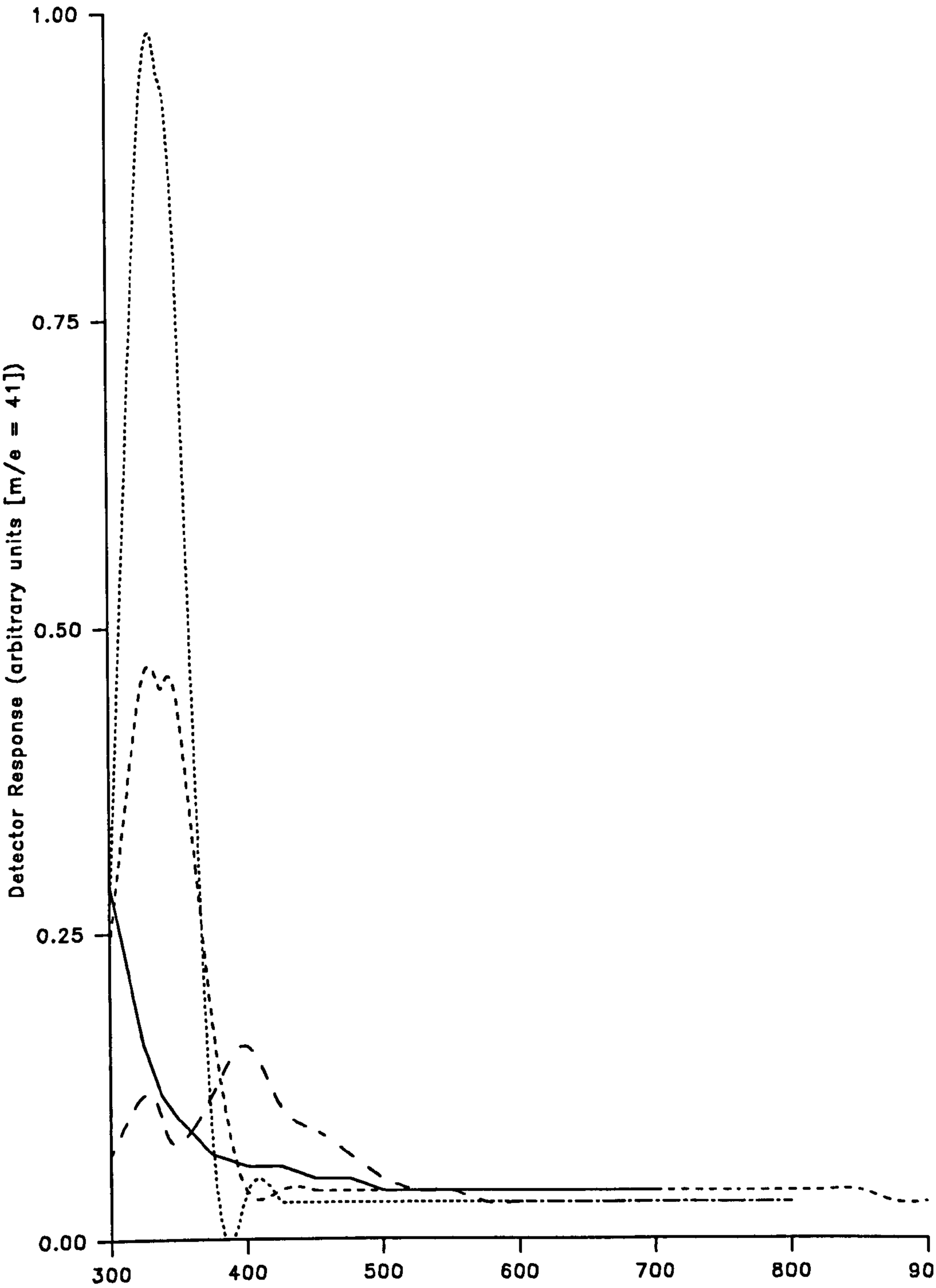

Figure 3.29: T.P.D. Spectra of Propene Desorption from Pure and Metallised Titanium Dioxide (Reduced/Oxidised Samples)

untreated catalyst. The TPD profile for Pt(0.5)/P25(T) shows a rather broad and large single desorption peak occurring over the temperature range 300 - 500K, with the maximum at 335K. On the high temperature side of this peak, a much smaller desorption peak, having a maximum at 425K, can also be seen. Again this indicates the presence of two distinct adsorption sites for propene are present on the surface of the untreated catalyst.

It is worth noting that for the platinised materials, desorption of propane, due to the occurrence of propene hydrogenation, will also make a small contribution to the observed TPD profiles.

b) Reduced Catalysts

The results obtained from this series of experiments are plotted in terms of mass spectrometer detector response (arbitrary units) vs temperature (K) in Fig. 3.31. It can be seen that the TPD profiles for all three pre-reduced adsorbates are very similar, each showing a single low temperature desorption peak, with the maximum occurring at 325K. The quantity of propene desorbed from reduced P25 titania is small in comparison to the amount desorbed from the platinised catalysts, which in both cases is quite considerable.

c) Reduced/Oxidised Catalysts

The TPD profiles obtained from this series of experiments are plotted in terms of mass spectrometer detector response (arbitrary units) vs temperature (K) in Fig. 3.32. The TPD profile obtained for propene

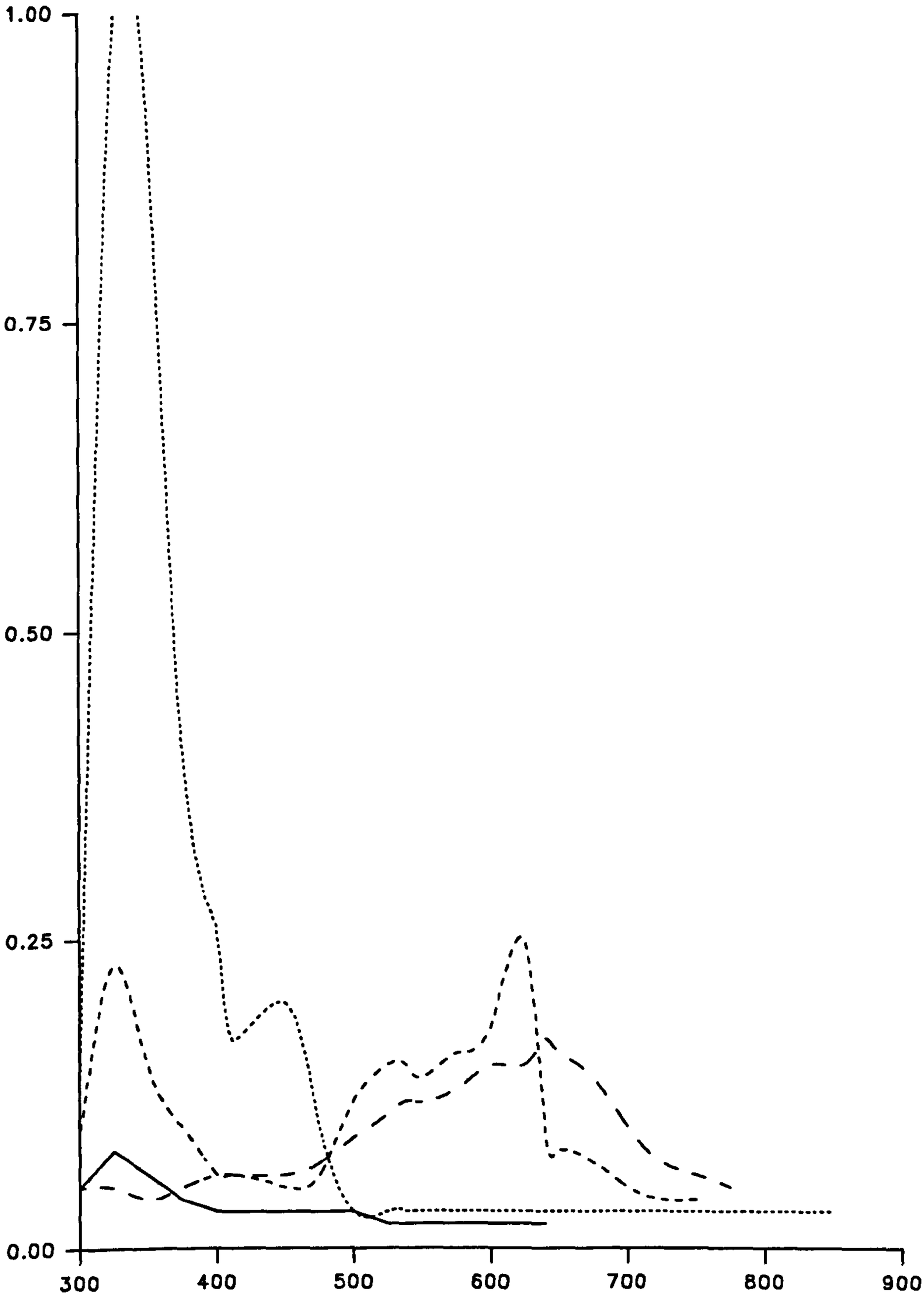

Figure 3.30: T.P.D. Spectra of Propene Desorption in the Presence of Hydrogen from Pure and Metallised Titanium Dioxide (Untreated Samples)

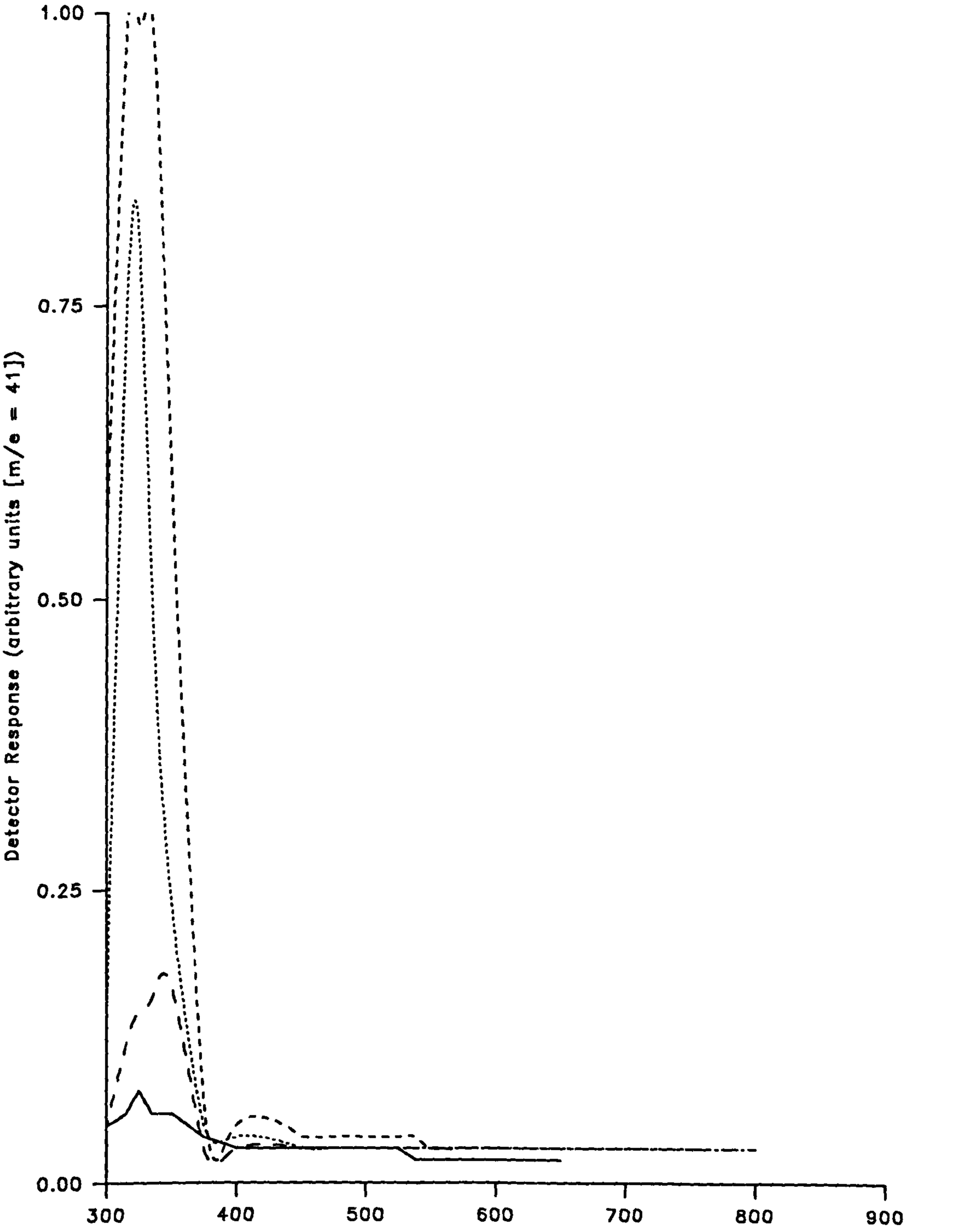

Figure 3.31: T.P.D. Spectra of Propene Desorption in the Presence of Hydrogen from Pure and Metallised Titanium Dioxide (Reduced Samples)

desorption from reduced/oxidised P25 titania, previously exposed to propene/H_2, is virtually identical to that obtained using pure propene as the adsorbate. Thus, the profile shows desorption occurring in the temperature range 300 - 500K, with two distinct peaks, having maxima at 325K and 395K, being distinguishable. The TPD profiles for reduced/oxidised Pt(0.5)/P25(P) and Pt(0.5)/P25(T) are very similar, each showing a single low temperature desorption peak, with the maxima occurring at ~333K and 325K respectively. The quantity of propene desorbed from the thermally-prepared catalyst can be seen to be much greater than that desorbed from the photodeposited catalyst.

3.2.3 CO Desorption Experiments

a) Untreated Catalysts

The results obtained from this series of experiments are plotted in terms of mass spectrometer detector response (arbitrary units) vs temperature (K) in Fig. 3.33. The background desorption profile for CO, obtained with no adsorbate present, shows a large low temperature peak, with the maximum occurring at ~315K, which falls slightly to a constant high level over the entire temperature range investigated. This observation shows that large amounts of CO are adsorbed onto the surfaces of the vacuum system, which then desorb at a fairly constant rate, since most of the vacuum system remains at ambient temperature, when the system is opened to the mass spectrometer. Untreated P25 titania shows significant CO desorption above and beyond that observed when no adsorbate

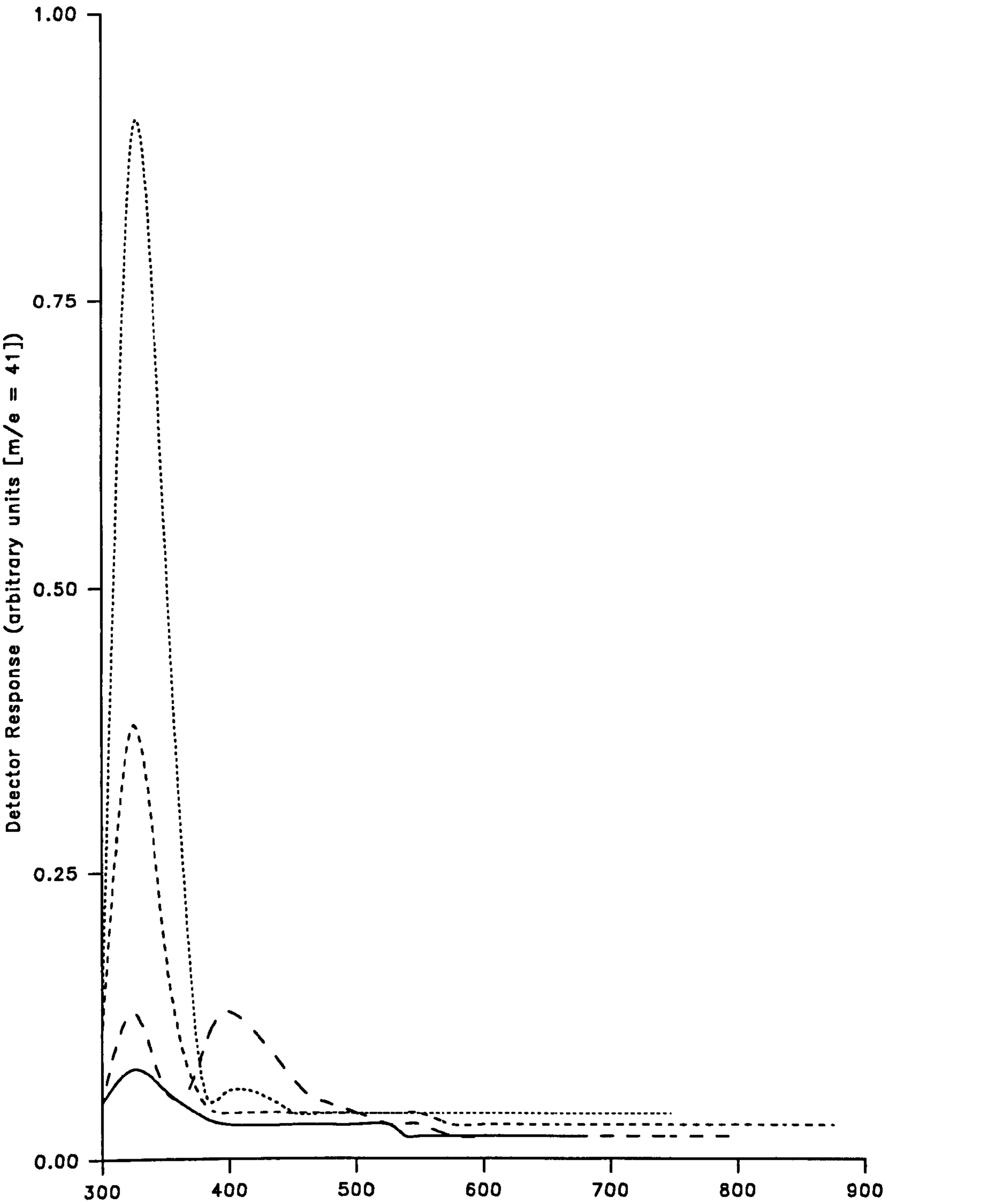

Figure 3.32: T.P.D. Spectra of Propene Desorption in the Presence of Hydrogen from Pure and Metallised Titanium Dioxide (Reduced/Oxidised)

is present, the TPD profile being fairly complicated. A series of four distinct desorption peaks, having maxima at ~415K, 490K, 600K and 690K, can be seen, indicating the presence of at least four different sites for CO adsorption, or different forms of adsorbed CO, on the surface of untreated P25 titania. For untreated Pt(0.5)/P25(P) catalyst, the TPD profile of CO desorption shows a large low temperature peak, with the maximum occurring at 390K. On the low temperature side of this peak, two distinct shoulders can be seen, indicating the presence of at least three different forms of adsorbed CO, which are very similar in energy terms, on the surface of this material. Above 450K, the TPD profile is very similar to that obtained with no adsorbate present, implying that the CO desorbed over the remaining temperature range is from the vacuum system rather than the catalyst. The TPD profile of CO desorption from untreated Pt(0.5)/P25(T) has much structure in the low temperature region, with at least three distinct peaks, having maxima at 360K, 400K and 465K, being observable. This observation suggests that, as in the case of the photodeposited catalyst, at least three different forms of adsorbed CO exist on the surface of this material, although these forms are more different in energy terms than those present on the surface of the photo-deposited catalyst. Above 525K, the TPD profile is very similar to the background desorption profile, indicating CO desorption from the vacuum system rather than the adsorbate catalyst.

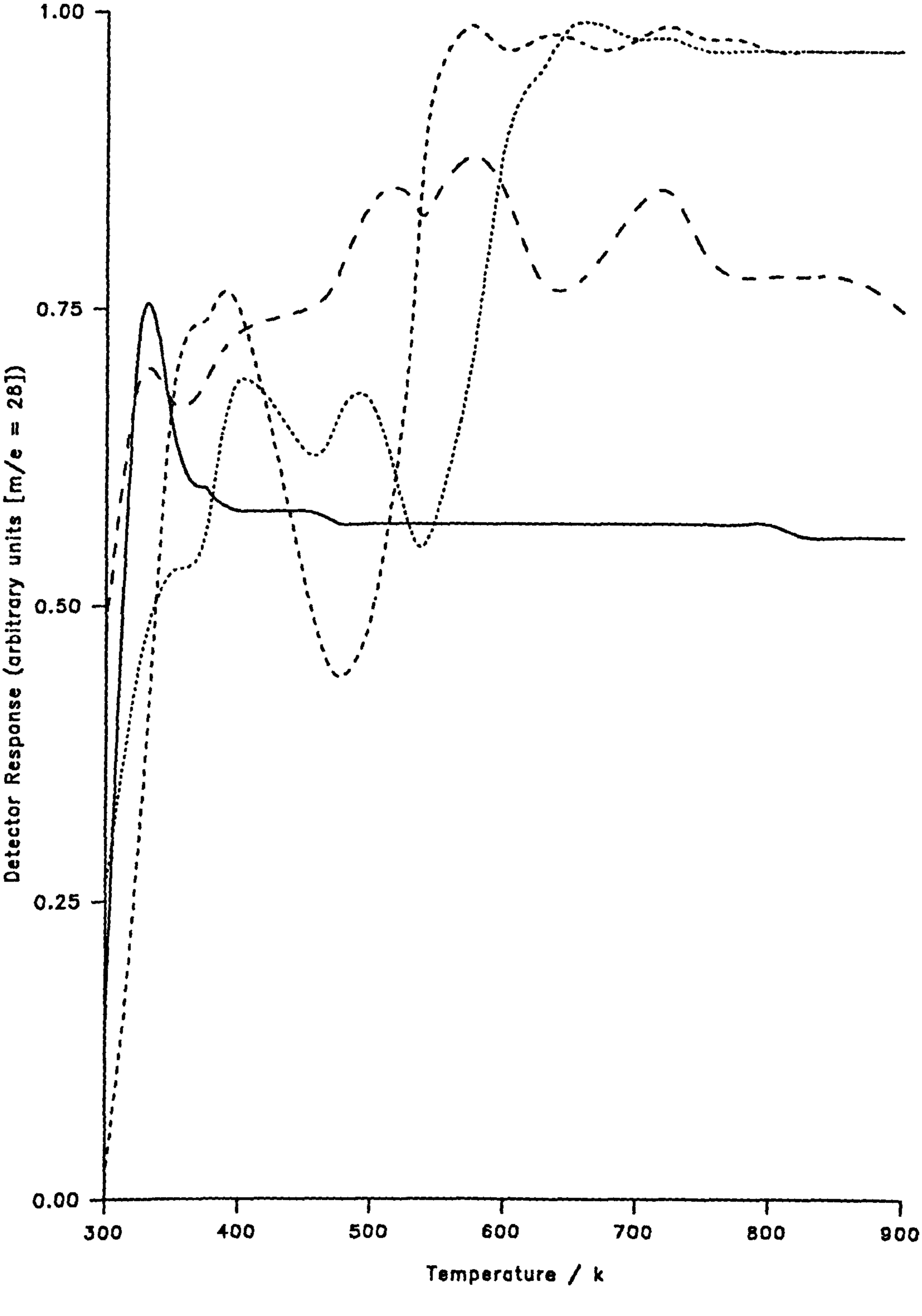

Figure 3.33: T.P.D. Spectra of CO Desorption from Pure and Metallised Titanium Dioxide (Untreated Samples)

b) Reduced Catalysts

The results obtained from this series of experiments are plotted in terms of mass spectrometer detector response (arbitrary units) vs temperature (K) in Fig. 3.34. The TPD profile for CO desorption from P25 titania previously reduced in hydrogen at high temperature, is very similar to that observed when no adsorbate is present, although the total amount of CO desorbed is considerably reduced. This suggests that CO adsorption onto P25 titania is suppressed following such pretreatment and that the observed CO desorption is from the vacuum system rather than the adsorbate. The low background level of adsorbed CO is possibly due to the presence of presorbed hydrogen, originating from the high temperature reduction of the P25 titania, on the surfaces of the vacuum system.

Reduced Pt(0.5)/P25(P) catalyst shows significant CO desorption over the entire temperature range investigated. Three distinct desorption peaks, having maxima at ~335K, 525K and ~665K, can be seen in the TPD profile, indicating the existence of three different adsorption sites, or adsorbed forms of CO, on the surface of the reduced catalyst. This is very different to that found for the corresponding untreated material. Above 700K, large quantities of CO are desorbed and the profile becomes a flat plateau, similar to that observed when no adsorbate is present. As with the photodeposited material, reduced Pt(0.5)/P25(T) shows significant CO desorption over the entire temperature range investigated. The TPD profile shows a low temperature desorption peak, with the maximum occurring at 325K. This peak becomes a distinct plateau on the high temperature side, from 375 - 425K, before falling again, suggesting the

existence of two similar, in energy terms, adsorption sites for, or forms of, CO on the surface of the reduced material. Again, this is very different to that observed in the case of the corresponding untreated catalyst. Significant CO desorption occurs in the region 500 - 900K, although no further structure is observable in the TPD profile in this temperature range.

c) Reduced/Oxidised Catalysts

The results of this series of experiments are plotted in terms of mass spectrometer detector response (arbitrary units) vs temperature (K) in Fig. 3.35. Significant CO desorption is observed to occur from P25 titania following high temperature re-oxidation, with the TPD profile showing a large low temperature desorption peak, with the maximum occurring at ~340K, and a much smaller and broader peak around 475K. Above 500K, significant CO desorption is observed, although the TPD profile possesses no distinguishable structure over the remaining temperature range. The TPD profile for reduced/oxidised Pt(0.5)/P25(P) catalyst shows a fairly small low temperature CO desorption peak, with the maximum occurring at 335K. On the high temperature side of this peak, a plateau region, in the range 375 - 475K, is observed, indicating the existence of two closely associated, in energy terms, adsorption sites for, or adsorbed forms of, CO on the surface. Above 475K, CO desorption falls rapidly and no further significant desorption is observed over the remaining temperature range. The TPD profile of CO desorption from reduced/oxidised Pt(0.5)/P25(T) catalyst shows a low temperature desorption

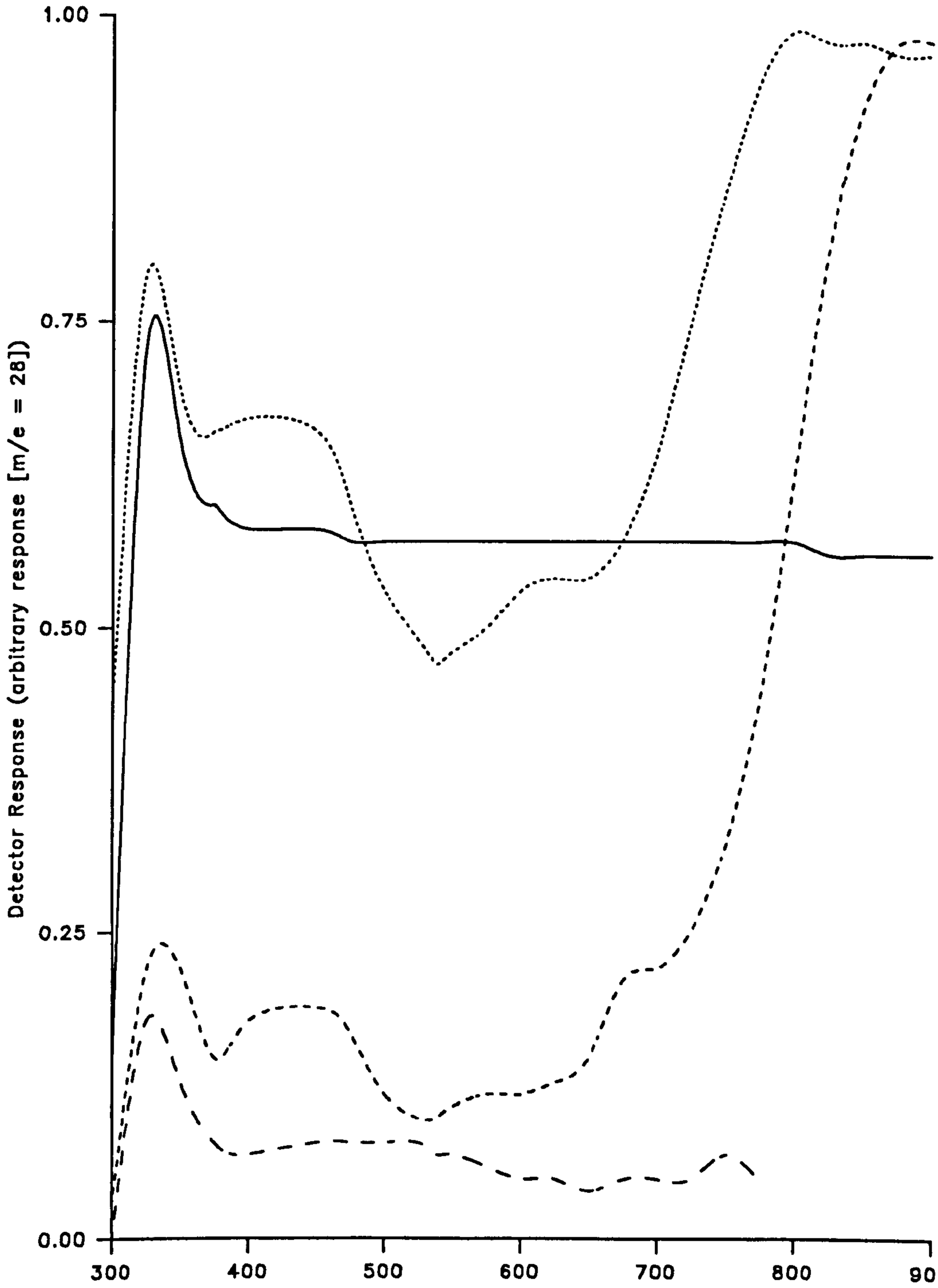

Figure 3.34: T.P.D. Spectra of CO Desorption from Pure and Metallised Titanium Dioxide (Reduced Samples)

peak, with the maximum occurring at 325K. As observed with the photo-deposited catalyst, the high temperature side of this peak forms a plateau over the range 375 - 450K, before rising again to give a much smaller peak centred around 480K and then falling off. Above 500K no further significant CO desorption is observed until a high temperature peak, with maximum occurring at ~865K, is formed. These observations suggest the existence of three very similar and one very different adsorption sites for, or adsorbed forms of CO, on the surface of reduced/oxidised Pt(0.5)/ P25(T).

3.2.4 CO_2 Desorption Experiments

a) Untreated Catalysts

The results obtained from this series of experiments are plotted in terms of mass spectrometer detector response (arbitrary units) vs temperature (K) in Fig. 3.36. The background TPD profile, obtained with no adsorbate present, shows a small, fairly broad low temperature peak, with the maximum occurring at 400K. Above 500K CO_2 desorption is observed to increase gradually as the temperature is increased to 900K. No definite structure to the profile can be seen in this high temperature region, implying that the CO_2 is being generally desorbed from the surfaces of the vacuum system. For untreated P25 titania significant CO_2 desorption is observed over the entire temperature range investigated and the resulting TPD profile is quite complicated. A series of five distinct peaks, having maxima at 350K, 400-425K, ~590K, ~685K and 800K, can be seen,

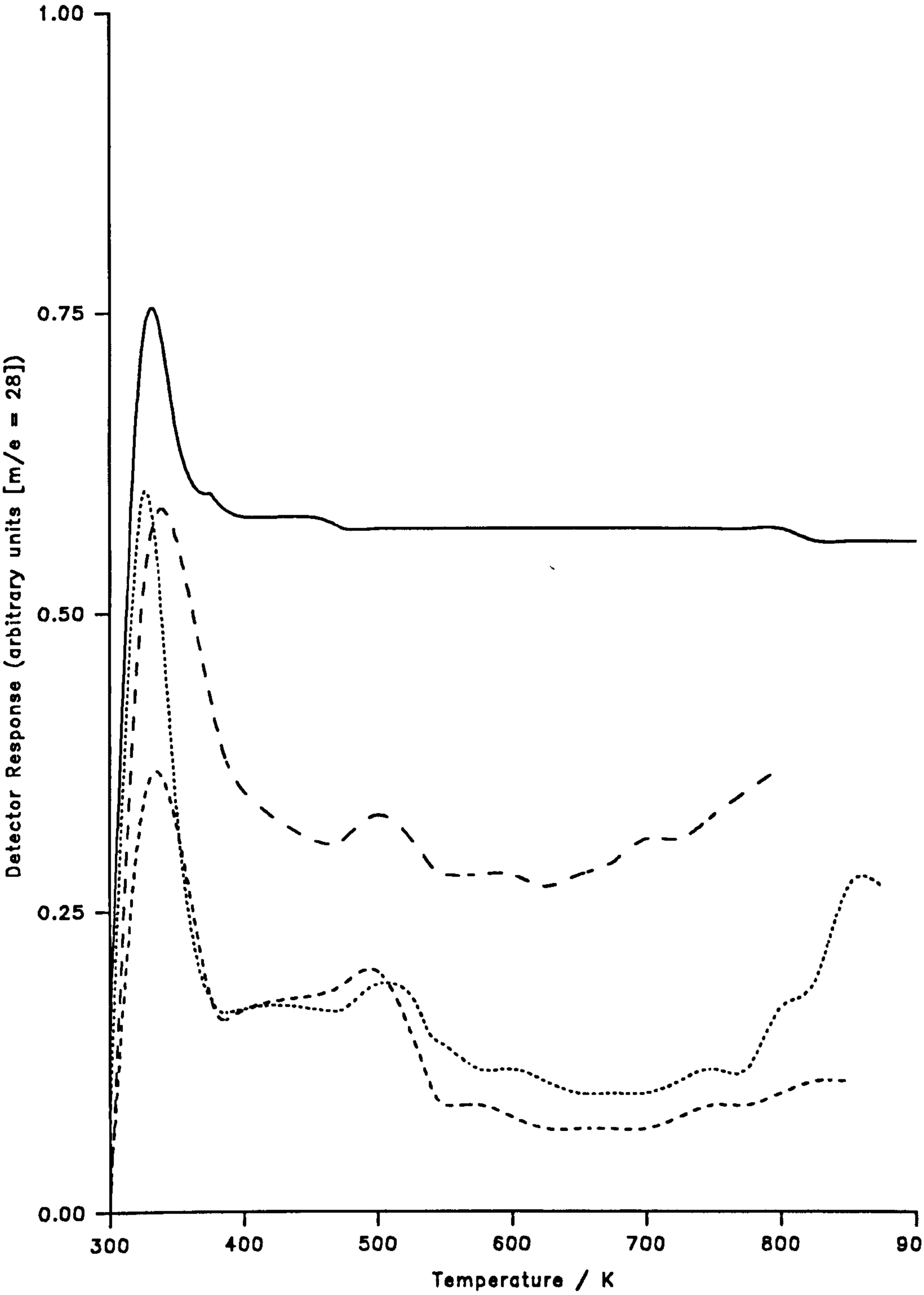

Figure 3.35: T.P.D. Spectra of CO Desorption from Pure and Metallised Titianium Dioxide (Reduced/Oxidised Samples)

indicating that five different sites for adsorption, or adsorbed forms, CO_2 are present on the surface of untreated P25 titania.

Untreated Pt(0.5)/P25(P) catalyst also shows significant CO_2 desorption over the entire temperature range investigated. The TPD profile shows a large, very broad low temperature desorption peak, with the maximum occurring at 390K, extending over the range 300 - 550K. Above 500K CO_2 is desorbed in very large quantities, such that the profile becomes a featureless plateau over the remaining temperature range. These observations suggest that at least one discrete site for CO_2 adsorption is present on the catalyst surface and that, above 500K, CO_2 is formed and then desorbed from the surface generally, with no specific sites involved. For untreated Pt(0.5)/P25(T) catalyst, CO_2 is observed to be desorbed in large quantities over the entire temperature range investigated, with no distinct peaks being observable in the TPD profile. As with the photodeposited material, this observation suggests that CO_2 is formed and desorbed from the surface of the catalyst generally, with no specific sites involved in the process.

b) Reduced Catalysts

The results obtained from this series of experiments are plotted in terms of mass spectrometer detector response (arbitrary units) vs temperature (K) in Fig. 3.37. Reduced P25 titania shows only limited CO_2 desorption in the temperature range investigated. The TPD profile shows a very small low temperature peak, with the maximum occurring at ~337K, which, on the high temperature side, forms a plateau over the range 375 -

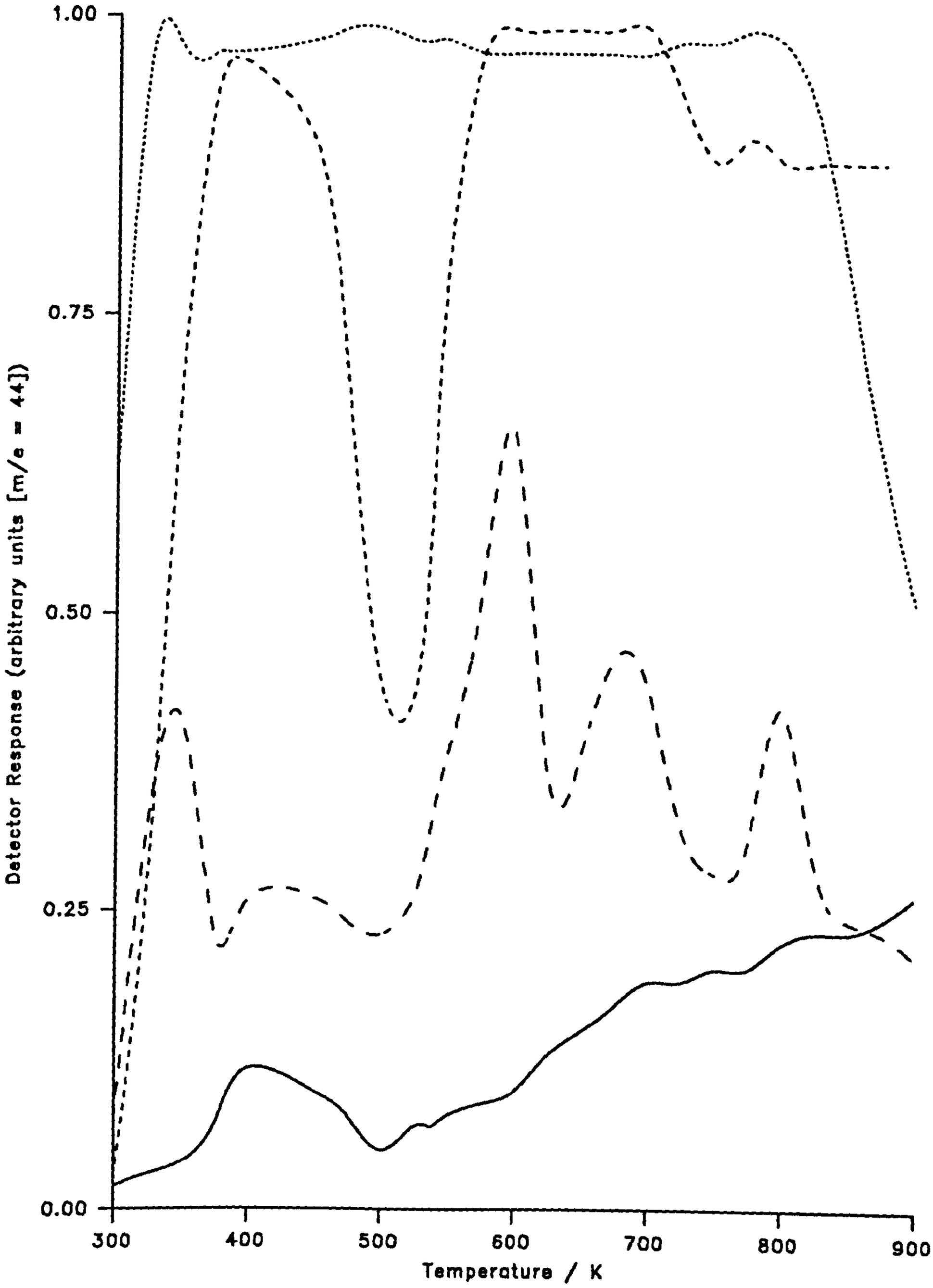

—— Background - – P25 TiO_2 ---- Pt(0.5)/P25(P) ..... Pt(0.5)/P25(T)

Figure 3.36: T.P.D. Spectra of CO_2 Desorption from Pure and Metallised Titanium Dioxide (Untreated Samples)

425K. Beyond this plateau region, the amount of CO_2 desorbed gradually falls, such that above 500K no further significant CO_2 desorption is observed. The TPD profile of CO_2 desorption from reduced Pt(0.5)/P25(P) shows two very small low temperature peaks, having maxima at 340K and ~415K, then no further significant desorption up to 600K. Above this temperature a much larger and broader peak, with the maximum occurring at 825K, is observed, which appears to gradually fall off slowly at temperatures in excess of 900K. The TPD profile for reduced Pt(0.5)/P25(T) catalyst is very similar to that observed for the photodeposited material, in that a small broad desorption peak occurs over the temperature range 300 - 500K. A much larger and broader peak is observed in the high temperature region, with the peak maximum occurring at ~820K, which also appears to fall off gradually at temperatures in excess of 900K.

c) Reduced/Oxidised Catalyst

The results obtained from this series of experiments are plotted in terms of mass spectrometer detector response (arbitrary units) vs temperature (K) in Fig. 3.38. For re-oxidised P25 titania, the TPD profile for CO_2 desorption shows a very large and broad low temperature peak, with the maximum occurring at ~337K, which then falls to the background level, observed with no adsorbent present, in the range 475 - 900K. No structure can be seen in the profile above 475K, suggesting that CO_2 is rapidly formed and desorbed from the surface at fairly low temperatures. A similar low temperature desorption peak can be seen in the TPD profile obtained for the re-oxidised photodeposited catalyst, although in this case

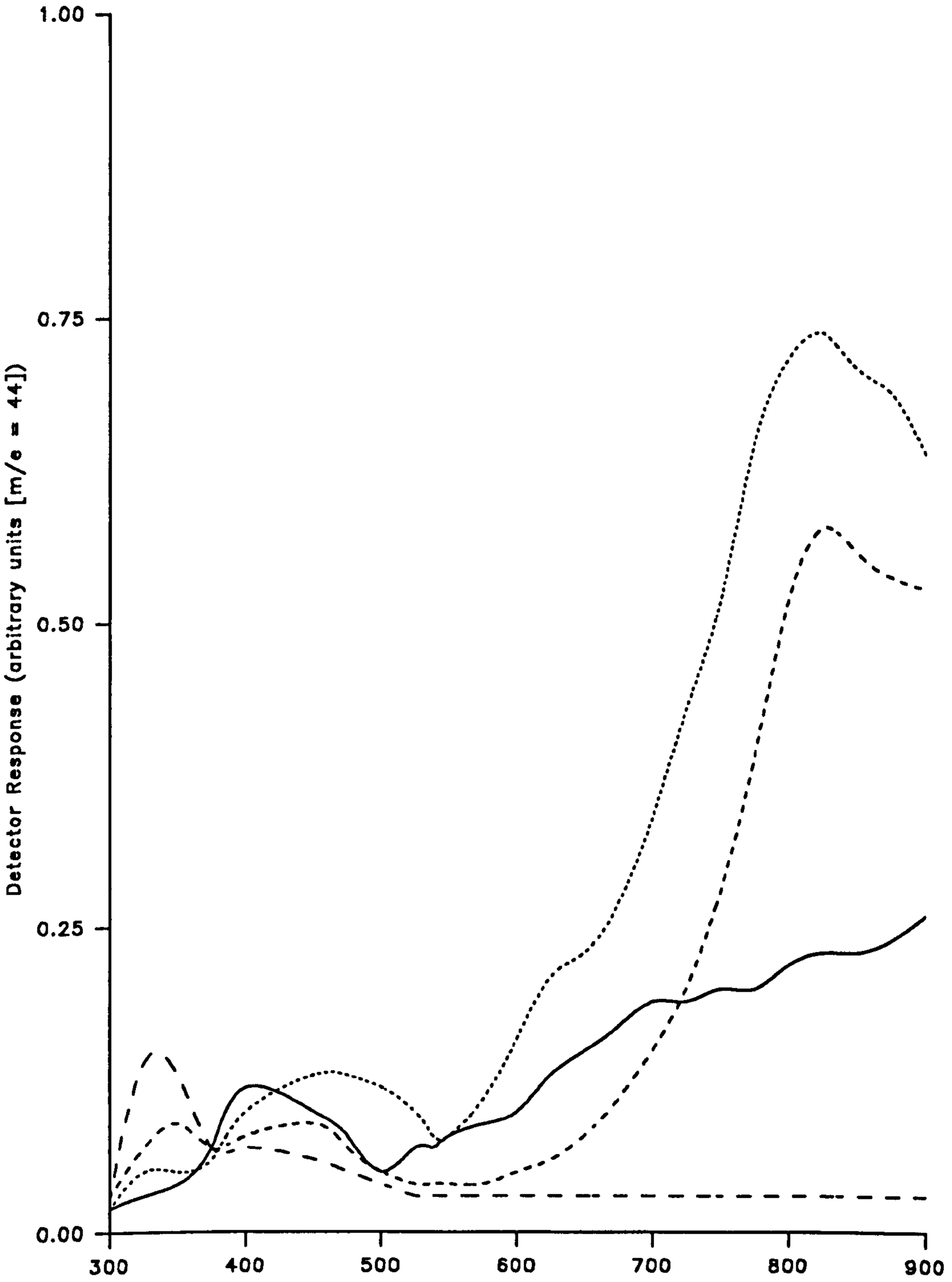

Figure 3.37: T.P.D. Spectra of CO_2 Desorption from Pure and Metallised Titanium Dioxide (Reduced Samples)

the amount of CO_2 desorbed appears to be much greater. Above 500K, further CO_2 desorption is occurs and a small, but broad, high temperature peak, with the maximum occurring at 875K, is observed in the profile. The TPD profile of CO_2 desorption from re-oxidised Pt(0.5)/P25(T) catalyst also shows a very large and broad peak at low temperatures, which very gradually falls off to a minimum at ~650K. A further large, but very sharp, desorption peak is observed around 775K.

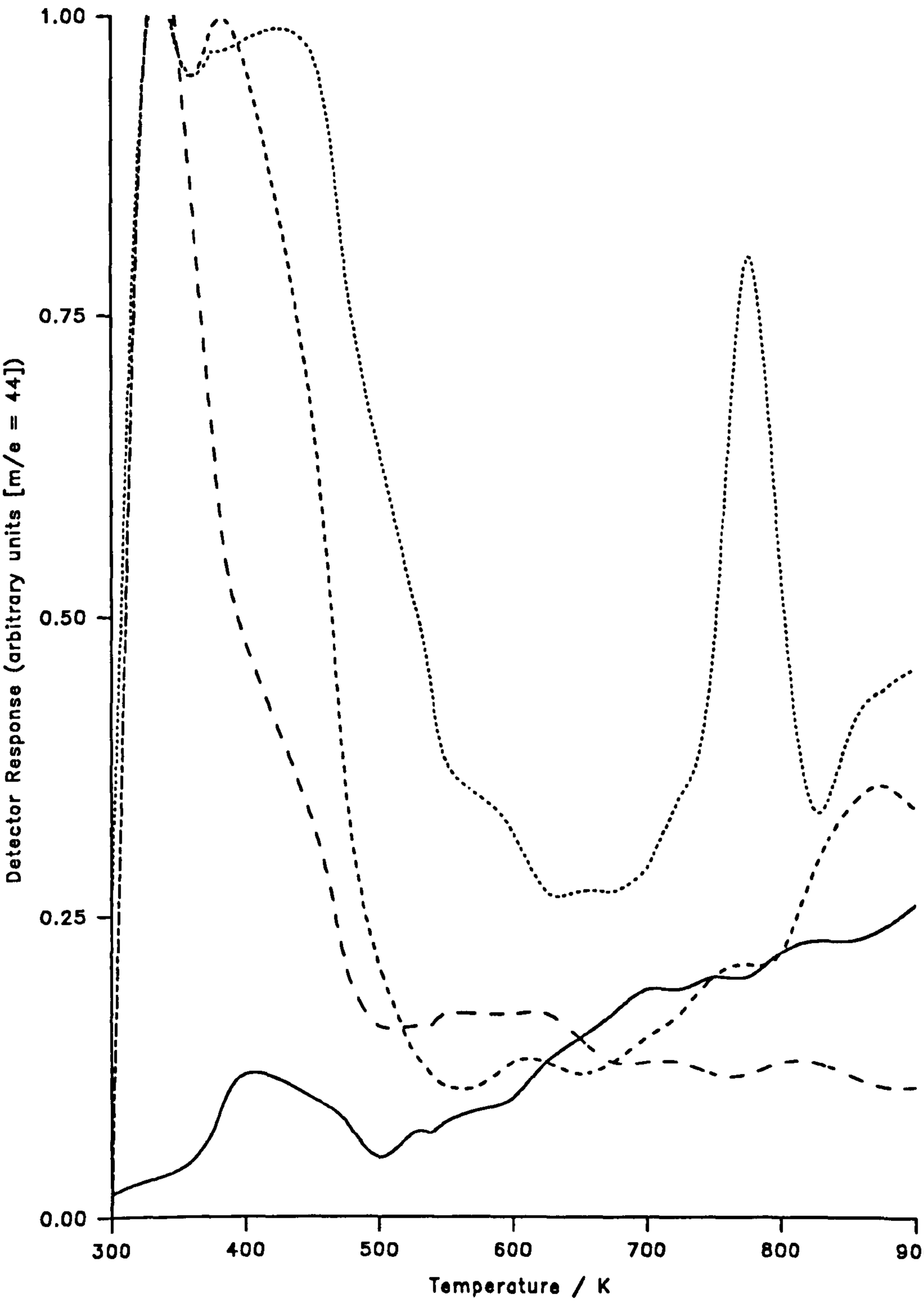

Figure 3.38: T.P.D. Spectra of CO_2 Desorption from Pure and Metallised Titanium Dioxide (Reduced/Oxidised Samples)

3.3 Liquid-Phase Photocatalytic Dehydrogenation Studies

On the basis of the results obtained during the gas-phase thermal hydrogenation experiments, it was proposed, at this stage of the project, that the behaviour of metal/TiO_2 catalysts in a particular reaction type might be determined largely by the method of preparation. In order to investigate this hypothesis, it was decided to study a reaction type which was completely different to gas-phase thermal hydrogenation. It was felt that a reaction which was mediated by UV light (i.e. photo-catalytic), but which also involved adsorption of hydrogen, would be particularly suitable for such an investigation. The reaction chosen was the photocatalytic dehydrogenation of propan-2-ol, on the basis that it fulfilled the criteria outlined above and also that the apparatus required to study this reaction type was readily available.

The experimental apparatus and the procedure used for all the photocatalytic experiments are described in detail in Sections 2.2 and 2.5.6(b), respectively. The results of these experiments are given in the following text. It is worth mentioning at this point that a significant dark reaction was observed to occur for all catalysts containing Pt metal, as shown by the presence of detectable quantities of propanone at time zero, just prior to the commencement of irradiation with UV light.

3.3.1 Photocatalytic Dehydrogenation of Propan-2-ol:

Effect of Metal Type

In this series of experiments, activity for the photocatalytic dehydrogenation of propan-2-ol, at 293K, was investigated using various metals supported on P25 titania, at a level of 0.5 mass%. Specifically, these catalysts were: Pt(0.5), Pd(0.5), Rh(0.5) and Ir(0.5)/P25, all prepared by photodeposition, and Pt(0.5)/P25, prepared by impregnation/-reduction. A sample of pure P25 titania was also included in this series of catalysts, in order to assess the contribution to reaction progress made by this material.

The results obtained in this series of experiments are summarised in Table 3.52 and plotted in terms of propanone concentration (mol dm^{-3}) vs time (mins) in Fig. 3.39. Overall, it can be seen that, in terms of decreasing activity for the photocatalytic reaction, the catalysts used in this experiment lie in the order:

Pt(0.5)/P25(P) ~ Pt(0.5)/P25(T) > Pd(0.5)/P25(P) ~ Rh(0.5)/P25(P) > > Ir(0.5)/P25(P) > P25 titania ~ 0.

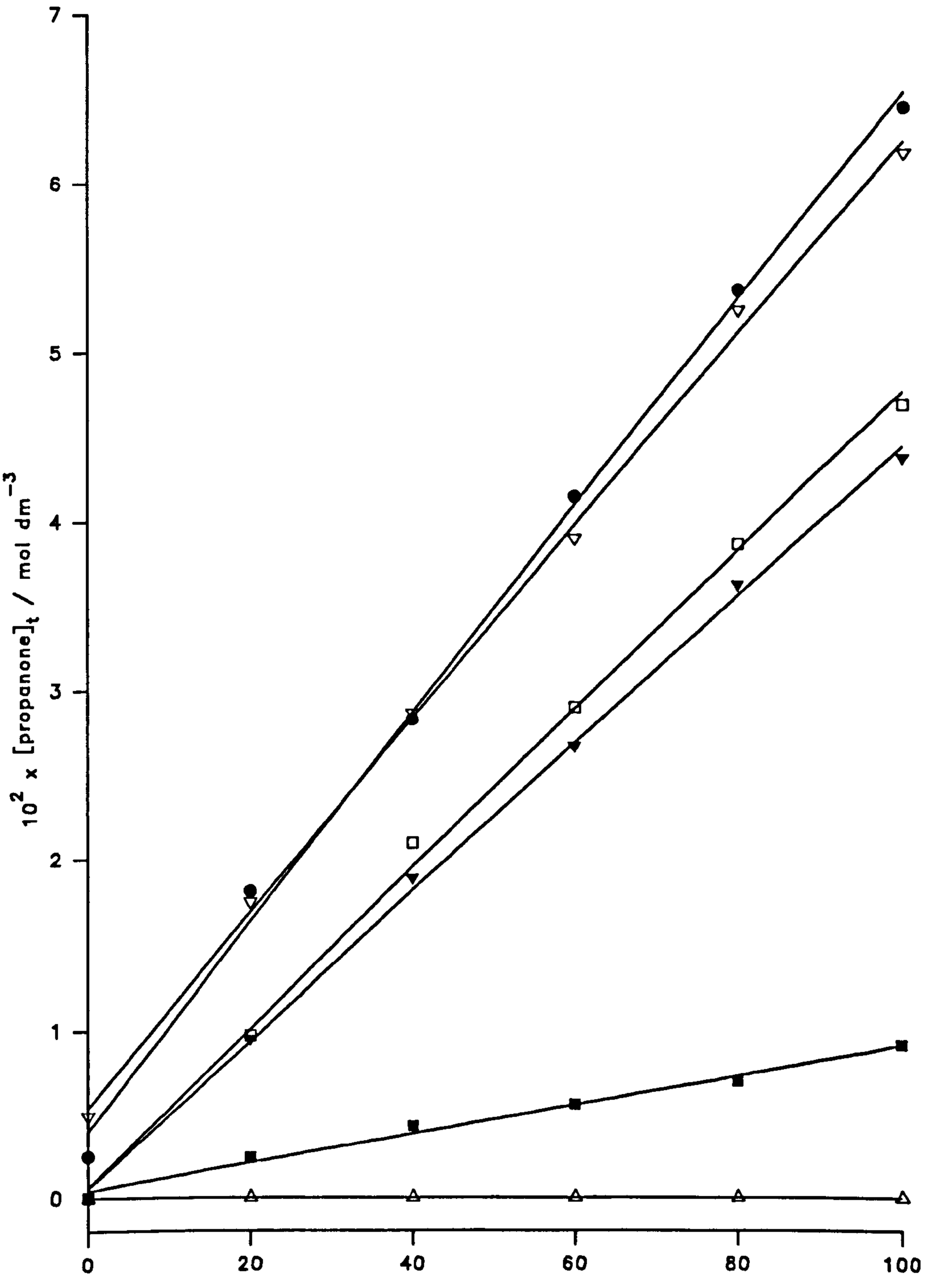

Figure 3.39: Propanone Concentration as a Function of Time for the Photocatalytic Dehydrogenation of Propan-2-ol over Various M(0.5)/P25 Catalysts

Table 3.52

Time / mins	10^2 x [propanone] / mol dm^{-3}					
	Pt(0.5)/P25(P)	Pt(0.5)/P25(T)	Pd(0.5)/P25(P)	Rh(0.5)/P25(P)	Ir(0.5)/P25(P)	P25 titania
0	0.25	0.49	0.00	0.00	0.00	0.00
20	1.81	1.74	0.95	0.97	0.24	0.00
40	2.83	2.86	1.88	2.09	0.43	0.00
60	4.15	3.90	2.67	2.90	0.56	0.00
80	5.38	5.26	3.63	3.87	0.70	0.00
100	6.48	6.20	4.38	4.70	0.91	0.00
10^5 x Rate / mol dm^{-3} s^{-1}	1.09	0.98	0.74	0.79	0.15	0.00

3.3.2 Photocatalytic Dehydrogenation of Propan-2-ol:

Effect of Pt Content

In this series of experiments, activity as a function of metal content was investigated for a series of platinised P25 titania catalysts by measuring the photocatalytic dehydrogenation rate of propan-2-ol at 293K. Three catalysts, all prepared by the photo-deposition technique and possessing Pt contents of 0.25, 1.0 and 2.0 mass% were used in this study. The results obtained are summarised in Table 3.53 and plotted in terms of propanone concentration (mol dm^{-3}) vs time (mins) in Fig. 3.40. The activities of the catalysts, including the result obtained for Pt(0.5)/P25(P) in Section 3.3.1, are plotted in terms of propanone formation rate (mol dm^{-3} s^{-1}) vs Pt metal content (mass%), in Fig. 3.41. It can be seen that all the catalysts are active for the photocatalytic reaction although a maximum in activity is observed at a level of 0.5 mass% Pt.

Table 3.53

Time / mins	10^2 x [propanone] / mol dm^{-3}			
	Pt(0.25)/ P25(P)	Pt(0.5) /P25(P)	Pt(1.0) /P25(P)	Pt(2.0) /P25(P)
0	0.02	0.25	0.42	0.33
20	0.87	1.81	1.68	1.34
40	1.68	2.83	2.45	2.09
60	2.80	4.15	3.19	3.03
80	3.82	5.38	3.64	3.52
100	4.67	6.48	5.01	4.78
10^5 x Rate / mol dm^{-3} s^{-1}	0.79	1.09	0.80	0.60

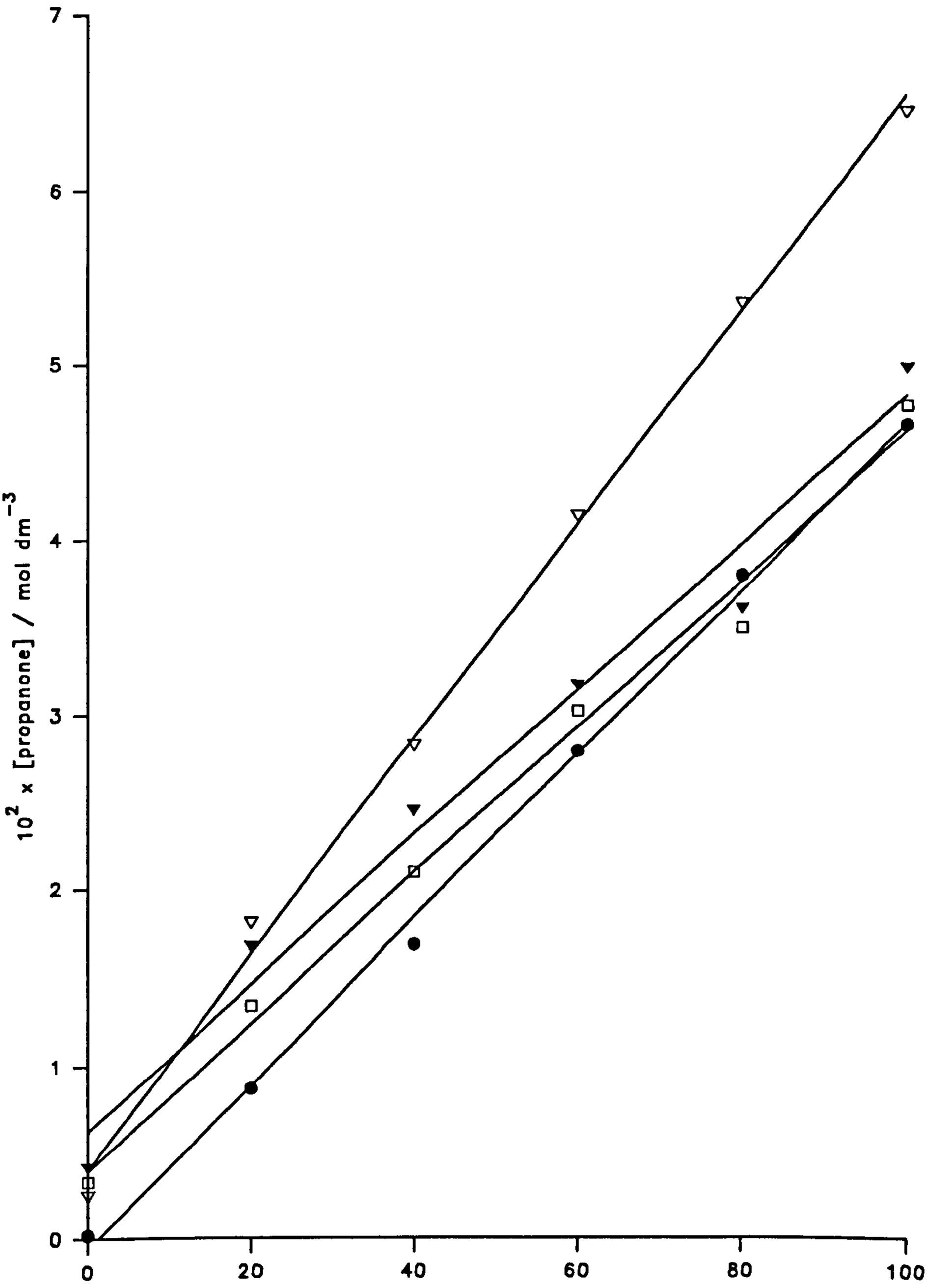

Figure 3.40: Propanone Concentration as a Function of Time for the Photocatalytic Dehydrogenation of Propan-2-ol over Various Pt/P25 Catalysts Prepared by Photodeposition

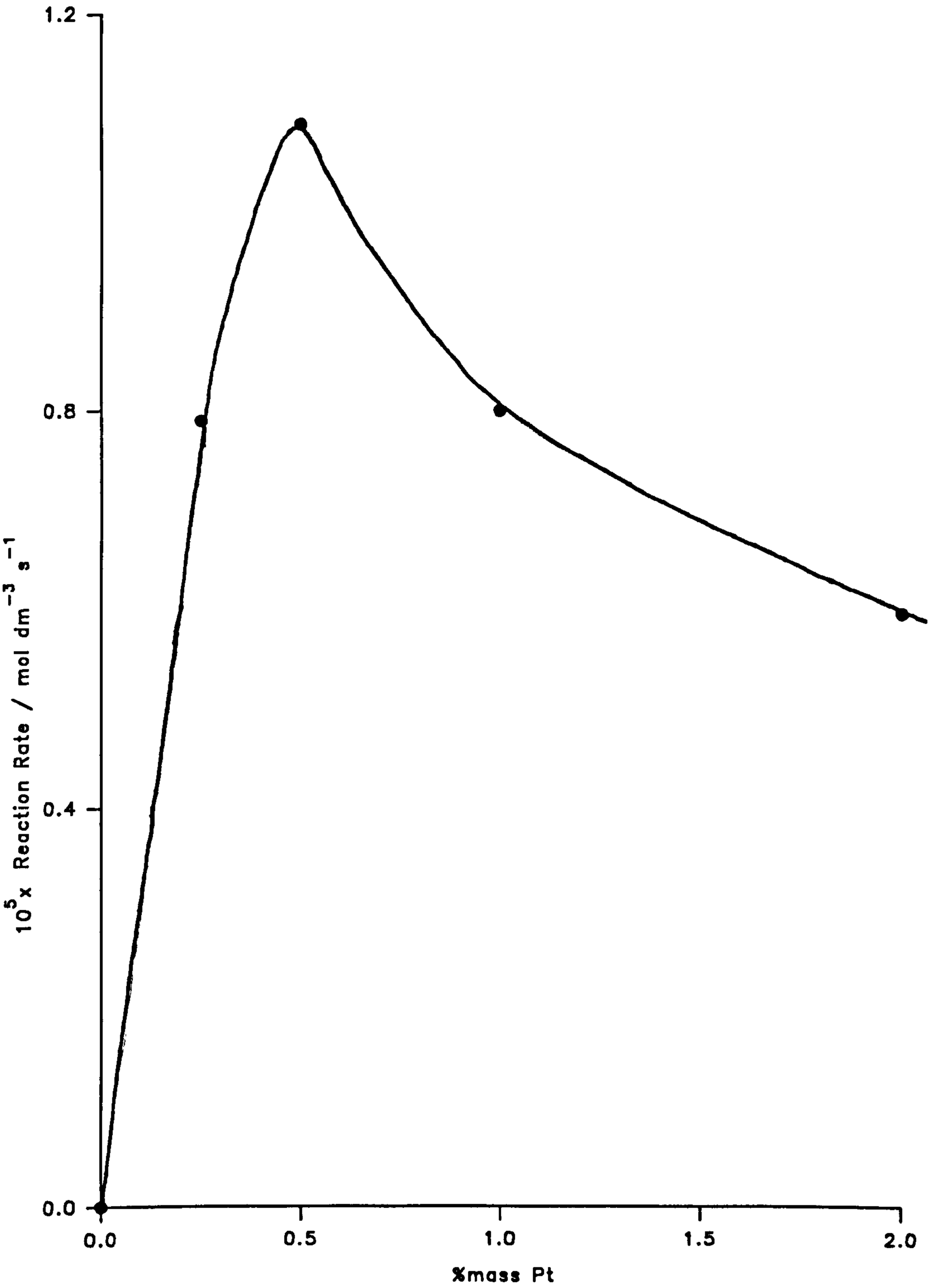

Figure 3.41: Rate of Propanone Formation as a Function of Pt Content for the Photocatalytic Dehydrogenation of Propan-2-ol over Pt(x)/P25(P) Catalysts

3.3.3 Photocatalytic Dehydrogenation of Propan-2-ol:

Effect of Temperature

In this series of experiments, the activities of four platinised catalysts, for the photocatalytic dehydrogenation of propan-2-ol, were measured as a function of temperature, in the range 278 - 303K. The catalysts included in this series were Pt(0.5)/P25(P), Pt(0.5)/P25(T), Pt(0.5)/anatase(P) and Pt(0.5)/rutile(P). All experiments were carried out in accordance with the procedure detailed in Section 2.5.6(b), the reaction temperature being increased in 5K intervals.

The results obtained for each catalyst are summarised in Tables 3.54 - 3.57 and plotted in terms of propanone concentration (mol dm^{-3}) vs time, for each reaction temperature, in Figs. 3.42 - 3.45. Generally, for each catalyst studied, the photocatalytic reaction rate was found to increase with increasing reaction temperature. It can be seen that for Pt(0.5)/rutile(P), increasing the reaction temperature from 278K to 303K produces only a small increase in the photocatalytic reaction rate, relative to the increases observed for the other three catalysts over the same temperature range. In order of decreasing activity for the photocatalytic reaction, the catalyst lie in the order:

Pt(0.5)/P25(T) > Pt(0.5)/P25(P) > Pt(0.5)/anatase(P) > >

Pt(0.5)/rutile(P)

within the temperature range investigated. Fig. 3.46 shows the appropriate Arrhenius plots for each of the catalyst studied, constructed from the data gained in this series of experiments. From these plots the following activation energies for the photocatalytic dehydrogenation of propan-2-ol,

over the temperature range 278 - 303K, were calculated for each catalyst:

Catalyst	Activation Energy / kJ mol^{-1}
Pt(0.5)/P25(P)	18 ± 1
Pt(0.5)/P25(T)	15 ± 1
Pt(0.5)/anatase(P)	16 ± 1
Pt(0.5)/rutile(P)	14 ± 1

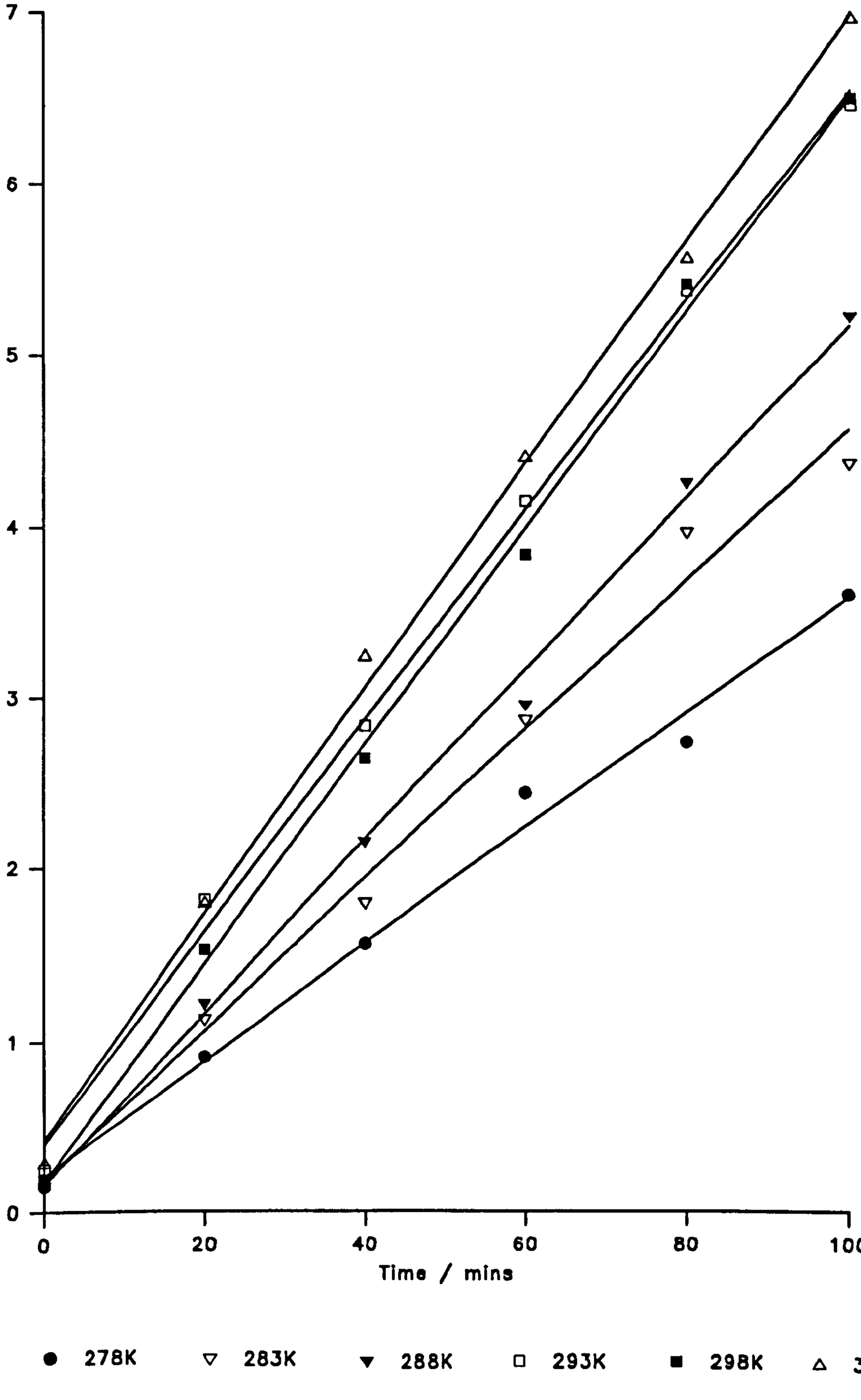

Figure 3.42: Propanone Concentration as a Function of Time at Various Temperature for the Photocatalytic Dehydrogenation of Propan-2-ol over Pt(0.5)/P25(P)

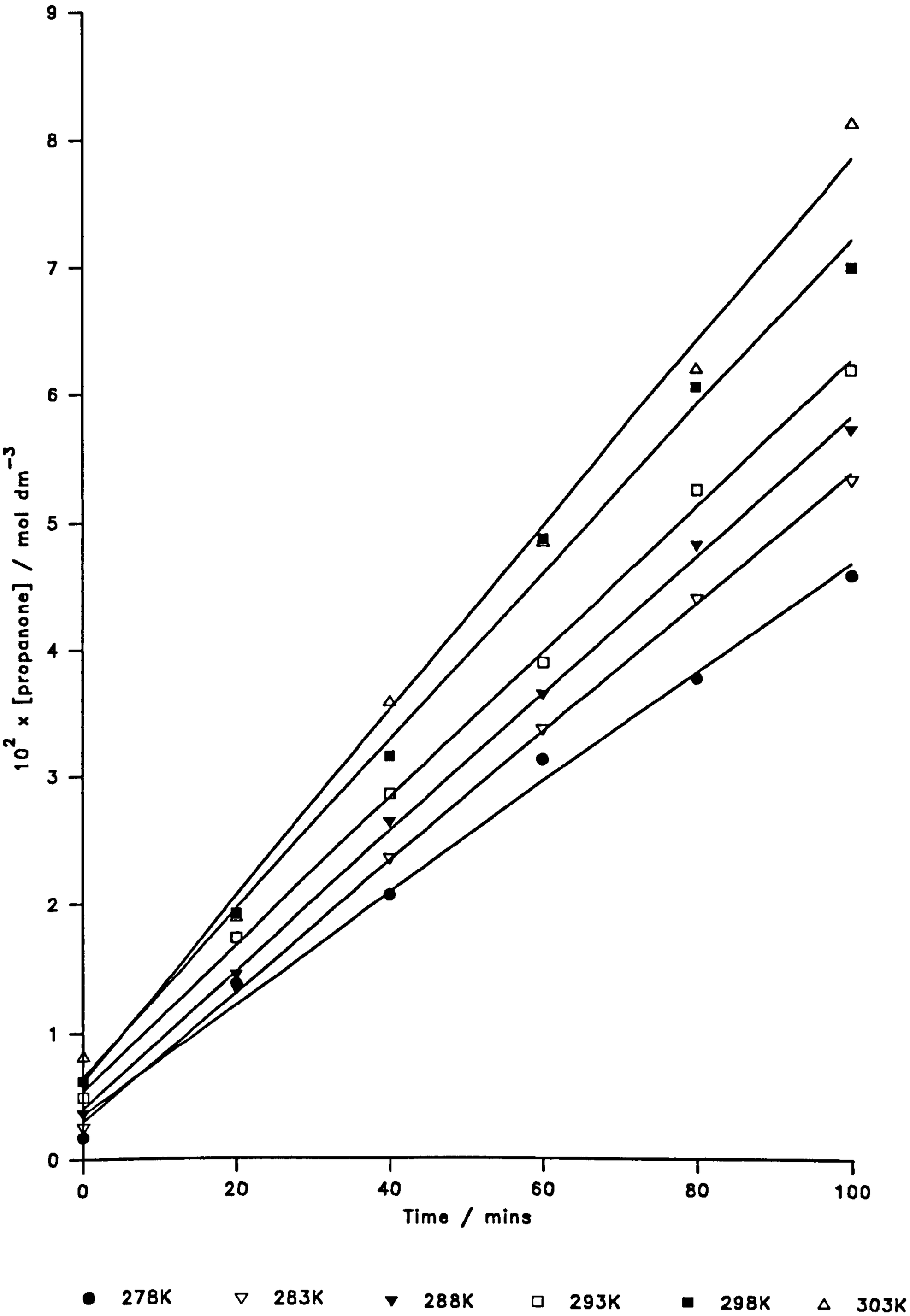

Figure 3.43: Propanone Concentration as a Function of Time at Various Temperature for the Photocatalytic Dehydrogenation of Propan-2-ol over Pt(0.5)/P25(T)

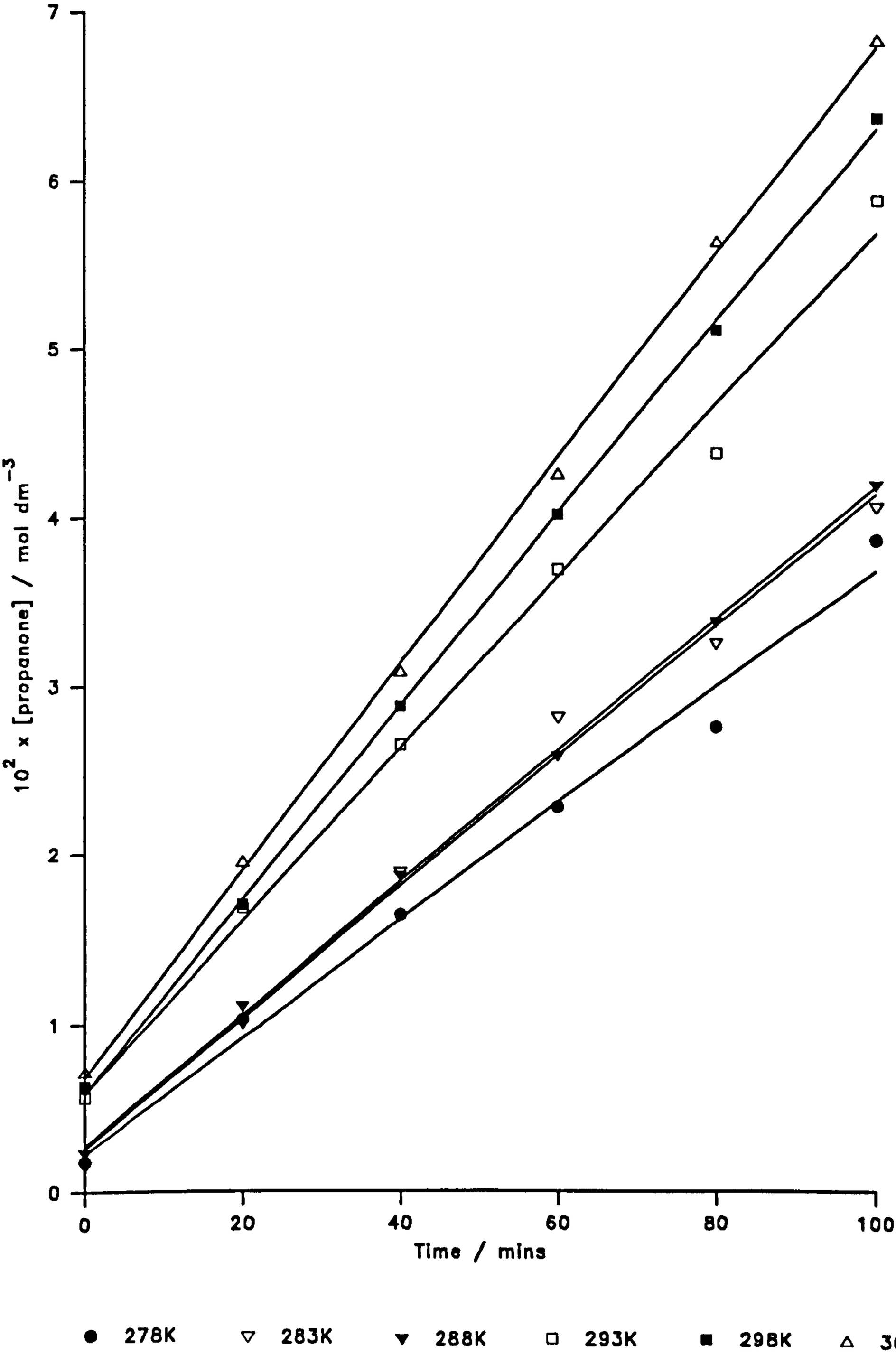

Figure 3.44: Propanone Concentration as a Function of Time at Various Temperature for the Photocatalytic Dehydrogenation of Propan–2–ol over Pt(0.5)/anatase(P)

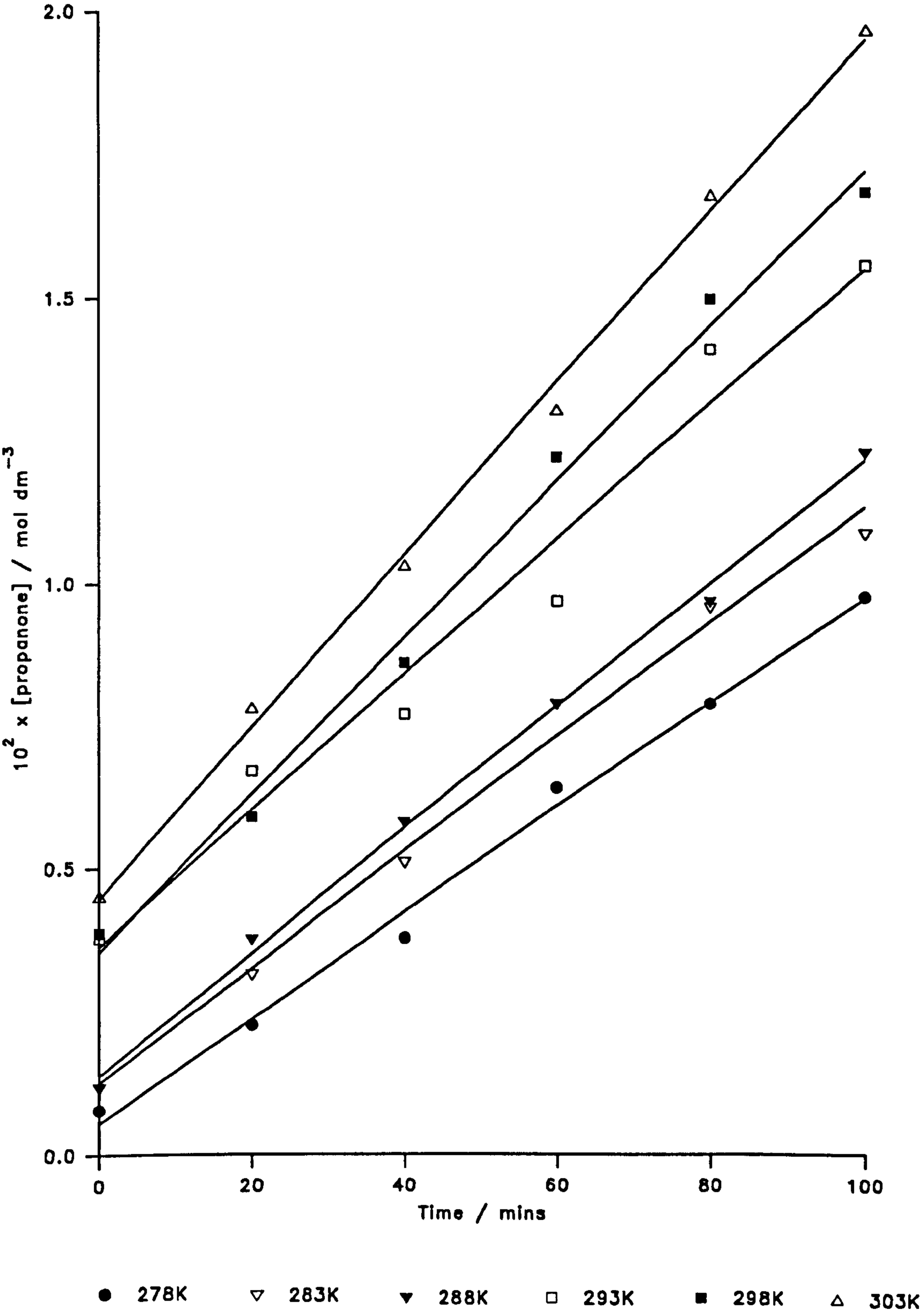

Figure 3.45: Propanone Concentration as a Function of Time at Various Temperature for the Photocatalytic Dehydrogenation of Propan–2–ol over Pt(0.5)/rutile(P)

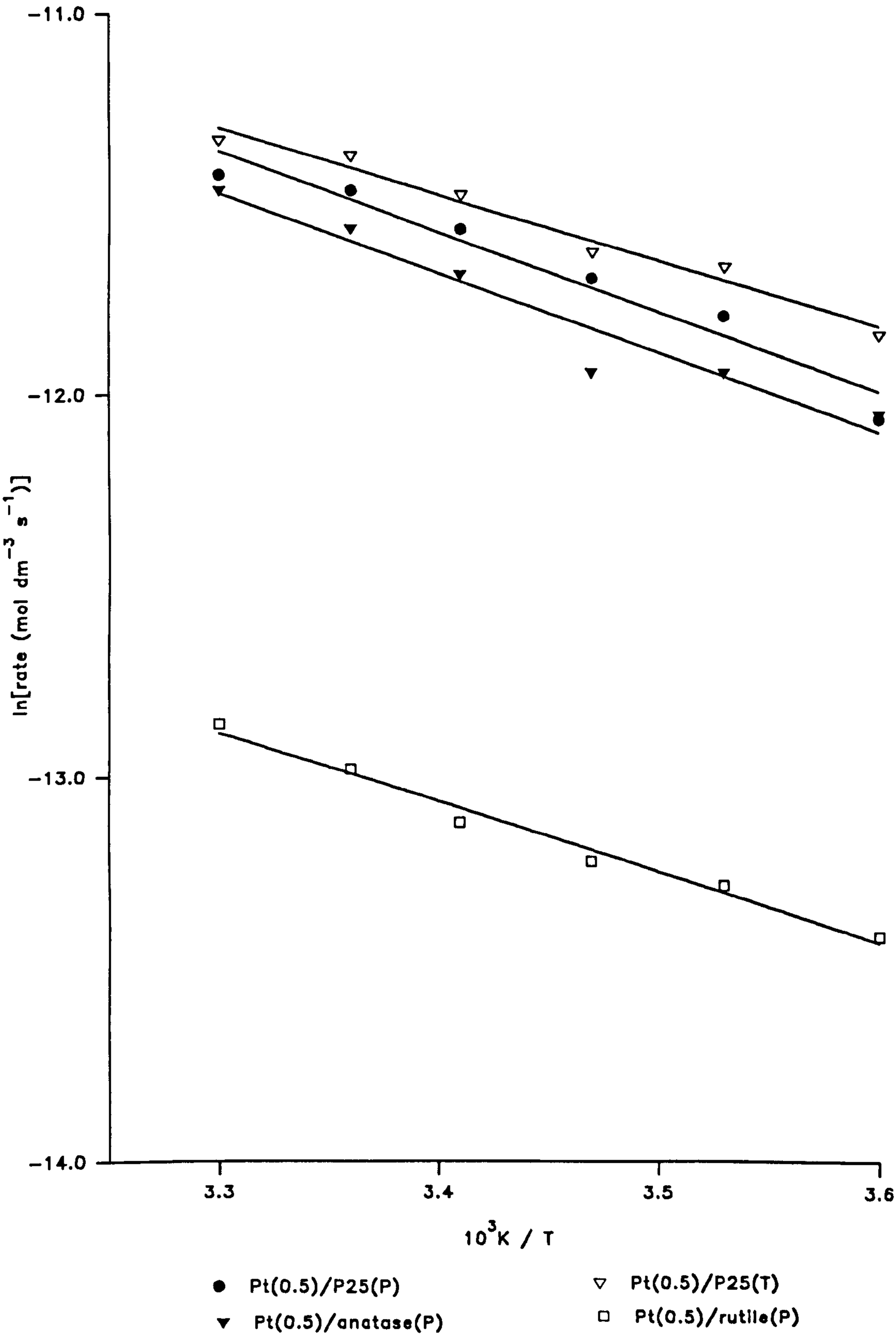

Figure 3.46: Arrhenius Plots for Photocatalytic Propanone Formation over Various Platinised Titania Catalysts

Table 3.54

Catalyst: Pt(0.5)/P25(P)

Time / mins	10^2 x [propanone] / mol dm^{-3}					
	278K	283K	288K	293K	298K	303K
0	0.15	0.15	0.19	0.25	0.19	0.28
20	0.91	1.13	1.22	1.81	1.53	1.79
40	1.56	1.79	2.15	2.83	2.64	3.24
60	2.44	2.87	2.96	4.15	3.84	4.40
80	2.74	3.97	4.26	5.38	5.42	5.57
100	3.61	4.37	5.24	6.48	6.52	6.98
10^5Rate / mol dm^{-3} s^{-1}	0.58	0.76	0.84	0.95	1.06	1.11

Table 3.55

Catalyst: Pt(0.5)/P25(T)

Time / mins	10^2 x [propanone] / mol dm^{-3}					
	278K	283K	288K	293K	298K	303K
0	0.17	0.25	0.36	0.49	0.62	0.81
20	1.39	1.35	1.46	1.74	1.93	1.90
40	2.07	2.35	2.64	2.86	3.16	3.58
60	3.13	3.37	3.65	3.90	4.88	4.85
80	3.78	4.41	4.83	5.26	6.06	6.20
100	4.60	5.34	5.73	6.20	7.02	8.15
10^5Rate / mol dm^{-3} s^{-1}	0.72	0.86	0.90	1.04	1.15	1.21

Table 3.56

Catalyst: Pt(0.5)/anatase (P)

Time / mins	10^2 x [propanone] / mol dm^{-3}					
	278K	283K	288K	293K	298K	303K
0	0.18	0.16	0.23	0.56	0.63	0.71
20	1.03	1.01	1.11	1.68	1.70	1.95
40	1.64	1.89	1.87	2.65	2.88	3.08
60	2.28	2.82	2.59	3.70	4.02	4.25
80	2.76	3.26	3.39	4.38	5.12	5.64
100	3.88	4.07	4.20	5.90	6.39	6.84
10^5Rate / mol dm^{-3} s^{-1}	0.58	0.65	0.65	0.85	0.95	1.02

Table 3.57

Catalyst: Pt(0.5)/rutile (P)

Time / mins	10^2 x [propanone] / mol dm^{-3}					
	278K	283K	288K	293K	298K	303K
0	0.08	0.12	0.12	0.38	0.39	0.45
20	0.23	0.32	0.38	0.67	0.59	0.78
40	0.38	0.51	0.58	0.77	0.86	1.03
60	0.64	0.79	0.79	0.97	1.22	1.30
80	0.79	0.96	0.97	1.41	1.50	1.68
100	0.98	1.09	1.23	1.56	1.69	1.97
10^5Rate / mol dm^{-3} s^{-1}	0.15	0.17	0.18	0.20	0.23	0.24

CHAPTER 4: DISCUSSION

4.1 Introductory Discussion

The emphasis of the project work reported in this thesis was to compare the performance of TiO_2-supported metal catalysts, in terms of activity and stability, produced by two very different routes. The first method involved reduction of the appropriate metal salt solution via photo-electrons generated in the oxide support material by irradiation with UV light. This was conducted under an inert atmosphere at room temperature. In contrast, the second method of preparation involved impregnation of the oxide support with the appropriate metal salt solution, followed by reduction in H_2 at 753K. The overall hypothesis to be tested was that more finely dispersed TiO_2-supported metal could be achieved via the photodeposition route, compared with the thermal reduction route, consequently giving catalysts with much higher activities. The reasoning behind this hypothesis was that the high-temperature reduction method was more likely to lead to significant sintering of the supported metal and also probably induce metal - support effects, via the generation of non-stoichiometry within the oxide support. Therefore, the main thrust of the project was to investigate the influence the method of preparation may have on the catalytic performance of TiO_2-supported metals.

The main catalytic reactions selected for the assessment of metal/TiO_2 catalytic performance were the thermal hydrogenations of gaseous propene and cyclopropane. This choice of reactions to be studied

was based on the fact that pure Group VIII metals, such as platinum, palladium, rhodium, which were to be used in the project work, are known to be active catalysts of these hydrogenation reactions at fairly low temperatures. The criterion of relatively low reaction temperatures was important, since exposure of the metal/TiO_2 catalysts to high reaction temperatures during experiments would probably result in extensive sintering and enhancement of metal - support effects. This in turn would mask any differences arising from the use of different preparation methods. However, as is discussed in more detail later, even the relatively mild reaction conditions used during the thermal hydrogenation reactions were sufficient to destroy the activities of the metal/TiO_2 catalysts produced via the photodeposition route.

The reverse reaction of dehydrogenation was also studied during the course of the project. Thermal dehydrogenation reactions generally only proceed at reasonable rates at fairly high reaction temperatures, $\geq$ 500K. Therefore, such reactions were not suitable for investigating potential differences in metal/TiO_2 catalysts arising from different preparation routes. As an alternative, the photocatalytic dehydrogenation of propan-2-ol was chosen, since this reaction occurs in the presence of metal/TiO_2 catalysts and UV light of the appropriate wavelength at low temperatures. Thus, potential problems of inducing metal sintering and metal - support effects during the catalytic reaction would hopefully be avoided.

4.2 Gas - Phase Propene Hydrogenation Studies

4.2.1 Effect of Catalyst Pretreatment

Figure 4.1 summarise the effect of pretreatment in either H_2 or H_2 followed by O_2, in the range 300 - 750K, on the activity of Pt(0.5)/P25(P) for prolonged propene hydrogenation at 300K. It can be readily seen that pre-reduction of the catalyst in H_2 at increasingly higher temperatures, in the range 400 - 600K, gradually eliminated hydrogenation activity. Pre-reduction in H_2 at temperatures above 600K was found to render the catalyst completely inactive for the hydrogenation of propene at 300K. It is well-known that high temperature reduction of catalysts comprising Group VIII metals supported on reducible transition metal oxides leads to suppression of their chemisorptive, and hence catalytic, capabilities. This effect was first described by Tauster et al[147], who attributed the loss of catalytic properties to the occurrence of some form of strong metal-support interactions (SMSI). The SMSI phenomenon has been the subject of many investigations, although the exact origin of the effect has not yet been fully elucidated. It is generally accepted that hydrogen spillover from metal sites, active for H_2 chemisorption, onto the supposedly inert support material is the first essential step in the inception of SMSI effects. However, the precise role which spillover hydrogen plays in the generation of SMSI is still the subject of much debate and several theories have been proposed to explain the SMSI phenomenon. These include the "encapsulation model", which suggests that the metal sites are covered by mobile sub-oxide species arising from the reduction of the support

material, electron enrichment of the metal sites by transfer of electronic charge from the reduced support to the metal and the formation of intermetallic compounds, e.g. Pt_nTiO_x. The literature covering this topic has been reviewed in detail in Section 1.5.

The results of the experiments investigating the relationship between pre-reduction temperature and subsequent catalyst activity reported here, show that the chemisorption, and hence catalytic, capacity of Pt(0.5)/P25(P) is only partially suppressed following pre-reduction in H_2 at temperatures below 600K. Complete suppression of catalytic ability is only achieved by pre-reduction in H_2 at temperatures above 600K. This suggests that the inception of SMSI occurs in two distinct stages, the first occurring at temperatures below 600K, and the second at temperatures greater than 600K. In most studies of the SMSI phenomenon, the effect of pre-reduction temperature is largely ignored and metal-support effects are induced simply by pre-reducing the catalyst in question at high temperatures, most usually 773K. However, more recently, Belzunegui et al[241] have used ^1H NMR to study the influence of the degree of support reduction on metal-support interactions, for a Rh/TiO_2 catalyst prepared by impregnation/reduction. On the basis that the ^1H NMR spectra obtained following hydrogen reduction of the catalyst in the range 373 - 673K were quite different from those obtained following similar pre-reduction at temperatures above 673K, these workers proposed that the establishment of SMSI occurs in two distinct stages. The first stage, occurring between 373 and 673K, was linked to a loss in hydrogen chemisorption at the metal sites and attributed to the incorporation of hydride species into

oxygen vacancies at the metal-support interface. Above 673K, such hydride species cannot be stabilised at the interface and the loss in metal chemisorptive ability was attributed to both an electronic interaction between the metal and the reduced support together with encapsulation of the metal by TiO_x overlayers. The role of hydrogen in the generation of SMSI has recently been studied by Munuera et al[242,243], using XPS and ion - scattering spectroscopy to study the diffusion of Ni and titanium sub-oxides in model Ni-TiO_x systems. On the basis of the results obtained, these workers proposed that treatment of the model systems in H_2 at elevated temperature leads to the incorporation of hydrogen, in the form of hydride-like species, into the titanium oxide lattice. Furthermore, it was suggested that incorporation of the hydride-like species resulted in enhanced mobility of both titanium suboxide species and of atoms of the metallic phase through the TiO_x lattice. Unfortunately, the effect of increasing reduction temperature was not investigated and the observations related only to a single high temperature reduction carried out at 773K. However, it would appear that the results of Munuera et al[243] support the proposition of Belzunegui et al[241] that the generation of SMSI during hydrogen reduction of metal/TiO_2 catalysts occurs in two distinct stages. The first stage would appear to be the incorporation of hydride-like species in the defect oxide lattice and the second encapsulation of the metal particles by TiO_x layers, which may also be enhanced by diffusion of metal atoms into the defect support lattice. Bonneviot and Haller[244] have studied the effect of low (513K), medium (573K) and high (773K) temperature reduction on the H_2 and CO chemisorption capacity

and the n-butane isomerisation and hydrogenolysis activity of Pt/TiO_2 catalyst. Inhibition of the chemisorptive and catalytic properties of the catalyst was found to occur in two distinct steps and also the overall effect could be reversed by treatment in oxygen. It was proposed that the first stage, which occurred at medium reduction temperature, was due to an apparent flattening of the metal particles, leading to the exposure of less active, low index planes. The second stage, found to occur at high reduction temperature, was attributed to the blocking of metal sites by TiO_x overlayers. However, the results of a recent ^{195}Pt NMR study of the SMSI effect in high temperature reduced Pt/TiO_2 catalysts recently conducted by Bucher et al[245] suggest that no significant changes in the morphology of the Pt deposits occur during the pretreatment. A moderate loss in bulk metal properties was observed and attributed to changes in the electronic structure of the metal particles. Furthermore, preliminary experiments on samples containing very small, highly dispersed Pt particles suggested the occurrence of substantial rearrangements in the electronic structure at the $Pt\text{-}TiO_2$ interface. These results are clearly in conflict with the proposal of Bonneviot and Haller[244] that the first stage of the establishment of SMSI involves a substantial morphological change in the supported metal at medium reduction temperatures.

Figure 4.1 also show the effect of re-oxidation in O_2 at increasingly higher temperatures on the activity of Pt(0.5)/P25(P), previously reduced in hydrogen at 750K, for propene hydrogenation at 300K. It can been seen that the chemisorptive, and hence catalytic ability, of SMSI Pt(0.5)/P25(P) was gradually restored by oxidative pretreatment at increasingly

higher temperatures in the range 300 - 700K. This demonstrates the reversibility of the SMSI effect in such catalysts and the results obtained here are in complete agreement with the observations made by other workers[147,185,202]. Removal of SMSI is usually explained as being the reverse of the process responsible for the establishment of the effect in the first place and can therefore be attributed to the removal of TiO_x overlayers, the relocation of electronic charge from the metal to the oxide support or the breaking of intermetallic compounds. The results of this study show that whilst re-oxidation of SMSI Pt(0.5)/P25(P) in oxygen, in the range 300 - 500K, initially restores catalytic activity, the stabilities of such pretreated catalysts are extremely poor and their activities during prolonged propene hydrogenation at 300K rapidly fall to very low values. Only re-oxidation of SMSI Pt(0.5)/P25(P) at temperatures well above 500K completely restored catalytic activity and resulted in good stability during prolonged hydrogenation. These observations provide support for the theory of two stages of SMSI inception, since presumably removal of SMSI effects would also show two temperature-dependent steps during re-oxidation of SMSI catalysts at increasingly higher temperatures. In a further ^1H NMR study, Belzunegui et al[246] investigated the effect of re-oxidation temperature on SMSI Rh/TiO_2 and noted that two distinct stages occurred for the removal of the SMSI state. The first, occurring in the range 273 - 473K, was attributed to the progressive elimination of electronic perturbations of the metal and was characterised by a partial restoration of chemisorption capacity. However, complete removal of SMSI effects could only be achieved by re-oxidation at 673K, this being

attributed to the removal of TiO_x overlayers partially blocking the metal surfaces. It is also worth noting that Bucher et al[245] found that re-oxidation of SMSI Pt/TiO_2 catalyst at temperatures below 600K was not sufficient to fully restore the ^{195}Pt spectra to their original form.

Although the concept that the establishment of SMSI in TiO_2-supported metal catalysts occurs in two distinct temperature-dependent stages is fairly recent, the results obtained in this study would appear to support this theory. The fact that reduction of Pt(0.5)/P25(P) in H_2 at temperatures up to 600K gradually eliminates catalytic activity, whereas reduction at temperatures above 600K completely removes all activity would suggest the occurrence of two temperature-dependent processes. This is further supported by the fact that unless SMSI Pt(0.5)/P25(P) is re-oxidised at temperatures well above 500K, the stability of the re-oxidised catalyst during prolonged propene hydrogenation is found to be extremely poor. This instability might be due to the partial restoration of catalytic activity and re-incorporation of hydride-like species at the metal - support interface, rich in TiO_x due to incomplete re-oxidation, during the hydrogenation of propene at 300K, via a mechanism involving spillover hydrogen. Such an explanation, although entirely speculative, is consistent with the observations and hypotheses of Belzunegui et al[241,246] and Bucher et al[245].

Many workers[147,191,246] have found that the most efficient method of restoring chemisorptive, and hence the catalytic, ability of SMSI catalysts is high temperature re-oxidation, followed by a further mild, low temperature reduction in hydrogen. The positive effect of the second

reduction stage is frequently attributed to the removal of PtO_x species formed during the high temperature re-oxidation step. However in the experiments reported here, no significant differences, in terms of both activity and stability during prolonged propene hydrogenation, were observed between samples of SMSI Pt(0.5)/P25(P) which were either re-oxidised at 700K or re-oxidised at 700K and then subjected to a second reduction stage in H_2 at 400K. However, the exposure of Pt(0.5)/P25(P), re-oxidised at 700K only, to propene/hydrogen mix at 300K may have been sufficient to eliminate any differences in activity between that sample and the one subjected to the second mild reduction step. One possible method of testing this hypothesis would be to investigate the activities of similarly pretreated Pt/TiO_2 catalysts for a reaction not involving hydrogen.

4.2.2 Effect of Platinum Loading

The influence of increasing the amount of supported Pt metal, in the range 0.25 - 2.0 %mass, on the initial activities of 'as prepared' Pt(x)/P25(P) catalysts for propene hydrogenation at 300K, is shown in Fig. 4.2. As would be expected, an increase in Pt content is generally accompanied by an increase in the measured hydrogenation activity of the catalyst. However, there appears to be no direct relationship between %mass of supported Pt and the corresponding measured reaction rate. The two catalysts containing 0.5 %mass Pt, in particular that prepared by photodeposition, exhibit greater than expected activities in comparison

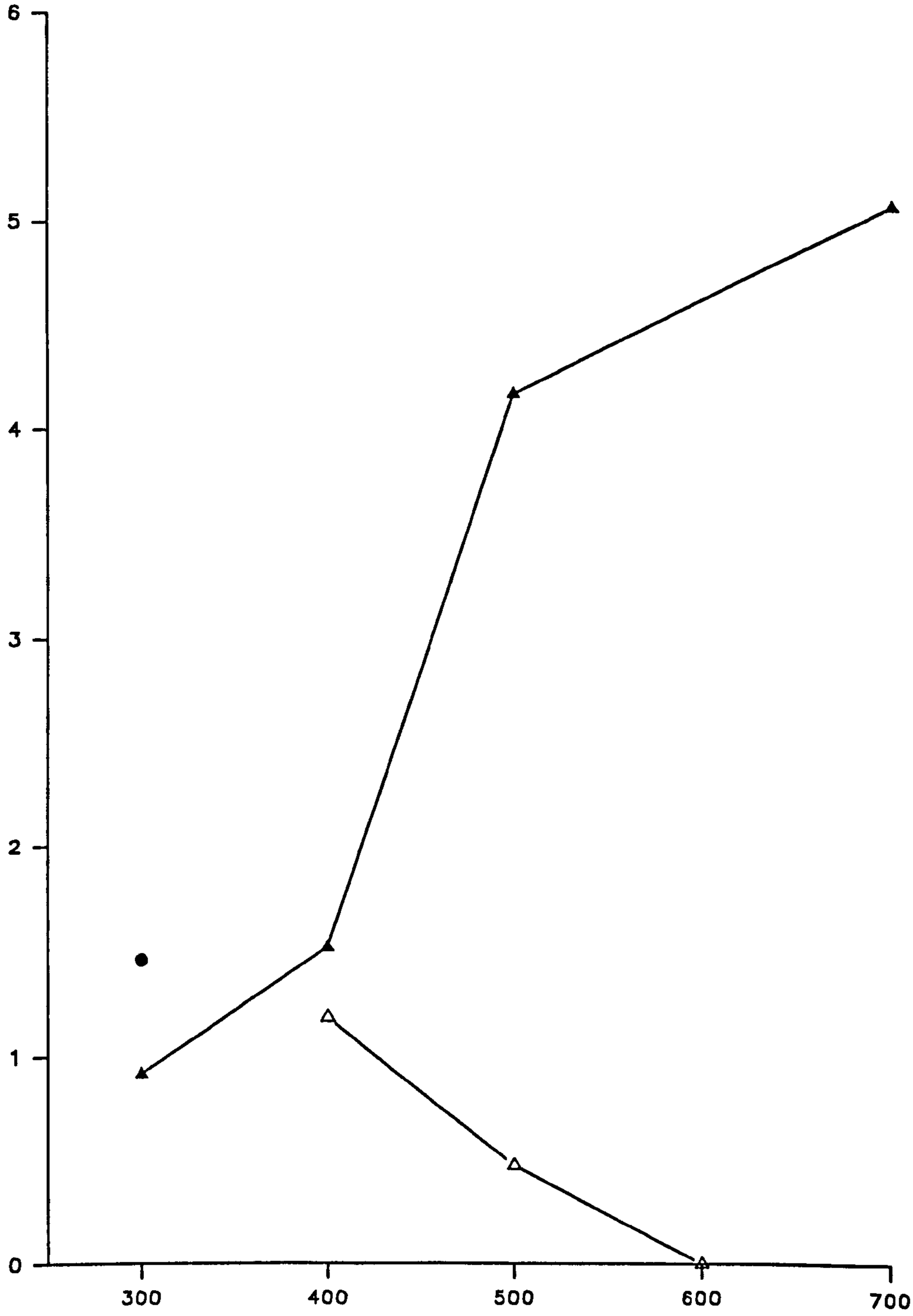

- ● No pretreatment
- △ Reduction in H_2 for 3hrs
- ▲ Reduction in H_2 for 3hrs, then oxidation in O_2 for 3hrs

Figure 4.1: Summary of the Effect of Reduction and Reduction/ Oxidation on the Absolute Initial Propene Hydrogenation Rate over Pt(0.5)/P25(P) Catalyst

with the other catalysts. A similar comparison between Pt/TiO_2 catalysts, prepared by both photodepostion and impregnation/reduction methods, has been conducted by Dunn and Bard[146], who investigated the activities of these catalysts for the liquid-phase hydrogenation of benzene. It was observed that the activity of the photodeposited catalyst was significantly greater than that observed for the corresponding catalyst prepared by the thermal method. The difference in activities was attributed to the fact that the thermal preparative route involves pre-exposure of the material to hydrogen at elevated temperatures, which may induce a certain degree of SMSI in the resulting catalyst. However, the results obtained in this study would suggest that such an explanation is incorrect, since Pt(0.5)/P25(T) is observed to be almost as active as Pt(1.0)/P25(P), despite the fact that latter catalyst comprised approximately twice as much supported metal and was not exposed to hydrogen at all during preparation. A more likely explanation of the observed results is that the photodeposition technique produces catalysts in which the initial dispersion of the metal is somewhat variable, regardless of the final metal content, which in turn gives rise to the variable activities observed for the 'as prepared' catalysts. Also, differing extents of surface contamination by preparation by-products, in particular chloride ions, may have a significant effect on the activities of the 'as prepared' materials.

The above hypothesis is supported by the observation that all the catalysts exhibited significantly enhanced activities for the hydrogenation reaction, relative to the corresponding 'as prepared' samples, following reduction in H_2 and subsequent re-oxidation in O_2 at elevated tempera-

tures. Such marked increases in catalytic activity in all cases is presumed to be a consequence of an increase in the surface area of active metal presented to the reactants. This can be explained in terms of enhanced diffusion of the metal atoms through a defect titanium oxide lattice, in the presence of hydrogen, at elevated temperatures, as postulated by Munuera et al[242,243]. The occurrence of metal atom diffusion in this manner could conceivably give rise to catalysts with much greater metal dispersions, and hence metal surface areas, following high temperature reduction and re-oxidation, relative to the 'as prepared' materials. In terms of initial hydrogenation activities immediately following pretreatment, the catalysts were found to lie in the order:

Pt(0.5)(P) > Pt(2.0)(P) ~ Pt(1.0)(P) ~ Pt(0.5)(T) >> Pt(0.25)(P).

Thus, a maximum in hydrogenation activity is observed with a Pt loading of 0.5 %mass, deposited by photodeposition, following high temperature reduction and subsequent re-oxidation, Fig 4.3. However, from Fig. 3.10, it can be seen that the stabilities of both Pt(0.25)/P25(P) and Pt(0.5)/P25(P) catalysts, during prolonged propene hydrogenation, are very poor, relative to the three other Pt/TiO_2 catalysts. These two issues can be explained in terms of morphological differences, with respect to the supported Pt metal, arising as a consequence of the two different preparative routes used, and are discussed in more detail in Section 4.5.

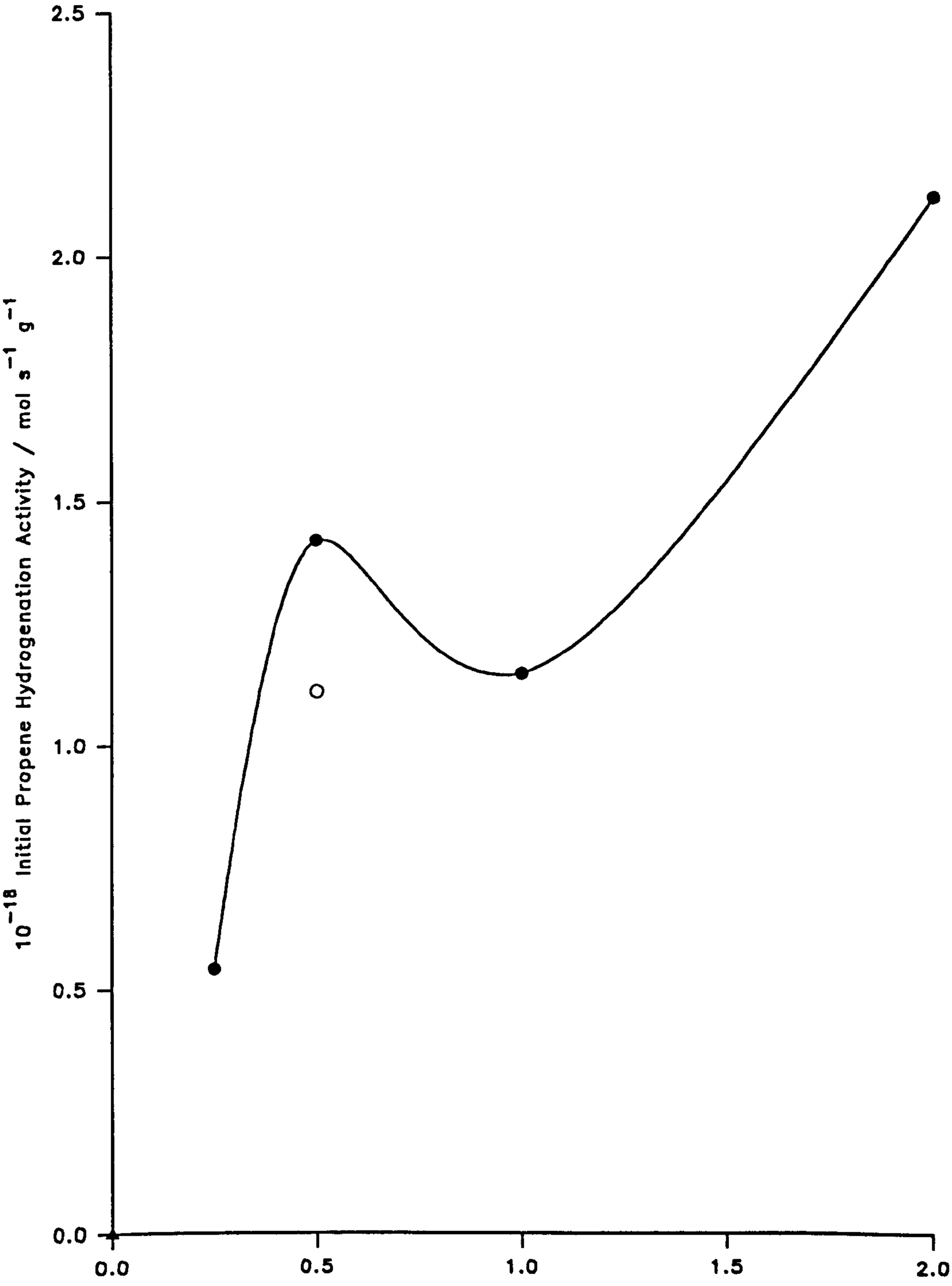

Figure 4.2: Initial Propene Hydrogenation Activity as a Function of Metal Content for Various Untreated Pt/TiO_2 Catalysts

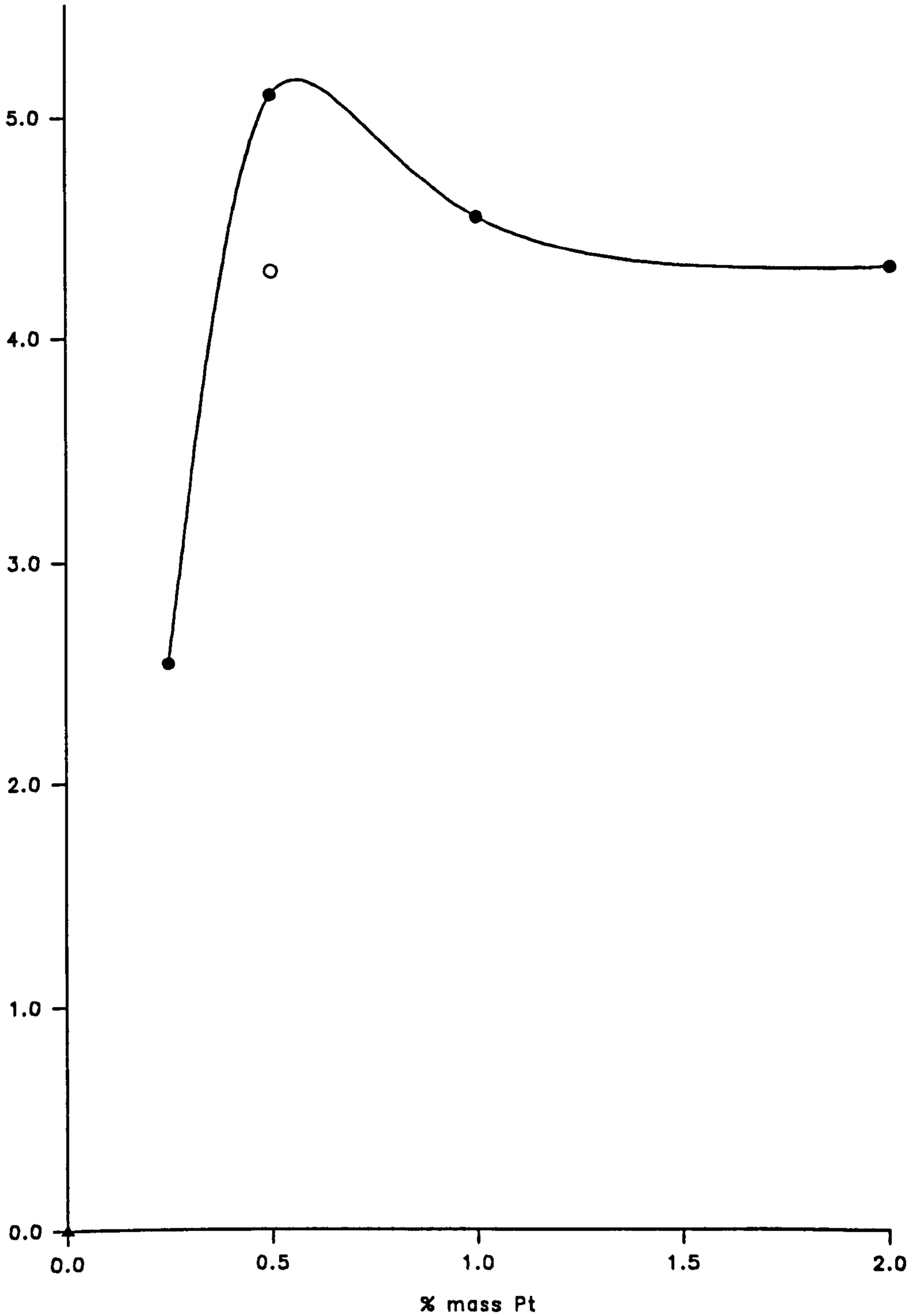

Figure 4.3: Initial Propene Hydrogenation Activity as a Function of Metal Content for Various Reduced/Oxidised Pt/TiO_2 Catalysts

4.2.3 Temperature Dependence

Fig. 3.11 shows the influence of increasing temperature, in the range 260 - 345K, on the rate of propene hydrogenation over reduced/oxidised Pt(0.5)/P25(P) and Pt(0.5)/P25(T) catalysts. For both catalysts, the rate of reaction was observed to increase rapidly with increasing temperature until a maximum was reached, then fall gradually as the temperature was further increased. However, the temperature at which the maximum reaction rate occurred with each of the catalysts was found to be different; 275K for the thermal catalyst and 295K for the photodeposited catalyst. The corresponding Arrhenius plots are shown in Fig. 4.4 and, as would be expected on the basis of Fig. 3.11, are very similar in form, being linear as the temperature increases from the start point, changing to non-linear and then back to linear as the temperature further increases. For the photodeposited catalyst, an activation energy of $+55 kJ\ mol^{-1}$ is estimated for the hydrogenation reaction over the temperature range 273 - 295K. As can be seen from Fig. 4.4, the data obtained using this catalyst are not very reproducible and as a consequence the apparent activation energy lies somewhere in the range $+30$ - $130 kJ\ mol^{-1}$. Above 300K a different activation energy, estimated to be - $10 \pm 8 kJ\ mol^{-1}$, is associated with the hydrogenation of propene. The activation energy for propene hydrogenation over the thermally-prepared catalyst also shows a similar dependence on temperature, estimated to be $+45 \pm 2 kJ\ mol^{-1}$ in the range 260 - 275K and $-2 \pm 0.5 kJ\ mol^{-1}$ in the range 280 - 345K. Unlike that obtained with the photodeposited catalyst, the data for the thermal catalyst are much more reproducible and consist-

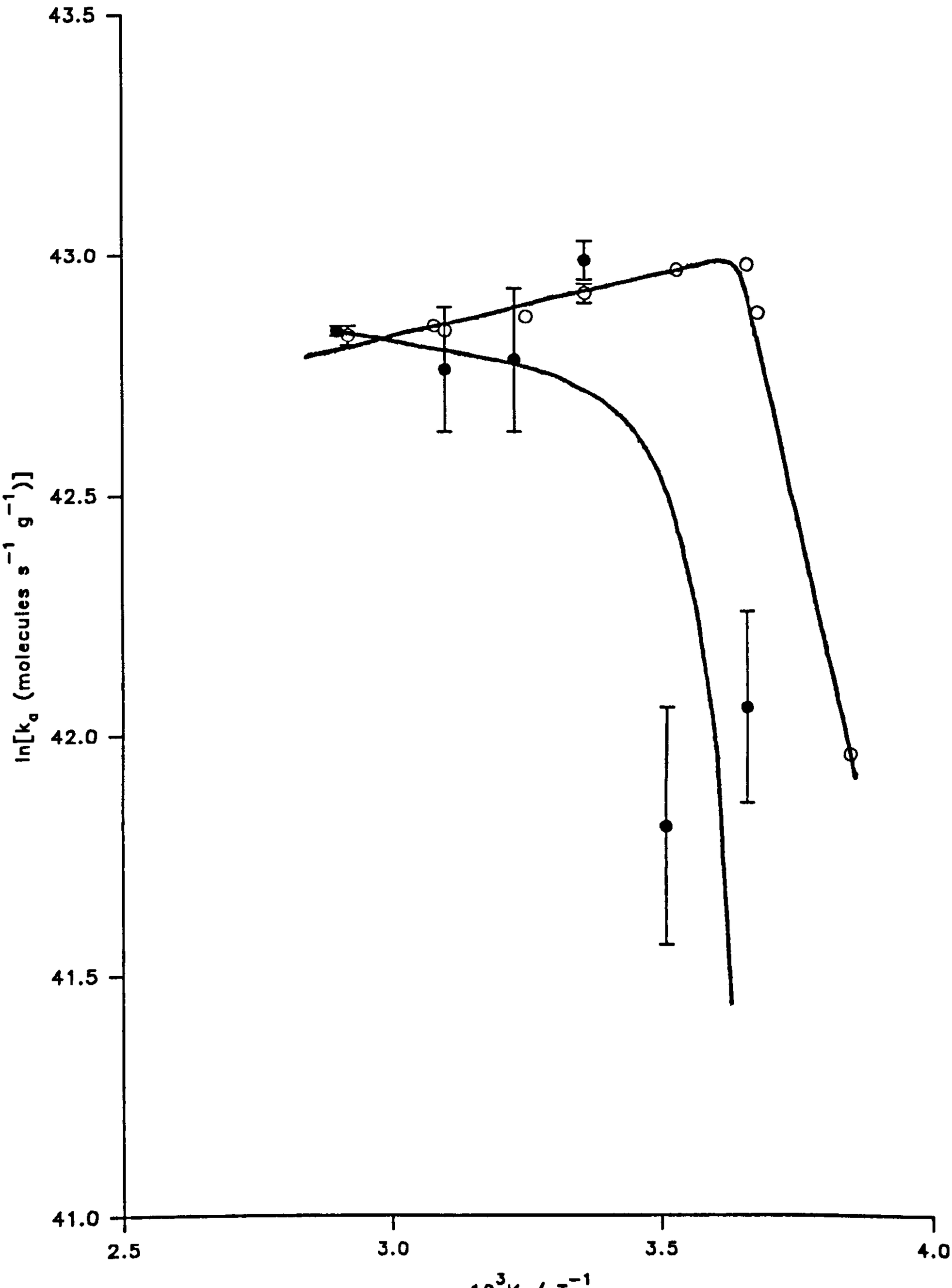

Figure 4.4: Arrhenius Plots for Propene Hydrogenation over Reduced/Oxidised Pt(0.5)/P25(P) and Pt(0.5)/P25(T) Catalysts

ent so that the margin of error with respect to the estimated values of the apparent activation energies is considerably smaller. This would suggest that reduced/oxidised Pt(0.5)/P25(P) is more sensitive to variations in temperature than the corresponding catalyst prepared by impregnation/reduction, thereby giving rise to the considerable variability in the data obtained. Since the activities of these catalysts are determined to a large extent by the nature of the deposited metal, it is possible that differences in the morphologies of the Pt deposits, arising from the different preparative techniques used, could account for the observed differences in behaviour of the two catalysts. This topic is discussed in more detail in Section 4.5.

The change in the estimated activation energies from positive to slightly negative values, as a consequence of increasing reaction temperature, indicates that these are apparent, rather than true, activation energies. In this case, these estimated values also include terms for the enthalpy of adsorption, ΔH_{ads}, of either, or possibly both, reactants onto the surface of the catalyst. It is known that in many catalytic reactions, enthalpies of adsorption are a function of the fractional surface coverage, θ, attained by the individual reactants. In turn, θ is usually determined by the experimental conditions of temperature and pressure, so that overall apparent activation energies are frequently dependent on the reaction conditions chosen. For example, it has been shown[247] that ΔH_{ads} for hydrogen adsorption onto pure metal surfaces decreases as the fractional surface coverage of hydrogen, θ_H, increases. However, since adsorption is an exothermic process, θ_H will decrease as the reaction temperature is

increased. The observed temperature dependence of the activation energy for propene hydrogenation over both Pt(0.5)/P25(P) and Pt(0.5)/P25(T) catalysts appears to be a general phenomenon in catalytic alkene hydrogenation reactions. In these cases, the activation energy for the reaction is observed to fall as the reaction temperature increases until, at a certain temperature, the value becomes zero. This critical temperature, at which a maximum in the rate is observed, is known as the "inversion temperature" and is denoted as T_{max}. At temperatures above T_{max}, the activation energy either remains at zero or attains a negative value. This effect has been observed with various forms of nickel[248,249], platinum[250,251] and even copper[252] catalysts. It has been observed[253] that T_{max} decreases with decreasing alkene pressure, which has been attributed[253] to alkene desorption. Thus, at temperatures above T_{max} it is necessary to subtract the enthalpy of adsorption of the alkene as well as that of hydrogen from the apparent activation energy in order to obtain the true value. Thus, for:

$$T < T_{max} \qquad E_{true} = E_{app} - \{-\Delta H_{ads}(H_2)\} \qquad [78]$$

$$T = T_{max} \qquad E_{true} = E_{app} \qquad [79]$$

$$T > T_{max} \qquad E_{true} = E_{app} - \{-\Delta H_{ads}(H_2)\} - \{-\Delta H_{ads}(alkene)\} \qquad [80]$$

Under conditions where $\theta << 1$, as is the case in the experiments described here, θ, and in turn ΔH_{ads}, for either, or much more likely, both reactants will be temperature dependent. Overall this means that the estimated apparent activation energies for the propene hydrogenation reaction over the Pt/TiO_2 catalysts will change as a function of increasing temperature, as is observed in this study.

An alternative explanation of the observed temperature dependence of the activation energies for propene hydrogenation is that the adsorption mechanism of the alkene onto the catalyst surface changes as a function of temperature. Such a change in the alkene adsorption mechanism would be reflected in the enthalpy of adsorption, although not necessarily in the fractional surface coverage under given experimental conditions. Studies[254-8] of ethene adsorption onto pure metals, such as platinum and palladium, using modern spectroscopic techniques, have shown that at temperatures below ~200K the adsorbed surface species can be represented as a 1,2-di-σ-adsorbed form, although there is some evidence to suggest that the π-complex form also exists. At temperatures between 200 - 300K, the adsorbed alkene species is observed to dehydrogenate to give a surface ethylidyne species, as shown below:

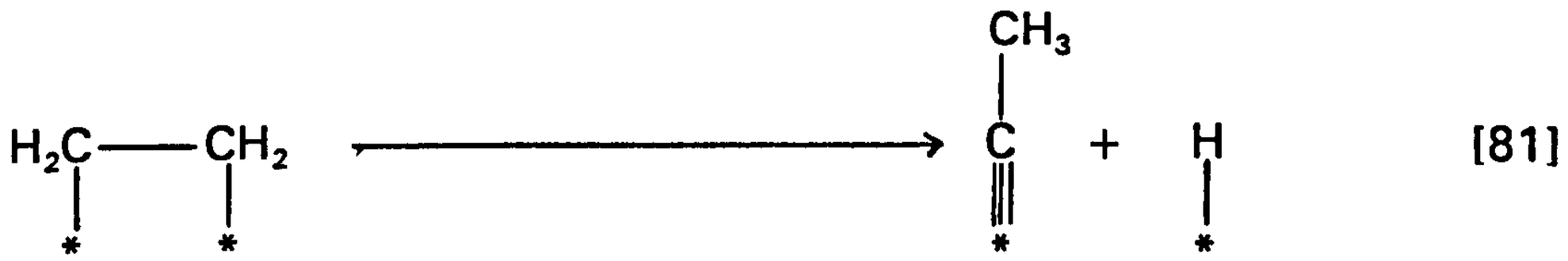

[81]

1,2-di-σ species

T < 200K

ethylidyne species

T > 200K

- where * = surface active site.

Spectroscopic evidence[254-8] suggests that the ethylidyne species adopts a p(2x2) form, although it has been proposed[259] that this species actually adopts a 3-(2x1) pattern. Ethylidyne formed on pure metal surfaces is apparently stable up to ~400K, at which point further dehydrogenation occurs to give carbonaceous surface deposits[260], although evidence for

the presence of ethylidyne on Pt black at 663K has been reported[261]. Similarly, it has been found[262] that cyclopentane also adsorbs onto pure metals to give a 1,2-di-σ-adsorbed species at low temperatures, which then converts to adsorbed cyclopentadienyl, C_5H_5, at higher temperatures. More recently, Mohsin et al[263] used IR spectroscopy to study ethene adsorption on alumina-supported Rh, Ir, Pt and Pd metals. At low temperatures, the 1,2-di-σ-adsorbed species was observed, which converted to the ethylidyne form as the temperature was raised. Adsorption of ethene at room temperature gave rise to IR bands corresponding to both π-complexed and adsorbed ethylidyne on the surface of each metal. Hensley and Kesmodel[264] have used HREELS to investigate the adsorption of ethene onto a model Pt-TiO_2 catalyst. Adsorption of ethene at 165K gave rise to the 1,2-di-σ species, which was observed to convert to ethylidyne on raising the temperature to 325K. In a similar study[265] using model Pt-alumina catalysts, these same workers observed the formation of both the π- and the 1,2-di-σ- species following ethene adsorption at 165K. However, it was noted that ethylidyne formation only occurred on larger Pt deposits, having an average size of 1.4nm as found by TEM, upon warming to 325K. Clearly, in the case of propene hydrogenation over Pt(0.5)/P25(P) and Pt(0.5)/P25(T) catalysts, the observed change in the apparent activation energies for the reaction, as the temperature was raised, may be attributed to a dramatic change in the adsorption mode of the alkene. Thus, below T_{max} propene is adsorbed as the 1,2-di-σ- and/or the π-species and above T_{max} as the propylidyne species. In this case, ΔH_{ads} for propene would almost certainly change as a function of temp-

erature, due to the change in adsorption mode, although θ for propene may not change significantly.

It is worth noting that the two possible explanations as to why the apparent activation energies change as the temperature is increased are not mutually exclusive and indeed both could be contributory factors to the observed temperature dependence of the apparent activation energy values. In order to resolve this issue, further studies on the thermodynamics of hydrogen and alkene adsorption onto TiO_2-supported metal catalysts, in conjunction with spectroscopic experiments in order to identify the adsorbed alkene species, are required. Unfortunately, in this study there were insufficient amounts of any of the supported catalysts to conduct such detailed experiments, which require larger amounts of material, preferably from the same batch. Finally, the above explanations, and in particular the first, imply that propene hydrogenation over the Pt/TiO_2 catalysts proceeds via a Langmuir-Hinshelwood mechanism. Evidence to support this proposal is provided in the next section, in which the effect of varying reactant partial pressures is discussed.

4.2.4 Effect of Changing Reactant Partial Pressures

During the initial stages of this project, it was assumed that the hydrogenation of propene over TiO_2-supported metal catalysts obeyed first-order kinetics, with respect to the alkene. However, preliminary results, obtained by use of mass spectrometry and given in Section 3.1.1.(iii) and summarised in Fig. 4.5, indicated that the hydrogenation

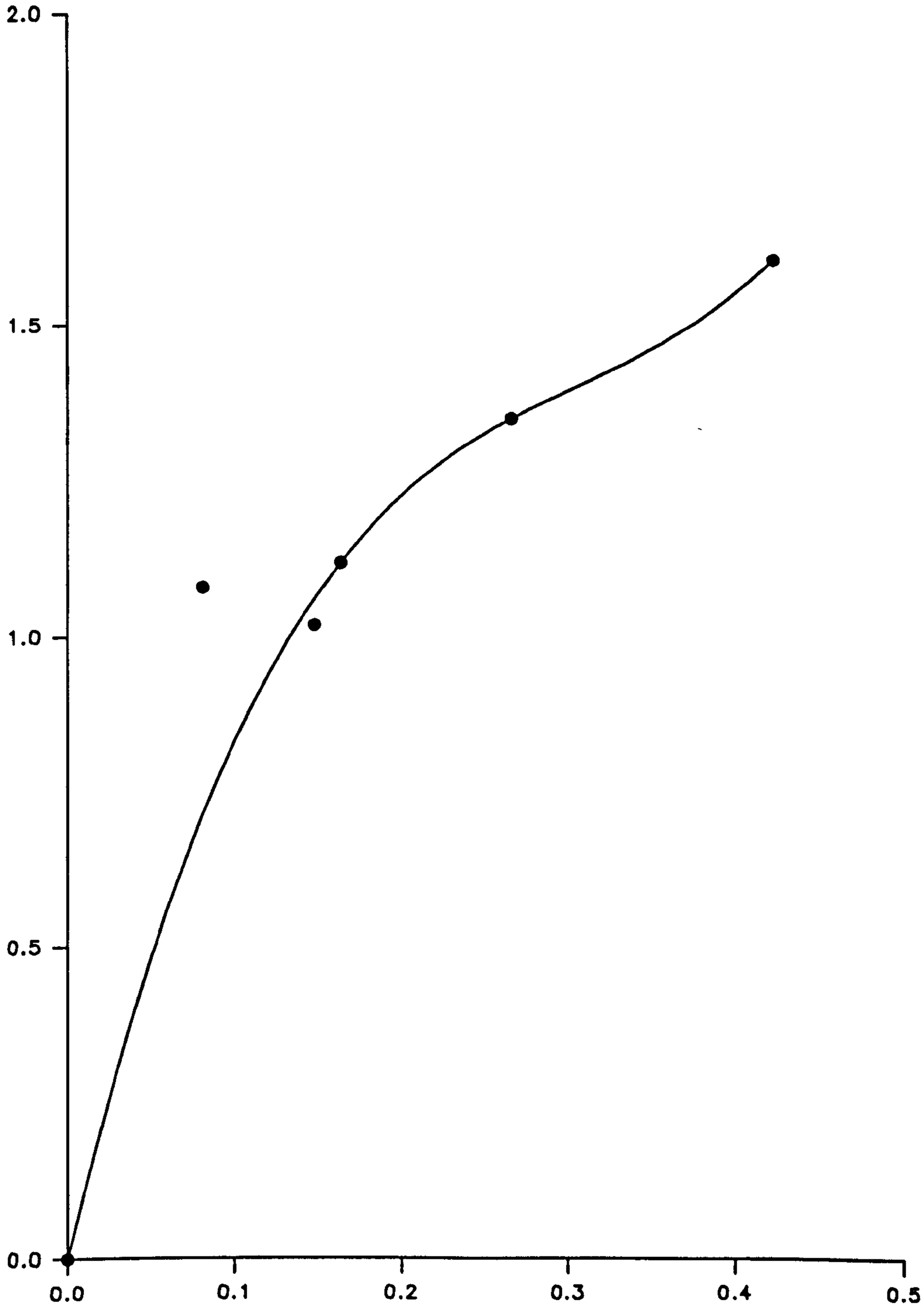

Figure 4.5: Absolute Initial Reaction Rate as a Function of Initial Propene Partial Pressure for Propene Hydrogenation over Untreated Pt(0.5)/P25(P)

reaction is less than first-order with respect to propene, although individual experiments obey first-order kinetics with respect to departure from equilibrium. This observation is supported by the fractional orders of reaction found for both hydrogen and alkenes in alkene hydrogenation reactions over both pure and supported metal catalysts, as reported in the literature[266].

At a later stage, a more comprehensive study of the pressure dependency, with respect to both hydrogen and propene, of the hydrogenation reaction, over both Pt(0.5)/P25(P) and Pt(0.5)/P25(T) catalysts, was undertaken. Fig. 3.13 shows how the reaction rate, over both types of catalyst, changes as a function of increasing propene partial pressure, with the hydrogen partial pressure being kept constant. A plot of $\log_{10}$ (rate) vs $\log_{10}$ (initial propene partial pressure), over the range 0.05 - 0.4kPa, is shown in Fig. 4.6, for both catalysts. In each case the order of reaction with respect to propene was calculated to be +0.5, although for the photodeposited catalyst a change in this reaction order was observed to occur as the propene partial pressure was increased above ~0.3kPa. Two possible explanations can be proposed for the observed fractional order of reaction with respect to propene. In the first explanation it is assumed that adsorption of propene onto the catalyst surface occurs non-dissociatively and follows a normal Langmuir isotherm, in which the reaction order changes from first- to zero-order as the surface coverage of propene increases with increasing propene partial pressure. Thus, under the reaction conditions employed, it is possible that $\theta_{propene} > 0$ but < 1, corresponding to the region of the Langmuir isotherm where the order of

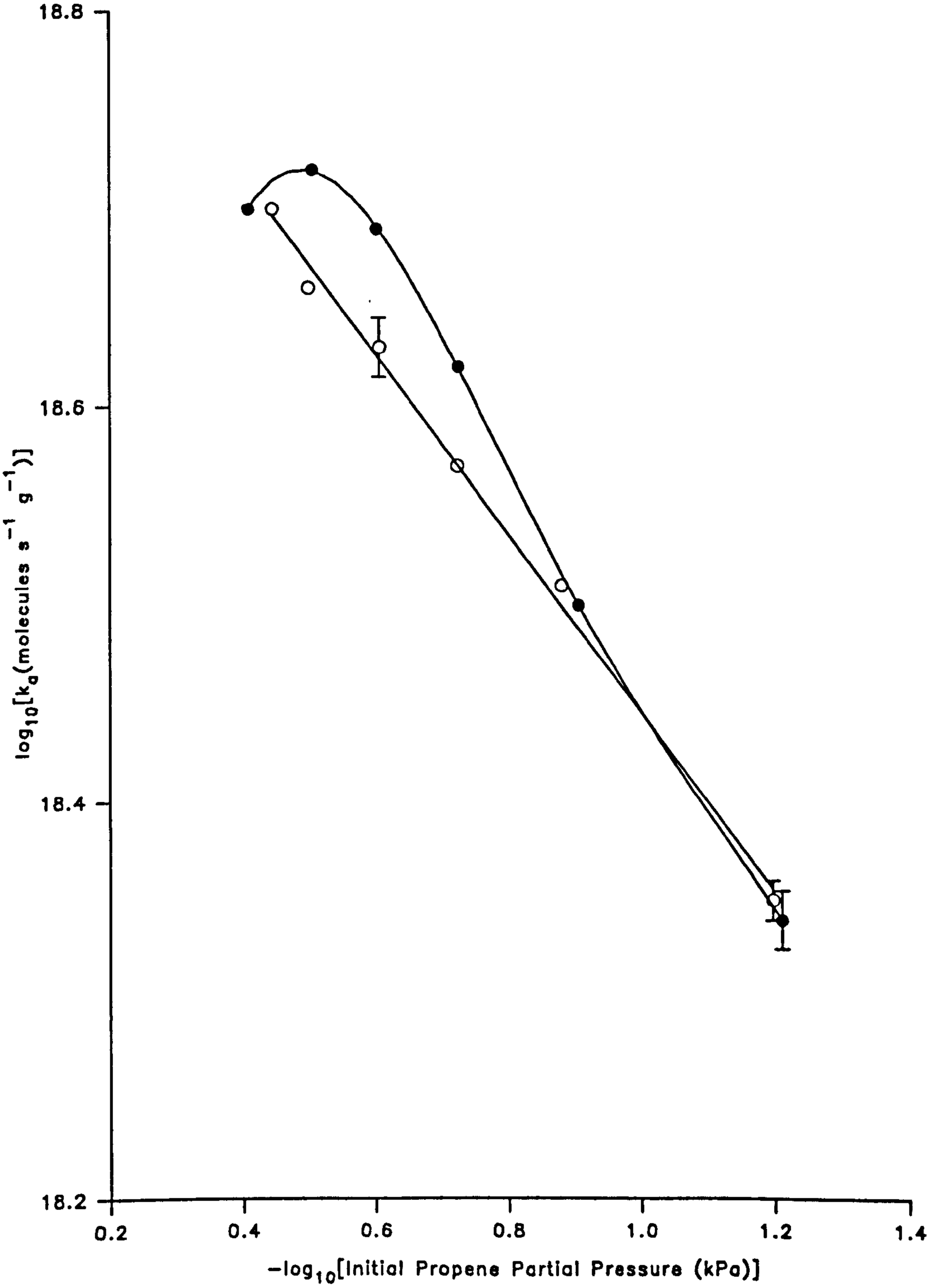

Figure 4.6: Plots of $\log_{10}$(Absolute Initial Propene Hydrogenation Rates) vs $\log_{10}$(Initial Propene Partial Pressure) for Reduced/Oxidised Pt(0.5)/P25(P) and Pt(0.5)/P25(T)

reaction with respect to propene is fractional, as shown in Fig. 4.7. The alternative explanation is that propene adsorption, under the reaction conditions employed, occurs via the formation of the propylidyne species, according to Eq.[81]. Adsorption of propene via such a mechanism is effectively dissociative adsorption, since two surface species, the propylidyne species and monatomic hydrogen, are generated. Such a process clearly requires two active surface sites for each propene molecule adsorbed, which will give rise to the fractional reaction order, with respect to propene, observed. As stated earlier, further studies are required to establish the adsorption mode of alkenes onto Pt/TiO_2 catalysts under the reaction conditions employed in this study. This in turn would indicate which of the two explanations for the observed fractional reaction order with respect to propene is correct.

The effect of increasing hydrogen partial pressure, whilst maintaining a constant propene partial pressure, on the rate of hydrogenation over both catalysts is shown in Fig. 3.15, with the corresponding $\log_{10}$ (rate) vs $\log_{10}$ (initial hydrogen partial pressure) plot given in Fig. 4.8. For the photodeposited catalyst, the order of reaction with respect to hydrogen, in the partial pressure range 0.2 - 0.4kPa, is calculated to be ~+0.6. This fractional order implies that H_2 is most probably dissociatively adsorbed at the catalyst metal sites:

$$H_2 + 2\,* \longrightarrow 2\,H{-}{-}* \qquad [82]$$

- where * = surface active site.

The positive sign indicates that in this pressure range, hydrogen is not competing with propene for active surface sites and is therefore not act-

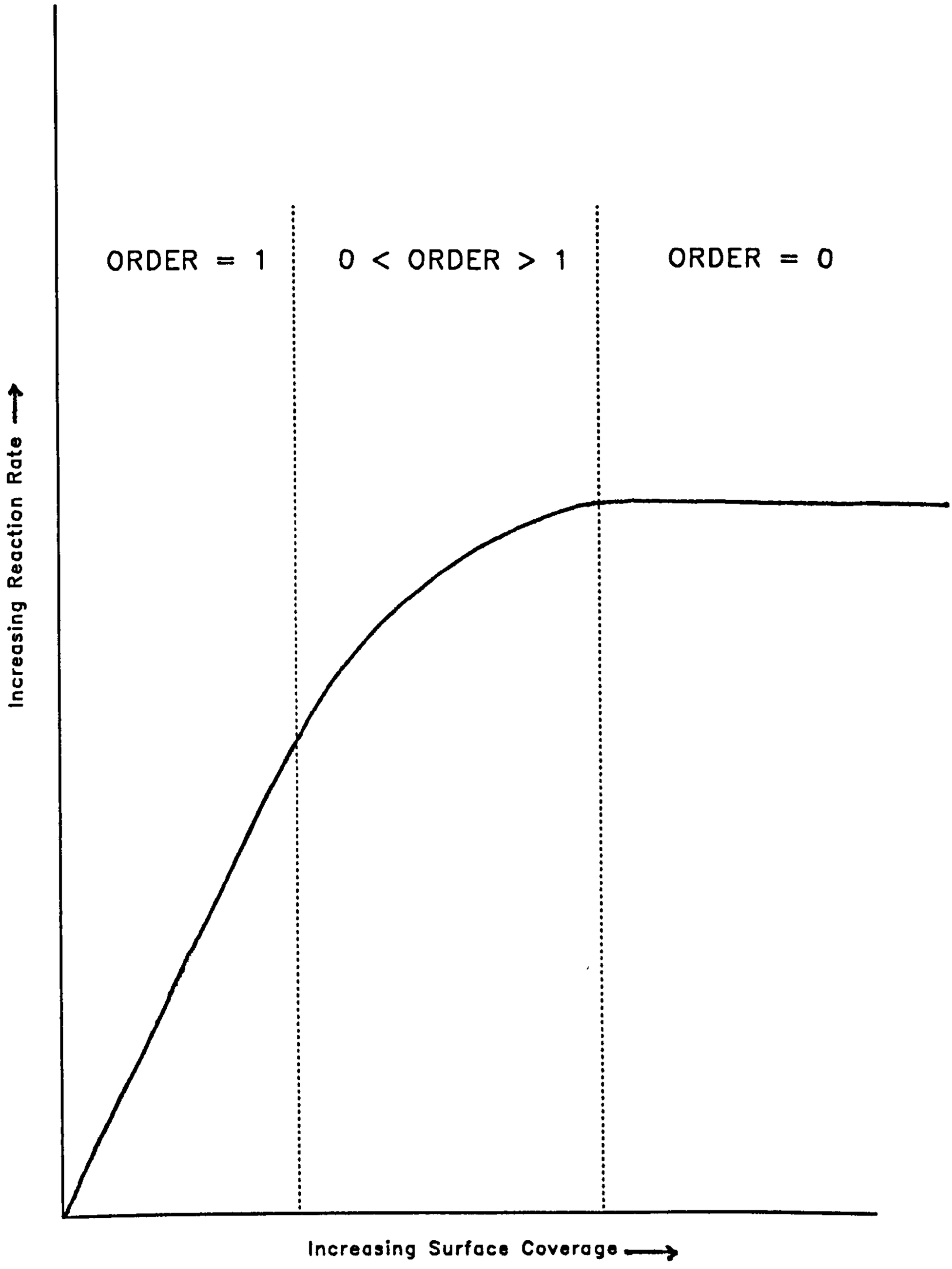

Figure 4.7: Schematic Representation of Changing Reaction Order as a Function of Increasing Surface Coverage Based on Non-dissociative Adsorption Following a Langmuir Isotherm

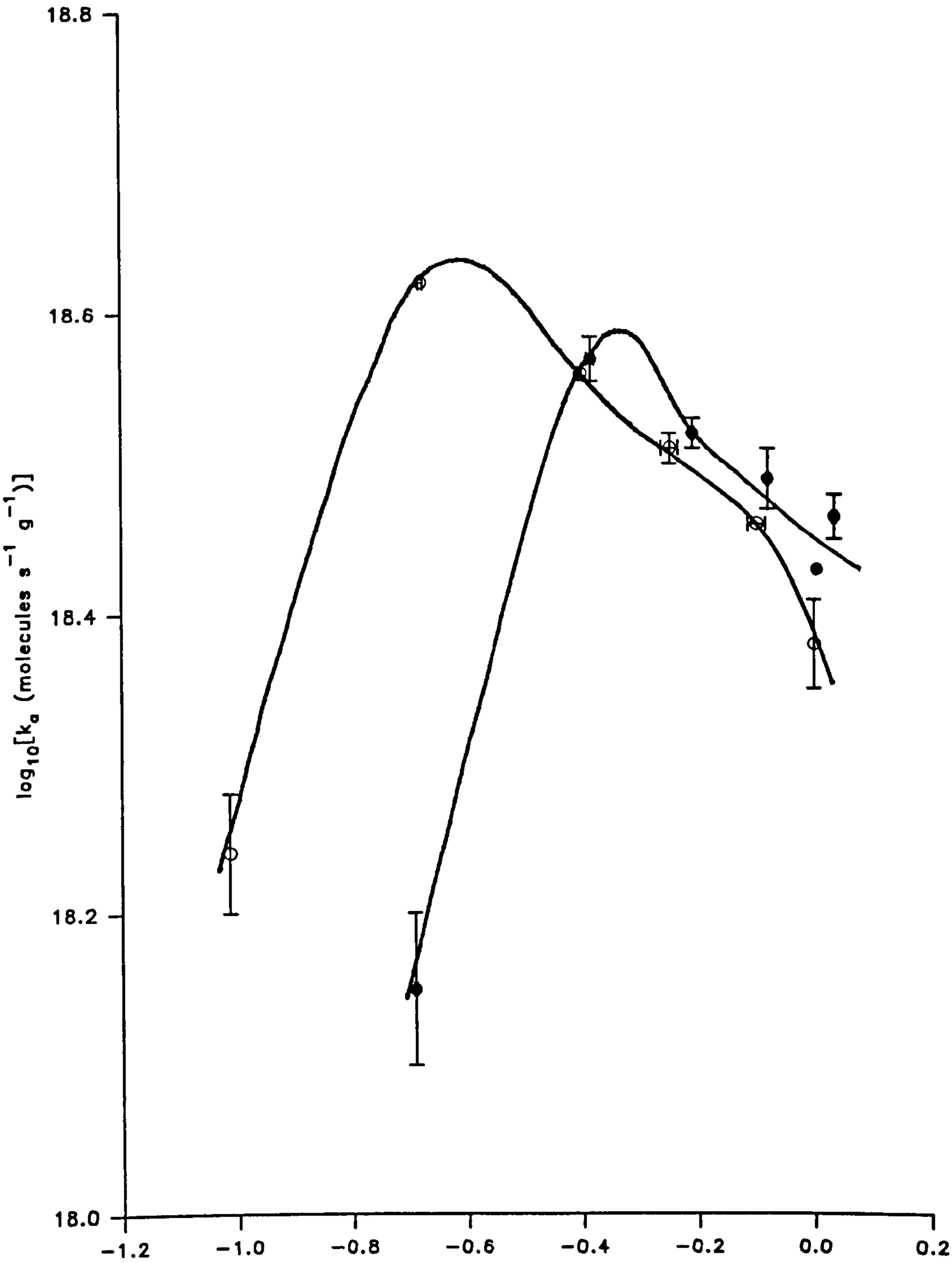

Figure 4.8: Plots of $\log_{10}$(Absolute Initial Propene Hydrogenation Rate) vs $\log_{10}$(Initial Hydrogen Partial Pressure) for Reduced/Oxidised Pt(0.5)/P25(P) and Pt(0.5)/P25(T)

ing as a poison. This could be because propene and hydrogen are adsorbed at different surface sites and the hydrogenation reaction occurs at the interfaces of these different sites, as shown in Fig. 4.9. Thus:

$$\theta_{C3H6} = k_1(P_{C3H6})^{0.5} \qquad \theta_{H2} = k_2(P_{H2})^{0.6} \qquad [83]$$

$$\text{Rate} = k_3\,\theta_{C3H6}\,\theta_{H2} \qquad [84]$$

$$\therefore\ \text{Rate} = k'(P_{C3H6})^{0.5}\,(P_{H2})^{0.6} \qquad [85]$$

An alternative, and probably more likely, explanation is that, under these reaction conditions, $\theta_{propene} << 1$, leaving many sites available for H_2 adsorption. This assumes that hydrogen and propene are adsorbed at the same surface sites, in which case it would be expected that, at sufficiently high partial pressures, hydrogen would act as a poison by competing with propene for active sites. This is indeed observed since in the partial pressure range 0.4 - 0.6kPa, the log-log plot becomes distinctly curved, indicating a rapidly changing reaction order with respect to hydrogen. Above 0.6kPa the plot becomes linear again and the hydrogen reaction order is calculated to be -0.5. Again, this value is indicative of dissociative adsorption of hydrogen at active surface sites, although now both reactants are competing for the same surface sites, as shown by the negative sign. Presumably this change in reaction order, from positive to negative value, occurs because at the higher partial pressures, $\theta_{hydrogen}$ approaches unity and impedes the adsorption of the alkene onto the catalyst surface, resulting in the observed decrease in reaction rate at H_2 partial pressures above 0.6kPa. For Pt(0.5)/P25(T) catalyst the order of reaction with respect to hydrogen is calculated to be -0.3 in the partial

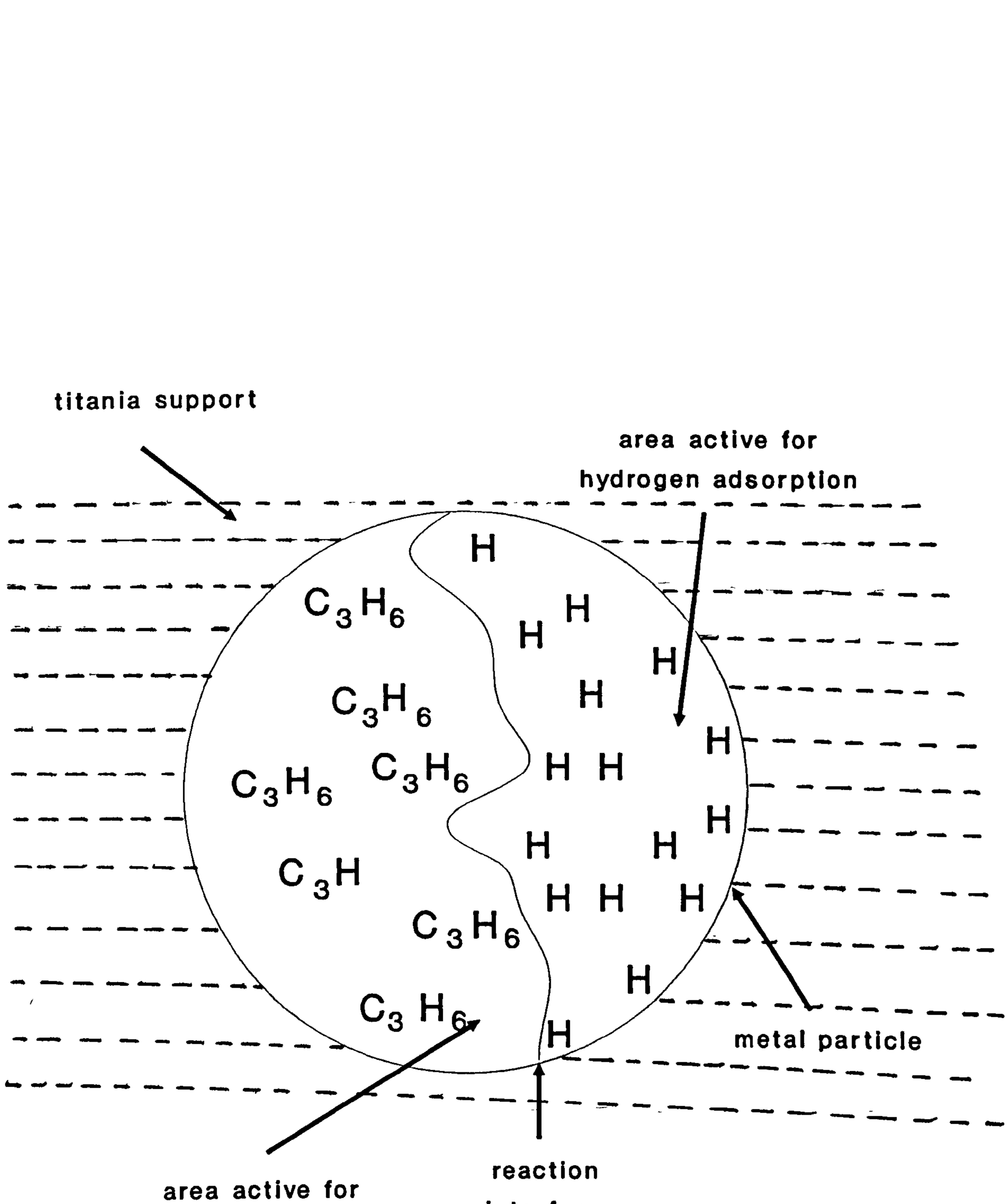

Figure 4.9: Schematic Representation of Different Adsorption Sites for Propene and Hydrogen Separated by a Reaction Interface on a Single Metal Particle

pressure range 0.25 - 0.65kPa. As in the case of the photodeposited catalyst, this negative fractional value indicates competitive, dissociative adsorption of hydrogen at the active metal sites.

For both types of catalyst, the plots of rate of reaction against hydrogen partial pressure show that the rate initially increases with increasing hydrogen pressure, until a maximum value is attained and then decreases as the hydrogen pressure is further increased. Such an observation clearly indicates that the hydrogenation of propene over both catalysts proceeds via a Langmuir-Hinshelwood mechanism, in which both reactants are chemisorbed onto the catalyst surface, where they react to form the alkane product, which is then desorbed rapidly to leave exposed surface active sites at which the reaction cycle can proceed again. Thus, the mechanism of propene hydrogenation over Pt/TiO_2 catalysts is:

i) $$CH_3CH{=}CH_{2\,(g)} \longrightarrow CH_3CHCH_{2\,(ads)} \qquad [86]$$

ii) $$H_{2\,(g)} + 2^*_{(s)} \longrightarrow 2\,H{-}^*_{(ads)} \qquad [87]$$

iii) $$CH_3CHCH_{2\,(ads)} + 2\,H{-}^*_{(ads)} \longrightarrow CH_3CH_2CH_3{-}^*_{(ads)} + 2^*_{(s)} \qquad [88]$$

iv) $$H_3CH_2CH_3{\sim\sim}^*_{(ads)} \longrightarrow CH_3CH_2CH_{3\,(g)} + ^*_{(s)} \qquad [89]$$

In the above mechanism, no assumption is made about the nature of the surface-adsorbed alkene species formed in (i), so that one or two surface active sites may be involved. Furthermore, it is possible that the addition of two hydrogen atoms to the adsorbed alkene species, as described in

step (iii), occurs either simultaneously or in a step-wise manner. The latter situation, in which a half-hydrogenated adsorbed species is formed, was first proposed by Horiuti and Polyani[267] and has since been widely accepted as the most probable sequence of events. In this case, step (iii) is actually the sum of two individual steps in which the half-hydrogenated species is formed before the fully-hydrogenated, adsorbed alkane is formed. In the Langmuir-Hinshelwood mechanism outlined above, step (iii), or the two individual sub-steps, is clearly the rate-determining step and will occur fastest when an optimum balance between the surface coverage of the alkene and that of hydrogen is achieved. From Fig. 4.10 it can be seen that, for the photodeposited catalyst, the maximum rate of hydrogenation is observed when the hydrogen: propene ratio ~ 4, whereas for the thermal catalyst, the maximum rate is observed when hydrogen:propene ratio ~ 2. Assuming that the reaction proceeds via a Langmuir-Hinshelwood mechanism and that there are no differences in alkene adsorption mechanism onto the two catalyst types, then the differences in the hydrogen:propene ratios at which the maximum hydrogenation rates occur, arise because of a difference in the number of surface sites available for reaction on the catalyst surfaces. Thus, there are fewer active sites on the surface of Pt(0.5)/P25(T) in which case $\theta_{hydrogen}$ approaches unity, with a concomitant reduction in reaction rate, at a much lower hydrogen:propene ratio, compared with that observed for Pt(0.5)/P25(P) catalyst. This is supported by the fact that in the case of the photodeposited catalyst, the order of reaction with respect to hydrogen shows that H_2 is adsorbed dissociatively, but non-competitively, at

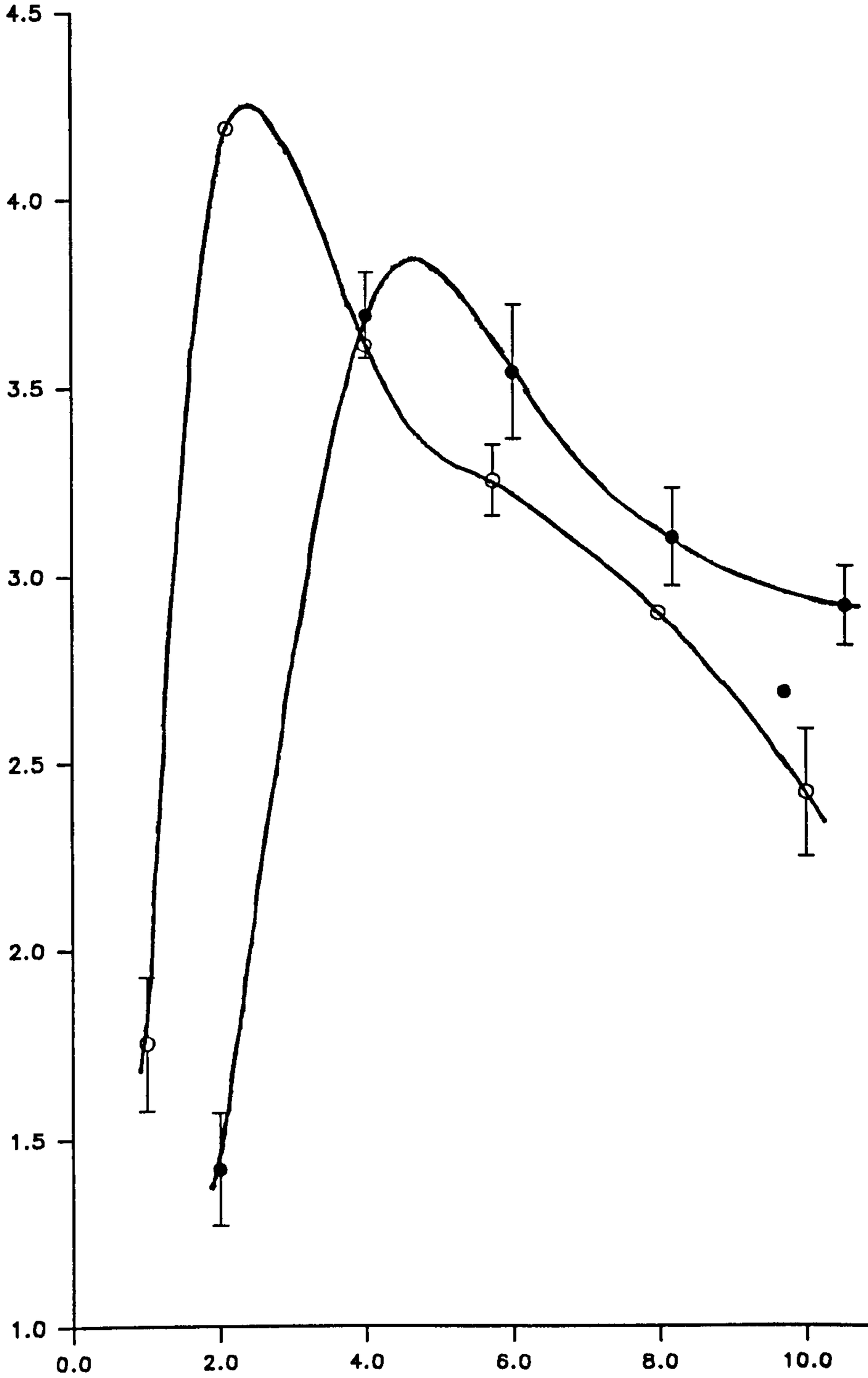

Figure 4.10: Propene Hydrogenation Rate as a Function of Initial Hydrogen:Propene Partial Pressure Ratio for Reduced/ Oxidised Pt(0.5)/P25(P) and Pt(0.5)/P25(T)

low partial pressures of hydrogen, although this changes to competitive dissociative adsorption at higher hydrogen partial pressures. For the thermal catalyst, H_2 was found to adsorb dissociatively in a competitive manner, even at low hydrogen partial pressures. It is unlikely that differences in the strengths of adsorption of either or both of the reactants, as a function of catalyst type, could account for the differences in the hydrogen: propene ratios at which the maximum rates are observed, since the apparent activation energies for the hydrogenation reaction are very similar for both catalysts, as discussed in the previous section. Therefore, the evidence strongly suggests that there is a significant difference with respect to supported metal morphology, between the photodeposited and the thermal catalysts. This issue will be discussed in much more detail at a later stage in this Chapter.

4.3. Gas-Phase Cyclopropane Hydrogenation Studies

The gas-phase hydrogenation of cyclopropane has been studied using TiO_2-supported metal catalysts prepared via the photodeposition technique. A catalyst containing 0.5mass% Pt, prepared by impregnation /reduction, was also included for the purpose of comparison. For the photodeposited catalysts, the hydrogenation reaction was investigated as a function of metal type, metal content and morphology of the support titania. In all experiments, catalyst samples were subjected either to high-temperature reduction or high-temperature reduction, followed by subsequent re-oxidation, in order to remove any variations in catalyst activity arising from contamination during preparation. Since all the photodeposited catalysts exhibited very similar behaviour during cyclopropane hydrogenation, which was found to be dependent only upon the pretreatment prior to reaction, the results of all studies are discussed together below. The results obtained during the cyclopropane hydrogenation studies are given in Sections 3.3.1 - 3.3.3, and are shown graphically in Figs. 3.17 - 3.22 inclusive.

4.3.1 Cyclopropane Hydrogenation over Reduced Catalysts

Following high-temperature reduction in hydrogen, all the photodeposited catalysts, regardless of metal type, metal content or the morphological nature of the support material, were found to be inactive for cyclopropane hydrogenation in the range 370 - 420K. Such inactivity clearly arises due to a very strong suppression of the chemisorptive, and

hence catalytic, ability of these catalysts. This is characteristic of catalysts in a deep SMSI state, which has been discussed previously. In contrast, the activity of reduced Pt(0.5)/P25(T) catalyst was observed to increase as the reaction temperature was increased in the range 370 - 420K. This increase in activity was not merely a function of increasing reaction temperature, since a second measurement of activity at 370K was found to be significantly higher than that initially measured at this temperature, prior to raising the reaction temperature. The apparent recovery in catalyst activity during the hydrogenation of cyclopropane can be explained in terms of removal of excess hydrogen from the surface of the catalyst. Immediately following high-temperature reduction, the metal sites active for hydrogenation will be covered with adsorbed hydrogen, arising from the pretreatment. On exposure to the cyclopropane/hydrogen mixture, rapid adsorption of the alkane occurs, where it reacts with adjacent presorbed hydrogen to give propane, which is then rapidly desorbed and results in the formation of free active metal sites. Cyclopropane is then preferentially adsorbed at these free sites and the presorbed hydrogen is progressively removed from the surface of the catalyst, leading to the observed increase in catalytic activity during the reaction. Two possible reasons can be put forward to explain the initial adsorption of cyclopropane onto the catalyst surface, immediately following pre-reduction. In the first case, exposure of the reduced catalyst to the high vacuum system may result in some hydrogen desorption occurring or, alternatively, metal sites which are inactive for hydrogen, but active for cyclopropane, adsorption exist on the catalyst surface. It seems unlikely that hydrogen

desorption during the initial exposure of the reduced catalyst to a high vacuum does occur, since no recovery in activity was observed for any of the photodeposited catalysts, except reduced Pt(2.0)/P25(P). This is also true for the hydrogenation of propene over reduced Pt(0.5)/P25(T), indicating that sites active for the adsorption of cyclopropane, but not propene or hydrogen, exist on the surface of this catalyst. It is worth noting that, as mentioned above, reduced Pt(2.0)/P25(P) catalyst also exhibited a small increase in activity during the hydrogenation of cyclopropane, similar to that observed for the thermal catalyst, and the same explanation of this effect is suggested.

The fact that reduced Pt(0.5)/P25(T) exhibited some ability to adsorb cyclopropane, whereas the photodeposited catalysts, with the exception of Pt(2.0)/P25(P), did not, strongly suggests that the two preparative routes give rise to catalysts in which the supported metal morphologies are somewhat different. The difference in metal morphology results in the photodeposited catalysts being much more susceptible to metal-support effects compared with the thermally-prepared catalyst, and as a consequence high-temperature reduction destroys all the chemisorptive ability of these catalysts. The fact that reduced Pt(2.0)/P25(P) catalyst also exhibits a slight recovery in activity indicates that some resistance to SMSI effects can be found in photodeposited catalysts possessing a relatively high metal content. This implies that at loadings of < 2 mass%, the supported metal morphology of photodeposited catalysts is different to that of the supported metal of the thermal catalyst, but at

higher metal contents such differences become rather less pronounced.

This topic is discussed in more detail in Section 4.5.

4.3.2 Cyclopropane Hydrogenation over Reduced/Oxidised Catalysts

From the results given in Sections 3.3.1 - 3.3.3, it can be seen that immediately following high-temperature reduction and subsequent re-oxidation, all catalysts, regardless of preparation method, metal type, metal content or support morphology, exhibited very similar activities for the hydrogenation of cyclopropane at 370K, although Rh(0.5)/P25(P) was observed to be slightly less active than the other catalysts. Ir(0.5)/P25(P) exhibited very atypical behaviour since it remained virtually inactive for the hydrogenation reaction in the range 370 - 420K, despite high-temperature re-oxidation. The reason for this is far from clear and is in conflict with the observed behaviour of Ir/TiO_2 catalysts, subjected to similar pretreatment, in a different study[268]. It is possible that SMSI effects in reduced Ir(0.5)/P25(P) are so well developed that re-oxidation at higher temperatures or much longer times than employed in this study are required to break them and restore catalytic activity. Alternatively, there may be such dramatic morphological changes occurring during high-temperature pretreatments, that all metal sites potentially active for the adsorption of cyclopropane are removed, thus rendering the catalyst inactive for this particular reaction, regardless of whether or not it is in the SMSI state.

The fact that all catalysts possessed very similar activities for the hydrogenation of cyclopropane immediately following re-oxidation at 700K, would suggest that the dispersion of the metals on the support surfaces was much the same in all cases. However, as the results show, the stabilities of all the photodeposited catalysts, without exception, were extremely poor, indicating that the cause of this effect was independent of metal type, metal content or support morphology. In stark contrast, reduced/oxidised Pt(0.5)/P25(T) catalyst exhibited excellent stability during the hydrogenation reaction, its activity being virtually independent of reaction temperature. The most probable explanation for such a marked difference in catalyst behaviour is that whilst initially the metal dispersions are fairly similar, the morphologies of the supported metals, as determined by preparation, are very different. In the case of the photodeposited catalysts, the metal morphology is such that the catalysts are susceptible to induced metal-support effects and therefore exhibit poor stability during a fairly demanding reaction, such as the hydrogenation of cyclopropane. On the other hand, the morphology of the supported metal in the thermal catalyst is such that it is much more stable with respect to metal-support interactions, and is therefore unaffected during the demanding hydrogenation reaction.

As stated previously, the activity of re-oxidised Pt(0.5)/P25(T) for cyclopropane hydrogenation was found to be virtually independent of reaction temperature in the range 370 - 420K. However, Fenoglio et al[269] have recently investigated the hydrogenolysis of methylcyclopentane over Rh/SiO_2 and Rh/TiO_2 catalysts, prepared by the standard impregnation

technique, and Rh/TiO_2 catalyst prepared by an ion-exchange method. These workers observed that, following oxidation at 673K, subsequent reduction at increasing temperatures produced a gradual increase in catalyst activity, such that a maximum in activity was observed when the reduction temperature was approximately 550K. Reduction at higher temperatures was found to produce correspondingly lower activities. Although both the SiO_2- and TiO_2-supported catalysts exhibited similar behaviour, the most pronounced effect was observed for Rh/TiO_2 catalysts in which the metal dispersion was very high, as determined by temperature-programmed reduction and TEM analysis. On the basis of TEM observations, these findings were explained in terms of morphological changes of the supported metal, occurring during the oxidation/reduction cycles. Thus, reduction following oxidative treatment initially rendered the metal particles in a very disperse state, giving rise to low catalytic activity since large ensembles of metal particles were thought to be necessary for the reaction to proceed. Increasing the reduction temperature resulted in annealing of the metal particles, such that reduction at ~550K produced an optimum metal configuration, corresponding to the observed maximum in catalyst activity. Further reduction at temperatures above 550K resulted in greater annealing and, in the case of the TiO_2-supported catalysts, metal-support interactions, which produced a decrease in catalyst activity. These observations are in direct contradiction to the results obtained for Pt(0.5)/P25(T) catalyst during this study, since exposure of this catalyst to hydrogen at increasing temperatures, during the hydrogenation reaction, did not produce any significant change

in catalyst activity. However, the results of Fenoglio et al[269] do show that considerable morphological changes can occur in supported metal catalysts during exposure to hydrogen, even at the relatively low temperatures employed during this investigation into the hydrogenation of cyclopropane using similar catalysts. It seems highly probable that the poor stabilities of the photodeposited catalysts observed during the hydrogenation of cyclopropane can be attributed to the occurrence of significant morphological changes of the supported metal during the initial stages of the reaction.

4.3.3 Cyclopropane Hydrogenation over Reduced/Oxidised Pt(0.5)/P25(T): Effect of Varying Reactant Partial Pressures

The effect of increasing cyclopropane partial pressure, whilst maintaining a constant hydrogen partial pressure, on the rate of reaction over reduced/oxidised Pt(0.5)/P25(T) at 370K is shown in Fig. 3.23. The plot shows that the reaction rate rapidly increases as the cyclopropane partial pressure is increased in the range 0.06 - 0.30kPa. At partial pressures above 0.30kPa, the reaction rate tends towards a plateau, indicating that an optimum in the product of $\theta_{cyclopropane}$ and $\theta_{hydrogen}$, (Eq.[84]), and hence in catalyst activity, is achieved when the hydrogen:cyclopropane ratio is ~2. A similar result was obtained for propene hydrogenation over this catalyst, where the maximum reaction rate was observed to occur with a hydrogen:propene ratio ~2.

From the gradient of the plot of $\log_{10}$(initial rate) vs $\log_{10}$(initial cyclopropane partial pressure), shown in Fig. 4.11, the order of reaction with respect to cyclopropane is calculated to be +0.50, in the approximate partial pressure range 0.06 - 0.40kPa. As in the case of propene adsorption, this fractional reaction order may arise for one of two reasons. Firstly, adsorption of cyclopropane is associative and described by a normal Langmuir isotherm, which, under the reaction conditions employed, corresponds to the region of the isotherm where there is a transition from first- to zero-order, Fig. 4.7. In this case the adsorption mode might be:

(i)

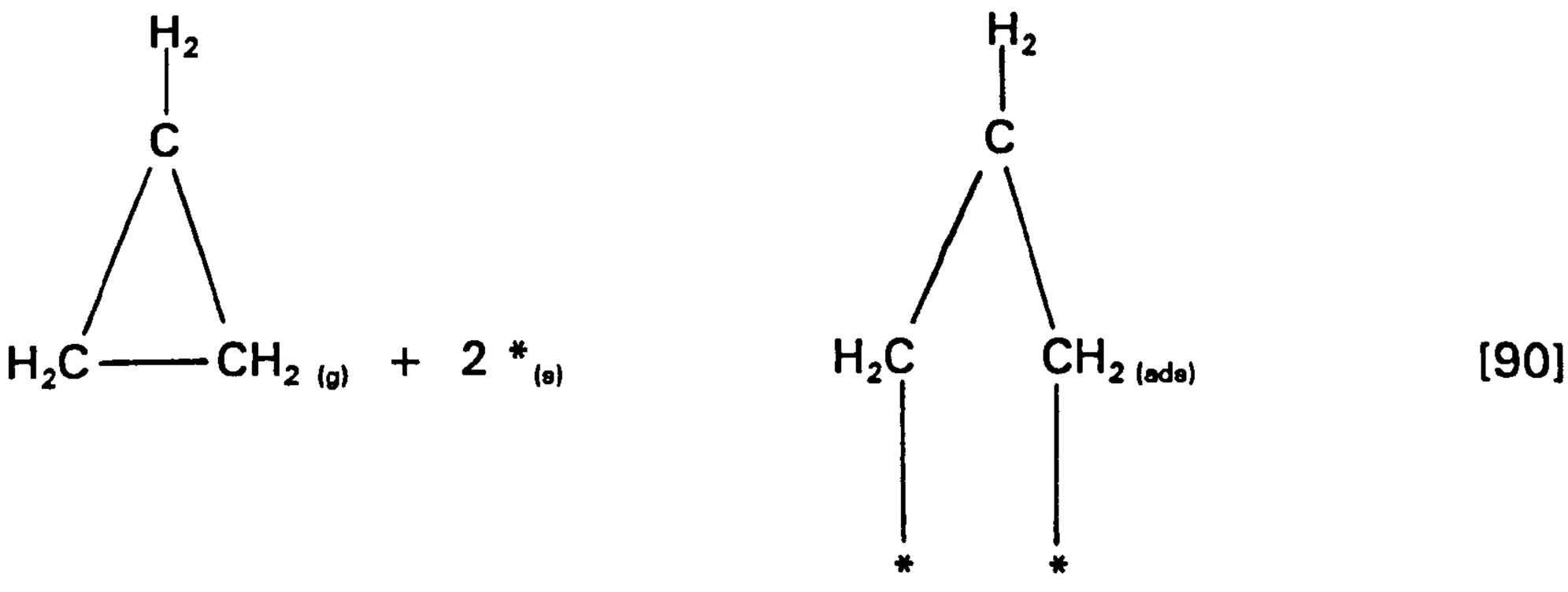

[90]

The second possible reason is that cyclopropane is adsorbed onto Pt/TiO_2 in the form of the alkylidyne species, in which case adsorption is dissociative and two active surface sites are required, viz:

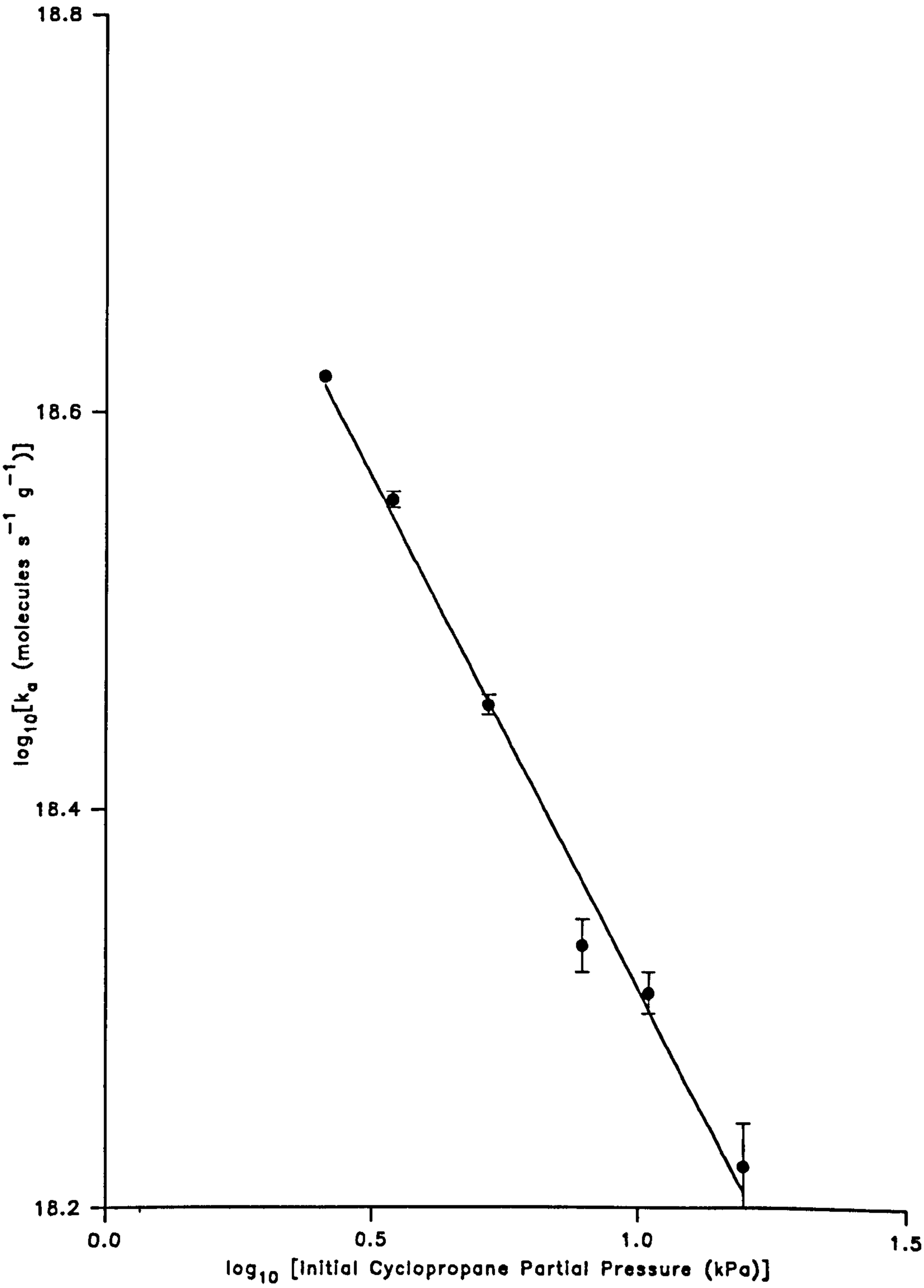

Figure 4.11: Plot of $\log_{10}$(Absolute Initial Cycloprpane Hydrogenation Rate) vs $\log_{10}$(Initial Cyclopropane Partial Pressure for Reduced/Oxidised Pt(0.5)/P25(T)

(ii)

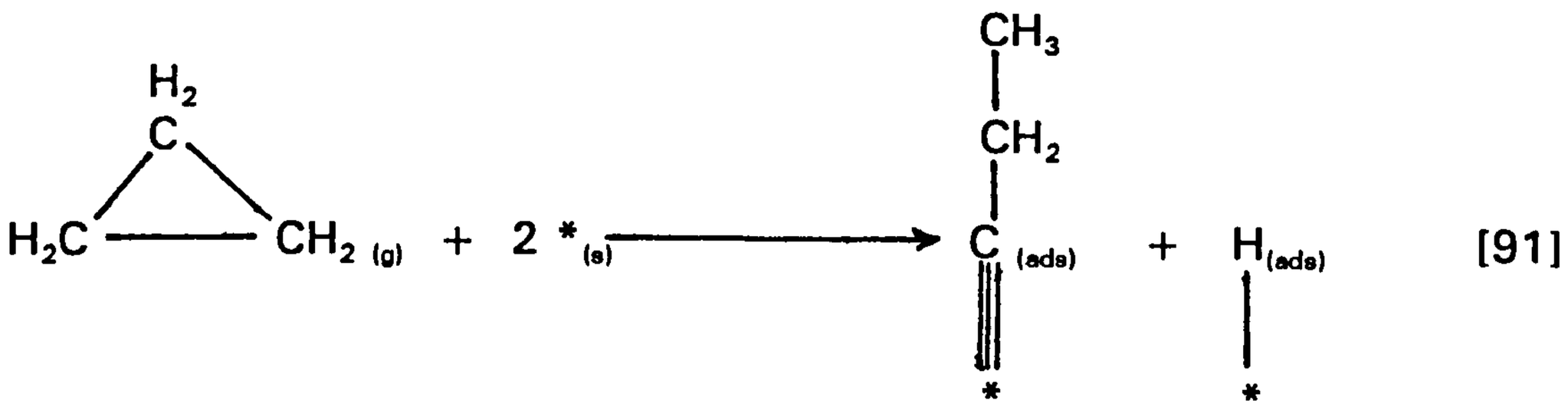

[91]

The hydrogenation of cyclopropane has been extensively studied[270-273] using catalysts comprising Group VIII metals supported on pumice and orders of reaction with respect to both cyclopropane and hydrogen reported. For cyclopropane, orders of reaction between 0.2 and 1.0 have been observed[273], depending upon reaction temperature and fixed hydrogen pressure. On the grounds that the reaction kinetics are not consistent with the dissociative adsorption of c-C_3H_6, mechanism (ii) above has been excluded. Mechanism (i) has also been ruled out on the grounds that the 1,3-di-σ-adsorbed species should be as strongly adsorbed as linear alkenes, which has not been observed. An alternative mechanism has been proposed[266] in which cyclopropane is adsorbed via π-complexation with the supported metal, where the partially delocalised electrons of the carbon ring interact with the incompletely filled d-orbitals of the metal, i.e.:

(iii)

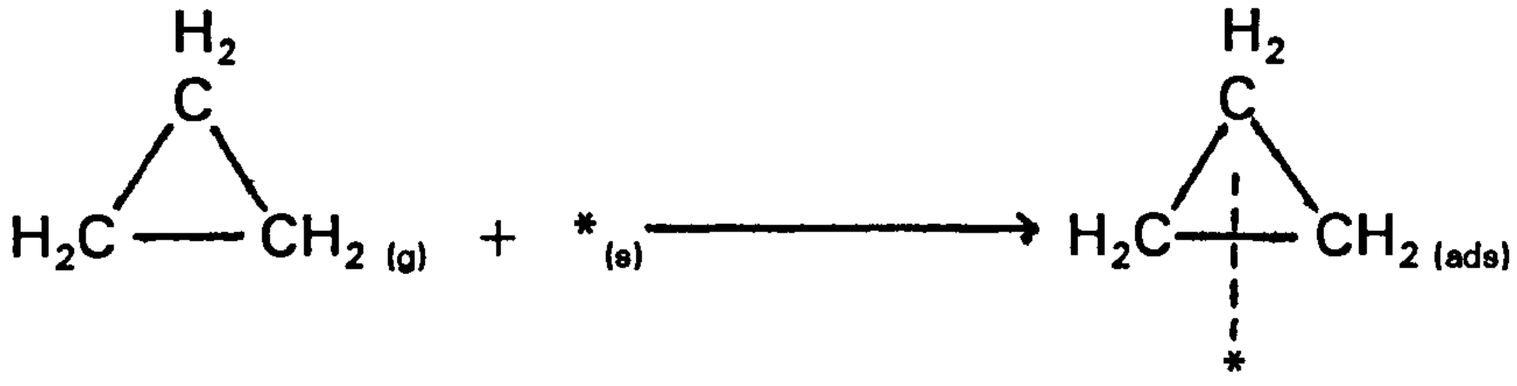

[92]

This hypothesis is supported by the finding[273] that methylcyclopropane is more strongly adsorbed than cyclopropane, presumably because of the electron releasing ability of the methyl group. Consideration of steric hinderance would suggest that methylcyclopropane would be not be as strongly adsorbed as cyclopropane, indicating that electronic, rather than steric, factors play a greater role in the adsorption of alicyclic hydrocarbons onto pumice-supported metal catalysts. Furthermore, the order of activity of these catalysts for cyclopropane hydrogenation was found[271] to be, in terms of decreasing activity:

$$Rh > Ir > Pt > Pd > Ni.$$

This observation is consistent with the proposed mechanism of cyclopropane adsorption since the percentage 'd-character' of the above metals lie the same decreasing order. Higher percentage 'd- character' favours activity since the d-orbitals of the metal become progressively more available to accept electron density from the adsorbing gas, which produces a stronger interaction. However, in the current investigation, the initial order of activity for cyclopropane hydrogenation, albeit for the unstable photodeposited catalysts, was found to be, in terms of decreasing activity:

$$Pt \sim Pd > Rh >> Ir \sim 0.$$

This observation implies that adsorption via π-complex formation is not the dominant mechanism for cyclopropane adsorption onto TiO_2-supported metal catalysts. Also, as stated before, it would seem very likely that the adsorption of cyclopropane onto these catalysts occurs via a similar mechanism to that for alkene adsorption, which, on the basis of recent evidence, appears to be via the formation of a surface alkylidyne species. Therefore, mechanism (i) shown above is probably the mechanism for cyclopropane adsorption onto TiO_2-supported metal catalysts. It is worth noting that during the reaction between cyclopropane and D_2 over pumice-supported metal catalysts[272], deuterium exchange was observed to occur, indicating that cyclopropane adsorption via mechanism (i) did occur to some extent. Unfortunately, it appears that no recent studies of the adsorption of alicyclic hydrocarbons onto supported metal catalysts, using modern spectroscopic techniques, have been conducted and so the question of the true adsorption mechanism for cyclopropane onto such catalysts remains unresolved.

Fig. 3.25 shows that increasing hydrogen partial pressure, in the range 0.099 - 0.660kPa, whilst maintaining a constant cyclopropane partial pressure, results in decreasing rate of cyclopropane hydrogenation over reduced/oxidised Pt(0.5)/P25(T) at 370K. This observation implies that competitive adsorption at the active metal sites occurs between hydrogen and cyclopropane under these conditions. The corresponding plot of $\log_{10}$(initial rate) vs $\log_{10}$(initial hydrogen partial pressure), given in Fig. 4.12, is of reasonably good linearity. The order of reaction with respect to hydrogen, over the partial pressure range 0.099 - 0.660kPa, is

calculated to be -0.3, indicating that hydrogen is dissociatively adsorbed. As is the case for propene hydrogenation over this same catalyst, the results of this study show that cyclopropane hydrogenation also proceeds via a Langmuir-Hinshelwood mechanism, involving competitive adsorption of both reactants at the supported metal sites, followed by reaction between the adsorbed species to give the alkane product. Thus the reaction scheme for cyclopropane hydrogenation over reduced/oxidised Pt(0.5)/P25(T) catalyst is similar to that described in Section 4.2.4. A Langmuir-Hinshelwood mechanism has also been proposed for the hydrogenation of alicyclic hydrocarbons, including cyclopropane, over pumice-supported Group VIII catalysts[273] and the results obtained in this particular study are in accordance with the observations made in the earlier studies.

In the study of propene hydrogenation over TiO_2-supported Pt catalysts, the reaction rate was found to vary with temperature, in the range 260 - 345K. This was explained in terms of a temperature dependence of the enthalpies of adsorption for one or both of the reactants, possibly due to a change in the adsorption mode of the alkene. However, the rate of cyclopropane hydrogenation over reduced/oxidised Pt(0.5)/P25(T), was found to be independent of temperature, in the range 370 - 420K, indicating that the apparent activation energy for the reaction is effectively zero. In this case, there is no change in the enthalpies of adsorption for either reactant, implying that neither the surface coverage or adsorption mode of the reactants are temperature dependent, in the range employed during this study.

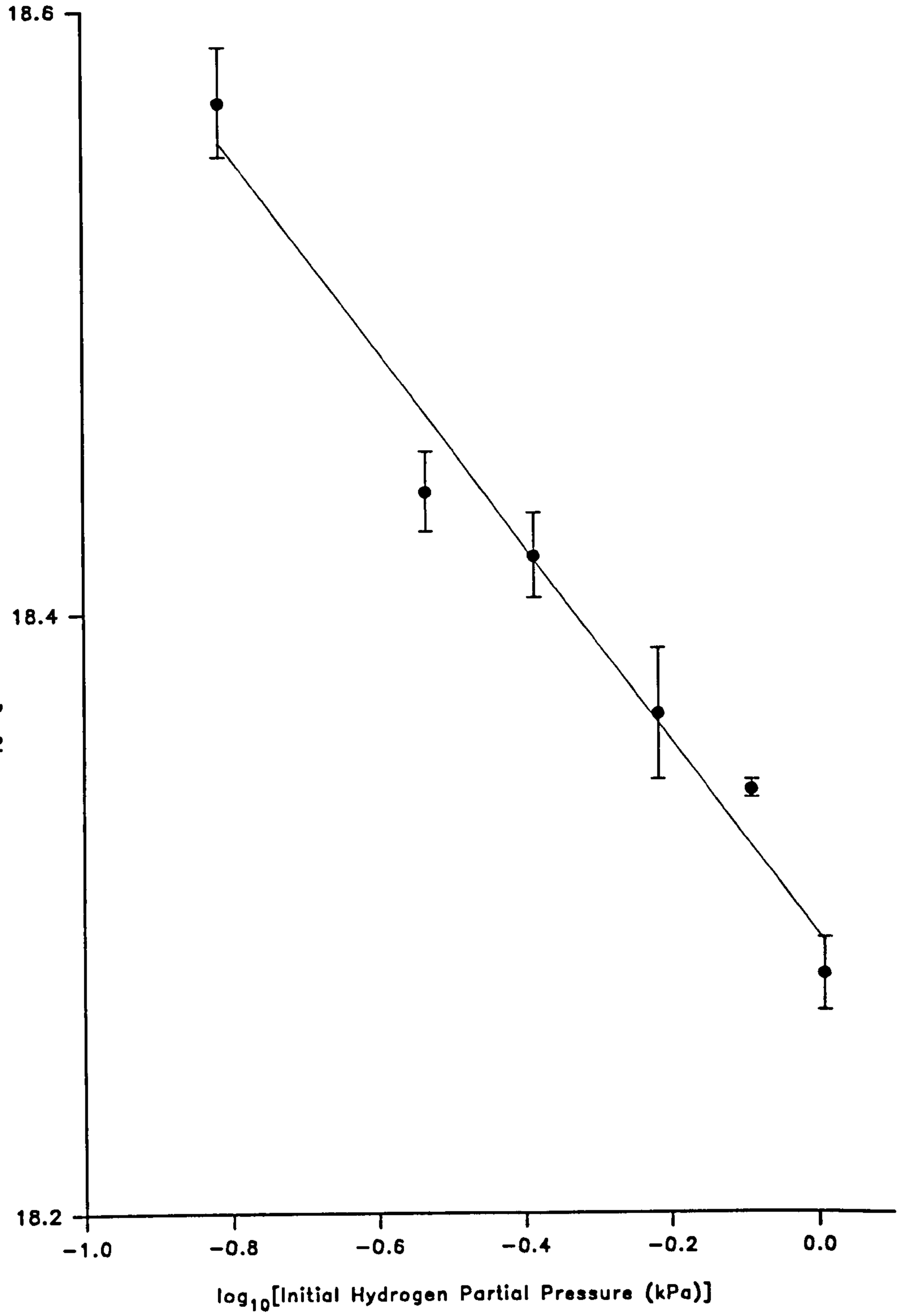

Figure 4.12: Plot of $\log_{10}$(Absolute Initial Cyclopropane Hydrogenation Rate) vs $\log_{10}$(Initial Hydrogen Partial Pressure) for Reduced/Oxidised Pt(0.5)/P25(T)

4.4 Temperature Programmed Desorption Experiments

Temperature programmed desorption was employed in an attempt to probe possible morphological differences between platinum metal deposited onto TiO_2 by photodeposition and that deposited via the thermal technique. The results obtained during the course of these experiments are given in Section 3.3 and discussed in detail below. Unfortunately, no quantitative data, with respect to the amount of gas desorbed as a function of temperature, was obtained during the TPD experiments and therefore only qualitative comparisons between the various adsorbents can be made. However, it was expected that any significant differences in the morphologies of the supported metals would lead to different strengths of adsorption of the adsorbate gases, which would be reflected in the resulting TPD profiles. In this way it was hoped that any morphological differences would at least be qualitatively detected.

4.4.1 Propene Desorption

Figs. 3.27 - 3.29 show the TPD spectra obtained for 'as prepared', high-temperature reduced and high-temperature reduced/oxidised Pt(0.5)/P25(P), Pt(0.5)/P25(T) and pure P25 TiO_2, using propene as the adsorbate. The single, fairly sharp propene desorption peak, with a maximum occurring at ~325K, observed for 'as prepared' Pt(0.5)/P25(T) would suggest a reasonably uniform dispersion of metal had been achieved using the thermal preparative method. In this case, the strength of adsorption of propene is fairly uniform on all metal deposits, giving rise

to the sharp desorption peak observed. For 'as prepared' Pt(0.5)/P25(P), a broad, rather flat, propene desorption region, extending over the range 300 - 425K, is observed in the TPD profile. Although only a qualitative observation, it can be seen that less propene is desorbed from this catalyst than from 'as prepared' Pt(0.5)/P25(T). This would suggest that a certain degree of heterogeneity in the metal deposits, in terms of size and possibly shape, exists for this catalyst. Such differences, arising during preparation, result in differing strengths of propene adsorption, which is then reflected in the corresponding TPD profile, as is observed. The fact that only one desorption peak, or region, is observed for both types of catalyst, suggests that there is only one adsorption mode for propene onto the active metal sites. As discussed in Section 4.2.3, there is considerable spectroscopic evidence to suggest that the adsorbed alkene species is propylidyne, particularly at 300K, which is the adsorption temperature employed during these studies. However, other possible adsorption modes, such as the di-σ-adsorbed or π-complexed species, cannot be ruled out, especially since these catalysts are in the 'as prepared' state. Furthermore, extensive hydroxylation of the titania support, due to dissociative chemisorption of water[44-46] during storage of the catalysts under ambient atmosphere, may result in a certain quantity of propene being adsorbed via a hydrogen-bonding interaction with surface hydroxyl groups. Desorption of such adsorbed propene may then contribute to the observed TPD peak, which would account for the different quantities of propene desorbed from the two catalyst types.

Untreated P25 TiO_2 shows two distinct propene desorption peaks, the maxima occurring at ~550K and ~650K respectively. IR spectroscopic studies conducted by various workers[94-96] have suggested that alkene adsorption onto titania occurs only via a hydrogen-bonding interaction between surface hydroxyl groups and the alkene double bond. It has also been proposed[96] that weak π-complex formation may occur at exposed Ti^{4+} cations. However, these adsorption mechanisms are fairly weak interactions and it is unlikely that they could account for the two, relatively high temperature desorption peaks observed in the TPD spectrum. It has been proposed[95,96] that thermal activation of TiO_2, following alkene adsorption, can produce surface alkoxide species. The thermal decomposition of alcohols, to alkenes, ethers and water via dehydration processes and to ketones and CO via dehydrogenation processes, on titania has been attributed to the formation and subsequent reaction of alkoxide species[71,73,78]. Therefore, it is possible that during this TPD experiment, adsorbed propene was converted to isopropoxide ions via thermal activation, which then decomposed to various compounds, including propene via dehydration, at still higher temperatures. These processes would then explain the occurrence of the two high temperature peaks observed in the propene desorption profile obtained for P25 TiO_2. It is relevant that Flinn[274] recorded a propene desorption peak occurring at ~500K, following propan-2-ol adsorption onto the surface of anatase. The fact that high temperature propene desorption peaks were not recorded for TiO_2-supported metal catalysts suggests that the surfaces of these materials are dominated by the presence of Pt metal, which possibly blocks the sites at

which propene is adsorbed onto titania. Alternatively, some form of SMSI effect may suppress propene desorption from platinised TiO_2 at high temperatures.

The TPD profile for propene desorption from high-temperature reduced Pt(0.5)/P25(T) is very similar to that observed for the 'as prepared' material, showing a fairly sharp, single desorption peak with the maximum at ~330K. Surprisingly, the quantity of propene desorbed is much greater from the pretreated catalyst, compared with the 'as prepared' material, even though earlier studies have shown that high-temperature reduction rendered the catalyst virtually inactive for thermal hydrogenation due to SMSI effects. This observation implies that the reduced catalyst remains active for propene adsorption, although it is in an SMSI state and therefore inactive for propene hydrogenation. Thus, it would appear that only hydrogen chemisorption onto the SMSI catalyst is suppressed, which is a well-known effect. If this is indeed the case, the question remains as to how significant propene adsorption can occur on reduced Pt(0.5)/P25(T), since the dispersed metal is either covered by TiO_x overlayers or electron-enriched due to electron transfer from the reduced oxide support. One possible explanation is that the surface of the TiO_2 support becomes highly hydroxylated during high-temperature reduction, due to extensive hydrogen spillover from the metal sites onto the support material. This may then give rise to propene adsorption at such surface hydroxyl groups via a 'hydrogen-bond' type of interaction with the π-bond of the alkene. Such a process would account for the observed single, sharp low temperature desorption peak and the fact that much

more propene is desorbed from the reduced catalyst relative to the 'as prepared' catalyst. Also, limited propene adsorption at metal sites cannot be discounted since it has been observed that the rate of cyclopropane hydrogenation over reduced Pt(0.5)P25/(T) increases on repeated exposure to the cyclopropane/H_2 mixture, indicating the occurrence of cyclopropane adsorption at metal sites even when the catalyst is in a deep SMSI state. Therefore, propene adsorption onto the reduced catalyst may occur at both surface hydroxyl groups and, to a certain extent, at metal sites. This proposition is supported by the fact that the TPD profile of propene desorption from reduced Pt(0.5)/P25(P) also shows a similar sharp low temperature peak, occurring at ~330K, although the quantity of desorbed propene is considerably less. It is observed that this peak has a very long tail, extending to ~700K, which would not be expected if only fairly weak adsorption via hydrogen-bonding at surface hydroxyl groups occurs on such pretreated catalysts. This would suggest that propene is adsorbed, to a limited extent, at metal sites, despite SMSI effects. The TPD spectrum of propene desorption from high-temperature reduced P25 titania shows only a very small propene desorption peak, with the maximum occurring at ~330K. This observation is consistent with the idea that propene adsorption onto reduced Pt/TiO_2 catalysts occurs mainly via a hydrogen-bonding interaction at surface hydroxyl groups. However, hydrogen chemisorption onto TiO_2 has been observed at temperatures above 623K, with the concomitant formation of surface hydroxyl groups[94]. Since, in this study, high-temperature reduction was conducted at 773K, it would be expected that the surface of reduced TiO_2 was

extensively hydroxylated, in which case a large propene desorption peak would also be expected. However, it is likely that far more surface hydroxyl groups are formed on the platinised catalyst since these materials would be much more active for hydrogen chemisorption than pure titania. Furthermore, hydrogen spillover, with the concomitant hydroxylation of the support surface, will also occur during high-temperature reduction of the platinised catalysts. The fact that the small propene desorption peak observed for reduced P25 TiO_2 occurs at the same temperature as those observed for the platinised catalysts would suggest that propene adsorption onto all three adsorbates occurs via the same mechanism and that the observed differences in the quantities of desorbed propene arise from differing extents of surface hydroxyl group formation during high-temperature reduction.

The TPD profiles of propene desorption from reduced/oxidised Pt(0.5)/P25(T) and Pt(0.5)/P25(P) catalysts are virtually identical, each showing a single sharp desorption peak with the maxima occurring at ~325K. It can be seen that the quantity of propene desorbed from the thermal catalyst is approximately twice that desorbed from the photodeposited catalyst, although in both cases the quantity of desorbed propene is far greater than that observed for the corresponding 'as prepared' catalysts. This implies that reduction and subsequent re-oxidation at high temperatures produces a metal dispersion greater than that achieved by either of the preparative techniques used. The fact that high-temperature reduction and re-oxidation was found to give catalysts which were more active for the thermal hydrogenation of alkenes than the correspon-

ding 'as prepared' catalysts produced by both methods, although removal of contaminants may contribute to the increased activity. It is probable that there is some contribution to the observed desorption peaks due to propene adsorbed onto the TiO_2 surface, although in view of the pretreatment, the extent of surface hydroxylation is likely to be small. In this case, adsorption of propene onto the support would be at exposed Ti^{4+} cations, via weak π-complex formation. The TPD profile of propene desorption from reduced/oxidised P25 titania shows two small, but distinct, peaks occurring at ~325K and ~400K. The low temperature peak is probably due to propene adsorbed at exposed surface Ti^{4+} cations via π-complex formation, as described above. However, the origin of the higher temperature peak, which does not occur in the TPD profiles of propene desorption from the platinised catalysts, is more obscure and cannot be explained at present.

4.4.2 Propene Desorption in the Presence of Hydrogen

Figs. 3.32 - 3.34 show the TPD profiles of propene desorption of 'as prepared', high-temperature reduced and reduced/oxidised Pt(0.5)/P25(P), Pt(0.5)/P25(T) and P25 TiO_2, using propene/H_2 as the adsorbate. Overall, these spectra are very similar to those obtained using pure propene as the adsorbate, particularly in the case of the pretreated samples. This indicates that the presence of hydrogen in the adsorbate has little effect on the adsorption, and subsequent desorption, of propene, which is not too unexpected since it is likely that adsorbed hydrogen is

quickly removed from the metal sites via alkene hydrogenation. The quantity of desorbed propene observed for reduced Pt(0.5)/P25(P) catalyst is quite surprising since it is clearly in excess of that desorbed from reduced Pt(0.5)/P25(T), opposite to the trend usually observed for these two materials. However, this probably reflects differing extents of surface hydroxylation, and consequently, differing amount of propene adsorbed at the reduced oxide surface via weak hydrogen bonding interactions at surface hydroxyl groups as discussed earlier, rather than any significant differences in catalyst structures.

Fig. 3.32 shows that the propene TPD profile obtained for 'as prepared' Pt(0.5)/P25(T) using propene/H_2 as the adsorbate is rather different from that obtained using pure propene as the adsorbate. In this case, a definite shoulder on the high temperature side of the usual peak, extending to ~450K, is observed and also the quantity of desorbed propene is much greater. This is not too surprising since any presorbed hydrogen remaining after preparation would be displaced by oxygen during storage of the catalyst under ambient atmosphere. Thus, the presence of hydrogen in the TPD adsorbate may give rise to such differences in the resulting TPD profile, relative to that obtained using propene alone as the adsorbate. It is possible that this extended region of propene desorption indicates the existence of metal sites of slightly different morphologies, leading to slightly different strengths of propene adsorption. The TPD profiles obtained for 'as prepared' Pt(0.5)/P25(P) and P25 TiO_2 obtained using propene/H_2 as the adsorbate are very similar to those obtained using pure propene as the adsorbate. High temperature peaks tentatively

assigned as being due to the formation and subsequent dehydrogenation of surface alkoxide species on TiO_2 can be seen to occur in the TPD spectrum for 'as prepared' Pt(0.5)/P25(P), in Fig. 3.32, but not in that obtained by use of pure propene. This may be because the presence of hydrogen in the adsorbate results in extensive hydroxylation of the support surface, via a hydrogen spillover mechanism. However, the same peaks would be expected to occur in the TPD spectra obtained for 'as prepared' Pt(0.5)/P25(T), regardless of whether or not H_2 is present in the adsorbate, since this material is exposed to hydrogen during preparation, with the consequent hydroxylation of the oxide surface. The fact that no such peaks are observed in any of the TPD spectra obtained for Pt(0.5)/P25(T) would suggest that some differences between the two 'as prepared' catalyst types exist, although the exact nature of such differences is not known.

The slight differences observed between the TPD profiles obtained using propene/H_2,and those obtained using pure propene, as the adsorbate, for the 'as prepared' materials, are probably due to variations between the samples of each adsorbent. Such observations are probably a consequence of the fact that the catalysts prepared by both deposition techniques are unlikely to be truly homogeneous throughout in terms of metal particle size and shape, as perhaps would be expected. Of course, the extent of such variations between samples of the same catalyst, as observed in TPD experiments, gives some indication of the uniformity of metal dispersion achieved using each preparative technique. The results of the propene and propene/H_2 desorption experiments suggest that, on the

whole, the uniformity of metal dispersion achieved by use of both photo-deposition and impregnation/reduction is reasonably good, with little or no differences between the two types of catalyst being detected by use of TPD.

4.4.3 CO Desorption

As can be seen from Fig. 3.35, the CO TPD profiles obtained for 'as prepared' Pt(0.5)/P25(P), Pt(0.5)/P25(T) and P25 TiO_2 are fairly complicated compared to those obtained for propene desorption. At first sight, the TPD profile obtained for P25 TiO_2 suggests that quite extensive CO desorption from this material occurs over the range 300 - 900K. However, it has been concluded that CO is only weakly adsorbed onto the TiO_2 surface and that such adsorbed CO can be readily removed by evacuation at room temperature[43,99,100]. Therefore, it seems unlikely that the TPD profile observed in this study can be attributed to continued CO desorption from P25 titania at elevated temperatures and it is probable that much of the observed profile arises from continued CO desorption from the surfaces of the high vacuum and mass spectrometer system which, on the whole, remains at ambient temperatures. It has been proposed[99,100] that surface carboxylate species can be formed via reaction of CO, reversibly adsorbed at Ti^{4+} sites, with adjacent oxygen atoms at temperatures between 473 - 573K. Above 573K, these surface carboxylate species decompose with the concomitant evolution of CO_2. Thus, the desorption of CO observed to occur at high temperatures may in fact be

due to CO_2 desorption, formed via the carboxylate mechanism described, with the CO being derived from the surfaces of the vacuum system. In this case, the detection of CO would be due to the cracking of CO_2 in the mass spectrometer. Overall, it is probable that the large quantities of desorbed CO, observed at high temperatures, arises partly due to persistent desorption from the vacuum system which remains at ambient temperature, as shown by the high background trace obtained in the presence of no adsorbent, and from CO_2 desorption as a result of surface carboxylate decomposition. Support for this proposition has been obtained by monitoring CO_2 desorption from these materials, following exposure to CO adsorbate, as discussed later.

The TPD profile of CO desorption obtained for 'as prepared' Pt(0.5)/P25(P) shows a single, fairly broad, desorption peak occurring over the approximate temperature range 300 - 450K. Since, as discussed above, CO adsorption onto TiO_2 occurs only via a very weak interaction and is readily desorbed during evacuation, this desorption peak can be ascribed to CO adsorbed at Pt metal sites. Above 500K, large quantities of desorbed CO are detected, with the profile becoming a rather featureless plateau up to the final temperature of 900K. The high temperature desorption of large quantities of CO probably arises from both the vacuum system and CO_2 evolution via surface carboxylate decomposition, as discussed above for P25 TiO_2. In the case of 'as prepared' Pt(0.5)/P25(T), two distinct CO desorption peaks, the peaks occurring at ~400K and ~475K, are observed in the TPD profile. These low temperature peaks are ascribed to CO desorption from Pt metal sites, suggesting that either two

distinct metal sites, or different CO adsorption modes, occur on this catalyst. Since only one low temperature desorption peak is observed for the 'as prepared' photodeposited catalyst, it is possible that the presence of presorbed hydrogen, arising from preparation, influences the adsorption, or subsequent desorption, of CO onto, or from, 'as prepared' Pt(0.5)/P25(T) catalyst. At temperatures above ~550K, large quantities of desorbed CO were detected, the TPD profile becoming a featureless plateau up to the final temperature of 900K. Again, this observation is explained in terms of persistent desorption of CO from the surfaces of the vacuum system and CO_2 evolution via carboxylate decomposition.

The CO TPD profiles obtained for high-temperature reduced P25 TiO_2, Pt(0.5)/P25(P) and Pt(0.5)/P25(T) are shown in Fig. 3.36. The fact that very little CO desorption is observed to occur from reduced titania is consistent with the observations of other workers, who have proposed that CO adsorption onto TiO_2 surfaces occurs only at Ti^{4+} sites, via a weak interaction. However, CO desorption from both reduced platinised catalysts was clearly evident, particularly from the thermally-prepared catalyst. This is somewhat surprising since the suppression of CO adsorption is a well-known characteristic of Pt/TiO_2 catalysts in a deep SMSI state, as achieved by high-temperature reduction. It has been reported[275-279] that TiO_2-supported metal catalysts exhibit enhanced activity for CO hydrogenation following high-temperature reduction, which renders the catalysts in a deep SMSI state. Burch and Flambard[275] have proposed that the presence of special sites at the metal-oxide interface are responsible for such enhanced activity and that migration of titanium

sub-oxide species onto metal particles during high-temperature reduction produces an increased concentration of these special sites, consequently leading to enhanced methanation activity. There also appears to be conflicting evidence as to whether or not the reduced catalysts remain in the SMSI state during CO hydrogenation. Wang et al[276] found that H_2 and CO chemisorption, as measured by IR spectroscopy, remained low after CO methanation activity, implying that the catalyst was still in an SMSI state, whereas Anderson and Burch[277] reported partial restoration of H_2 chemisorption following exposure of an SMSI Pt/TiO_2 catalyst to CO/H_2 mixture. More recently, Blankenburg and Datye[278] have studied the restoration of hydrogenolysis activity of an SMSI Pt/TiO_2 catalyst by exposure to CO/H_2 and obtained evidence to suggest that CO hydrogenation leads to removal of TiO_x species covering the metal sites. They concluded that enhanced CO methanation activity of the SMSI catalyst is not due to the presence of titanium sub-oxide species covering the metal deposits, but rather to spillover of reaction intermediates onto the oxide support. Mao and Falconer[279] also came to a similar conclusion in their study of the CO hydrogenation activities of Pt/TiO_2 catalysts. These workers suggested that a methoxy (CH_3O) species is formed on the surface of the oxide support, via a CO spillover mechanism, and that the methoxy species is hydrogenated at a faster rate than CO adsorbed and hydrogenated at the Pt deposits.

On the basis of the above observations, it is possible that exposure of high-temperature reduced Pt(0.5)/P25 catalysts to CO leads to the removal of TiO_x overlayers covering the metal sites, via reaction of CO

with presorbed hydrogen arising from the pretreatment. Further adsorption of CO would then be possible, giving rise to the extensive CO desorption profiles observed for these materials. The fact that much more CO is desorbed from reduced Pt(0.5)/P25(T), relative to the photodeposited catalyst, would suggest that the removal of TiO_x species from the metal sites occurs to a greater extent with the former catalyst, this being indicative of some morphological differences between the two types of catalyst following hydrogen reduction. The continued desorption of CO over the entire experimental temperature range, particularly above ~700K, might be attributable to spillover CO, possibly occurring as the methoxy species discussed above.

The effect of high-temperature reduction, and subsequent re-oxidation, on CO adsorption and desorption from P25 TiO_2, Pt(0.5)/P25(P) and Pt(0.5)/P25(T) is shown in Fig. 3.37. Surprisingly, very little CO desorption is observed to occur from these pretreated materials, compared to the corresponding 'as prepared' and reduced samples. With all three re-oxidised samples, a single low temperature peak, the maxima occurring in the range 325 - 350K, is found in the TPD profiles. In each case, the high temperature side of this peak falls slightly and then extends as a featureless plateau up to ~500K. Above 500K, no further significant CO desorption is observed to occur for the platinised samples, although in the case of P25 TiO_2 the level of CO desorption remains fairly high up to the final temperature of 800K. The relatively small quantities of CO desorbed from the platinised catalysts, relative to the 'as prepared' and reduced samples, is not easily explained. The occurrence of the low

temperature desorption peak in both cases can be attributed to CO adsorbed at surface Ti^{4+} cations, since the same peaks is observed for pure titania. However, high-temperature re-oxidation no doubt results in the surfaces of the platinised materials being covered with presorbed oxygen, arising from the pretreatment, which would presumably react with the adsorbed CO to form CO_2. Also, the formation, and subsequent decomposition to CO_2 of surface carboxylate species is expected to be quite significant under these conditions. As discussed earlier, the formation and desorption of significant amounts of CO_2 detected in the mass spectrometer via cracking to CO, would then register on the TPD profile. It may be that saturation of the metal with presorbed oxygen prevents CO adsorption at these sites, which means that only CO desorbing from Ti^{4+} cations is observed for the re-oxidised catalysts. However, detection of CO at high temperatures should still occur due to CO_2 evolution via decomposition of surface carboxylate species, as observed with re-oxidised P25 titania. The presence of presorbed oxygen on the surfaces of the vacuum system may also contribute to the low overall levels of CO desorption observed following re-oxidative pretreatment, by preventing CO adsorption and subsequent persistent desorption during the TPD experiments.

4.4.4 CO_2 Desorption

The TPD spectra of CO_2 desorption obtained following CO adsorption onto 'as prepared', high-temperature reduced and reduced/ oxidised Pt(0.5)/P25(T), Pt(0.5)/P25(P) and P25 TiO_2 are shown in Figs. 3.38 - 3.40. For 'as prepared' Pt(0.5)/P25(T), CO_2 desorption is observed to occur over virtually the entire temperature range investigated, with the TPD profile being a flat, featureless plateau. 'As prepared' Pt(0.5)/P25(P) shows a rather large CO_2 desorption region over the range 300 - 550K, with the maximum occurring at ~400K. Above 500K, large quantities of CO_2 are desorbed and the TPD profile becomes a flat plateau, with no structure, up to the final temperature of 900K. The desorption of CO_2 formed at Pt metal sites by reaction of adsorbed CO with presorbed oxygen, derived from the ambient atmosphere the catalysts were stored in, will clearly contribute to significantly to the observed TPD profiles for these two catalysts and probably explains the large desorption peak observed for Pt(0.5)/P25(P). It is also possible that some of the observed CO_2 is derived via the decomposition of surface carboxylate species formed from CO reversibly adsorbed at Ti^{4+} sites and adjacent oxygen atoms, as discussed previously. There is also spectroscopic evidence [60,94,101] for the formation of surface bicarbonate and carbonate species via the interaction of CO_2 with hydroxylated titania surfaces. It is possible that the high temperature CO_2 desorption observed for both catalyst types arises due to the decomposition of such species formed by the reaction of CO_2, produced at Pt metal sites, with adjacent surface hydroxyl groups. The fact that much more CO_2 is desorbed from Pt(0.5)/P25(T), compared

to Pt(0.5)/P25(P), can be explained in terms of differing extents of hydroxylation of the oxide surface, likely to be much greater for the thermal catalyst due to hydrogen spillover during preparation. The TPD profile of CO_2 desorption from P25 TiO_2, following exposure to CO adsorbate, shows that much less CO_2 is desorbed from this material compared to the platinised catalysts. However, at least four distinct desorption peaks are observable in the profile, with the maxima occurring at ~350K, ~600K, ~675K and ~800K. As suggested earlier, these peaks, particularly the high temperature ones, probably correspond to the decomposition of surface carboxylate species formed by interaction of CO, reversibly adsorbed at Ti^{4+} sites, with surface oxygen atoms, to give CO_2. The low temperature peak may be due to the decomposition of surface bicarbonate species, which are more thermolabile than carboxylate species.

High-temperature reduction of the platinised catalysts and P25 TiO_2 resulted in a dramatic reduction in the amount of CO_2 desorbed from all three adsorbents, as can be seen from the TPD profiles shown in Fig. 3.39. In the case of reduced P25 TiO_2, virtually no CO_2 desorption is observed to occur over the entire temperature range investigated. This result is expected since it is thought that CO is only weakly adsorbed onto titania at Ti^{4+} sites, such that high-temperature reduction of TiO_2, which leads to the formation of Ti^{3+} sites, suppresses CO adsorption on this material. The observed lack of CO, and hence CO_2, desorption from reduced P25 TiO_2 is consistent with this hypothesis. For the platinised catalysts, significant CO_2 desorption is observed to occur only at temp-

eratures in excess of 700K, with the amount of desorbed CO_2 being greater for the thermal catalyst, relative to the photodeposited catalyst. The adsorption of CO onto high-temperature reduced Pt/TiO_2 catalysts, ostensibly in a deep SMSI state, has been discussed previously in Section 4.4.3. However, significant CO_2 desorption from reduced platinised catalysts would not be expected, since high-temperature reduction results in the removal of presorbed oxygen and the creation of surface hydroxyl groups and anion vacancies, thereby suppressing the formation of CO_2 on the catalyst surface. This is consistent with the observed CO_2 TPD profiles observed for the reduced Pt(0.5)/P25 catalysts. The high temperature desorption of CO_2 from these reduced catalysts suggests that the formation, and subsequent decomposition, of some kind of surface species, possibly methoxy or carboxylate species, does occur to a limited extent.

The CO_2 TPD profiles for reduced/oxidised P25 TiO_2, Pt(0.5)/P25(T) and Pt(0.5)/P25(P), following exposure to CO, are shown in Fig. 3.40. A very large desorption region, extending from 300 - 500K, is observed for all three adsorbents. Qualitatively, the amount of CO_2 desorbed from these materials is, in ascending order:

$$\text{P25 } TiO_2 < \text{Pt(0.5)/P25(P)} < \text{Pt(0.5)/P25(T)}.$$

This observation is consistent with the adsorption of CO at both Ti^{4+} and Pt metal sites, followed by reaction with presorbed oxygen arising from the pretreatment, to give adsorbed CO_2. The fact that more CO_2 is found to desorb from the thermal catalyst, relative to the photodeposited material, suggests that the Pt metal morphology in the former is some-

what different to that in the latter. This hypothesis is further supported by the observation that above 500K, no further CO_2 desorption occurs for both P25 TiO_2 and Pt(0.5)/P25(P), whereas significant CO_2 desorption from Pt(0.5)/P25(T) continues to ~650K. Furthermore, a single, sharp high temperature desorption peak, the maximum occurring at ~775K, is observed for the thermal catalyst only. This would suggest the formation, and subsequent decomposition, of a surface species, possibly carboxylate species, as discussed earlier. However, the evident lack of this peak in the TPD profile obtained for either P25 TiO_2 or Pt(0.5)/P25(P), clearly indicates a difference in supported metal morphology between the two catalyst types.

4.5. Photocatalytic Dehydrogenation of Propan-2-ol

4.5.1 Occurrence of the Dark Reaction

Within this project, the photocatalytic dehydrogenation of propan-2-ol, in the presence of various metallised TiO_2 catalysts, was studied. A consistent observation made during these experiments was the occurrence of a dark reaction in the presence of all catalysts containing platinum metal, regardless of metal content or method of preparation. The dark reaction was characterised by the formation of detectable quantities of propanone, prior to initiation of the reaction by exposure to UV radiation. Catalysts containing other Group VIII metals were not found to produce such a dark reaction. A similar dark reaction was observed by Hussein and Rudham[213,240] when $Pt(0.5)/TiO_2$, prepared by impregnation and subsequent H_2 reduction at 753K, was contacted with various primary and secondary alcohols, including propan-2-ol, under a nitrogen atmosphere. These workers concluded that the reaction represents the limited oxidation of alcohol to the corresponding carbonyl compound via a thermal mechanism. For all the alcohols studied, with the exception of methanol, the reaction was found to obey first-order kinetics with respect to departure from a common temperature-independent equilibrium yield of the appropriate carbonyl compound of 0.45×10^{-2} mol dm^{-3}. Although the methanol dark reaction was found to follow the same kinetics, the equilibrium yield of methanal was found to be lower than that observed for the other alcohols. This was thought to be due to further oxidation of methanal to CO_2, via methanoic acid. An activation energy of 120 ± 5kJ

mol^{-1}, was calculated for the oxidation of propan-2-ol to propanone via the dark reaction, in the temperature range 278 - 293K. The mechanism of this dark reaction was proposed to involve the interaction of the alcohol with the O_2^- species, formed via the adsorption of oxygen onto non-stoichiometric TiO_2 support, generated during high temperature reduction in H_2. Hence:

$$2\ R'R''CHOH + O_2^- \longrightarrow 2\ R'R''CO + 2H_2O + e^-_{(to\ catalyst)} \qquad [93]$$

The authors postulated[213] that the observed first-order kinetics reflected the limited amount of adsorbed O_2 present as a chemisorbed monolayer on the catalyst surface and that the high activation energy was a consequence of the relatively low reactivity of the O_2^- species, compared to other possible adsorbed oxygen species. This activation energy is quite characteristic of thermal catalytic processes and so may be a reflection of the fact that the dark reaction is a thermal process. Furthermore, high temperature oxidation of the thermally-prepared catalyst was found to result in complete suppression of the dark reaction, whereas reduction of a similar catalyst prepared by photodeposition, which did not initially exhibit any dark reaction capacity, was subsequently found to enable the dark reaction. These observations were taken as further supporting evidence for the postulated mechanism of the dark reaction.

Although the occurrence of a dark reaction was observed during this study, several discrepancies exist between the results reported here and those found by the previous workers. In this study, the amount of

propanone formed via the dark reaction appeared to be dependent upon both the reaction temperature, Fig. 4.13, and the Pt content of the catalyst, Fig. 4.14. It is possible that in the current experiments, insufficient time was allowed for completion of the dark reaction prior to commencement of irradiation with UV light of the reaction mixture. However, the fact that all plots for the photocatalytic evolution of propanone as a function of time are clearly linear strongly suggests that the dark reaction was indeed complete prior to irradiation of the reaction mixture. Furthermore, in the case of Pt(0.5)/P25(T) and Pt(0.5)/anatase(P) catalysts, the concentrations of propanone formed via the dark reaction, at temperatures ≥ 293K, were found to exceed the equilibrium yield of 0.45×10^{-2} mol dm^{-3} reported earlier. These observations imply that, for the Pt/TiO_2 catalysts used in this study, temperature-dependent equilibrium yields of propanone exist for the dark reaction. Also in contrast to the results reported by Hussein and Rudham[213,240], it was found that Pt/TiO_2 catalysts prepared by photodeposition also exhibited a pronounced dark reaction, in addition to the catalyst prepared by the thermal reduction method. This observation indicates that non-stoichiometry is induced in the support oxide by both preparative routes, assuming that the dark reaction occurs via the mechanism proposed by Hussein and Rudham[213]. However, if this is so, it would be expected that catalysts containing other Group VIII metals, prepared via the photodeposition route, would also exhibit a pronounced dark reaction, which was not observed during these experiments.

The discrepancies between the results reported here and those of Hussein and Rudham, reported earlier, are not easily explained. The

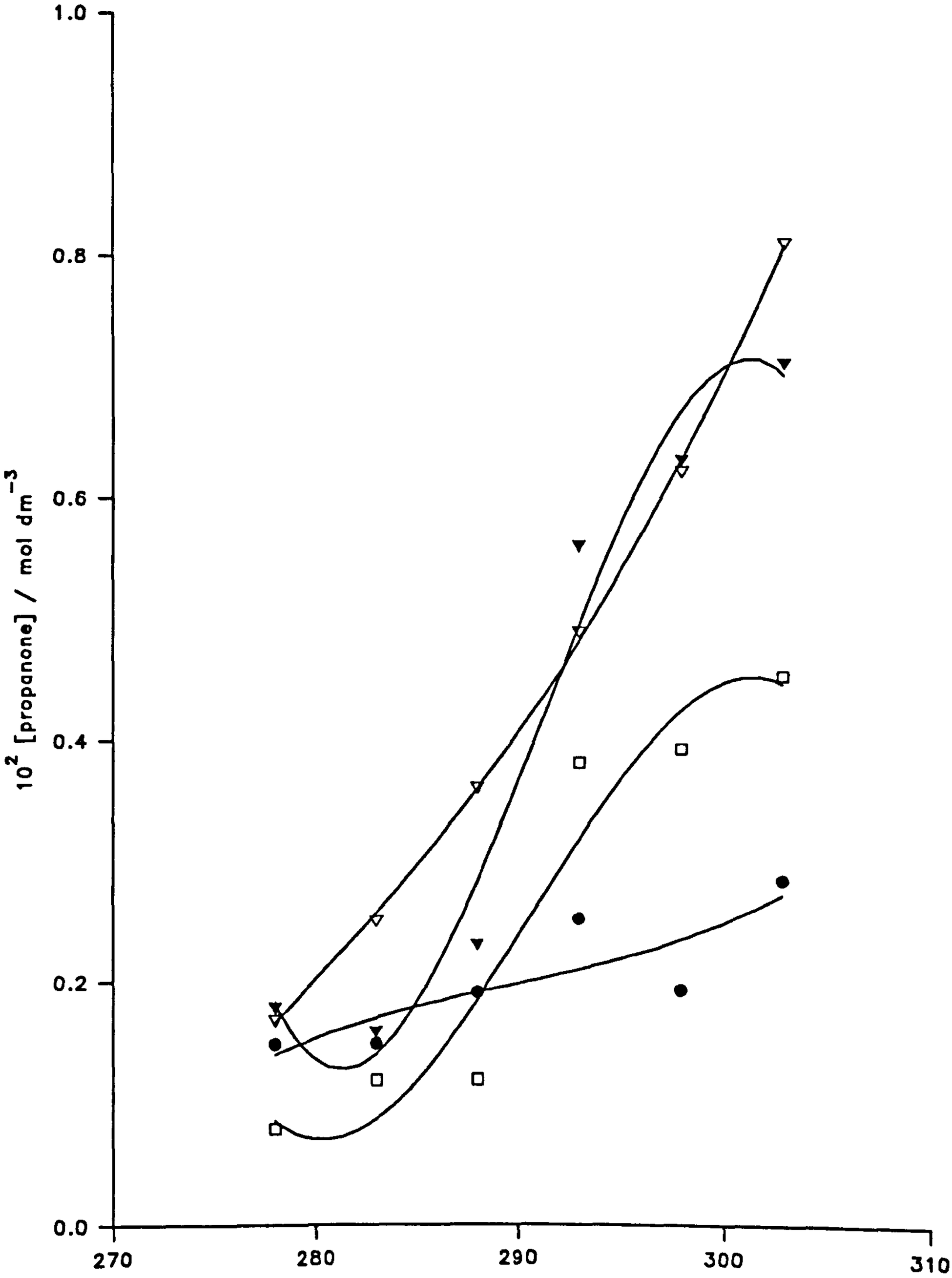

Figure 4.13: Propanone Concentration as a Function of Temperature Formed as a Consequence of the Dark Reaction over Various Pt/TiO_2 Catalysts

results reported in this current study would seem to suggest that the presence of platinum metal is essential for the occurrence of the dark reaction. One possible explanation of the discrepancies between the two studies, is that the Pt/TiO_2 catalysts used in this study contained a much greater quantity of impurities, arising from the preparation of these catalysts, than those employed by Hussein and Rudham. The presence of varying quantities of such impurities would presumably modify the electronic structure of the Pt/TiO_2 catalysts to differing extents. In this case, oxygen adsorption, and hence the dark reaction, would be dependent upon the extent to which the catalyst electronic structure was modified, as determined by the presence of varying quantities of impurities. Along these lines, the absence of an observed dark reaction with other Group VIII metals may arise because the electronic structures of such catalysts are sufficiently different to that of Pt/TiO_2, such that the presence of impurities does not lead to the chemisorption of oxygen. Furthermore, this hypothesis can explain the observed temperature-dependent propanone equilibrium yield, since increasing temperature may result in an increase in the transfer of thermal electrons from impurities to oxygen.

4.5.2 The Effect of Metal Type

The influence of TiO_2-supported metal type, at a level of 0.5 mass%, on the rate of photocatalytic dehydrogenation of propan-2-ol at 293K is shown in Fig. 3.39. It is immediately obvious that the presence of a metal is required for the reaction to proceed, since zero activity for

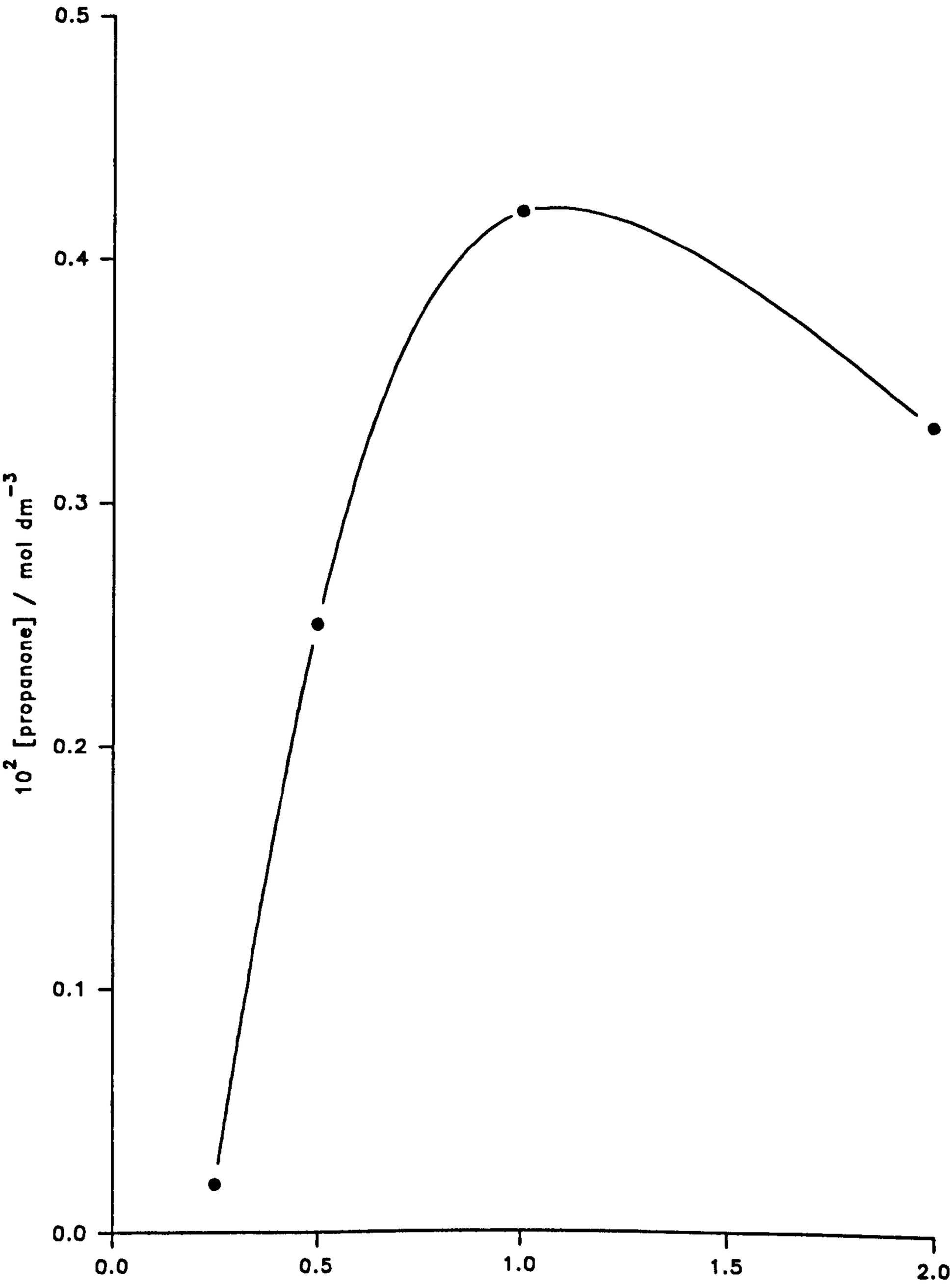

Figure 4.14: Propanone Concentration as a Function of Pt Content Formed as a Consequence of the Dark Reaction over Various Photodeposited Pt/TiO_2 Catalysts

the reaction was observed with pure P25 TiO_2. The results obtained here show that, in the presence of metal, the rate of reaction is clearly dependent upon the nature of the supported metal. In terms of decreasing activity for the photocatalytic reaction, the metals are seen to lie in the order:

$$Pt > Pd > Rh >> Ir > \text{none} \sim 0.$$

With respect to the platinised catalysts, the measured rates of reaction are very similar, implying that the method of catalyst preparation has little influence on catalyst activity for this photocatalytic reaction.

The above order of activities for the photocatalytic reaction, as a function of metal type, is very similar to that observed in the thermal cyclopropane hydrogenation experiments, although in the latter case the catalysts were subjected to high temperature reduction and oxidation prior to reaction. In combination, these two sets of results strongly suggest that the degree of metal dispersion is a dominant factor in determining, at least initial, catalyst activity for the two reaction types. Therefore, on the basis of catalyst activity, it would appear that Pt metal is most disperse and Ir metal the least disperse, on the supporting oxide surface. In a similar study, Pichat et al[239] measured the photocatalytic dehydrogenation activity of Pt and Rh/TiO_2 catalysts and observed that Pt/TiO_2 was much more active than Rh/TiO_2 for the reaction. The authors also measured the degree of metal dispersion for these catalysts and found that the Pt metal dispersion was greater than the Rh metal dispersion. This result was used to explain the observed difference in the photocatalytic activities of the two catalysts. Unfortunately, the absence of any

quantitative metal dispersion data precludes further testing of the above hypothesis in this study.

4.5.3 Effect of Pt Content

The effect of changing the quantity of TiO_2-supported Pt metal, in the range 0.25 - 2.0 mass%, on the rate of photocatalytic dehydrogenation of propan-2-ol is shown in Fig. 3.41. The results show that all catalysts were active for the reaction, indicating that a minimum quantity of metal is not required for the reaction to proceed, as would be expected. A maximum in activity for the reaction was observed with 0.5 mass% Pt, which is in good agreement with the observations of other workers[239,280]. It has been proposed[280] that good catalyst activity is achieved by the use of relatively low levels of supported Pt metal, since a high degree of metal dispersion can be achieved, which in turn minimises recombination of photogenerated electrons and holes. The results obtained in these current photocatalytic experiments are in good agreement with those obtained from the thermal propene hydrogenation experiments, in which it was found that both the 'as prepared' and the reduced/oxidised 0.5 mass % Pt catalysts were much more active for the reaction than would be expected, relative to those catalysts containing higher levels of Pt metal. The most likely explanation of these results is that an optimum degree of metal dispersion on the oxide support is achieved at approximately 0.5 mass% metal. This would explain the higher than expected activity of 0.5 mass% Pt catalysts for the thermal reactions and the maximum in activity

observed for the photocatalytic reaction, based on the assumption that an optimum metal loading is required to achieve optimal separation of photogenerated electrons and holes. Again, the absence of quantitative data with respect to metal dispersions precludes further testing of this hypothesis within the current study, although it does seem that the use of higher, ≥ 1 mass%, metal contents in TiO_2-supported catalysts is not particularly beneficial in terms of catalyst activity.

4.5.4 Effect of Temperature

The effect of varying temperature on the photocatalytic dehydrogenation of propan-2-ol for various 0.5 mass% Pt catalysts is shown in Figs. 3.42 - 3.45., with the corresponding Arrhenius plots shown in Fig. 3.46. The use of various TiO_2 supports, possessing very different surface areas, means that the four calculated activation energies for the photocatalytic reaction cannot be compared with each other. However, the results obtained for Pt(0.5)/P25(P) and Pt(0.5)/P25(T) are comparable, since the same oxide support was utilised. Previous studies [125,213] have shown that the photocatalytic oxidation of propan-2-ol using TiO_2 and the photocatalytic dehydrogenation of propan-2-ol using photo-deposited Pt/TiO_2, are both associated with an activation energy of ~20 kJ mol^{-1}. These results were explained in terms of reaction mechanisms involving the transport of photogenerated holes and electrons through the oxide bulk to the surface, where they are trapped. It has been proposed that the common activation energy for the two types of reaction arises

due to photo-electron trapping processes occurring during the transport process through the bulk oxide. Exposure of Pt/TiO_2 catalyst to hydrogen at 753K, either during or after catalyst preparation, was found to give a much lower activation energy, ~8 kJ mol^{-1}, for the photocatalytic dehydrogenation reaction. This was explained in terms of a reduction in the photo-electron trap depth, due to the generation of non-stoichiometry in the oxide support. Therefore, differences in activation energies for the photocatalytic dehydrogenation reaction reflect differing extents of reduction of the oxide support, such that a greater degree of reduction leads to a correspondingly smaller activation energy. It can be seen that the activation energy of 18 ± 1 kJ mol^{-1} calculated for Pt(0.5)/P25(P) in these current experiments, is in reasonable agreement with the proposed reaction and photo-electron transport mechanisms. The lower activation energy of 15 ± 1 kJ mol^{-1} calculated for Pt(0.5)/P25(T) is also expected, since exposure of this catalyst to H_2 at elevated temperatures during preparation would result in the reduction of the oxide support. However, this value is significantly higher than that reported previously for a similar catalyst, which suggests that the degree of oxide non-stoichiometry in Pt(0.5)/P25(T) is somewhat limited. A possible explanation for this difference is that the catalyst used in the current study was stored under ambient atmosphere for a considerably longer time before use than in previous studies. In this case, a certain degree of non-stoichiometry may have been eliminated via the slow uptake of oxygen by the catalyst.

For Pt(0.5)/anatase and Pt(0.5)/rutile, both prepared by photodeposition, activation energies of 16 ± 1 and 14 ± 1 kJ mol^{-1} respect-

ively, were calculated for the photocatalytic dehydrogenation of propan-2-ol between 278 - 303K. Harvey et al[124] studied the photocatalytic oxidation of propan-2-ol using low surface area anatase and rutile catalysts and found that the activation energy for the reaction increased dramatically as the oxide surface area decreased or the extent of doping increased. The anatase, rutile and P25 TiO_2 used in this current study possessed very different surface areas and are not strictly comparable, as mentioned previously. However, in contrast to the findings of Harvey et al[124], the results obtained in this study suggest that the surface area of the oxide support is not a critical factor influencing the photocatalytic dehydrogenation rate of propan-2-ol, although the presence and level of impurities is clearly an important consideration. This implies that the photogenerated electrons are trapped at the Pt metal sites, rather than the oxide surface, as would be expected and that the extent of oxide reduction is far more important than oxide surface area considerations. However, on this basis, it would be expected that the three photodeposited catalysts give rise to very similar activation energies for the photocatalytic reaction, which is not observed.

The unexpected variations in activation energies for the photocatalytic dehydrogenation of propan-2-ol obtained with the Pt/TiO_2 catalysts may be due to differing levels of impurities, arising during preparation. Such impurities are a potential source of photo-electron trap centres and variable impurity levels would result in variable activation energies, as is observed. The presence of variable levels of impurities in these catalysts has already been suggested as the cause of the dark reaction

observed with all platinum catalysts, as discussed previously. It is also thought that the variable behaviour of the 'as prepared' Pt/TiO_2 catalysts in the thermal hydrogenation reactions may be a result of variable impurity levels, which were subsequently removed during high temperature pretreatment. In combination, all these observations strongly suggest that the 'as prepared' Pt/TiO_2 catalysts used in this study were contaminated with variable levels of impurities, presumably arising during catalyst preparation. It is clear that further investigations into the effects of such impurities on catalyst performance during photocatalytic, as well as thermal, reactions is required in order to resolve these issues. In the context of this study, there appears to be very little difference in the photocatalytic behaviour of Pt(0.5)/P25(P) and Pt(0.5)/P25(T) catalysts. This is presumably because the reaction is not demanding enough to highlight any differences, with respect to activity or stability and hence potential morphological differences, between the two catalyst types. This is in clear contrast to the results obtained during the thermal hydrogenation experiments, which highlighted several important differences between those catalysts prepared via photodeposition and that prepared via high temperature reduction in hydrogen.

4.6 Effect of Preparation Method on Catalyst Behaviour

Throughout the course of this discussion chapter, continual reference has been made to the possible existence of morphological differences between Pt metal deposited on TiO_2 via photodeposition and that deposited by impregnation, followed by high-temperature reduction in H_2. Much indirect evidence to support this hypothesis has been found from many of the experiments, particularly in the case of the thermal hydrogenation investigations, conducted during this project. Briefly, the most important differences between the two catalyst types are can be summarised as follows:

1. Following high-temperature reduction and subsequent re-oxidation, the photodeposited catalysts generally exhibited very poor stability during prolonged thermal hydrogenation reactions, relative to the thermally-prepared catalyst. This difference in behaviour was particularly evident with respect to the more demanding cyclopropane hydrogenation reaction, in which all the photodeposited catalysts were found to rapidly and irreversibly decline in activity. Furthermore, reduced/oxidised Pt(0.25)/P25(P) and Pt(0.5)/P25(P) were also found to be very unstable during prolonged propene hydrogenation, which is a relatively undemanding reaction.

2. The activity of high-temperature reduced Pt(0.5)/P25(T) catalyst was observed to increase upon exposure to cyclopropane/H_2 mixture, whereas all similarly pretreated photodeposited catalysts, with the exception of Pt(2.0)/P25(P), remained inactive for the reaction.

3. The calculated activation energies for the hydrogenation of propene over Pt(0.5)/P25(P) and Pt(0.5)/P25(T), previously reduced and then re-oxidised at high temperature, were found to be very different. It is proposed that this difference is a result of differing reactant adsorption behaviour on the two catalysts types, which in turn is thought to arise because of differences in supported metal morphology.

4. Although the hydrogenation of both propene and cyclopropane appears to occur via a Langmuir-Hinshelwood mechanism for both types of catalysts, maximum rates of reaction were observed to occur at different hydrocarbon:H_2 ratios. Again, this indicates different reactant adsorption behaviour, which is presumed to be a consequence of differing supported metal morphologies.

On the basis of the above observations, it would be expected that the TPD experiments would show some clear differences in the desorption behaviour of the adsorbates studied from the photodeposited and the thermally-prepared catalyst. Unfortunately, although some differences in desorption behaviour were observed, these were not as significant as was hoped and no firm evidence to support the hypothesis of different metal morphologies was obtained from the TPD experiments.

Although there is a lack of direct evidence, the above results clearly indicate that the method of preparation has a significant influence on the subsequent behaviour of TiO_2-supported catalysts, particularly with

respect to gas-phase thermal hydrogenation reactions. This effect appears to be most marked in the photodeposited catalysts containing less than 1.0 mass% supported metal, which were found to be very unstable during the thermal hydrogenation reactions. A possible explanation for this effect is that the photodepostion method of catalyst preparation, which is conducted under very mild conditions, results in a very high degree of dispersion of the metal on the oxide surface, particularly at low metal contents. In this case it is probable that the metal forms very thin, but discrete "rafts" or "islands" of metal on the catalyst surface, similar to the "pill-box" morphology suggested by Baker et al[153,176]. Thermal preparation of TiO_2-supported metal catalysts, which involves exposure to H_2 at elevated temperatures, leads to the formation of larger crystallites of metal on the oxide surface, possibly as a consequence of sintering effects. The fact that photodeposited catalysts containing higher levels, $\geq$ 1.0 mass%, of supported metal were found to be only slightly more active than those containing 0.5 or less mass% metal, suggests that similar crystallites can be formed via the photodeposition of higher levels of metal. Thus, it is proposed that very similar supported metal morphologies exist for Pt(0.5)/P25(T), Pt(1.0)/P25(P) and Pt(2.0)/P25(P), whereas the supported metal morphology for photodeposited catalysts containing less than 0.5 mass% metal are distinctly different. This difference is shown conceptually in Fig. 4.15(a).

Accepting that such differences in supported metal morphologies do indeed exist, the results obtained with the 'as prepared' catalysts suggest that such differences are not important in determining catalyst

performance. The variations in the behaviour of 'as prepared' catalysts are thought mainly to be due to different levels of impurities arising from preparation, rather than significant differences in the degree of metal dispersion. However, it is possible that such differences in metal morphology can be used to explain the differences in the observed behaviour of the various catalysts following high-temperature reduction in hydrogen. Overall, the results show that such pretreatment of the photodeposited catalysts rendered them completely inactive for the thermal hydrogenation reactions, a consequence of the generation of SMSI effects. Although the exact origins of the SMSI effect are still unknown, there is considerable evidence to support the theory of coverage of the dispersed metal by TiO_x overlayers, the so-called "decoration model". On the basis of such a model, it can be seen that for the photodeposited catalysts, where the metal adopts a very thin, raft-like morphology, complete coverage of the metal by titania sub-oxide species would occur readily. It also seems likely that this effect would be enhanced by diffusion of the supported metal into the bulk oxide. Applying the same model of SMSI to the thermal catalyst, in which the metal is proposed to exist as larger crystallites, it seems logical that it would be harder to completely cover the metal with TiO_x overlayers and that diffusion of the metal into the bulk oxide would not be as marked. Therefore, the thermal catalyst should be more resistant to SMSI effects, relative to the photodeposited catalysts, as shown by the results of the cyclopropane hydrogenation experiments. The low activity exhibited by reduced Pt(2.0)/P25(P) for cyclopropane hydrogenation gives support to the proposition that, for photodeposited catalysts

containing high levels of metal, the morphology of the metal begins to resemble that achieved via thermal catalyst preparation. This is shown in Fig. 4.15(b).

Continuing along these lines, high-temperature oxidation of the SMSI catalysts will result in the removal of TiO_x overlayers from the supported metal and, it is suggested, redispersion of the metal on the oxide surface. This effect is likely to be greatest for the photodeposited catalysts, particularly those with low levels of metal, but will lead to the observed increase in activity for all catalysts, relative to the corresponding 'as prepared' materials, as shown in Fig. 4.15(c) . Redispersion of supported Pt catalysts, during oxidative treatments, has been studied by Lee and Kim[281]. These workers concluded that redispersion of Pt/TiO_2 only occurred in the presence of chloride ion impurities during oxidation and suggested that a molecular migration model, involving the spreading of platinum oxide, could best account for the results obtained. However, it has already been proposed that highly dispersed supported metal catalysts are susceptible to metal - support effects. The fact that both Pt(0.25)/P25(P) and Pt(0.5)/P25(P), subjected to high-temperature reduction and oxidation, exhibited poor stability during prolonged propene hydrogenation, a relatively undemanding reaction, lends support to this proposition. The instability exhibited by all reduced/oxidised photodeposited catalysts during cyclopropane hydrogenation shows that the photodeposition method of catalyst preparation gives rise to supported metal catalysts which are susceptible to metal - support effects, even at higher metal contents. In contrast, preparation via high-temperature reduction in

Figure 4.15: Schematic Representation of Proposed Supported Metal Morphologies as a Function of Pretreatment for Various Pt/TiO_2 Catalysts

a) 'As Prepared' Catalysts

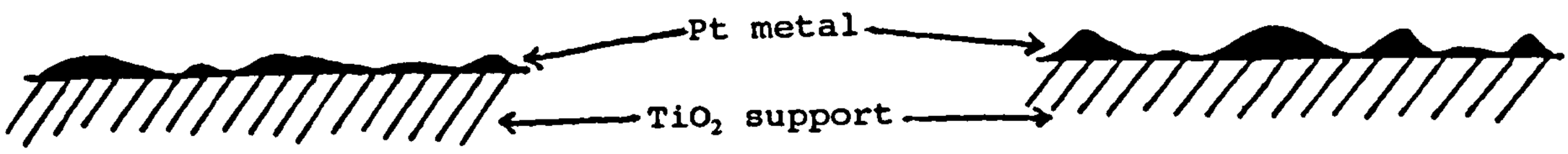

photodeposited catalysts
(≤ 2.0 %mass Pt)

thermal catalyst
(0.5 %mass Pt)

reduction
H_2/750K/3hrs

b) reduced catalysts

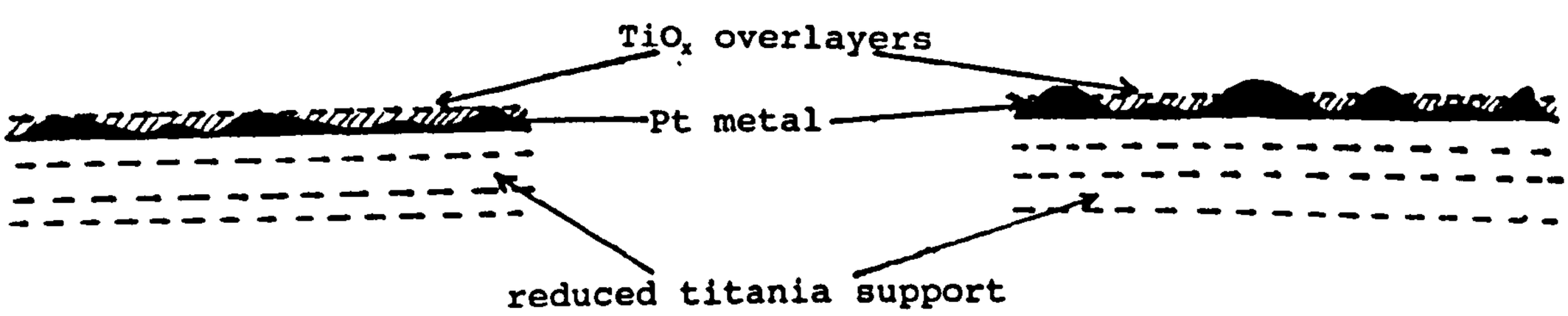

photodeposited catalysts
(≤ 1.0 %mass Pt)

thermal catalyst (0.5 %mass Pt)

photodeposited catalyst (2.0 %mass Pt)

oxidation
O_2/700K/3hrs

c) reduced/oxidised catalysts

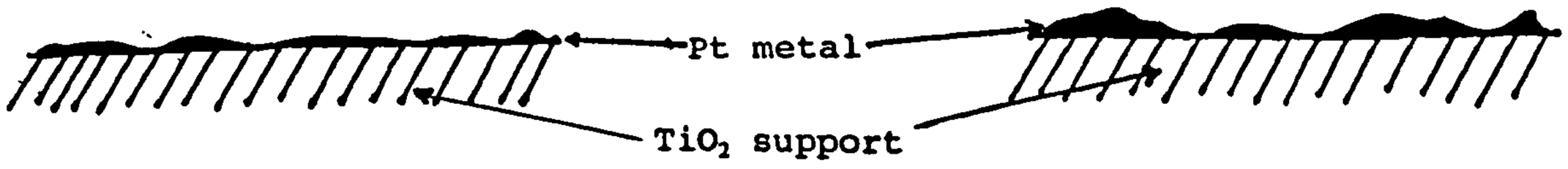

photodeposited catalysts
(≤ 0.5 %mass Pt)

thermal catalyst (0.5 %mass Pt)

photodeposited catalysts (≥ 1.0 %mass Pt)

H_2 produces catalysts with good stability characteristics, even at relatively low metal content.

The above explanation of the observed behaviour of the catalysts studied during this project is speculative, although indirect evidence, as outlined earlier, to support the hypothesis can be found in the experimental results. However, there is a clear need to investigate the nature of the supported metal directly and to obtain quantitative data, particularly with respect to metal dispersions. During this project some exploratory scanning electron microscopy (SEM) investigations were conducted using a Cambridge Instruments 1509 Scanning Electron Microscope. A small quantity of the catalyst sample was mounted on a thin aluminium disc using a cyanoacrylate adhesive and then coated with a very thin layer of gold via sputtering under vacuum. It was hoped that this technique could be used to analyse the morphology of TiO_2-supported metal and provide direct evidence for the existence of differences between the photodeposited and the thermally-prepared catalysts. Unfortunately, all attempts to locate and visualise Pt metal deposits directly were unsuccessful. There are several possible reasons that may account for the lack of success in the SEM investigations. Firstly, the electron microscope used was fairly old and the maximum resolution attainable was not as good as that possible on more modern machines. This problem was compounded by the fact that use of too high an electron beam energy led to the build up of charge on the disc holding the catalyst sample, which limited the maximum obtainable resolution, using this method of sample presentation. It is probable that the metal deposits were too small to be

detected and resolved using this particular machine. This is supported by the fact that analysis of the subsequent energy dispersive x-ray spectrum from the sample, following exposure to the intense electron beam, failed to reveal any peak which could be clearly attributed to Pt metal. Most electron microscopic studies of similar metal/TiO_2 catalysts reported in the literature have been conducted using high resolution transmission electron microscopy (HRTEM) techniques. It is worth noting that the average metal particle sizes, as measured using TEM, quoted in the literature are usually in the range 10 - 100nm, depending upon the metal loading of the catalyst studied[191,195,281,282]. Therefore, in order to directly visualise the metal deposits in the Pt/TiO_2 catalysts used in the current study, it would seem that the more powerful HRTEM, rather than SEM, techniques would be necessary. Such techniques were not available to the author when the experimental work for this project was conducted. Furthermore, other quantitative data are required to augment any electron microscopic investigations, in particular metal dispersions. Such data can be obtained via gas adsorption measurements, using hydrogen or carbon monoxide, and calculating H/M or CO/M ratios from gas volume uptake by the catalyst. Although some workers use hydrogen to calculate metal dispersions, spillover effects can give rise to misleading data, so the use of CO, where spillover can be detected using IR spectroscopy, is preferred. Unfortunately, limited quantities of the various Pt/TiO_2 catalysts used in the current study, meant that such quantitative data could not be obtained.

4.7 Overall Conclusions

The project reported here was primarily concerned with investigating the influence that preparation method has on the performance of TiO_2-supported metal catalysts. The main hypothesis of the project was that photodeposition of metals, conducted under mild conditions, would lead to more finely dispersed metal, relative to the alternative thermal reduction method, on the oxide support, thereby producing catalysts of higher activity. The results obtained within this study, particularly those relating to the thermal hydrogenation reactions, show that the hypothesis was incorrect, in that the catalysts prepared via the photodeposition procedure were found to be considerably less stable than that produced via the thermal reduction route. Ironically, the instability of the photodeposited catalysts is believed to arise because a higher degree of metal dispersion is actually achieved via the photodeposition method of preparation, particularly at low metal contents (≤ 1 mass%), which results in these catalysts being more prone to metal-support effects. This in turn leads to inherent catalyst instability, even for relatively undemanding reactions such as the hydrogenation of propene at low temperatures. That the method of preparation appears to be the dominant factor in determining subsequent catalyst stability, is shown by the fact that all photodeposited catalysts, regardless of the nature of the supported metal or metal loading, up to 2 mass%, exhibited very poor stability for cyclopropane hydrogenation at relatively low temperatures. In stark contrast, the catalyst prepared via thermal reduction in H_2, was found to be very stable, retaining its initial activity under the same reaction conditions. Similar experi-

ments also showed that the crystalline habit of the TiO_2 support made no, difference to the stability of the photodeposited catalysts.

The idea that the method of catalyst preparation, and subsequent pretreatments, has a strong influence of the morphology of the supported metal, and hence catalyst performance, is conjecture based on indirect evidence. Attempts to obtain direct evidence to support this hypothesis within this project, via the TPD and electron microscopy experiments, proved to be disappointing for a number of reasons. It is clear that in order to gain direct quantitative data to either support or disprove this hypothesis, further investigations are required, including electron microscopy, in particular HRTEM, experiments, determination of metal dispersions via gas adsorption and, possibly, by use of more specialised techniques such as ^{195}Pt NMR, UPS or a variety of X-ray analytical methods.

It was found that both propene and cyclopropane hydrogenation occurs via a Langmuir-Hinshelwood mechanism over both types of catalyst. However, the temperature and hydrocarbon:hydrogen ratio at which the maximum rate of propene hydrogenation occurred and the associated activation energies, were not the same for both catalysts, indicating difference in supported metal morphologies. It has been proposed that the kinetic differences between the two catalyst types, observed for the propene hydrogenation reaction, may be due to different adsorption behaviour of the reactants, as influenced by the different metal morphologies. Again, no direct evidence to support such a hypothesis was obtained within this project and further investigations are required, perhaps in the form of IR spectroscopy experiments to monitor adsorption behaviour as a

function of temperature. Improvements of the TPD methodology, particularly with respect to gaining more quantitative data, and the use of other similar techniques, such as temperature-programmed reaction experiments, may prove to be very useful in this area.

Finally, the reader is referred to back to Section 1.7 in this thesis, where a number of questions, which the work reported in this thesis was designed to answer, were posed. It is the belief of the author that these questions have been answered to a certain extent, although further work is obviously required to provide conclusive data and to answer some of the questions raised by the work conducted in this project.

REFERENCES

1. C. Renz; Helv. Chim. Acta; 4, 961, (1921).

2. L. Vegard; Phil. Mag.; 32, 65, (1916).

3. R.W.G. Wyckoff; "Crystal Structure", Vol.1, ChapterIV, p.7; Interscience, New York, (1960).

4. L. Pauling, J.H. Sturdivant; Zeits. Krist.; 68, 239, (1928).

5. S.R. Yoganarasimhan, C.N.R. Rao; Trans. Farad. Soc.; 58, 1579, (1962).

6. R.D. Shannon, J.A. Pask; J. Amer. Chem. Soc.; 48, 391, (1965).

7. C.N.R. Rao, S.R. Yoganarasimhan, P.A. Faeth; Trans. Farad. Soc.; 57, 504, (1961).

8. Y. Hara, M. Nicol; Phys. Status Solidi B; 94, 317, (1979).

9. J.F. Mammone, M. Nicol, S.K. Sharma; Solid State Commun.; 34, 799, (1980).

10. Y.Y. Bobyrenko, A.B. Zholnin, V.K. Konovalova; Russ. J. Phys. Chem.; 46, 749, (1972).

11. N.B. Hannay, C.P. Smyth; J. Amer. Chem. Soc.; 68, 111, (1946).

12. H.P. Boehm; Adv. Catal.; 16, 249, (1966).

13. M.D. Earle; Phys. Rev.; 61, 56, (1942).

14. A-L. Companion, R.E. Wyatt; J. Phys. Chem. Solids; 24, 1025, (1963).

15. F.G. Wakim; Phys. Status Solidi B; 1, 479, (1970).

16. A.K. Ghosh, F.G. Wakim, R.R. Addiss Jr; Phys. Rev.; 184, 979, (1969).

17. W.A. Weyl, T. Førland; Ind. Eng. Chem.; 42, 357, (1950).

18. V.N. Bogomolov, I.A. Smirnov, E.V. Shadrichev; Soviet Phys. - Solid State; 11, 2606, (1970).

19. W.F. Sullivan; Progr. Org. Coatings; 1, 157, (1972).

20. A.K. Ghosh, R.B. Lauer, R.R. Addiss Jr; Phys. Rev. B; 8, 4842, (1973).

21. H.J. Gerristen; Proc. 1st Intern. Conf. Paramag. Res.; 1, 3, (1962).

22. T.I. Barry; Solid State Commun.; 4, 123, (1966).

23. T.J. Gray, N. Lowery; Disc. Farad. Soc.; 4, 132, (1972).

24. T. Iida, H. Nazaki; Bull. Chem. Soc. Jpn.; 42, 929, (1969).

25. D.A Melnick; J. Phys. Chem.; 28, 1136, (1957).

26. R.R. Addiss Jr, F.G. Wakim; Photographic Sci. Eng.; 13, 111, (1969).

27. L.A. Bursill, B.G. Hyde, O. Terasaki, D Watanabe; Phil. Mag.; 20, 347, (1969).

28. L.A. Bursill, B.G. Hyde; Acta Cryst.; B27, 210, (1971).

29. L.A. Bursill, B.G. Hyde, D.K. Philip; Phil. Mag.; 23, 1501, (1971).

30. D.L. Cronemeyer, M.A. Gilleo; Phys. Rev.; 82, 975, (1951).

31. P. Kofstad; J. Chem. Phys. Solids; 23, 1579, (1962).

32. K.S. Førland; Acta Chem. Scand.; 18, 1267, (1964).

33. P. Coufova, H. Arend; Czech. J. Phys.; B11, 845, (1961).

34. T. Hurlen; Acta Chem. Scand.; 13, 365, (1959).

35. P.F. Chester; J. Appl.Phys. Suppl.; 32, 2233, (1961).

36. R.D. Carnahan, J.O. Brittain; J. Amer. Ceramic Soc.; 48, 366, (1965).

37. J.B. Watchman Jr, L.R. Doyle; Phys. Rev.; 135, 276, (1964).

38. J.B. Watchman Jr, S.Spinner, W.B. Brower, T. Fridinger, R.W. Dickson; Phys. Rev.; 148, 811, (1966).

39. P. Kofstad; J. Less - Common Metals; 13, 635, (1965).

40. W. Jakubowski; Actaphysica Polo Nica; 33, 465, (1968).

41. V.I. Barbanel', V.N. Bogomolov, S.A. Borodin, S.I.Budarina; Soviet Phys. - Solid State; 11, 431, (1969).

42. H.P.Boehm; Angew. Chem. Intern. Ed.; 5, 541, (1966).

43. D.J.C. Yates; J. Phys. Chem.; 65, 746, (1961).

44. P. Jones, J.A. Hockey; Trans. Farad. Soc.; 67, 2669, (1971).

45. P. Jones, J.A. Hockey; Trans. Farad. Soc.; 67, 2679, (1971).

46. P. Jones, J.A. Hockey; Trans. Farad. Soc.; 68, 907, (1972).

47. D.E. Yates, R.O. James, T.W. Healy; J.C.S. Farad. Trans. I; 76, 1, (1980).

48. M. Primet, P. Pichat, M-V. Mathieu; C.R. Acad. Sci. Ser. B; 267, 799, (1968).

49. R. Kozlowski, R.F. Pettifer, J.M Thomas; J. Phys. Chem.; 87, 5172, (1982).

50. H.P. Boehm, M. Herrmann; Zeits. Anorg. Allgem. Chemie; 352, 156, (1967).

51. M. Primet, P. Pichat, M-V. Mathieu; J. Phys. Chem.; 75, 1216, (1971).

52. D.M. Griffiths, C.H. Rochester; J.C.S. Farad. Trans. I; 73, 1510, (1977).

53. P. Jackson, G.D. Parfitt; Trans. Farad. Soc.; 67, 2469, (1971).

54. G. Munuera, F.S. Stone; Disc. Farad. Soc.; 52, 205, (1971).

55. E. De Pauw, J. Marlen; J. Phys. Chem.; 85, 3550, (1981).

56. T. Morimoto, T. Iwaki; J.C.S. Farad. Trans. I; 83, 943, (1987).

57. T. Morimoto, T. Iwaki; J.C.S. Farad. Trans. I; 83, 957, (1987).

58. T. Morimoto, M. Nagao, F. Tokuda; J. Phys. Chem.; 73, 243, (1969).

59. H.P. Boehm; Disc. Farad. Soc.; 52, 264, (1971).

60. M. Primet, P. Pichat, M-V. Mathieu; J. Phys. Chem.; 75, 1221, (1971).

61 M. Herrmann, H.P. Boehm; Zeits. Anorg. Allgem. Chemie; 368, 73, (1969).

62. G.D. Parfitt, J. Ramsbottom, C.H. Rochester; Trans. Farad. Soc.; 67, 3100, (1971).

63. J. Graham, C.H. Rochester, R. Rudham; J.C.S. Farad. Trans. I; 77, 1973 (1981).

64. J. Graham, C.H. Rochester, R. Rudham; J.C.S. Farad. Trans. I; 77, 2735 (1981).

65. J. Graham, C.H. Rochester, R. Rudham; J.C.S. Farad. Trans. I; 77, 2845 (1981).

66. C. Morterra; J.C.S. Farad. Trans. I; 84, 1617, (1988).

67. G.D. Parfitt; Progr. Surf. Membr. Sci.; 11, 181, (1976).

68. R.E. Day; Progr. Org. Coatings; 2, 169, (1973/4).

69. T.J. Wiseman; "Characterisation of Powder Surfaces", (Eds. G.D. Parfitt & K.S.W. Sing); Academic Press, New York / London, (1976).

70. Y.M. Shchekochikin, V.N. Filimonov, N.P. Keier, A.N. Terenin; Kinet. Catal.; 5, 94, (1964).

71. P. Jackson, G.D. Parfitt; J.C.S. Farad. Trans. I; 68, 1443, (1972).

72. G. Munuera, I. Carrizosa; Acta Cient. Venez. Suppl.; 24, 226, (1973).

73. C.H. Rochester, J. Graham, R. Rudham; J.C.S. Farad. Trans. I; 80, 2459 (1984).

74. I. Carrizosa, G. Munuera; J. Catal.; 49, 174, (1977).

75. I. Carrizosa, G. Munuera; J. Catal.; 49, 189, (1977).

76. S.J. Gentry, R. Rudham, K.P. Wagstaff; J.C.S. Farad. Trans. I; 71, 657, (1975).

77. I. Carrizosa, G. Munuera, S. Castanar; J. Catal.; 49, 265, (1977).

78. K.S. Kim, M.A. Barteau, W.E. Farneth; Langmuir; 4, 533, (1988).

79. J-M. Herrmann, P.Vergnon, S.J. Teichner; Bull. Chim. Soc. Fr.; 30, 3034, (1972).

80. P. Gravelle, F. Juillet, P. Meriaudeau, S.J. Teichner; Disc. Farad. Soc.; 52, 140, (1971).

81. R.D. Iyengar, M. Codell; Adv. Coll. Interf. Sci.; 3, 365, (1972).

82. J.M Thomas, W.J. Thomas; "Introduction to the Principles of Heterogeneous Catalysis"; Academic Press, London, (1967).

83. J. Cunningham, E. Finn, N. Samman; Disc. Farad. Soc.; 58, 160, (1974).

84. A.A. Davydov, M.P. Komarova, V.F. Anufrienko, N.G. Maksimov; Kinet. Catal.; 14, 1519, (1973).

85. A.I. Mashchenko, V.B. Kazanskii, G.B. Pariiskii, V.M. Sharapov; Kinet. Catal.; 8, 853, (1967).

86. A.P. Griva, V.V. Nikisha, B.N. Shelimov, V.B. Kazanskii; Kinet. Catal.; 15, 86, (1974).

87. A.P. Griva, V.V. Nikisha, B.N. Shelimov, V.B. Kazanskii, G.M. Zhidomirov; Kinet. Catal.; 14, 1693, (1973).

88. H.W. Gundlach, K.E. Heusler; Z. Phys. Chem. Neue Folge; 112, 101, (1978).

89. H.W. Gundlach, K.E. Heusler; Z. Phys. Chem. Neue Folge; 119, 213, (1980).

90. W.J. Lo, Y.W. Chung, G.A. Somorjai; Surf. Sci.; 71, 199, (1978).

91. E. Serwicka, R.N. Schindler, R. Schumacher; Ber. Bunsenges Phys. Chem.; 85, 192, (1981).

92. T. Iwaki; J.C.S. Farad. Trans. I; 79, 137, (1983).

93. T. Iwaki, K. Katsuta, M. Miura; J. Catal.; 68, 492, (1981).

94. P. Jackson, G.D. Parfitt; J.C.S. Farad. Trans. I; 68, 896, (1972).

95. T. Nakajima, H.Miyata, Y. Kubokawa; Bull. Chem. Soc. Jpn.; 55, 609, (1982).

96. J. Graham, R. Rudham, C.H. Rochester; J.C.S. Farad. Trans. I; 80, 895 (1984).

97. F. Al-Mashta, C.V. Davanzo, N. Sheppard; J.C.S. Chem. Commun.; 1258, (1983).

98. B.I. Brookes, R. Bird, C.Kemball, H.F. Leach; J.C.S. Farad. Trans. I; 85, 2173, (1989).

99. M. Primet, J. Bandiera, C. Naccache, M-V. Mathieu; J. Chim. Phys.; 67, 535, (1970).

100. M. Primet, J. Bandiera, C. Naccache, M-V. Mathieu; J. Chim. Phys.; 67, 1030, (1970).

101. K. Tanaka, J.M. White; J. Phys. Chem.; 86, 4708, (1982).

102. V. Bolis, B. Fubini, E. Garrone, C. Morterra; J.C.S. Farad. Trans. I; 85, 1383, (1989).

103. Th. Wolkenstein; Progr. Surf. Sci.; 6, 213, (1975).

104. C. Naccache, P. Meriaudeau, M. Che, A.J. Tench; Trans. Farad. Soc.; 67, 506, (1971).

105. D.R. Kennedy, M. Ritchie, J. Mackenzie; Trans. Farad. Soc.; 54, 119, (1958).

106. P. Meriaudeau, J.C. Vedrine; J.C.S. Farad. Trans I; 72, 472, (1976).

107. S. Fukuzawa, K.M. Sancier, T. Kwan; J. Catal.; 11, 364, (1968).

108. R.I. Bickley, F.S. Stone; J. Catal.; 31, 389, (1973).

109. R.I. Bickley, R.K.M. Jayanty; Disc. Farad. Soc.; 58, 194, (1974).

110. A.H. Boonstra, C.A.H.A. Mutsaers; J. Phys. Chem.; 79, 1694, (1975).

111. Y. Oosawa, M. Grätzel; J.C.S. Farad. Trans I; 84, 197, (1988).

112. G. Munuera, V. Rives-Arnau, A. Saucedo; J.C.S. Farad. Trans I; 75, 736, (1979).

113. A.R. Gonzalez-Elipe, G. Munuera, J. Soria; J.C.S. Farad. Trans I; 75, 748, (1979).

114. G. Munuera, A.R. Gonzalez-Elipe, J. Soria, J. Sanz; J.C.S. Farad. Trans I; 76, 1535, (1980).

115. K. Tanaka; J. Phys. Chem.; 78, 555, (1974).

116. H. Courbon, M. Formenti, P. Pichat; J. Phys. Chem.; 81, 550, (1977).

117. S. Sato, T. Kadowaki, K. Yamaguti; J. Phys. Chem.; 88, 2930, (1984).

118. S. Sato; J. Phys. Chem.; 91, 2895, (1987).

119. I.S. M°Lintock, M. Ritchie; Trans. Farad. Soc.; 61, 1007, (1965).

120. Y.P. Solonitsyn, C.N. Kuz'min, A.L. Shurygin, V.M. Yurkin; Kinet. Catal.; 17, 1092, (1976).

121. R.I. Bickley, G. Munuera, F.S. Stone; J. Catal.; 31, 398, (1973).

122. R.B. Cundall, R. Rudham, M.S. Salim; J.C.S Farad. Trans. I; 72, 1642, (1976).

123. J. Cunningham, B. Doyle, E.M. Leahy; J.C.S Farad. Trans. I; 75, 2000, (1979).

124. P.R. Harvey, R. Rudham, S. Ward; J.C.S. Farad. Trans. I; 79, 1381, (1983).

125. P.R. Harvey, R. Rudham, S. Ward; J.C.S. Farad. Trans. I; 79, 2975, (1983).

126. N. Djeghri, M. Formenti, F. Juillet, S.J. Teichner; Disc. Farad. Soc.; 58, 185, (1974).

127. J-M. Herrmann, J.Disdier, M-N. Mozzanega, P.Pichat; J. Catal; 60, 369, (1979).

128. N. Djeghri, S.J. Teichner; J. Catal; 62, 99, (1980).

129. M. Formenti, F. Juillet, P. Meriaudeau, S.J. Teichner; "Proc. 5th Intern. Congr. Catal.;", (Ed. J.H. Hightower), p.1101; North Holland / American Elsevier, (1973).

130. M. Fujihira, Y. Satoh, T. Osa; Nature; 293, 206, (1981).

131. M. Fujihira, Y. Satoh, T. Osa; Bull. Chem. Soc. Jpn.; 55, 666, (1982).

132. L.P. childs, D.F. Ollis; J. Catal.; 67, 35, (1981).

133. M. Anpo, N. Aikawa, S. Kodama, Y. Kubokawa; J. Phys. Chem.; 88, 2569, (1984).

134. A.H. Boonstra, C.A.H.A. Mutsaers; J. Phys. Chem.; 79, 2025, (9175).

135. Z-S. Cai, R.R.Kuntz; Langmuir; 4, 830, (1988).

136. J-M. Herrmann, P.Pichat; J.C.S. Farad. Trans. I; 76, 1138, (1980).

137. P.R. Harvey, R. Rudham; J.C.S. Farad. Trans. I; 84, xxxx, (1988).

138. S.N. Frank, A.J. Bard; J. Phys. Chem.; 81, 1484, (1977).

139. L.V. Lyashenko, Y.B. Gorokhovat-skii; Theoret. Exptl. Chem.; 10, 138, (1975).

140. V.S. Zakharenko, A.E. Cherkashin, A.M. Volodin, N.P. Keier; React. Kinet. Catal. Letts.; 10, 329, (1979).

141. B. Kraeutler, C.D. Jaeger, A.J. Bard; J. Amer. Chem. Soc.; 100, 2239, (1978).

142. B. Kraeutler, C.D. Jaeger, A.J. Bard; J. Amer. Chem. Soc.; 100, 4903, (1978).

143. B. Kraeutler, A.J. Bard; J. Amer. Chem. Soc.; 100, 5985, (1978).

144. B. Kraeutler, A.J. Bard; J. Amer. Chem. Soc.; 100, 4318, (1978).

145. A.J. Bard, W.W. Dunn, B. Kraeutler; US Patent 4,264,421; (1981).

146. W.W. Dunn, A.J. Bard; Nouv. J. Chimie; 5, 651, (1981).

147. S.J. Tauster, S.C. Fung, R.L. Garten; J. Amer. Chem. Soc.; 100, 170, (1978).

148. P. Pichat, J-M. Herrmann, J. Disdier, H. Courbon, M-N. Mozzanega; Nouv. J. Chimie; 5, 627, (1981).

149. A. Takeuchi, J.R. Katzer; J. Phys. Chem.; 85, 937, (1981).

150. S.Fuentes, A. Vázquez, R. Silva, J.G. Pérez-Ramirez, M.J. Yacamán; J. Catal.; 111, 353, (1988).

151. A. Mills; J.C.S. Chem. Commun.; 367, (1982).

152. A.A. Slinkin, A.V. Kucherov, E.A. Fedorovskaya, L.V. Ermolov, G.A. Ashsvskaya, L. Kempinski, J. Jablonski; Kinet. Catal.; 29, 594, (1988).

153. R.T.K. Baker, E.B. Prestridge, R.L.Garten; J. Catal; 56, 390, (1979).

154. R.I. Bickley; S.P.R.- Catalysis; 5, 308, (1982).

155. M. Koudelka, J. Sanchez, J. Augustynski; J. Phys. Chem.; 86, 4277, (1982).

156. C. Sungbom, M. Kawai, K. Tanaka; Bull. Chem. Soc. Jpn.; 57, 871, (1984).

157. J.S. Curran, J. Domenech, N. Jaffrezic-Renault, R. Philippe; J. Phys. Chem.; 89, 957, (1985).

158. J-M. Herrmann, J. Disdier, P. Pichat; J. Phys. Chem.; 90, 6028, (1986).

159. H. Yoneyama, N. Nishimura, H. Tamura; J. Phys. Chem.; 85, 268, (1981).

160. H. Nakamatsu, T.Kawai, A. Koreeda, S. Kawai; J.C.S. Farad. Trans. I; 82, 527, (1985).

161. J-M. Herrmann; J. Catal.; 89, 404, (1984).

162. G.C. Bond; "Heterogeneous Catalysis - Principles and Applications", Chapter 7, p.78; Oxford University Press, 1987.

163. S. Khoobiar; J. Phys. Chem.; 68, 411, (1964).

164. J.E. Benson, H.W. Kohn, M. Boudart, J. Catal.; 5, 307, (1966).

165. M. Lacroix, G.M. Pajonk, S.J. Teichner; Bull. Chem. Soc. Fr.; 1, 87, (1981).

166. P.A. Sermon, G.C. Bond; J.C.S. Farad. Trans. I; 72, 745, (1976).

167. P. Gajardo, T.M. Apple, C.Dybowski; Chem. Phys. Letts.; 74, 306, (1980).

168. J.C. Conesa, J. Soria; J. Phys. Chem.; 86, 1392, (1982).

169. T. Huizinga, R. Prins; J. Phys. Chem.; 85, 2156, (1981).

170. J-M. Herrmann, P. Pichat; Stud. Surf. Sci. Catal.; 17, 77, (1983).

171. D.D. Beck, J.M. White; J. Phys. Chem.; 88, 174, (1984).

172. D.D. Beck, J.M. White; J. Phys. Chem.; 88, 2764, (1984).

173. D.D. Beck, A.O. Bawagan, J.M. White; J. Phys. Chem.; 88, 2764, (1984).

174. P.A. Sermon, G.C. Bond; Catal. Rev.; 8, 211, (1973).

175. G.C. Bond; Stud. Surf. Sci. Catal.; 17, 1, (1983).

176. R.T.K. Baker, E.B. Prestridge, R.L. Garten; J. Catal.; 59, 293, (1979).

177. R.T.K. Baker, E.B. Prestridge, L.L. Murrell; J. Catal.; 79, 348, (1983).

178. T. Huizinga, R. Prins; J. Phys. Chem.; 87, 173, (1983).

179. X-Z. Jiang, T.F. Hayden, J.A. Dumesic; J. Catal.; 83, 168, (1983).

180. A.J. Simeons, R.T.K. Baker, D.J. Dwyer, C.R.F. Lund, R.J. Madon; J. Catal.; 86, 359, (1984).

181. H.R. Sadeghi, V.E. Henrich; J. Catal.; 87, 279, (1984).

182. C.S. Ko, R.J. Gorte; J. Catal.; 90, 59, (1984).

183. H. Brumberger, F. Dehaglio, J. Goodisman, M.G. Phillips, J.A. Schwarz, P. Sen; J. Catal.; 92, 199. (1985).

184. Y-M. Sun, D.N. Belton, J.M. White; J. Phys. Chem.; 90, 5178, (1986).

185. A.D. Logan, E.J. Braunschweig, A.K. Datye, D.J. Smith; Langmuir; 4, 827, (1998)

186. J.A. Horsley; J. Amer. Chem. Soc.; 101, 2870, (1979).

187. J-M. Herrmann, P. Pichat; J. Catal.; 78, 425, (1982).

188. S.C. Fung; J. Catal.; 76, 225, (1982).

189. B.A. Sexton, A.E. Hughes, K.F. Foger; J. Catal.; 77, 85, (1982).

190. P. Meriaudeau, O.H. Ellestad, M. Dufaux, C. Naccache; J. Catal.; 75, 243, (1982).

191. B-H. Chen, J.M. White; J. Phys. Chem.; 86, 3534, (1982).

192. B-H. Chen, J.M. White; J. Phys. Chem.; 87, 1327, (1983).

193. M.S. Spencer; J. Phys. Chem.; 88, 1046, (1984).

194. D.N. Belton, Y-M. Sun, J.M. White; J. Phys. Chem.; 88, 1690, (1984).

195. J.H.A. Martens, R. Prins, H. Zandbergen, D.C. Koningsberger; J. Phys. Chem.; 92, 1903, (1988).

196. D.N. Belton, Y-M. Sun, J.M. White; J. Amer. Chem. Soc.; 106, 3059, (1984).

197. D.N. Belton, Y-M. Sun, J.M. White; J. Phys. Chem.; 88, 5172, (1984).

198. D.N. Belton, Y-M. Sun, J.M. White; A.C.S. Symp. Ser. - Catal. Characterisation Sci.; 288, 80, (1985).

199. S. Takatani, Y-W. Chung; J. Catal.; 90, 75, (1975).

200. T. Sheng, X. Guoxing, W. Hongli; J. Catal.; 111, 136, (1988).

201. H-C. zur Loye, A.M. Stacy; Langmuir; 4, 1261, (1988).

202. S.J. Tauster, S.C. Fung, R.T.K. Baker, J.A. Horsley; Science; 211, 1121, (1981).

203. G.C. Bond, X. Yide; J.C.S. Farad. Trans. I; 80, 3103, (1984).

204. K. Foger; J. Catal.; 78, 406, (1982).

205. J. Schwank, J.Y. Lee, J.R. Goodwin Jr; J. Catal.; 108, 495, (1987).

206. J.P.S. Badyal, A.J. Gellman, R.M. Lambert; J. Catal.; 111, 383, (1988).

207. M.E. Levin, M. Salmeron, A.T. Bell, G.A. Somorjai; J. Catal.; 106, 401, (1987).

208. T. Mori, S. Taniguchi, Y. Mori, T. Hattori, Y. Murakami; J. Catal,; 108, 501, (1987).

209. G.C. Bond, R. Burch; S.P.R.- Catalysis; 6, 54, (1983).

210. M. Kawai, S. Naito, K. Tamaru, T. Kawai; Chem. Phys. Letts.; 98, 377, (1983).

211. M. Kawai, T. Kawai, S. Naito, K. Tamaru; Chem. Phys. Letts.; 110, 58, (1984).

212. T. Sakata, T. Kawai; Chem. Phys. Letts.; 80, 341, (1981).

213. F.H. Hussein, R. Rudham; J.C.S. Farad. Trans. I; 83, 1631, (1987).

214. Y. Oosawa; J.C.S. Chem. Commun.; 221, (1982).

215. Y. Oosawa; J.C.S. Farad. Trans. I; 80, 1507, (1984).

216. A. Fujishima, K. Honda; Nature; 238, 37, (1982).

217. E. Borgarello, J. Kiwi, E. Pelizzetti, M. Visca, M. Grätzel; J. Amer. Chem. Soc.; 103, 6324, (1981).

218. E. Yesodharan, M. Grätzel; Helv. Chimica Acta; 66, 2145, (1983).

219. S. Sato, J.M. White; J. Amer. Chem. Soc.; 102, 7206, (1980).

220. S-C. Tsai, C-C. Kao, Y-W. Chung; J. Catal.; 79, 451, (1983).

221. A.J. Bard; J. Photochem.; 10, 59, (1979).

222. S. Sato, J.M. White; Chem. Phys. Letts.; 72, 83, (1980).

223. S. Sato, J.M. White; J. Catal.; 69, 128, (1981).

224. J. Kiwi, E. Borgarello, E. Pelizzetti, M. Visca, M. Grätzel; Angew. Chem. Intern. Ed.; 19, 646, (1980).

225. D. Duonghong, E. Borgarello, M. Grätzel; J. Amer. Chem. Soc.; 103, 4685, (1981).

226. R.H. Baker, J. Lilie, M. Grätzel; J. Amer. Chem. Soc.; 104, 422, (1982).

227. D. Duonghong, J. Ramsden, M. Grätzel; J. Amer. Chem. Soc.; 104, 2977, (1982).

228. M. Grätzel; Farad. Disc. Chem. Soc.; 70, 359, (1980).

229. J-M. Lehn; "Photochemical Conversion and Storage of Solar Energy"; Academic Press, New York, 1981.

230. A.J. Bard; J. Phys. Chem.; 86, 172, (1982).

231. A. Harriman; S.P.R.- Photochemistry; 14, 513, (1983).

232. L. Milgrom; New Scientist; p.26, 02/02/84.

233. S-M. Fang, B-H. Chen, J.M. White; J. Phys. Chem; 86, 3126, (1982).

234. S. Sato, J.M. White; Chem. Phys. Letts.; 70, 131, (1980).

235. S. Sato, J.M. White; J. Phys. Chem.; 85, 336, (1981).

236. W.G. Leighton, G.S. Forbes; J. Amer. Chem. Soc.; 52, 3139 (1930).

237. M.I. Christie, G. Porter; Proc. Royal Soc. London; A212, 390 (1952).

238. J.G. Calvert, J.N. Pitts; "Photochemistry"; J. Wiley & Son; (1966).

239. P. Pichat, M-N. Mozzanega, J. Disdier, J-M. Herrmann; Nouv. J. Chim.; 6, 559, (1982).

240. F.H. Hussein, R. Rudham; J.C.S. Farad. Trans. I; 80, 2817, (1984).

241. J.P. Belzunegui, J. Sanz, J.M. Rojo; J. Amer. Chem. Soc.; 112, 4066, (1990).

242. G. Munuera, A.R. González-Elipe, J.P. Espinós; Surf. Sci.; 211/212, 1113, (1989).

243. A.R. González-Elipe, A. Fernández, J.P. Espinós, G. Munuera; J. Catal.; 131, 51, (1991).

244. L. Bonneviot, G.L. Haller; J. Catal.; 130, 359, (1991).

245. J.P. Bucher, J.J. van der Klink, M. Grätzel; J. Phys. Chem.; 94, 1209, (1990).

246. J.P. Belzunegui, J.M. Rojo, J. Sanz; J. Phys. Chem.; 95, 3463, (1991).

247. P.R. Norton, J.A. Davies, T.E. Jackman; Surf. Sci.; 121, 103, (1982).

248. E.K. Rideal; J. Chem. Soc.; 121, 309, (1922).

249. G.I. Jenkins, E.K. Rideal; J. Chem. Soc.; 2490, (1955).

250. G.C. Bond; Trans. Farad. Soc.; 52, 1235, (1956).

251. E.B. Maxted, C.H. Moon; J. Chem. Soc.; 1190, (1935).

252. R.N. Pease, C.A. Harris; J. Amer. Chem. Soc.; 57, 1147, (1935).

253. H. zur Strassen; Z. Phys. Chem.; A169, 81, (1934).

254. L.L. Kesmodel, L.H. Dubois, G.A. Somorjai; Chem. Phys. Lett.; 56, 267, (1978).

255. L.L. Kesmodel, D.G Castner, G.A. Somorjai; Chem. Phys. Lett.; 70, 5234, (1980).

256. L.L. Kesmodel, J.A. Gates; Surf. Sci.; 111, L747, (1981).

257. P. Skinner, M.W. Howard, I.A. Oxton, S.F.A. Kettle, D.B. Powell, N. Sheppard; J.C.S Farad. Trans. II; 77, 1203, (1981).

258. F. Zaera, G.A. Somorjai; J. Phys. Chem.; 89, 3211, (1985).

259. N. Freyer, G. Pirug, H.P. Bonzel; Surf. Sci.; 125, 327, (1983).

260. P. Berlowitz, C. Megiris, J.B. Butt, H.H. Kung; Langmuir; 1, 206, (1985).

261. Z. Paál, E. Fülöp, D. Marton; React. Kinet. Catal. Lett.; 38, 131, (1989).

262. N.R. Avery; Surf. Sci.; 137, L109, (1984).

263. S.B. Mohsin, M. Trenary, H.J. Robota; J. Phys. Chem.; 95, 6657, (1991).

264. D.A. Hensley, L.L. Kesmodel; Surf. Sci.; 231. 361, (1990).

265. D.A. Hensley, L.L. Kesmodel; J. Phys. Chem.; 95, 1368, (1991).

266. G.C. Bond; "Catalysis by Metals"; Chapter 11; Academic Press, London (1962).

267. J. Horiuti, M. Polanyi; Trans. Farad. Soc.; 30, 1164, (1934).

268. D.E. Resasco, G.L. Haller; J. Phys. Chem.; 88, 4552, (1984).

269. R.J. Fenoglio, G.M. Nuñez, D.E. Resasco; J. Catal.; 121, 77, (1990).

270. G.C. Bond, J. Sheridan; Trans. Farad. Soc.; 48, 713, (1952).

271. G.C. Bond, J. Turkevich; Trans. Farad. Soc.; 50, 1335, (1954).

272. J. Addy, G.C. Bond; Trans. Farad. Soc.; 53, 368, 383, 388, (1957).

273. G.C. Bond, J. Newham; Trans. Farad. Soc.; 56, 1501, (1960).

274. C. Flinn; PhD Thesis, Nottingham University, (1987).

275. R. Burch, R.J. Flambard; J. Catal.; 78, 389, (1982).

276. S.Y. Wang, S.H. Moon, M.A. Vannice; J. Catal.; 71, 167, (1981).

277. J.B.F. Anderson, R. Burch; Appl. Catal.; 25, 173, (1986).

278. K.J. Blankenburg, A.K. Dayte; J. Catal.; 128, 186, (1991).

279. T.F. Mao, J.L. Falconer; J. Catal.; 123, 443, (1990).

280. S. Teratani, J. Nakamichi, K. Taya, K. Tanaka; Bull. Chem. Soc. Jpn.; 55, 1688, (1982).

281. T.J. Lee, Y.G. Kim; J. Catal.; 90, 279, (1984).

282. S. Fuentes, A. Vázquez, J.G. Pérez, M.J. Yacamán; J. Catal.; 99, 492, (1986).

APPENDIX 1: BASIC PROGRAM TO MONITOR GAS PRESSURE AS A FUNCTION OF TIME VIA CUBAN-12A ADC CARD

```
10 CLS:MODE131
20 PRINT" HYDROGENATION PRESSURES _ DATA COLLECTION"
30 PRINT" ============================"
40 PRINT:PRINT"This program collects pressure readings at set intervals
                from the "
50 PRINT:PRINT"MKS Baratron via the Cuban-12A A to D card by
               sampling the output"
60 PRINT:PRINT"voltage of the Baratron. If rapid sampling of the
               pressure is required during"
70 PRINT:PRINT"the initial stages of the reaction, this option is available"
80 PRINT:PRINT"The data is the stored on disk in a user-named file"
90 PRINT:PRINT"The appropriate disk must be inserted in DRIVE ! and
                the correct directory"
100 PRINT:PRINT"set before this program is run. DO NOW IF
             REQUIRED!!"
110 PRINT:PRINT"PRESS SPACEBAR TO CONTINUE"
120 X$=GET$:IF X$<>" " THEN120
125 REM LINES 130 TO 260 DEFINE DATA COLLECTION PATTERN AS
    A FUNCTION OF TIME FOR
130 CLS:PRINT
140 n=0:IRT=0
150 INPUT "Do you require rapid sampling during the initial stages of the
reaction (Y/N)";L$
160 IF L$="N" THEN 220
170 PRINT:INPUT"Enter initial rapid sampling time (mins)";IRT
180 irt=(IRT*60):PRINT
190 INPUT"Enter initial rapid sampling read interval (secs)";IRI:
          IRS=(IRI*100):PRINT
200 n = 1+INT(irt/IRI)
```

```
210 PRINT"No. of rapid read points = "n
220 PRINT:INPUT"Enter overall run time (mins)";RT:RT=(RT*60):PRINT
230 INPUT"Enter delayed read interval (secs)";RI:RS=(RI*100):PRINT
240 N=INT((rt-irt)/RI)
250 DP=n+N
260 PRINT"Total no. of data points = "DP
270 REM DATA COLLECTION PROCEDURE FROM MKS BARATRON VIA
    CUBAN-12A A TO D CARD
280 PRINT:PRINT:PRINT"PRESS SPACEBAR TO COMMENCE DATA
                          COLLECTION PROCEDURE"
290 Y$=GET$:IF Y$<>" " THEN290
300 TIME=0
310 DIM S(DP), V(DP), P(DP)
320 JIM=&FD80:REM HEX address for CUBAN-12A
330 PROCassemble(JIM)
340 PROCinit
350 STOPCLEAR (420)
360 ROW=1
370 REPEAT
380 count=count+1
390 X%=0
400 PROCresult
410 UNTIL count=DP
420 PRINT:PRINT:PRINT"PRESS SPACEBAR TO START FILE CREATION"
430 Z$=GET$:IF Z$<>" " THEN430
440 PROCcreate_file
450 END

500 REM INITIALISE CUBAN-12A DATA COLLECTION
510 DEFPROCinti
520 CALL setup
525 REM Remove cursor from screen
```

```
530 CLS:VDU23,1,0;0;0;0
540 PRINTTAB(3)"Time (s)";TAB(25)"Voltage (V)";TAB(50)"Pressure
          (kPa)"
550 PRINTTAB(2)"--------";TAB(24)"----------";TAB(49)"----------"
560 ENDPROC

600 REM SET UP CUBAN-12A VIA ADDRESSES
610 DEFPROCassemble(VIA%)
620 LL% = &FCFF
630 ?LL% = &DC
640 PORTB% = VIA%
650 PORTA% = VIA% + 1
660 DDRB% = VIA% + 2
670 DDRA% = VIA% + 3
680 ifr% = VIA% + &0D
690 PCR% = VIA% + 0C
700 PORTQ% = VIA% + &0F
710 DIM CODE 100
720 FOR pass%0 TO 3 STEP 3
730 P% = CODE
735 REM ASSEMBLY LANGUAGE CONTAINED BETWEEN [ AND ]
740 [
750 OPT pass%
760 .setup          LDA £&08
770                 STA PCR%
780                 LDA £&00
790                 STA DDRA%
800                 LDA £&FF
810                 STA DDRB%
820                 RTS
830 .ADC            STX PORTB%
840                 LDA PORTA%
```

```
850 .loop       LDA ifr%
860             AND £&02
870             BEQ loop
880             LDA PORTB%
890             ORA £&10
900             STA PORTB%
910             LDX PORTQ%
920             AND £&EF
930             STA PORTB%
940             LDA PORTQ%
950             RTS
960 .delay      LDX £&10
970 .outer      DEX
980             BNE outer
990             RTS
1000 ]
1010 NEXT
1020 ENDPROC

1500 REM RESULTS PROCESSING SUBROUTINE
1510 DEFPROCresult
1520 T=TIME
1530 total%=USR(ADC)
1540 value=total% AND &0FFF
1545 REM sound warning when data collection time near end
1550 IF count > DP-2 THEN SOUND 1,-15,100,30
1555 REM Convert data into seconds, voltage and pressure readings
1560 V(count)=value%/1000
1570 P(count)=(V(count)*0.6736)+0.0072
1580 S(count)=INT(10*(T/100+0.5))/10
1590 P(count)=INT(10^4*P(count)+0.5)/10^4
1595 REM Ensure correct number of decimal places and consistent
```

```
1600 B$ =STR$(V(count))
1610 B=INSTR((B$,".")
1620 B$ =LEFT$(B$,B+3)
1630 C$ =STR$(P(count))
1640 C=INSTR(C$,".")
1650 C$ =LEFT$(C$,C+4)
1660 ROW=ROW+1
1670 IF ROW<23 THEN 1710
1680 CLS:ROW=2
1690 PRINTTAB(2)"Time (s)";TAB(24)"Voltage (V)";TAB(49)"Pressure
                (kPa)"
1700 PRINTTAB(2)"--------";TAB(24)"----------";TAB(49)"-------------"
1710 @%=&20106:PRINTTAB(2,ROW) S(count)
1720 @%=&0402:PRINTTAB(24,ROW) B$;TAB(49,ROW) C$
1730 IF count<n THEN STOPCLEAR (IRS) ELSE STOPCLEAR (RS)
1740 ENDPROC

2000 REM Store data on disk under user-defined name
2010 DEFPROCcreate_file
2020 CLS:PRINT:INPUT"Please enter desired name of file";file$
2030 CH%=OPENOUT(file$)
2040 FOR I=1 TO DP
2050 PRINT£CH%,S(I),V(I),P(I)
2060 NEXTI
2070 CLOSE£CH%
2080 ENDPROC

2100 END
```

APPENDIX 2: PHYSICO-CHEMICAL CHARACTERISTICS OF TiO_2 SUPPORTS USED IN THIS STUDY

	Degussa P25	CLDD2078/1	CLDD2078/2
Cl, %	-	0.015	0.8
ZrO_2, ppm	-	30	50
Nb_2O_5, ppm	-	< 10	< 10
P_2O_5, ppm	-	300	200
SiO_2, ppm	-	< 100	200
SO_3, ppm	-	< 100	100
CaO, ppm	-	100	30
Al_2O_3, %	< 0.3	-	-
Fe_2O_3, %	< 0.2	-	-
TiO_2, %	> 97	> 98	> 98
Crystal Form	mainly anatase	anatase	rutile
Surface Area ($m^2\ g^{-1}$)	50 ± 15	63.0	15.4

[Data kindly supplied by Degussa GmBH and Tioxide Group PLC]